# MASSIVE HYDRAULIC FRACTURING EXPERIMENTS OF THE DEVONIAN SHALE IN LINCOLN COUNTY, WEST VIRGINIA

## COLUMBIA/DOE CONTRACT E (46-1)-8014

## APPENDICES

Contributing Authors:

S. P. CREMEAN
S. F. McKETTA
G. L. OWENS
E. C. SMITH

Reviewed by:

R. M. FORREST

Approved by:
W. F. MORSE

JANUARY, 1979



RESEARCH DEPARTMENT

COLUMBIA GAS SYSTEM
SERVICE CORPORATION

Open File No. 199
Volume 2 - Appendices

# TERRA TEK REPORT

## IN SITU STRESS DETERMINATION IN THE DEVONIAN SHALE (IRA MCCOY 20402) WITHIN THE ROME BASIN

# VOLUME II

# APPENDICES

# APPENDIX I

# APPENDIX 1: AN EXPLANATION OF GAS CONTENT TERMINOLOGY AND ANALYTICAL METHODS

## Standarization of Reserve Terminology

Considering the importance of the reported gas reserve estimates to exploration planning, caution should be exercised when referring to any of the reported values, especially when such figures might be subject to public scrutiny. At some future time, we shall be called to account for the gas reserves which have been published. If it is generally known that some given quantity of gas is contained in the Eastern Devonian Shales, it may be difficult to explain after the fact that only a fraction of the reserves are exploitable. With this in mind, it seems logical to select those figures which most closely reflect the economically producible gas reserves.

The most reliable information is the "produced gas" as given by actual production records, but this can only be determined after a well has ceased production. However, well log and reservoir test data are used to estimate the amount of "free gas in place" and "recoverable gas," and with additional production data one may accurately calculate the recoverable gas reserves. The fraction of the gas in place which is recoverable will depend on the back pressure in the gas lines and technical and economic factors. Perhaps the best reserves figures are based on either produced or producible gas values, but in order to use these estimates to determine the reserves elsewhere, we must assume a drainage volume for each well, make the assumption that the reservoir contains a similar gar concentration at every location and the stimulation method is effective. Such assumptions will introduce an undetermined amount of error.

In the present attempts to calculate reserves for the entire Appalachian Basin from the analyses of canned rock samples, it would be most desirable to base the calculations on some reference pressure, as we cannot continue to produce below the line back pressure. Columbia's estimates relate the gas content to the pressure increase observed in sealed sample containers--that is, the final gauge pressure. Samples which contain some hydrocarbon gas but yield no measurable pressure increase are considered to contain no producible gas. Although the true producible portion will vary depending on the actual collection line pressure, it is felt that our values which we shall call "off gas" are the most applicable. Moreover, the term "off gas" doesn't imply any physical state, but merely that it is mobile gas of some sort. It should be noted that the "off gas" as measured does not include any gas originally present in fractures, or other permeable zones.

Battelle's "free gas" values are more difficult to apply since the gas pressure includes the initial air pressure of 14.7 psi. Even if these figures are multiplied by the hydrocarbon fraction of the contained gas, this will include gas which is not producible with a back pressure of zero psig. Battelle's "weight loss" values from thermogravimetric measurements are almost entirely due to water vapor release. Consequently, they are of no use to us. Our own low mobility hydrocarbon content is also of limited economic interest at this time.

"Gas yield," "oil yield," "Fischer Assay," "gas equivalent of carbon content" and related hydrocarbon content figures are not measures of the gas content of a formation; but are, in fact, the hydrocarbon fractions which may only be generated and liberated by heating rock volumes to a sufficent temperature under proper conditions. These figures must not be confused with gas contents or true gas reserves, as the economics of exploitation differ markedly. It is difficult to compare the gas yield and gas equivalent results from different laboratories due to differences in analytical procedures (temperatures, pressures, addition of hydrogen, and catalytic agents). The ultimate gas-equivalent reserves can only be determined by that retorting procedure which generates the maximum possible amount of gas.

In summary, in the absence of production or well test data, the most applicable type of rock or core gas measurement is one based on observed pressure increases due to hydrocarbon gas release as is being done by the Columbia Gas Research Department. It is proposed that this fraction of the total gas content be referred to as the "off gas" content. The adoption of some standard terminology appears to be a first step in working towards a basis of comparison for results, and a basin-wide extension of reserve estimates based on core analyses.

Categories of Hydrocarbons and Other Organic
Matter in Relation to Resource Evaluation

Anyone who reviews the existing literature on the hydrocarbon reserves of organic rich sediments will find a bewildering range of reported values. These differences in gas and oil content may be real and due to actual horizontal and vertical gradations, or may be only apparent and related to nomenclature differences, the inclusion of only one or several physical states of hydrocarbons in the rock, differences in methods of measurement or content calculation models. The following outline is an attempt to clarify some of this confusion.

I. Nomenclature and Physical Forms of Hydrocarbons and Organic Compounds:

A. Light, hydrocarbons which are gases under standard conditions include free gas, adsorbed gas and trapped gas.

1. "Gas in place" is the total content of light hydrocarbons which would be gaseous under standard conditions. This corresponds to the maximum recoverable volume if economic factors are disregarded, but below the temperatures at which kerogen decomposes. (Includes all of the other forms: free, adsorbed, trapped, fracture content, etc.).

2. "Produced gas" is that volume of gas actually recovered according to production records.

3. "Recoverable gas" is that calculated portion of the total gas in place which can be exploited economically against a given line pressure.

4. "Off gas" refers to those lighter hydrocarbons which can escape from a rock volume under ambient conditions given sufficient time without any heat stimulation and without grinding the rock. This term does not imply that the gas is in any one physical state <u>in situ</u>.

5. "Fracture gas" is that gas which is contained in the fracture volume. (Cannot be accurately measured at present).

6. "Adsorbed gas" also includes the gas which will eventually be released without grinding or heat treatment, but may include trapped gas which is totally enclosed by mineral grains and cement. (Research conducted at Juniata College suggests that what has been called free gas may behave entirely as an adsorbed phase. The adsorption model allows for multiple layer concentrations which would have a density similar to a liquid).

7. Low Mobility hydrocarbons include that portion totally surrounded by mineral grains (trapped gas) and other heavy hydrocarbons which are only released at a noticeable rate at temperatures of about 300°C.

B. Heavy hydrocarbons exist as liquids under standard conditions.

1. Oil and related compounds

C. Solids

1. Bitumens are solvent extractable.

2. Kerogen is a residual macromolecular residue which is insoluble.

II. Methods of Measuring Hydrocarbon Content

A. Light hydrocarbons (gas components) may be measured by:

1. Determining the volume and pressure of gases released at ambient temperature (off gas or gas in place).

2. Determining the weight loss of a sample with a thermogravimetric balance at temperatures ranging up to 100°C as was done by Battelle mostly shows the amount of adsorbed water rather than the hydrocarbon gas content.

3. Determining gas released by grinding samples in sealed containers. (trapped gas).

4. Determining gas actually produced from a well assuming a given drainage volume. (producible gas or gas in place)

B. Heavy hydrocarbons may be measured by:

1. Retorting (oil yield)

2. Solvent extraction (content of various fractions)

C. Solids may be measured by:

1. Retorting, distillation, pyrolysis (oil/gas yield--variable yields due to variable operating conditions. At temperatures near 300°C, kerogen appears to begin to break down).

2. Solvent extraction (content of various fractions)

## GAS CONTENT CALCULATIONS

1. "Off gas" values determined by Columbia's core gas analyses from Lincoln County, West Virginia core samples (Method of measurement described previously in the test):

   Range 0 to 1.8 scf/cf shale
   Mean 0.2 scf/cf shale

2. Values reported by Battelle and referred to by them as "free gas" from our Lincoln County samples (Includes the air sealed in the cans; therefore, the values are high):

   Range 1.4 to 2.9 scf/cf shale

3. Rejected recoverable gas reported by Columbia by K. L. Brooks and R. M. Forrest, 1974, based on recorded production from the Big Sandy Field of 198 MMcf assumed drainage area of 40 acres ans stimulated section thickness of 500 feet.

   Calculated gas content = .23 scf/cf shale

4. "Adsorbed gas" from Lincoln County samples

   A. Measured by Battelle by TGA weight loss described subsequently. This is determined after the "off gas" has been removed. The weight loss now known to be due to water vapor desorption.

      Range 18 to 50 scf/cf shale

   B. Juniata is progressing toward an "adsorbed gas" content calculation based on the gas released into the sample containers, but no values have been reported yet.

5. "Trapped gas" in shale cores as reported by Columbia is determined from the area under the 250°C peak on a plot of the total hydrocarbon gas released per unit time as 1-3 gram samples are heated from ambient temperature to 600°C.

6. Gas yield from retorting, distillation, or pyrolysis (Care should be exercised in comparing these results because of differences in the analytical techniques.)

   A. Based on values in the literature (Ashley and other papers), and some experiments by K. Brooks whereby shale samples were heated to 300°C or more, Columbia has referred to a value of 1 Mcf/ton or

      gas yield = 87 scf/cf shale

   (Due to the lack of detail as to the exact temperatures and other related Parameters, the exact significance of these results is questionable. It is, therefore, difficult to compare these values, and better not to refer to them.)

B. Based on Battelle's values reported for gas equivalent of the carbon content:

gas yield - from 50 to 360 scf/cf shale
(All carbon is converted to gas.)

C. Columbia's Kerogen-derived gas is measured by the area under the 450°C peak of a pyrolysis temperature plot similar to the trapped gas.

Recoverable Gas Potential

Shale sequences are generally considered to be the principal loci of hydrocarbon generation and are known to contain certain volumes of natural gas. They are typically low in permeability. Due to the low permeability, shale gas production has been restricted to highly fractured zones where a network of interconnecting fractures can provide a suitable reservoir. The goal of our shale fracturing program is to create similar open fracture systems of sufficient surface area to permit a rapid transfer of gas from the shale bodies to the well bore. The formation porosity, formation permeability, actual gas content, and the mode of occurrence of the gas are of primary importance in determining the resource potential of a shale sequence. Porosity measures the maximum volume within the formation which could be occupied by free gas. Permeability determines the rate at which gas can move through the shale (from which we may estimate a theoretical gas production rate). From a knowledge of the gas content, we can assign a limit to the production we may expect from a given area or shale volume. A knowledge of the mode of gas occurrence (gaseous, liquid or adsorbed phase) will also be necessary to determine the equations for calculating the gas content.

Measurements of these properties have been performed on samples from Well 20155-T in Belmont County, Ohio and Well 20403-T in Lincoln County, West Virginia. The analytical work on the Belmont County samples was done at Battelle Memorial Institute, Columbus, Ohio and at the Chemistry Department of Juniata College, Huntingdon, Pennsylvania. Samples from the Lincoln County well have been analyzed at Core Laboratories, Dallas, Texas; Halliburton Services, Duncan, Oklahoma; and Columbia Gas System Service Corporation, Marble Cliff, Ohio. Schlumberger and Birdwell logs also contain porosity values for these wells.

A considerable range of values has been reported for the gas reserves of the eastern Devonian Shale. The U.S.G.S. claims yields of over 1,000 cubic feet of gas may be produced by "distillation" of one ton of shale. Values as high as 30 cubic feet of natural gas per cubic foot of shale have been reported (Battelle), but other values as low as one cubic foot per ton are reported. In view of the importance of these reserve figures, it is highly desirable to determine the precision and accuracy of the data upon which we shall base our estimates. The porosity and gas content values reported for our Devonian Shale samples have shown a wide range of values which, in turn, would give rise to a large range in the calculated gas reserves. Although actual variations in the gas content of the shale are to be expected for different locations and depths, some apparent variation is related to differences in the methods used to determine gas content and porosity.

Methods:

Porosity Determination

The porosity values reported by Battelle were obtained by standard gravimetric techniques--bulk density, apparent density (from weight suspended in $CCl_4$), and true density (from pycnometer measurements). From the three types of measurements, one may calculate the open, closed, and total porosities. There appear to be two possible sources of error in the procedures used by Battelle: (1) the samples might have expanded or cracked while they were being oven-dried before the measurements were made causing an erroneously high porosity or (2) the samples might not have been totally saturated with $CCl_4$ during the apparent density measurements which would give rise to erroneously low values. However, Battelle observed no change in the appearance or physical size of the samples upon drying. Because of the small sample size and the time allowed for saturating the sample, it seems unlikely that the apparent density would be measurably low; especially since Battelle's values were the highest. The values reported by Battelle are probably the most accurate.

The porosity and permeability determinations performed by Core Lab and Halliburton are both made using equipment and procedures developed by Core Lab. The porosity of core samples is measured in a helium porosimeter. After allowing two hours for the helium to permeate all of the open pores, the gauge reading appeared to be stable. However, considering the size of the sample and the number of days which were required to remove the contained natural gas from similar samples, it would seem that this method should yield erroneously low values. The values reported by Halliburton and Core Lab are both very low, but probably represent only the most accessible pore fraction.

The porosity values reported by the well logging companies result from two separate logging tools-- a neutron log and a density log. Density logs measure the concentration of electrons in a formation and yield fairly accurate bulk density values. Provided that the grain density of a rock and the density of any contained fluids are well defined, the porosity may also be found.

Neutron logging devices respond primarily to the concentration of hydrogen atoms in a volume rock. In general, these measurements are related to the amount of pore space filled with water or heavy hydrocarbons (gaseous hydrocarbons are not sufficiently dense to be detected). A better estimate of porosity may be obtained from cross-plots of the neutron and density log values for specific rock types. These cross-plot values are usually good approximations of the actual porosity.

A comparison of the porosimeter, gravimeter, and well log porosities shows that Battelle's values are very high (14.29% and 19.42%) for the two samples analyzed. Schlumberger's log readings are lower (.6% and 5.1%) for the corresponding depths, and the values from Core Lab and Halliburton for samples from the Lincoln County well are all extremely low (all less than 1.6%).

There was no correlation between the porosimetry readings and the well log porosities for the corresponding depths. However, it is difficult to ascertain whether the core and log depths are, in fact, the same. With only two values from Battelle, it is not possible to develop a correlation but their bulk density values agree with the log values and are within the expected range. After reviewing the possibilities for error inherent in the methods, the technique used by Battelle appears to be the most sound.

Permeability Measurements

Juniata College, Battelle, and Core Lab have reported Devonian shale permeabilities. However, Juniata's research actually involves diffusion rates rather than true permeabilities. The Core Lab procedure measures the time required for a fluid of known viscosity to travel through a sample with a measured length and cross-section in response to a fixed pressure drive. On the other hand, Juniata's work suggests that the diffusion model should be more applicable to the capillary-sized passages in the shale.

Gas Content Measurements

The methods used to detect and measure gas contained in shale samples and the form in which the gas is held are of primary importance to reserve estimate calculations. Some gas may occur in interconnecting pores and will be escaping from the sample at ambient temperatures with time (free gas). Totally enclosed pore spaces may contain gas which is trapped until the pores are physically ruptured (trapped gas). Gas may also be sorbed onto mineral surfaces and/or organic matter within the shale. Any sorbed gas which occurs along the interconnected pore network may also be released with time. In addition, if the kerogen contained in rock samples is heated under proper conditions, it can break down to form gaseous and liquid hydrocarbons. Bacteria may also produce methane, ethylene, and propylene from certain organic materials.

Columbia has been concerned chiefly with measurements of the free gas content, although measurements of the trapped gas content and amount producible by kerogen breakdown are also being made. Only free and sorbed gas are presently considered as potentially available through hydraulic fracturing since shale must be pulverized or heated to remove the trapped gas or degrade the kerogen.

Battelle determined the gas content in one shale sample from Belmont County, Ohio by thermogravimetric analyses at several temperatures. The gas volume was calculated from the weight loss of the sample (measured as a function of time), and the composition of the gases released was determined by mass spectrometry. As before, some gas was lost prior to canning, plus additional gas would have been lost when the core was removed from the can and the shale was cut to the proper size for analysis. In spite of these losses, they still reported a high gas content (30 cubic feet per cubic foot of shale). Subsequent investigations indicated that these values were far too high.

Well logs can also detect the presence of pore spaces occupied by gas by comparing neutron porosity and density logs, but the data cannot be used to derive quantitative estimates of the gas content.

Trapped Gas and Kerogen

Pyrolysis techniques are being used at Columbia Gas to study the changes in the trapped gas and kerogen content of shale samples. Colin Baker (1975) reports that as samples are heated, the gas pressure in closed pores increases until the enclosing mineral grains are forced apart. The released gas is detected as a distinct peak on a continuous trace from a total hydrocarbon detector. At higher temperatures, the gas produced from the breakdown of kerogen is similarly recorded. Several of our samples were also pulverized in sealed containers to measure the trapped gas content without applying heat.

Juniata College has also conducted some pyrolysis investigations. The results indicated an endothermic process occurring from 80°C to 113°C (interpreted as due to water desorption) and an exothermic process beginning at about 300°C which has been tied to the breakdown of kerogen. The gas produced from the kerogen breakdown contained large amounts of hydrogen, hydrogen sulfide, and carbon dioxide compared to the hydrocarbon content. From .05 to .41

millimoles of gas were produced per gram of shale and the calculated calorific value of the shale was from .66 to 36.1 calories per gram.

The validity of Columbia's gas content estimates rests on the assumption that the gas contained in the rock samples behaves as free gas in spite of whether the gas is actually free or adsorbed. This assumption appears to be justified from the results of previously mentioned experiments. However, the values may be subject to change when the open porosity has been verified by gravimetric methods. It is evident that for samples with such high gas contents that it is physically impossible for the total quantity to exist as a gas; the contents cannot be calculated by ideal gas laws.

There is also strong evidence to support the existence of an adsorbed gas phase within the shale, as shown by Paul Schettler of Juniata College. The adsorption model proposed by the Juniata research team is based on the work of Brunauer, Emmett and Teller. For all practical purposes, one should consider the shale "off-gas" and adsorbed gas to be one and the same.

# APPENDIX II

## APPENDIX II: GAS CONTENTS OF SHALE SAMPLES

## WELL #20402 LINCOLN COUNTY, WEST VIRGINIA

| Point No. | Depth (Feet) | Off Gas Cu.Ft. Gas Cu.Ft. Shale | Trapped Gas Cu.Ft. Gas Cu.Ft. Shale | Kerogen Derived Gas Cu.Ft. Gas Cu.Ft. Shale |
|---|---|---|---|---|
| 1 | 2660 | .01 | | |
| 2 | 2665 | .00 | | |
| 3 | 2670 | .00 | | |
| 4 | 2675 | .00 | | |
| 5 | 2680 | .03 | | |
| 6 | 2685 | .03 | | |
| 7 | 2690 | .01 | | |
| 8 | 2695 | .03 | | |
| 9 | 2700 | .003 | .09 | 1.12 |
| 10 | 2716 | .00 | | |
| 11 | 2721 | .01 | .15 | 1.53 |
| 12 | 2726 | .00 | | |
| 13 | 2731 | .00 | | |
| 14 | 2736 | .00 | | |
| 15 | 2741 | .00 | .21 | 2.84 |
| 16 | 2746 | .02 | | |
| 17 | 2751 | .00 | | |
| 18 | 2756 | .09 | | |
| 19 | 2766 | .00 | | |
| 20 | 3005 | .11 | | |
| 21 | 3010 | .11 | | |
| 22 | 3015 | .08 | | |
| 23 | 3020 | .06 | | |
| 24 | 3030 | .15 | 1.07 | 1.25 |
| 25 | 3035 | .11 | | |
| 26 | 3040 | .13 | | |
| 27 | 3045 | .20 | | |
| 28 | 3055 | .10 | | |
| 29 | 3061 | .21 | .44 | 4.74 |
| 30 | 3066 | .45 | | |
| 31 | 3071 | .33 | | |
| 32 | 3076 | .23 | | |
| 33 | 3081 | .12 | .40 | 3.33 |
| 34 | 3086 | .11 | | |
| 35 | 3091 | .27 | .78 | 11.67 |
| 36 | 3096 | .09 | | |
| 37 | 3106 | .17 | | |
| 38 | 3111 | .05 | | |
| 39 | 3116 | .50 | | |
| 40 | 3298 | .07 | .47 | 1.23 |
| 41 | 3308 | .63 | | |
| 42 | 3313 | .80 | | |
| 43 | 3318 | .74 | | |
| 44 | 3323 | .22 | | |
| 45 | 3333 | .10 | | |
| 46 | 3338 | .23 | | |
| 47 | 3343 | .13 | | |
| 48 | 3348 | .46 | | |
| 49 | 3353 | .00 | | |

| Point No. | Depth (Feet) | Off Gas Cu.Ft. Gas Cu.Ft. Shale | Trapped Gas Cu.Ft. Gas Cu.Ft. Shale | Kerogen Derived Gas Cu.Ft. Gas Cu.Ft. Shale |
|---|---|---|---|---|
| 50 | 3358 | .26 | | |
| 51 | 3363 | .12 | | |
| 52 | 3368 | .21 | | |
| 53 | 3373 | 1.16 | | |
| 54 | 3383 | .83 | | |
| 55 | 3388 | .22 | 2.48 | 9.49 |
| 56 | 3393 | .09 | | |
| 57 | 3398 | 1.22 | | |
| 58 | 3403 | .12 | | |
| 59 | 3408 | .26 | 3.35 | 49.27 |
| 60 | 3413 | .00 | | |
| 61 | 3418 | .26 | 9.09 | 32.51 |
| 62 | 3423 | .58 | | |
| 63 | 3433 | .08 | | |
| 64 | 3438 | .00 | 12.79 | 31.03 |
| 65 | 3443 | .27 | | |
| 66 | 3449 | .80 | 8.07 | 25.40 |
| 67 | 3454 | .15 | | |
| 68 | 3459 | .67 | 4.72 | 20.00 |
| 69 | 3464 | .74 | | |
| 70 | 3469 | .82 | 7.05 | 21.65 |
| 71 | 3473 | 1.27 | | |
| 72 | 3483 | .29 | | |
| 73 | 3488 | .36 | | |
| 74 | 3493 | .35 | | |
| 75 | 3498 | .95 | 6.82 | 21.94 |
| 76 | 3503 | .16 | | |
| 77 | 3508 | .38 | 3.50 | 25.43 |
| 78 | 3513 | .08 | | |
| 79 | 3518 | .58 | | |
| 80 | 3523 | .74 | | |
| 81 | 3532 | .44 | 2.22 | 14.26 |
| 82 | 3537 | .00 | | |
| 83 | 3542 | .00 | 3.35 | 20.97 |
| 84 | 3547 | 2.03 | | |
| 85 | 3552 | .45 | | |
| 86 | 3557 | .30 | | |
| 87 | 3561 | .21 | 1.68 | 5.94 |
| 88 | 3566 | 1.18 | | |
| 89 | 3571 | .08 | | |
| 90 | 3576 | .00 | | |
| 91 | 3581 | .46 | 4.72 | 26.43 |
| 92 | 3586 | .73 | | |
| 93 | 3901 | .64 | | |
| 94 | 3906 | 2.12 | 10.40 | 21.20 |
| 95 | 3911 | 2.59 | | |
| 96 | 3917 | .00 | | |
| 97 | 3927 | .39 | | |
| 98 | 3937 | 1.91 | .00 | 4.60 |
| 99 | 3943 | 1.32 | | |
| 100 | 3948 | .57 | | |
| 101 | 3952 | .04 | | |
| 102 | 3957 | .00 | | |
| 103 | 3966 | 1.86 | | |

## WELL #20338 WISE COUNTY VIRGINIA

| Point No. | Depth (Feet) | Off Gas Cu.Ft. Gas Cu.Ft. Shale | Trapped Gas Cu.Ft. Gas Cu.Ft. Shale | Kerogen Derived Gas Cu.Ft. Gas Cu.Ft. Shale |
|---|---|---|---|---|
| 1 | 4871 | 3.64 | .470 | .820 |
| 2 | 4881 | 1.90 | .460 | .530 |
| 3 | 4890 | 2.95 | .000 | .000 |
| 4 | 4891 | 2.04 | .210 | .640 |
| 5 | 4901 | 3.22 | 1.190 | 3.260 |
| 6 | 4911 | 3.43 | 1.440 | 2.180 |
| 7 | 4921 | 2.34 | .650 | 1.010 |
| 8 | 4931 | 1.82 | .270 | .950 |
| 9 | 4941 | .17 | .470 | .560 |
| 10 | 4951 | .69 | .020 | .100 |
| 11 | 4961 | .00 | .050 | .110 |
| 12 | 4971 | .00 | .020 | .120 |
| 13 | 4981 | .15 | .070 | .060 |
| 14 | 5211 | .61 | .520 | .280 |
| 15 | 5221 | .45 | .040 | .130 |
| 16 | 5231 | .39 | .110 | .490 |
| 17 | 5241 | .61 | .280 | .390 |
| 18 | 5251 | .97 | .100 | .120 |
| 19 | 5261 | .13 | .050 | .030 |
| 20 | 5271 | 2.16 | | |
| 21 | 5281 | 1.47 | .260 | .930 |
| 22 | 5291 | .03 | .550 | 1.550 |
| 23 | 5302 | 2.93 | .180 | .090 |
| 24 | 5311 | .26 | .410 | 1.110 |
| 25 | 5321 | 1.86 | .620 | .810 |
| 26 | 5331 | .66 | .002 | .050 |
| 27 | 5341 | 2.72 | .510 | 1.170 |
| 28 | 5350 | 2.34 | .070 | .470 |
| 29 | 5361 | .02 | .080 | .120 |
| 30 | 5363 | 4.49 | | |
| 31 | 5366 | 2.76 | | |
| 32 | 5371 | 3.24 | 1.060 | .790 |
| 33 | 5380 | 1.26 | .120 | .440 |
| 34 | 5401 | 4.20 | .930 | 1.270 |
| 35 | 5411 | .70 | .230 | .600 |
| 36 | 5421 | 3.17 | .750 | 1.820 |
| 37 | 5431 | 2.20 | .060 | .050 |
| 38 | 5441 | 3.87 | | |
| 39 | 5445 | 2.93 | | |
| 40 | 5451 | 4.09 | .750 | .910 |
| 41 | 5461 | 1.78 | .530 | 2.430 |
| 42 | 5471 | 3.10 | .320 | .800 |
| 43 | 5688 | .11 | .040 | .090 |

WELL #20336 MARTIN COUNTY, KENTUCKY

| Point No. | Depth (Feet) | Off Gas Cu. Ft. Gas Cu. Ft. Shale | Trapped Gas Cu.Ft. Gas Cu.Ft. Shale | Kerogen Derived Gas Cu.Ft. Gas Cu.Ft. Shale |
|---|---|---|---|---|
| 1 | 2442 | .64 | | |
| 2 | 2452 | .06 | 4.424 | 5.547 |
| 3 | 2462 | .11 | 1.137 | .284 |
| 4 | 2472 | .00 | 2.097 | 8.059 |
| 5 | 2482 | 1.78 | 2.157 | 7.365 |
| 6 | 2490 | .00 | 3.063 | 7.775 |
| 7 | 2493 | .71 | 2.768 | 10.400 |
| 8 | 2503 | .26 | 2.299 | 8.252 |
| 9 | 2513 | .02 | .227 | .810 |
| 10 | 2523 | .00 | .114 | .213 |
| 11 | 2533 | .00 | .000 | .099 |
| 12 | 2543 | .19 | .037 | .043 |
| 13 | 2549 | .10 | .028 | .205 |
| 14 | 2553 | .00 | .023 | .085 |
| 15 | 2564 | .00 | .026 | .109 |
| 16 | 2574 | .00 | .284 | .386 |
| 17 | 2584 | .00 | .043 | .097 |
| 18 | 2587 | .32 | 1.279 | 3.538 |
| 19 | 2594 | .00 | .016 | .017 |
| 20 | 2604 | .00 | .158 | .473 |
| 21 | 2624 | .02 | .112 | .261 |
| 22 | 2644 | .00 | .061 | .033 |
| 23 | 2645 | .08 | .081 | .274 |
| 24 | 2654 | .00 | .189 | .426 |
| 25 | 2664 | .00 | .099 | .321 |
| 26 | 2674 | .00 | 3.717 | 13.515 |
| 27 | 2684 | .00 | 2.813 | 8.866 |
| 28 | 2694 | .00 | 3.740 | 10.162 |
| 29 | 2704 | .00 | 5.044 | 15.583 |
| 30 | 2716 | .00 | 3.373 | 7.490 |
| 31 | 2725 | .03 | .301 | .367 |
| 32 | 2735 | .00 | 1.989 | 3.279 |
| 33 | 2745 | .00 | .922 | 2.984 |
| 34 | 2755 | .05 | 1.515 | 4.217 |
| 35 | 2762 | .00 | .999 | 3.191 |
| 36 | 2765 | .00 | 2.262 | 8.445 |
| 37 | 2775 | .00 | 2.521 | 8.297 |
| 38 | 2785 | .00 | 3.728 | 8.763 |
| 39 | 2795 | .00 | .313 | .578 |
| 40 | 2805 | .04 | .250 | .261 |
| 41 | 2815 | .02 | .386 | .277 |
| 42 | 2820 | .06 | .199 | .125 |
| 43 | 2825 | .00 | 1.918 | 5.479 |
| 44 | 2835 | .00 | .159 | .253 |
| 45 | 2845 | .00 | 1.831 | 5.069 |
| 46 | 2855 | .68 | 3.308 | 6.786 |
| 47 | 2865 | .00 | .469 | .483 |

| Point No. | Depth (Feet) | Off Gas Cu.Ft. Gas Cu.Ft. Shale | Trapped Gas Cu.Ft. Gas Cu.Ft. Shale | Kerogen Derived Gas Cu.Ft. Gas Cu.Ft. Shale |
|---|---|---|---|---|
| 48 | 2875 | .09 | 2.606 | 5.001 |
| 49 | 2879 | .06 | 1.091 | 2.141 |
| 50 | 2885 | .00 | 2.404 | 7.070 |
| 51 | 2895 | .36 | .335 | .148 |
| 52 | 2905 | .09 | 2.373 | 5.456 |
| 53 | 2915 | .21 | 3.637 | 10.105 |
| 54 | 2925 | .00 | 4.015 | 11.707 |
| 55 | 2930 | .14 | .069 | .029 |
| 56 | 2935 | .00 | .591 | 1.157 |
| 57 | 2940 | .74 | 3.632 | 7.945 |
| 58 | 2947 | .27 | 3.779 | 11.776 |
| 59 | 2957 | .28 | 2.427 | 6.706 |
| 60 | 2967 | 2.02 | 3.666 | 11.889 |
| 61 | 2977 | .87 | 2.827 | 10.150 |
| 62 | 2987 | .05 | 3.168 | 9.968 |
| 63 | 2997 | 1.23 | 3.518 | 13.071 |
| 64 | 2998 | 1.53 | 3.714 | 17.175 |
| 65 | 3008 | .32 | .904 | 3.893 |
| 66 | 3018 | .00 | 3.151 | 11.128 |
| 67 | 3028 | .00 | .435 | .340 |
| 68 | 3034 | .00 | 1.068 | 1.571 |
| 69 | 3038 | 1.02 | 7.127 | 17.823 |
| 70 | 3048 | .00 | 5.388 | 16.174 |
| 71 | 3058 | .00 | 3.032 | 15.049 |
| 72 | 3068 | .00 | 1.938 | 14.958 |
| 73 | 3078 | .00 | 3.694 | 13.128 |
| 74 | 3088 | 2.05 | 2.751 | 14.958 |
| 75 | 3098 | 1.97 | 4.319 | 15.004 |
| 76 | 3105 | .05 | .696 | 2.657 |
| 77 | 3107 | .00 | 4.225 | 14.799 |
| 78 | 3117 | .04 | 7.331 | 22.585 |
| 79 | 3127 | .00 | .189 | .166 |
| 80 | 3137 | .00 | .308 | .767 |
| 81 | 3147 | .13 | .088 | .646 |
| 82 | 3157 | .11 | .195 | .000 |
| 83 | 3163 | .00 | .037 | .016 |
| 84 | 3168 | .07 | .412 | 1.165 |
| 85 | 3178 | .25 | .074 | .563 |
| 86 | 3188 | .00 | .021 | .115 |
| 87 | 3198 | .00 | 2.586 | 7.388 |
| 88 | 3209 | .00 | .007 | .000 |
| 89 | 3218 | .82 | .936 | 1.077 |
| 90 | 3220 | .00 | .114 | .017 |
| 91 | 3227 | .00 | .141 | .695 |
| 92 | 3237 | .04 | .027 | .833 |
| 93 | 3247 | .00 | .028 | .024 |
| 94 | 3257 | .08 | .027 | .037 |
| 95 | 3267 | .12 | .125 | .632 |
| 96 | 3277 | .00 | .092 | .000 |
| 97 | 3280 | .16 | .028 | .017 |

| Point No. | Depth (Feet) | Off Gas Cu.Ft. Gas Cu.Ft. Shale | Trapped Gas Cu.Ft. Gas Cu.Ft. Shale | Kerogen Derived Gas Cu.Ft. Gas Cu.Ft. Shale |
|---|---|---|---|---|
| 98 | 3287 | .30 | 4.910 | 13.230 |
| 99 | 3297 | .11 | .065 | .014 |
| 100 | 3307 | .04 | .081 | .134 |
| 101 | 3317 | .34 | .142 | .097 |
| 102 | 3317 | .14 | .000 | .000 |
| 103 | 3328 | .00 | .149 | .563 |
| 104 | 3338 | .06 | 4.274 | 13.003 |
| 105 | 3348 | .05 | .028 | .156 |
| 106 | 3358 | .80 | 1.770 | 15.174 |
| 107 | 3368 | .20 | 4.098 | 17.936 |
| 108 | 3378 | .64 | 5.700 | 21.369 |
| 109 | 3379 | .51 | .171 | 1.745 |
| 110 | 3388 | .75 | 3.154 | 7.873 |
| 111 | 3398 | .00 | 1.344 | 3.513 |
| 112 | 3408 | .00 | .210 | .371 |

## WELL #20403 LINCOLN COUNTY, WEST VIRGINIA

| Point No. | Depth (Feet) | Off Gas Cu.Ft. Gas Cu.Ft. Shale | Trapped Gas Cu.Ft. Gas Cu.Ft. Shale | Kerogen Derived Gas Cu.Ft. Gas Cu.Ft. Shale |
|---|---|---|---|---|
| 1 | 2735 | .00 | .074 | .551 |
| 2 | 2740 | .01 | .050 | .594 |
| 3 | 2745 | .00 | .124 | 1.729 |
| 4 | 2750 | .03 | | |
| 5 | 2755 | .01 | | |
| 6 | 2760 | .00 | | |
| 7 | 2765 | .00 | | |
| 8 | 2770 | .00 | | |
| 9 | 2775 | .03 | .034 | .446 |
| 10 | 2782 | .03 | | |
| 11 | 2787 | .04 | .077 | 1.165 |
| 12 | 2792 | .00 | .355 | .000 |
| 13 | 2797 | .00 | .105 | .906 |
| 14 | 2802 | .00 | .071 | .833 |
| 15 | 2807 | .04 | .073 | .997 |
| 16 | 2812 | .03 | | |
| 17 | 2817 | .00 | .055 | .727 |
| 18 | 2827 | .05 | .311 | 2.565 |
| 19 | 2832 | .05 | .148 | 10.593 |
| 20 | 2837 | .00 | .125 | 3.626 |
| 21 | 2842 | .05 | .109 | .698 |
| 22 | 2847 | .08 | .091 | 2.305 |
| 23 | 2852 | .02 | .054 | .438 |
| 24 | 2857 | .14 | .256 | .000 |
| 25 | 2862 | .00 | .219 | 2.475 |
| 26 | 2872 | .00 | .190 | 2.319 |
| 27 | 2877 | .00 | .119 | 1.554 |
| 28 | 2882 | .03 | | |
| 29 | 2887 | .11 | 1.097 | .199 |
| 30 | 2892 | .00 | 1.279 | .102 |
| 31 | 2897 | .07 | | |
| 32 | 2912 | .14 | .870 | .085 |
| 33 | 2917 | .29 | | |
| 34 | 2918 | .00 | | |
| 35 | 2922 | .00 | 1.284 | 8.627 |
| 36 | 2927 | .00 | | |
| 37 | 2933 | .03 | .398 | 1.489 |
| 38 | 2938 | .03 | | |
| 39 | 2943 | .00 | .651 | 2.907 |
| 40 | 2947 | .00 | | |
| 41 | 2952 | .01 | | |
| 42 | 2959 | .05 | | |
| 43 | 2964 | .05 | | |
| 44 | 2969 | .14 | | |
| 45 | 2974 | .11 | 2.694 | 10.336 |
| 46 | 2979 | .05 | | |
| 47 | 2984 | .17 | | |
| 48 | 2989 | .05 | | |

| Point No. | Depth (Feet) | Off Gas Cu.Ft. Gas Cu.Ft. Shale | Trapped Gas Cu.Ft. Gas Cu.Ft. Shale | Kerogen Derived Gas Cu.Ft. Gas Cu.Ft. Shale |
|---|---|---|---|---|
| 49 | 2994 | .06 | .546 | 8.082 |
| 50 | 2999 | .01 | | |
| 51 | 3004 | .08 | 6.695 | 29.837 |
| 52 | 3009 | .00 | | |
| 53 | 3014 | .17 | .447 | 3.876 |
| 54 | 3019 | .13 | | |
| 55 | 3024 | .11 | .995 | 7.184 |
| 56 | 3025 | .00 | | |
| 57 | 3029 | .15 | | |
| 58 | 3034 | .14 | 1.807 | 11.821 |
| 59 | 3035 | .09 | | |
| 60 | 3039 | .12 | | |
| 61 | 3044 | .08 | .648 | 2.251 |
| 62 | 3049 | .10 | | |
| 63 | 3054 | .08 | .466 | 4.643 |
| 64 | 3059 | .09 | | |
| 65 | 3064 | .09 | .989 | 6.700 |
| 66 | 3081 | .00 | | |
| 67 | 3085 | .22 | | |
| 68 | 3090 | .00 | | |
| 69 | 3095 | .16 | 3.183 | 12.651 |
| 70 | 3100 | .20 | | |
| 71 | 3106 | .48 | | |
| 72 | 3111 | .22 | | |
| 73 | 3116 | .15 | .602 | 6.161 |
| 74 | 3121 | .11 | | |
| 75 | 3126 | .22 | 1.080 | 8.127 |
| 76 | 3131 | .19 | | |
| 77 | 3135 | .21 | 2.876 | 13.128 |
| 78 | 3140 | .09 | | |
| 79 | 3145 | .06 | .887 | 5.104 |
| 80 | 3150 | .00 | | |
| 81 | 3155 | .14 | .557 | 7.275 |
| 82 | 3160 | .03 | | |
| 83 | 3165 | .06 | 2.205 | 9.434 |
| 84 | 3170 | .16 | | |
| 85 | 3175 | .11 | .932 | 5.251 |
| 86 | 3180 | .09 | | |
| 87 | 3185 | .24 | 1.364 | 9.866 |
| 88 | 3190 | .27 | | |
| 89 | 3198 | .14 | .318 | 2.216 |
| 90 | 3203 | .22 | | |
| 91 | 3208 | .04 | .284 | 1.898 |
| 92 | 3213 | .00 | | |
| 93 | 3218 | .15 | .227 | 2.228 |
| 94 | 3223 | .09 | | |
| 95 | 3228 | .10 | .369 | 1.353 |
| 96 | 3233 | .00 | | |
| 97 | 3238 | .05 | .281 | 1.824 |
| 98 | 3243 | .04 | | |
| 99 | 3248 | .16 | 1.853 | 10.139 |

| Point No. | Depth (Feet) | Off Gas Cu.Ft. Gas Cu.Ft. Shale | Trapped Gas Cu.Ft. Gas Cu.Ft. Shale | Kerogen Derived Gas Cu.Ft. Gas Cu.Ft. Shale |
|---|---|---|---|---|
| 100 | 3254 | .00 | | |
| 101 | 3263 | .12 | .216 | 1.057 |
| 102 | 3268 | .00 | | |
| 103 | 3273 | .00 | .727 | 3.651 |
| 104 | 3276 | .06 | | |
| 105 | 3280 | .29 | .261 | 2.637 |
| 106 | 3285 | .08 | | |
| 107 | 3290 | .00 | .239 | 1.654 |
| 108 | 3295 | .00 | | |
| 109 | 3300 | .10 | .344 | 1.284 |
| 110 | 3305 | .04 | | |
| 111 | 3310 | .07 | .256 | 1.165 |
| 112 | 3316 | .15 | | |
| 113 | 3321 | .00 | 1.444 | 16.368 |
| 114 | 3336 | .14 | | |
| 115 | 3341 | .19 | 3.762 | 11.673 |
| 116 | 3346 | .29 | | |
| 117 | 3351 | .12 | .943 | 2.194 |
| 118 | 3356 | .11 | | |
| 119 | 3361 | .00 | .494 | 1.540 |
| 120 | 3366 | .41 | | |
| 121 | 3371 | .20 | | |
| 122 | 3376 | .32 | | |
| 123 | 3381 | .18 | .318 | 1.239 |
| 124 | 3386 | .10 | | |
| 125 | 3391 | .13 | .222 | .779 |
| 126 | 3396 | .11 | | |
| 127 | 3401 | .00 | .318 | .585 |
| 128 | 3406 | .12 | | |
| 129 | 3411 | .14 | 5.297 | 14.992 |
| 130 | 3416 | .11 | | |
| 131 | 3421 | .15 | 5.592 | 13.356 |
| 132 | 3432 | .34 | 7.922 | 21.835 |
| 133 | 3437 | .66 | | |
| 134 | 3442 | .53 | .421 | 3.171 |
| 135 | 3447 | .78 | | |
| 136 | 3452 | .37 | 6.706 | 14.231 |
| 137 | 3457 | .49 | | |
| 138 | 3462 | .33 | 2.501 | 8.411 |
| 139 | 3467 | .21 | | |
| 140 | 3472 | .14 | .864 | 2.035 |
| 141 | 3477 | .45 | | |
| 142 | 3482 | .31 | 1.193 | 7.559 |
| 143 | 3487 | 1.03 | | |
| 144 | 3492 | .22 | 1.444 | 13.981 |
| 145 | 3498 | .08 | | |
| 146 | 3503 | .20 | | |
| 147 | 3508 | .38 | | |
| 148 | 3513 | .25 | 7.024 | 14.310 |
| 149 | 3518 | .20 | | |
| 150 | 3523 | .89 | 3.626 | 17.720 |
| 151 | 3528 | .18 | | |
| 152 | 3533 | .31 | 8.059 | 19.425 |

| Point No. | Depth (Feet) | Off Gas Cu.Ft. Gas Cu.Ft. Shale | Trapped Gas Cu.Ft. Gas Cu.Ft. Shale | Kerogen Derived Gas Cu.Ft. Gas Cu.Ft. Shale |
|---|---|---|---|---|
| 153 | 3538 | .65 | | |
| 154 | 3543 | .04 | | |
| 155 | 3548 | .17 | | |
| 156 | 3553 | .26 | 5.820 | 13.787 |
| 157 | 3558 | 1.16 | | |
| 158 | 3563 | .37 | 7.286 | 19.630 |
| 159 | 3568 | .62 | | |
| 160 | 3573 | .25 | 7.024 | 21.494 |
| 161 | 3578 | .35 | | |
| 162 | 3583 | .32 | | |
| 163 | 3588 | .250 | | |
| 164 | 3598 | .81 | | |
| 165 | 3606 | .21 | 2.467 | 12.980 |
| 166 | 3611 | .19 | | |
| 167 | 3616 | .36 | 3.865 | 18.016 |
| 168 | 3621 | .23 | | |
| 169 | 3626 | .12 | 3.433 | 12.333 |
| 170 | 3631 | .19 | | |
| 171 | 3636 | .27 | 10.159 | 26.597 |
| 172 | 3641 | .50 | .008 | .023 |
| 173 | 3646 | .24 | | |
| 174 | 3651 | .12 | | |
| 175 | 3656 | .10 | | |
| 176 | 3661 | .62 | | |
| 177 | 3666 | .00 | | |
| 178 | 3671 | .00 | | |
| 179 | 3676 | .06 | | |
| 180 | 3681 | .07 | | |
| 181 | 3686 | .14 | | |
| 182 | 3691 | .02 | | |
| 183 | 3696 | .26 | | |
| 184 | 3701 | .21 | | |
| 185 | 3706 | .34 | | |
| 186 | 3711 | .00 | | |
| 187 | 3716 | .01 | | |
| 188 | 3721 | .03 | .047 | .438 |
| 189 | 3726 | .004 | | |
| 190 | 3732 | .00 | | |
| 191 | 3737 | .18 | | |
| 192 | 3743 | .04 | | |
| 193 | 3748 | .40 | | |
| 194 | 3753 | .03 | | |
| 195 | 3759 | 1.42 | | |
| 196 | 3764 | .06 | | |
| 197 | 3768 | 1.32 | | |
| 198 | 3773 | 1.02 | | |
| 199 | 3777 | .19 | | |
| 200 | 3782 | 1.23 | | |
| 201 | 3787 | .05 | .182 | .375 |
| 202 | 3792 | .09 | | |
| 203 | 3797 | .01 | .003 | .128 |

| Point No. | Depth (Feet) | Off Gas Cu.Ft. Gas Cu.Ft. Shale | Trapped Gas Cu.Ft. Gas Cu.Ft. Shale | Kerogen Derived Gas Cu.Ft.Gas Cu.Ft. Shale |
|---|---|---|---|---|
| 204 | 3802 | .00 | | |
| 205 | 3807 | .60 | .119 | .905 |
| 206 | 3812 | .02 | | |
| 207 | 3818 | .02 | .026 | .055 |
| 208 | 3823 | .11 | | |
| 209 | 3829 | .00 | .025 | .388 |
| 210 | 3834 | .01 | | |
| 211 | 3839 | .00 | .202 | .000 |
| 212 | 3844 | .48 | | |
| 213 | 3849 | .08 | .010 | .065 |
| 214 | 3854 | .08 | | |
| 215 | 3859 | 1.69 | 1.080 | 2.961 |
| 216 | 3864 | .07 | | |
| 217 | 3869 | .08 | .051 | .079 |
| 218 | 3874 | .06 | | |
| 219 | 3879 | .53 | | |
| 220 | 3884 | .07 | | |
| 221 | 3888 | .06 | .094 | 1.502 |
| 222 | 3893 | .40 | | |
| 223 | 3898 | .15 | .187 | .764 |
| 224 | 3903 | 1.47 | | |
| 225 | 3908 | .19 | 1.176 | 1.489 |
| 226 | 3913 | .67 | | |
| 227 | 3918 | .17 | 2.569 | 1.563 |
| 228 | 3923 | .65 | | |
| 229 | 3928 | .46 | 2.103 | 4.205 |
| 230 | 3934 | .33 | | |
| 231 | 3939 | .16 | .824 | .960 |
| 232 | 3944 | .24 | | |
| 233 | 3950 | .28 | 1.040 | 2.756 |
| 234 | 3955 | .80 | | |
| 235 | 3959 | .78 | 4.137 | 8.525 |
| 236 | 3964 | 1.02 | | |
| 237 | 3969 | .81 | 3.546 | 6.081 |
| 238 | 3974 | 2.21 | | |
| 239 | 3979 | 1.35 | 8.400 | 10.650 |
| 240 | 3984 | 1.13 | | |
| 241 | 3998 | .57 | 6.615 | 6.956 |
| 242 | 4003 | .00 | | |
| 243 | 4010 | 1.35 | 4.091 | 7.002 |
| 244 | 4015 | .55 | | |
| 245 | 4020 | .96 | 2.296 | 4.467 |
| 246 | 4025 | .03 | | |
| 247 | 4025 | .25 | | |
| 248 | 4030 | 2.16 | 1.767 | 4.242 |
| 249 | 4030 | 2.09 | | |
| 250 | 4035 | 1.23 | | |
| 251 | 4035 | 1.22 | | |
| 252 | 4040 | 1.05 | .821 | 2.495 |
| 253 | 4049 | 2.28 | | |
| 254 | 4051 | .59 | | |

# APPENDIX III

# APPENDIX III: CORE DESCRIPTIONS

Well No. 20403

Core #1 (2720' - 2779'6")

| From | To | Lithologic Description |
|---|---|---|
| 2720' | 2779'6" | Medium gray-green laminated silty shale. |

| From | To | Fracture |
|---|---|---|
| 2722'6" | 2722'7" | Vertical |
| 2723'11" | 2724'2" | Vertical |
| 2728'7¼" | 2728'9 3/4" | Vertical |
| 2735'0" | 2735'3" | Vertical |
| 2742'4" | 2742'10" | Vertical |
| 2744'2" | 2744'4" | Vertical |
| 2748'1½" | 2748'5" | Vertical |
| 2751'1½" | 2751'3½" | Vertical |
| 2751'7½" | 2751'9½" | Vertical |
| 2764'6" | 2764'8½" | Vertical |
| 2778'½" | 2778'2½" | Vertical |

Distinct Black Kerogen Layers

2769'

Comments: Mud logger reported no indication of gas.

Core #2 (2779'6" - 2838')

| From | To | Lithologic Description |
|---|---|---|
| 2779'6" | 2795'6" | Medium dark gray laminated silty shale |
| 2795'6" | 2796'6" | Dark gray shale |
| 2796'6" | 2804'6" | Laminated medium gray silty shale |
| 2804'6" | 2805'6" | Medium green-gray shale |
| 2805'6" | 2809'6" | Medium dark gray silty shale |
| 2809'6" | 2821'6" | Medium to dark gray laminated silty shale |
| 2821'6" | 2823'6" | Medium gray shale |
| 2823'6" | 2831'6" | Medium and dark gray laminated silty shale |
| 2831'6" | 2832'6" | Medium gray shale |
| 2832'6" | 2838' | Medium dark gray silty shale |

| From | To | Fractures |
|---|---|---|
| 2783'11" | 2784'1" | Vertical |
| 2792'9" | 2793'7" | Vertical |
| 2794'7" | 2795'3" | Vertical, partially open |
| 2828'6" | 2829'6" | Vertical, partially open |
| 2829'9" | 2831'2" | Vertical |

Comments: Mud logger reported no indications of gas.

Core #3 (2838' - 2896'4")

| From | To | Lithologic Description |
|---|---|---|
| 2838' | 2853' | Medium to dark gray laminated silty shale but less silty than cores 1 and 2 |
| 2853' | 2855' | Dark gray shale |
| 2855' | 2866' | Medium dark gray laminated silty shale |
| 2866' | 2867' | Dark gray shale |
| 2867' | 2874' | Dark gray laminated silty shale |
| 2874' | 2876'3" | Dark gray shale with two silty layers ¼" thick |
| 2876'3" | 2881'8" | Dark gray laminated silty shale |
| 2881'8" | 2894' | Dark gray shale with light and dark beds grading downward into very dark gray shale |
| 2894' | 2896'4" | Very dark gray shale |

| From | To | Fractures |
|---|---|---|
| 2892'9" | 2894'11" | Vertical, open, with gas bleeding along fracture surface |

Comments: Mud logger reported no indications of gas. Core crumbled in places.

Core #4 (2896'4" - 2955'6")

| From | To | Lithologic Description |
|---|---|---|
| 2896'4" | 2904'4" | Very dark gray shale with several silty laminae |
| 2904'4" | 2908'4" | Dark gray shale with abundant dispersed silty layers |
| 2908'4" | 2910'4" | Very dark gray shale |
| 2910'4" | 2920'11" | Dark gray shale with dispersed lighter silty layers ¼" to 1" |
| 2920'11" | 2926'4" | Very dark gray shale with one 2" silty layer |
| 2926'4" | 2931'4" | Dark gray shale with dispersed silty layers |
| 2931'4" | 2932'4" | Very dark gray shale |
| 2932'4" | 2937'4" | Dark gray shale with dispersed silty layers |
| 2937'4" | 2938'4" | Very dark gray shale |
| 2938'4" | 2945'7½" | Dark gray shale with dispersed silty layers |
| 2945'7½" | 2948'4" | Very dark gray shale |
| 2948'4" | 2955'6" | Alternating bands of medium gray and very dark gray shale with occasional silty layers |

Comments: No indications of gas reported by mud logger. Core crumbled in places.

Core #5 (2955'6" - 3014')

| From | To | Lithologic Description |
|---|---|---|
| 2955'6" | 2962'6" | Very dark gray shale |
| 2962'6" | 2964'6" | Medium dark gray shale with dispersed silt and carbonate stringers |
| 2964'6" | 2975'6" | Very dark gray shale with four silty layers |
| 2975'6" | 2981'6" | Light to medium gray shale with several 1" silt-carbonate layers |
| 2981'6" | 2987'6" | Very dark gray shale |
| 2987'6" | 2999'6" | Very dark gray shale with dispersed ¼" silt-carbonate stringers |
| 2999'6" | 3014' | Very dark gray shale |

| From | To | Fractures |
|---|---|---|
| 2955'6" | 2959'10" | Vertical and open |
| 2968'8" | 2972'9½" | Vertical and open |
| 3009'8" | 3013'6" | Vertical and open |

Distinct Black Kerogen Layers

2981'
2995'
2996'9"
3000'
3005'

Comments: Mud logger reported no indication of gas. Very dark gray shale is brown when reduced to powder.

Core #6 (3014'-3073')

| From | To | Lithologic Description |
|---|---|---|
| 3014' | 3017' | Dark gray shale |
| 3017' | 3029'6" | Medium gray shale with siltier layers up to 2", pyrite layer along bedding plane at 3018' |
| 3029'6" | 3039' | Medium to dark gray shale |
| 3039' | 3053' | Medium to dark gray silty snale |
| 3053' | 3073' | Medium to dark gray shale with occasional silty shale horizons |

| From | To | Fractures |
|---|---|---|
| 3039'6" | 3046'6" | Vertical, mineralized |
| 3049'3" | 3053'6" | Vertical |
| 3049'3" | 3063'6" | Vertical, mineralized |
| 3053'6" | 3033'6 | Vertical |
| 3065'3½" | 3073' | Vertical |

Distinct Black Kerogen Layers

3030'

Comments: Mud logger detected "trip gas" after coring this interval.

Core #7 (3073'-3132'6")

| From | To | Lithologic Description |
| --- | --- | --- |
| 3073' | 3132'6" | Medium to dark gray shale with occasional darker bands - only rare and thin silty layers. |

| From | To | Fractures |
| --- | --- | --- |
| 3073' | 3084' | Vertical, mineralized |
| 3079' | 3119'1" | Vertical |
| 3119'1" | 3126'6" | Vertical |
| 3126'6" | 3130'6" | Vertical |

Core #8 (3132'6"-3192')

| From | To | Lithologic Description |
|---|---|---|
| 3132'6" | 3140'4" | Medium gray shale with 1" dark gray bands |
| 3140'4" | 3140'5-1/2" | Light gray, very silty shale to siltstone |
| 3140'5-1/2" | 3144'7" | Dark gray shale |
| 3144'7" | 3144'8-1/2" | Light gray very silty shale to siltstone |
| 3144'8-1/2" | 3150'1-1/2" | Dark to medium gray shale |
| 3150'1-1/2" | 3150'4" | Light gray, very silty shale to siltstone |
| 3150'4" | 3155'8" | Dark and medium dark gray shale |
| 3155'8" | 3155'11" | Light gray, very silty shale to siltstone |
| 3155'11" | 3165'1" | Dark to medium dark gray shale with numerous light gray siltstone laminae. |
| 3165'1" | 3165'5" | Light gray crossbedded argillaceous siltstone with dark gray shale bands |
| 3165'5" | 3183'5" | Dark to medium gray shale with numerous light gray siltstone bands up to 1" thick |
| 3183'5" | 3183'6" | Very light gray siltstone |
| 3183'6" | 3192' | Very dark gray to black shale (brown when reduced to powder) |

| From | To | Fractures |
|---|---|---|
| 3140' | 3140'6" | Vertical and open |
| 3141' | 3142' | Vertical and open |
| 3146' | 3146'10" | Vertical and open |
| 3148' | 3150' | Vertical and open |
| 3151'8" | 3152'7" | Vertical and open |
| 3154' | 3156'7" | Vertical and open |
| 3160'8" | 3161'4" | Vertical and open |
| 3164'6" | 3165' | Vertical and open |
| 3167'8" | 3169' | Vertical and open |
| 3169'8" | 3170'8" | Vertical and open |
| 3171' | 3172' | Vertical and open |
| 3173'3" | 3174' | Vertical and open |
| 3184' | 3186'4" | Vertical and open |
| 3186'6" | 3188'10" | Vertical and open |
| 3189' | 3192' | Vertical and open |

Core #9 (3192'-3251'1")

| From | To | Lithologic Description |
|---|---|---|
| 3192' | 3197'9" | Dark gray to black shale with a few medium gray 1" thick layers |
| 3197'9" | 3200'2" | Medium gray shale with several 1" dark and very dark gray layers |
| 3200'2" | 3200'4-1/2" | Light gray argillaceous siltstone |
| 3200'4-1/2" | 3220 | Medium and dark gray laminated shale with dark gray shale in 1/4" bands, three silt layers to 2" thick |
| 3220' | 3221'9" | Very dark gray to black shale |
| 3221'9" | 3227' | Medium gray and very dark gray banded shale |
| 3227' | 3230'3" | Medium gray shale with numerous very dark gray bands to 2" thick |
| 3230'3" | 3230'5-1/2" | Light gray argillaceous siltstone |
| 3230'5-1/2" | 3230'10'1/2" | Very dark gray to black shale |
| 3230'10-1/2" | 3246' | Medium and dark gray banded shale |
| 3246' | 3246'9" | Light gray argillaceous siltstone |
| 3246'9" | 3251'1" | Medium to very dark gray banded shale, very dark gray bands to 4" thick |

| From | To | Fractures |
|---|---|---|
| 3192'2" | 3193'3" | Vertical and open |
| 3193'10" | 3194'6" | Vertical and open |
| 3194'6" | 3197' | Vertical and open |
| 3197'2" | 3198'8" | Vertical and open |
| 3200'7" | 3202'6" | Vertical and open |
| 3202'7" | 3203'4" | Vertical and open |
| 3208'4" | 3209'9" | Vertical and open |
| 3210'7" | 3211'4" | Vertical and open |
| 3212' | 3213' | Vertical and open |
| 3213' | 3213'7" | Vertical and open |
| 3215'10" | 3216'10" | Vertical and open |
| 3217'3" | 3218'3" | Vertical and open |
| 3218'4" | 3219'3" | Vertical and open |
| 3222'3" | 3222'9" | Vertical and open |
| 3225'6" | 3227'2" | Vertical and open |
| 3228'8" | 3230'3" | Vertical and open |
| 3230'7" | 3239'1" | Vertical and open |
| 3239'3" | 3240'6" | Vertical and open |
| 3241'3" | 3244'8" | Vertical and open |
| 3244'8" | 3246' | Vertical and open |
| 3248' | 3251'1" | Vertical and open |

Core #10 (3251'1"-3310'6")

| From | To | Lithologic Description |
|---|---|---|
| 3251'1" | 3260'6" | Medium to dark gray shale with very dark gray to black bands up to 1-1/2" thick |
| 3260'6" | 3260'11" | Light gray argillaceous siltstone |
| 3260'11" | 3261'8" | Laminated medium gray shale and argillaceous siltstone |
| 3261'8" | 3310'3" | Very dark gray to black shale |
| 3310'3" | 3310'6" | Light gray siltstone |

| From | To | Fractures |
|---|---|---|
| 3255' | 3258'10" | Vertical and open |
| 3259'4" | 3260'6" | Vertical and open |
| 3261' | 3261'6" | Vertical and open |
| 3262' | 3262'10" | Vertical and open |
| 3264'10" | 3271'4" | Vertical and open |
| 3271'7" | 3274'6" | Vertical and open |
| 3275'2" | 3280'9" | Vertical and open |
| 3280'11" | 3283'6" | Vertical and open |
| 3283'6" | 3289'4" | Vertical and open |
| 3289'7" | 3291'6" | Vertical and open |
| 3291'10" | 3293'9" | Vertical and open |
| 3293'9" | 3297' | Vertical and open |
| 3297'4" | 3300'4" | Vertical and open |
| 3300'4" | 3301'8" | Vertical and open |
| 3301'10" | 3307'7" | Vertical and open |
| 3309'3" | 3310'5" | Vertical and open |

Core #11 (3310'6" - 3368'6")

| From | To | Lithologic Description |
|---|---|---|
| 3310'6" | 3314'2" | Medium gray shale with dark gray bands to 2" thick, severely broken |
| 3314'2" | 3323'10" | Dark and very dark gray shale with four 5" black bands |
| 3323'10" | 3336'4" | Medium gray shale with dark gray bands |
| 3336'4" | 3344'5" | Very dark gray to black shale (with brown streak) and medium gray bands |
| 3344'5" | 3344'7" | Light gray silty shale |
| 3344'7" | 3346'5" | Very dark gray to black shale (with brown streak) |
| 3346'5" | 3352'6" | Medium gray shale with very dark gray to black shale bands up to 8" thick |
| 3352'6" | 3363'6" | Medium gray shale with very dark and black bands to 1" thick, and silty layers to 1" in thickness |
| 3363'6" | 3366' | Dark gray shale with bands of medium and very dark gray shale, several light gray silty layers to 1" thick |
| 3366' | 3368'6" | Very dark gray to black shale |

| From | To | Fractures |
|---|---|---|
| 3347'8" | 3348'10" | Vertical and open |
| 3357'2" | 3358'3" | Vertical and open |
| 3310'6" | 3314'2" | Vertical and open |
| 3314'2" | 3315'1" | Vertical and open |
| 3314'1" | 3317'8" | Vertical and open |
| 3317'8" | 3319'6" | Vertical and open |
| 3319'6" | 3321'5" | Vertical and open |
| 3321'6" | 3323'11" | Vertical and open |
| 3325'5" | 3326'6" | Vertical and open |
| 3326'6" | 3331' | Vertical and open |
| 3337'6" | 3338'9" | Vertical and open |
| 3338'9" | 3339'10" | Vertical and open |
| 3340'4" | 3342'4" | Vertical and open |
| 3355'8" | 3356'9" | Vertical and open |
| 3358'2" | 3359'4" | Vertical and open |

Core #12 (3368'6" - 3428')

| From | To | Lithologic Description |
|---|---|---|
| 3368'6" | 3377'8" | Black shale (brown streak) |
| 3377'8" | 3377'9" | Light gray silty shale |
| 3377'9" | 3378'6" | Black shale |
| 3378'6" | 3381'6" | Medium gray shale with black bands, several with silty layers |
| 3381'6" | 3382'1" | Black shale |
| 3382'1" | 3391'4" | Medium gray shale with black bands several silty layers |
| 3391'4" | 3391'7" | Medium gray siltstones |
| 3391'7" | 3409'10" | Medium gray shale with black bands to 2" thick, and several light gray siltstones to 1" |
| 3409'10" | 3424'1" | Black shale with calcite veinlets |
| 3424'1" | 3428' | Very dark gray and black banded shale |

| From | To | Fractures |
|---|---|---|
| 3368'6" | 3370'10" | Vertical and open |
| 3370'11" | 3372'1" | Vertical and open |
| 3371'11" | 3373'9" | Vertical and open |
| 3374'11" | 3376'8" | Vertical and open |
| 3379'5" | 3381'4" | Vertical and open |
| 3388' | 3395'5" | Vertical and open |
| 3398'2" | 3399'3" | Vertical and open |
| 3411'2" | 3412'6" | Vertical and open |
| 3412'6" | 3415'4" | Vertical and open |
| 3416'4" | 3419' | Vertical and open |
| 3419' | 3424' | Vertical and open |
| 3424'3" | 3425'3" | Vertical and open |

Distinct Black Kerogen Layer

3422'5-1/2"

Core #13 (3428' - 3487')

| From | To | Lithologic Description |
|---|---|---|
| 3428' | 3448'9" | Black shale |
| 3448'9" | 3449'6" | Medium gray shale |
| 3449'6" | 3449'9" | Black shale |
| 3449'9" | 3450'9 1/2" | Medium gray shale |
| 3450'9 1/2" | 3451'5" | Black shale |
| 3451'5" | 3451'9" | Medium gray shale |
| 3451'9" | 3460'5" | Black shale |
| 3460'5" | 3462'5" | Medium gray shale with two 2" black bands |
| 3462'5" | 3468'5" | Medium gray shale with six black bands to 4", six silty layers to 2" and pyrite blebs and layers |
| 3468'5" | 3471'5" | Black shale |
| 3471'5" | 3474'5" | Medium gray and black shale bands |
| 3474'5" | 3479'1" | Black shale |
| 3479'1" | 3479'2" | Medium gray shale |
| 3479'2" | 3479'3" | Silty zone |
| 3479'3" | 3481' | Black shale |
| 3481' | 3483'8" | Dark gray and black shale |
| 3483'8" | 3484'10" | Medium gray shale |
| 3484'10" | 3485'1" | Blue gray siltstone |
| 3485'1" | 3485'4" | Medium gray shale |
| 3485'4" | 3486'3" | Dark gray shale |
| 3486'3" | 3487' | Black shale |

| From | To | Fractures |
|---|---|---|
| 3428'9" | 3431' | Vertical and open |
| 3430'9" | 3435'5" | Vertical and open |
| 3435'5" | 3436'8" | Vertical and open |
| 3437'4" | 3438'6" | Vertical and open |
| 3438'4" | 3441'8" | Vertical and open |
| 3441'8" | 3444'3" | Vertical and open |
| 3444'1" | 3449' | Vertical and open |
| 3452'2" | 3460'6" | Vertical and open |
| 3469'4" | 3472'2" | Vertical and open |
| 3461'8" | 3467' | Vertical and open |
| 3467'5" | 3469' | Vertical and open |

Distinct Black Kerogen Layers

3428'9
3460'1"
3471'
3478'

Core #14 (3487' - 3546'6")

| From | To | Lithologic Description |
|---|---|---|
| 3487' | 3487'9" | Medium gray shale with 1" silty layer |
| 3487'9" | 3493'5" | Black shale |
| 3493'5" | 3495'8" | Medium green-gray shale with two 1" black bands |
| 3495'8" | 3496'3" | Numerous pyrite blebs in black shale, one 1/4" pyrite stringer |
| 3496'3" | 3502' | Medium green gray shale, pyrite blebs, and one 1/2" and one 1-1/2" silty layer |
| 3502' | 3502'8" | Black shale |
| 3502'8" | 3503'11" | Medium green-gray shale with a 1" black shale band |
| 3503'11" | 3504'2" | Medium gray argillaceous siltstone |
| 3504'2" | 3504'10" | Medium gray silty shale |
| 3504'10" | 3505'10" | Black shale |
| 3505'10" | 3506'4" | Contorted black shale and siltstone |
| 3506'4" | 3508'5" | Hard, medium to light gray-green siltstone |
| 3508'5" | 3509'4" | Medium and black banded shale |
| 3509'4" | 3510'2" | Black shale |
| 3510'2" | 3510'6" | Medium gray and black shale (contorted bedding) |
| 3510'6" | 3510'10" | Black shale |
| 3510'10" | 3511' | Medium gray and black contorted shale |
| 3511' | 3518'1" | Black shale with a 1" pyrite band |
| 3518'1" | 3520'2" | Gray-green shale with two 3" black bands |
| 3520'2" | 3520'9" | Black shale |
| 3520'9" | 3521'9" | Green-gray shale with light gray silty layers |
| 3521'9" | 3523'3" | Black shale with 5 dark gray-green bands to 1" thick |
| 3523'3" | 3524'11" | Black shale |
| 3524'11" | 3525'3" | Medium gray-green shale |
| 3525'3" | 3529'3" | Black shale |
| 3529'3" | 3529'5" | Gray-green shale |
| 3529'5" | 3532'1" | Black shale |
| 3532'1" | 3532'4" | Gray-green shale |
| 3532'4" | 3533'9" | Black shale |
| 3533'9" | 3534'11" | Laminated gray-green and black shale |
| 3534'11" | 3541' | Black shale |
| 3541' | 3541'2" | Gray-green shale |
| 3541'2" | 3542'2" | Black shale |
| 3542'2" | 3544'8" | Medium gray green shale with 3 black layers 1/8" to 1" thick |
| 3544'8" | 3545'1" | Black shale with pyrite bands and blebs |
| 3545'1" | 3546'6" | Medium gray-green shale with one 2" black band |

Core #14 (Cont'd)

| From | To | Fractures |
|---|---|---|
| 3489' | 3492'1" | Vertical and open |
| 3492'1" | 3494' | Vertical and open |
| 3494'10" | 3501'6" | Vertical and open |
| 3502'2" | 3503'5" | Vertical and open |
| 3508'6" | 3519'1" | Vertical and open |
| 3521'9" | 3527'4" | Vertical and open |
| 3527'1" | 3531'6" | Vertical and open |
| 3531'6" | 3538'6" | Vertical and open |
| 3538'6" | 3541'7" | Vertical and open |
| 3544'1" | 3546'5" | Vertical and open |

Several Distinct Black Kerogen Layers

Complete distinct layers and partial layers were observed at several depths.

Core #15 (3546'6" - 3606')

| From | To | Lithologic Description |
|---|---|---|
| 3546'6" | 3553' | Medium to dark gray shale with parallel black layers (1/4" to 3") |
| 3553' | 3564'5" | Black shale with three 1" medium gray bands |
| 3564'5" | 3569'5" | Medium gray shale with four black bands (1/4" to 3") |
| 3569'5" | 3570'6" | Black shale |
| 3570'6" | 3570'9" | Medium gray shale |
| 3570'9" | 3570'11" | Medium gray siltstone |
| 3570'11" | 3571'5" | Black shale with pyrite |
| 3571'5" | 3571'8" | Medium gray shale |
| 3571'8" | 3580'10" | Black shale |
| 3580'10" | 3582'10" | Medium dark gray and black shale band 4-7" thick |
| 3582'10" | 3590'9" | Black shale |
| 3590'9" | 3593'4" | Black shale with five medium dark gray bands 3-5" thick |
| 3593'4" | 3595'6" | Black shale |
| 3595'6" | 3595'10" | Medium gray shale |
| 3595'10" | 3596'3" | Black shale |
| 3596'3" | 3596'11" | Medium gray shale |
| 3596'11" | 3598'8" | Black shale |
| 3598'8" | 3598'10" | Contorted medium gray shale |
| 3598'10" | 3599'4" | Black shale |
| 3599'4" | 3599'6" | Medium gray shale |
| 3599'6" | 3606' | Black shale |

| From | To | Fractures |
|---|---|---|
| 3548' | 3551'8" | Vertical and open |
| 3555'5" | 3557'6" | Vertical and open |
| 3557'8" | 3562'7" | Vertical and open |
| 3572' | 3580' | Vertical and open |
| 3582'1" | 3585'3" | Vertical and open |
| 3585'2" | 3588' | Vertical and open |
| 3589' | 3589'4" | Vertical and open |
| 3589'4" | 3591'10" | Vertical and open |
| 3596'8" | 3598' | Vertical and open |

Core #16 (3606'-3665')

| From | To | Lithologic Description |
|---|---|---|
| 3606' | 3612'3" | Black shale with contorted dark gray laminae |
| 3612'3" | 3613' | Medium dark gray shale |
| 3613' | 3613'5" | Black shale |
| 3613'5" | 3614'2" | Medium gray shale |
| 3614'2" | 3619'7" | Black shale |
| 3619'7" | 3620'3" | Medium gray shale |
| 3620'3" | 3620'6" | Black shale |
| 3620'6" | 3620'9" | Medium gray shale with silty layers |
| 3620'9" | 3621'3" | Black shale |
| 3621'3" | 3621'9" | Medium gray shale with black laminae |
| 3621'9" | 3623'5" | Black shale |
| 3623'5" | 3623'8" | Dark gray shale |
| 3623'8" | 3624' | Black shale |
| 3624' | 3624'9" | Medium gray shale |
| 3624'9" | 3625'5" | Black shale |
| 3625'5" | 3625'9" | Medium gray shale with black laminae |
| 3625'9" | 3628'3" | Black shale |
| 3628'3" | 3628'9" | Medium dark shale with black laminae |
| 3628'9" | 3629'4" | Black shale |
| 3629'4" | 3630' | Laminated dark gray and black shale |
| 3630' | 3632'5" | Black shale |
| 3632'5" | 3632'10" | Very dark shale with a 1/4" siltstone layer at base |
| 3632'10" | 3633'4" | Black shale |
| 3633'4" | 3633'9" | Very dark shale |
| 3633'9" | 3644'1" | Black shale with several very dark layers |
| 3644'1" | 3644'6-1/2" | Very dark gray shale |
| 3644'6-1/2" | 3644'8" | Medium gray argillaceous siltstone |
| 3644'8" | 3647'3" | Black shale |
| 3647'3" | 3648' | Black and very dark gray shale, one large pyrite bleb |
| 3648' | 3650'4" | Black shale |
| 3650'4" | 3650'11" | Black and dark gray shale |
| 3650'11" | 3651'2" | Black shale |
| 3651'2" | 3651'4" | Very dark gray shale |
| 3651'4" | 3651'7" | Black shale |
| 3651'7" | 3651'10" | Very dark gray shale |
| 3651'10" | 3652' | Black shale |
| 3652' | 3652'7" | Dark gray shale |
| 3652'7" | 3653'7" | Black shale |
| 3653'7" | 3653'9" | Very dark gray shale |
| 3653'9" | 3654' | Black shale |
| 3654' | 3654'4" | Very dark gray shale |
| 3654'4" | 3654'10" | Black shale |
| 3654'10" | 3655' | Very dark gray shale |
| 3655' | 3659'11" | Black shale |
| 3659'11" | 3661'7" | Medium gray shale with black laminae |
| 3661'7" | 3661'10" | Black shale |
| 3661'10" | 3662'2" | Medium dark gray shale |

Core #16 (Cont'd)

| From | To | Lithologic Description |
|---|---|---|
| 3662'2" | 3663'3" | Black shale with a 1/8" pyrite layer |
| 3663'3" | 3663'8" | Dark gray shale with black laminae |
| 3663'8" | 3663'11" | Black shale with 1/8" pyrite stringer at base |
| 3663'11" | 3664'9" | Medium gray shale |
| 3664'9" | 3665' | Black shale |

| From | To | Fractures |
|---|---|---|
| 3606' | 3606'5" | Vertical, open |
| 3608'2" | 3609'11" | Vertical, open |
| 3611' | 3612'3" | Vertical, open |
| 3615'3" | 3620'7" | Vertical, open |
| 3621'9" | 3622'11" | Vertical, open |
| 3630'2" | 3631'7" | Vertical, open |
| 3631'7" | 3632'9" | Vertical, open |
| 3632'9" | 3635'2" | Vertical, open |
| 3635'10" | 3637'10" | Vertical, open |
| 3638'3" | 3639'10" | Vertical, open |
| 3644'2" | 3646'7" | Vertical, open |
| 3648' | 3650'8" | Vertical, open |
| 3652'8" | 3656'3" | Vertical, open |
| 3656'3" | 3659'3" | Vertical, open |

Distinct Black Kerogen Layers:

3617'4"
3621'
3636'
3643'7"
3657'8"

Comment: Mud logger reported increase in gas show during Core #16.

Core #17 (3665'-3724'6")

| From | To | Lithologic Description |
|---|---|---|
| 3664' | 3665' | Black shale |
| 3665' | 3677'2" | Blue gray shale, abundant pyrite, numerous darker bands to 1" thick, a 1" silty layer at 3675'5". |
| 3677'2" | 3677'5" | Dark gray shale |
| 3677'5" | 3683'5" | Laminated dark gray and blue-gray shale |
| 3683'5" | 3684'5" | Blue-gray shale |
| 3684'5" | 3688'1" | Blue-gray and dark gray laminated shale |
| 3688'1" | 3688'8" | Dark gray shale |
| 3688'8" | 3691'7" | Laminated blue-gray and dark gray shale |
| 3691'7" | 3691'10" | Medium gray siltstone |
| 3691'10" | 3698'8" | Laminated blue-gray and dark gray shale |
| 3698'8" | 3698'11" | Dark gray laminated shale |
| 3698'11" | 3700'9" | Laminated blue-gray shale |
| 3700'9" | 3701'6" | Dark gray shale |
| 3701'6" | 3703'3" | Laminated blue-gray and dark gray shale |
| 3703'3" | 3704'6" | Blue-gray shale |
| 3704'6" | 3707'9" | Laminated blue-gray and dark gray shale |
| 3707'9" | 3711'1" | Blue-gray shale |
| 3711'1" | 3712'10" | Laminated blue-gray and dark gray shale |
| 3712'10" | 3712'11" | Light gray argillaceous siltstone |
| 3712'11" | 3716' | Blue-gray shale |
| 3716' | 3716'5" | Laminated dark gray and blue gray shale |
| 3716'5" | 3717'10" | Blue-gray shale |
| 3717'10" | 3718'2" | Laminated dark gray shale |
| 3718'2" | 3719' | Blue-gray shale |
| 3719' | 3720' | Laminated blue-gray and dark gray shale |
| 3720' | 3724'6" | Blue-gray shale |

| From | To | Fractures |
|---|---|---|
| 3679'5" | 3682'10" | Vertical, open |
| 3684' | 3690'11" | Vertical, open |
| 3699'11" | 3703'6" | Vertical, open |
| 3718'8" | 3718'9" | Folded zone with kerogen and pyrite fillings along a slickensided surface |

Core #18 (3724'6"-3764'6")

| From | To | Lithologic Description |
|---|---|---|
| 3724'6" | 3725' | Medium gray shale |
| 3725' | 3725'6" | Blue-gray shale |
| 3725'6" | 3725'9" | Blue-gray shale with one 2" black band |
| 3725'9" | 3726' | Blue-gray shale |
| 3726' | 3729' | Medium gray shale |
| 3729' | 3730'2" | Medium gray shale with four 1/4" light gray argillaceous siltstone layers |
| 3730'2" | 3730'10" | Blue-gray shale with black shale laminae and a 2" black band |
| 3730'10" | 3732'1" | Medium gray shale with a 2" light gray argillaceous siltstone |
| 3732'1" | 3732'11" | Blue-gray and black laminated shale |
| 3732'11" | 3733'1" | Blue-gray shale |
| 3733'1" | 3733'6" | Black shale with pyrite |
| 3733'6" | 3733'11" | Blue-gray shale |
| 3733'11" | 3735'5" | Medium gray shale |
| 3735'5" | 3736'2" | Blue-gray and black laminated shale |
| 3736'2" | 3736'8" | Blue-gray shale |
| 3736'8" | 3739'9" | Medium gray shale with one 1" silty band |
| 3739'9" | 3740'7" | Blue-gray shale with one 2" black band, black laminae |
| 3740'7" | 3743' | Medium gray shale |
| 3743' | 3743'4" | Blue-gray shale |
| 3743'4" | 3743'8" | Laminated blue-gray and black shale with two 2" black bands |
| 3743'8" | 3744'1" | Blue-gray shale |
| 3744'1" | 3746' | Medium gray shale with two 2" silty bands |
| 3746' | 3747'8" | Blue-gray and black laminated shale |
| 3747'8" | 3748'6" | Blue-gray shale |
| 3748'6" | 3748'9" | Blue-gray and black laminated shale |
| 3748'9" | 3750'8" | Blue-gray shale |
| 3750'8" | 3752'8" | Blue-gray and black laminated shale with four 2" black bands |
| 3752'8" | 3758'1" | Blue-gray shale, one 3" siltstone and one 3" black band with pyrite |
| 3758'1" | 3759'2" | Black shale with some blue gray laminae |
| 3759'2" | 3760'2" | Blue-gray shale |
| 3760'2" | 3761'11" | Medium gray shale |
| 3761'11" | 3762'3" | Black shale with pyrite |
| 3762'3" | 3763'10" | Medium gray shale |
| 3763'10" | 3764'2" | Black shale |
| 3764'2" | 3764'6" | Blue-gray shale |

Core #18 (3724'6"-3764'6")

| From | To | Fractures |
|---|---|---|
| 3729'3" | 3730'2" | Vertical, open |
| 3730'4" | 3731'1" | Vertical, open |
| 3733'1" | 3733'11" | Vertical, open |
| 3734'3" | 3736'3" | Vertical, open |
| 3738'3" | 3738'11" | Vertical, open |
| 3762'9" | 3763' | 45° slickensided surface |

Comment: Short core due to breakdown of booster.

Core #19 (3764'6"-3799'6")

| From | To | Lithologic Description |
|---|---|---|
| 3764'6" | 3766'4" | Medium gray shale |
| 3766'4" | 3766'8" | Black pyritic shale |
| 3766'8" | 3767'7" | Medium gray shale |
| 3767'7" | 3767'11" | Black pyritic shale |
| 3767'11" | 3768'6" | Medium gray calcareous shale |
| 3768'6" | 3771' | Medium gray slightly calcareous shale |
| 3771' | 3771'6" | Medium gray shale with calcareous siltstone |
| 3771'6" | 3772'11" | Medium gray calcareous shale with one 2" black band |
| 3772'11" | 3773'9" | Medium gray and black banded shale (non-calcareous) |
| 3773'9" | 3774'1" | Contorted black pyritic shale |
| 3774'1" | 3776' | Black shale |
| 3776' | 3777'4" | Blue-gray shale |
| 3777'4" | 3779' | Blue-gray and black laminated shale with two blue-gray bands 2" and 3" thick |
| 3779' | 3781'5" | Blue-gray calcareous |
| 3781'5" | 3782'7" | Black and blue-gray laminated shale with one blue-gray band 1" thick |
| 3782'7" | 3784'2" | Blue-gray shale |
| 3784'2" | 3784'5" | Black with blue-gray laminated shale |
| 3784'5" | 3785'6" | Blue-gray shale |
| 3785'6" | 3787'2" | Medium gray shale |
| 3787'2" | 3787'5" | Medium gray calcareous shale |
| 3787'5" | 3796'5" | Medium gray shale with one 5" dark gray band and one 1/8" silt band |
| 3796'5" | 3797'9" | Medium gray shale, one 2" calcareous zone and two 1" calcareous zones |
| 3797'9" | 3799'6" | Blue-gray and black laminated shale |

| From | To | Fractures |
|---|---|---|
| 3764'6" | 3765'10" | Vertical, open |
| 3767'2" | 3767'10" | Vertical, open |
| 3785' | 3786'4" | Vertical, open |
| 3786'4" | 3787'4" | Vertical, open |
| 3787'9" | 3788'9" | Vertical, open |
| 3793'2" | 3794'5" | Vertical, open |
| 3773'4" | 3774'1" | Contorted zone with slickensides |
| 3781'10" | 3782'6" | Two 45° slickensided surfaces |

Comment: Short core due to jamming of core barrel.

Core #20 (3799'6"-3858'4")

| From | To | Lithologic Description |
|---|---|---|
| 3799'6" | 3806'9" | Blue-gray shale with black laminae |
| 3806'9" | 3808'2" | Black laminated shale |
| 3808'2" | 3809'11" | Blue-gray shale |
| 3809'11" | 3810' | Gray calcareous shale with randomly oriented doubly terminated calcite crystals |
| 3810' | 3810'3" | Blue-gray shale |
| 3810'3" | 3814'3" | Laminated black and blue-gray shale |
| 3814'3" | 3814'4" | Calcite crystal cluster |
| 3814'4" | 3815'6" | Blue-gray shale |
| 3815'6" | 3816'9" | Laminated black and blue-gray shale |
| 3816'9" | 3822'11" | Blue-gray shale |
| 3822'11" | 3823'9" | Black and blue-gray laminated shale |
| 3823'9" | 3824'3" | Blue-gray shale |
| 3824'3" | 3824'4" | Blue-gray calcareous shale |
| 3824'4" | 3830'6" | Medium gray shale |
| 3830'6" | 3831'4" | Laminated dark gray and medium gray shale |
| 3831'4" | 3835'5" | Medium gray shale with one 1/8" light gray silty layer |
| 3835'5" | 3835'6" | Medium gray calcareous shale |
| 3835'6" | 3837' | Medium gray shale with three 1/4" silty layers |
| 3837' | 3838'9" | Laminated black and medium gray shale |
| 3838'9" | 3840'9" | Medium blue-gray shale |
| 3840'9" | 3843'6" | Blue-gray shale with dark bands up to 3" thick |
| 3843'6" | 3845'5" | Blue-gray shale |
| 3845'5" | 3845'10" | Blue-gray calcareous shale |
| 3845'10" | 3850'1" | Medium gray shale with four 1/8" silty zones |
| 3850'1" | 3850'5" | Dark gray to black laminated shale |
| 3850'6" | 3851'6" | Blue-gray shale |
| 3851'6" | 3853'3" | Blue-gray and very dark gray laminated shale |
| 3853'3" | 3855'4" | Blue-gray shale |
| 3855'4" | 3856'9" | Grading through blue gray, medium gray, dark gray, to very dark gray laminated shale |
| 3856'9" | 3858'1" | Blue-gray shale |
| 3858'1" | 3858'4" | Dark gray shale |

Fractures

No significant fractures

Core #21 (3858'4"-3916'6")

| From | To | Lithologic Description |
|---|---|---|
| 3858'6" | 3859'1" | Black shale |
| 3859'1" | 3859'6" | Medium gray shale with black bands |
| 3859'6" | 3861'4" | Black shale |
| 3861'4" | 3862'11" | Medium gray green pyritic shale |
| 3862'11" | 3863'6" | Black shale |
| 3863'6" | 3866'4" | Medium gray shale |
| 3866'4" | 3866'6" | Light gray calcareous shale |
| 3866'6" | 3868'10" | Medium gray shale with seven 1/8" to 1/4" light gray silty streaks and pyrite blebs |
| 3868'10" | 3869'3" | Black shale with a large pyrite bleb |
| 3869'3" | 3871'5" | Medium gray shale |
| 3871'5" | 3871'11" | Black shale |
| 3871'11" | 3875'4" | Medium gray shale with two 1/2" silty layers, one slightly calcareous, black laminae |
| 3875'4" | 3875'9" | Black shale |
| 3875'9" | 3878'1" | Medium gray shale |
| 3878'1" | 3878'6" | Black shale |
| 3878'6" | 3882'5" | Medium gray shale with eight 1/4" silty zones |
| 3882'5" | 3882'11" | Black shale |
| 3882'11" | 3886'2" | Green, medium gray and dark gray laminated shale with six 1/4" silty layers, pyrite and thin calcareous laminate at top |
| 33886'2" | 3886'4" | Black shale with reworked top |
| 3886'4" | 3889'7" | Medium gray, green gray, and dark gray laminated shale with two 1/2" silty layers |
| 3889'7" | 3889'11" | Black shale |
| 3889'11" | 3893' | Medium gray, green gray and dark gray laminated shale |
| 3893' | 3893'5" | Black shale |
| 3893'5" | 3895'11" | Medium gray, dark gray, green gray laminated shale with two 1/2" silty layers at base (one slightly calcareous) |
| 3895'11" | 3897'2" | Medium gray, green gray, dark gray laminated shale |
| 3897'2" | 3897'5" | Black shale |
| 3897'5" | 3899'8" | Medium gray, green gray, dark gray laminated shale |
| 3899'8" | 3900'1" | Black shale |
| 3900'1" | 3902'7" | Black gray and dark gray laminated shale (mostly medium gray) |
| 3902'11" | 3904'7" | Medium gray, green gray, dark gray laminated shale |
| 3904'7" | 3904'11" | Black shale |
| 3904'11" | 3909'2" | Medium gray and dark gray shale -- darker near base, nine lighter calcareous layers |
| 3909'2" | 3910'8" | Black and dark gray laminated shale |
| 3910'8" | 3911' | Medium gray and dark gray laminated shale, numerous pyrite blebs |
| 3911' | 3912'1" | Medium gray shale with some dark laminae, one calcareous layer |
| 3912'1" | 3913' | Dark gray and black laminated shale |
| 3913' | 3915'3" | Medium gray and dark gray laminated shale with abundant pyrite at top |

Core #21 (Cont'd)

| From | To | Lithologic Description |
| --- | --- | --- |
| 3915'3" | 3915'9" | Dark gray shale |
| 3915'9" | 3916'4" | Black shale |

| From | To | Fractures |
| --- | --- | --- |
| 3874' | 3874'6" | Vertical, open mineralized |

Core #22 (3916'6"-3956'6")

| From | To | Lithologic Description |
|---|---|---|
| 3916'6" | 3916'9" | Black shale |
| 3916'9" | 3919'3" | Medium gray and dark gray laminated shale with pyrite in places |
| 3919'3" | 3919'8" | Black shale |
| 3919'8" | 3921'8" | Medium gray and dark gray laminated shale |
| 3921'8" | 3922'2" | Black shale |
| 3922'2" | 3924'6" | Medium gray and dark gray laminated shale |
| 3924'6" | 3925'10" | Black shale with several ½" dark bands |
| 3925'10" | 3926'10" | Dark gray laminated shale |
| 3926'10" | 3928'8" | Medium gray shale with dark gray laminae |
| 3928'8" | 3928'11" | Black shale |
| 3928'11" | 3934'7" | Medium gray and dark gray laminated shale, many silty layers to 1/8" |
| 3934'7" | 3934'10" | Black shale |
| 3934'10" | 3939'4" | Medium gray shale with dark gray laminae and silty layers to 1/8", one calcareous layer ¼" |
| 3939'4" | 3940'1" | Medium gray shale |
| 3940'1" | 3942'2" | Medium gray and dark gray laminated shale, three silty streaks to ¼" |
| 3942'2" | 3942'4" | Black shale |
| 3942'4" | 3947'10" | Medium gray and dark gray shale, two 1/4" silty layers |
| 3947'10" | 3949'1" | Black shale |
| 3949'1" | 3952'6" | Medium and dark gray laminated shale with 1/16" pyrite bands near top |
| 3952'6" | 3953'2" | Black shale with pyrite blebs |
| 3953'2" | 3956'6" | Medium dark gray with darker laminae, pyrite bands to 1/4' |

| From | To | Fractures |
|---|---|---|
| 3917'6" | 3917'9" | 45° slickensided surface |
| 3924'6" | 3925'4" | Mineralized slickensided surface |
| 3935'6" | 3936'6" | 45° slickensided surface |
| 3950'9" | 3955' | Vertical, open |
| 3952'3" | 3953'2" | Mineralized slickensided surface |

<u>Comments</u>: Short core due to jamming of core barrel.

Core #23 (3956'6"-4007')

| From | To | Lithologic Description |
|---|---|---|
| 3956'6" | 3958'4" | Medium and dark gray laminated shale |
| 3958'4" | 3959'4" | Black shale |
| 3959'4" | 3962'4" | Black and dark gray laminated shale with pyrite laminae |
| 3962'4" | 3965'9" | Medium and dark gray laminated shale with pyrite laminae |
| 3965'9" | 3966' | Black shale |
| 3966' | 3966'3" | Dark gray shale |
| 3966'3" | 3966'9" | Black shale |
| 3966'9" | 3970'9" | Dark gray shale and black shale with pyrite blebs and laminae |
| 3970'9" | 3972'10" | Black shale |
| 3972'10" | 3973'4" | Dark gray shale with pyrite at top and base |
| 3973'4" | 3976'8" | Black shale |
| 3976'8" | 3977'2" | Dark gray and black laminated shale |
| 3977'2" | 3977'7" | Black shale |
| 3977'7" | 3977'8" | Medium gray silty, pyritic calcareous band |
| 3977'8" | 3978' | Dark gray and black laminated shale |
| 3978' | 3980'1" | Black shale |
| 3980'1" | 3980'11" | Medium gray and green gray laminated shale with pyrite blebs and laminae |
| 3980'11" | 3981' | Dark gray very calcareous silty shale |
| 3981' | 3981'3" | Black shale |
| 3981'3" | 3981'10" | Medium gray and green gray shale with pyrite laminae and blebs |
| 3981'10" | 3982'6" | Black shale with pyrite laminae |
| 3982'6" | 3984'4" | Dark gray and black laminated shale with pyrite laminae |
| 3984'4" | 3985'6" | Black shale with some pyrite |
| 3985'6" | 3987' | Dark gray and black laminated shale |
| 3987' | 3987'7" | Dark gray shale with green bands |
| 3987'7" | 3993'2" | Black and dark gray shale with pyrite laminae |
| 3993'2" | 3997'7" | Black shale with pyrite blebs |
| 3997'7" | 3999'10" | Very dark gray shale with pyrite laminae and a 2" slightly calcareous layer at top |
| 3999'10" | 4000'2" | Black shale with two ¼" pyrite bands |
| 4000'2" | 4000'5" | Dark gray shale |
| 4000'5" | 4002'8" | Black shale |
| 4002'8" | 4004'8" | Medium and black banded shale |
| 4004'8" | 4007' | Black shale |

| From | To | Fractures |
|---|---|---|
| 3977'3" | 3979'11" | Vertical, open |
| 3983'2" | 3984'7" | Intensely crumbled zone |
| 4000' | 4003'4" | Intensely crumbled zone |

Core #24 (4007'-4047'6")

| From | To | Lithologic Description |
|---|---|---|
| 4007' | 4014'3" | Black shale with pyrite laminae and vertical fillings, four calcareous bands and hairline calcite fillings |
| 4014'3" | 4014'6" | Calcareous, pyritic, silty layer with biotite (medium gray meta-bentonite |
| 4014'6" | 4016'3" | Folded and faulted black shale with pyrite laminae and dark calcareous shale band |
| 4016'3" | 4017'10" | Dark shale with many thin pyrite laminae |
| 4017'10" | 4019'7" | Black shale with several calcareous pyrite stringers, plus dark gray and green gray shale with calcareous pyrite layers to 1/8" |
| 4019'7" | 4025'1" | Very dark gray shale with calcareous pyrite bands |
| 4025'1" | 4026'6" | Laminated dark gray and gray green shale |
| 4026'6" | 4029' | Dark gray and black shale |
| 4029' | 4047'6" | Black shale (black in powder) with pyrite blebs and horizontal calcite veins along fractures |

| From | To | Fractures |
|---|---|---|
| 4024' | 4029' | Vertical, open fracture with slickensides |
| 4028'7" | 4029'9" | Mineralized vertical fracture |
| 4036' | 4036'10" | Vertical, open |

Core #25 (4047'6"-4056'6")

| From | To | Lithologic Description |
| --- | --- | --- |
| 4047'6" | 4051'3" | Black shale |
| 4051'3" | 4051'4" | Calcareous, pyritic fossiliferous zone |
| 4051'4" | 4054'10" | Medium gray fossiliferous limestone |
| 4054'10" | 4054'11½" | Medium gray flint |

| From | To | Fractures |
| --- | --- | --- |
| 4047'6" | 4051'3" | Vertical, open |

Well No. 20402

Core #1 (2654' - 2712'8")

| From | To | Lithologic Description |
|---|---|---|
| 2654' | 2682'3" | Gray green laminated shale with light gray siltstone layers showing cross-bedding up to 3" thick |
| 2682'3" | 2682'7" | Massive light gray siltstone |
| 2682'7" | 2703'5" | Green-gray laminated shale with light gray siltstone layers to 3" thick |
| 2703'5" | 2703'9" | Massive light gray siltstone |
| 2703'9" | 2712'8" | Green-gray laminated shale with light gray siltstone layers |

Fractures

No open fractures

Core #2 (2712'8" - 2771'3")

| From | To | Lithologic Description |
|---|---|---|
| 2712'8" | 2717'8" | Light gray laminated shale |
| 2717'8" | 2736'8" | Medium gray shale with dark gray laminae and argillaceous siltstone layers |
| 2736'8" | 2737'6" | Dark and medium gray shale layers about 2 1/2" thick |
| 2737'6" | 2742'8" | Medium gray shale with some dark gray laminae (less silty than above) |
| 2742'8" | 2770'8" | Medium and light gray laminated shale with light gray siltstone layers to 3" thick, and several dark shale layers up to 3" thick. |
| 2770'8" | 2771'3" | Dark gray shale |

| From | To | Fractures |
|---|---|---|
| 2716'8" | 2717'1" | Slightly mineralized fracture |
| 2726'9" | 2727'7" | Vertical, open |
| 2733' | 2733'7" | Vertical, open |
| 2733'11" | 2734'7" | Vertical, open |
| 2751'4" | 2751'7" | Vertical, open |

Core #3 (3000' - 3058'10")

| From | To | Lithologic Description |
|---|---|---|
| 3000' | 3001'9" | Medium gray laminated shale with several 1/2" dark bands |
| 3001'9" | 3003'4" | Dark gray shale |
| 3003'4" | 3005'10" | Medium and dark gray banded shale |
| 3005'10" | 3006'4" | Medium gray shale with lighter calcareous shale laminae |
| 3006'4" | 3007'4" | Medium and dark gray banded shale |
| 3007'4" | 3007'11" | Medium and dark gray laminated shale, light gray calcareous shale, one 2" argillaceous siltstone |
| 3007'11" | 3009'1" | Medium gray shale |
| 3009'1" | 3010' | Dark gray shale |
| 3010' | 3013'10" | Medium and dark gray shale with a 1" contorted siltstone layer at base |
| 3013'10" | 3014'9" | Dark gray shale |
| 3014'9" | 3021' | Medium and dark gray banded shale with several 1/4" calcite layers |
| 3021' | 3022'1" | Dark gray shale |
| 3022'1" | 3026'10 1/2" | Medium dark gray shale with calcareous shale layers |
| 3026'10 1/2" | 3027'4" | Dark gray shale |
| 3027'4" | 3029' | Medium gray shale with a few dark gray bands |
| 3029' | 3035'6" | Dark gray shale with some medium gray bands and one 1/4" calcite layer |
| 3035'6" | 3036'10" | Medium gray shale |
| 3036'10" | 3038'1" | Dark gray shale |
| 3038'1" | 3039'1" | Medium and dark gray banded shale |
| 3039'1" | 3040'10" | Dark gray shale |
| 3040'10" | 3041'5" | Medium and dark gray banded shale |
| 3041'5" | 3042'5" | Dark gray shale |
| 3402'5" | 3044'6" | Medium and dark gray banded shale with calcareous zones to 1/2" |
| 3044'6" | 3047'5" | Dark gray shale |
| 3047'5" | 3050'2" | Medium and dark gray shale |
| 3050'2" | 3052'6" | Dark gray shale |
| 3052'6" | 3053'7" | Medium and dark gray shale with calcareous layers |
| 3053'7" | 3054'11" | Dark gray shale |
| 3054'11" | 3057'10" | Medium gray shale with dark bands, two 1" calcareous layers near base |
| 3057'10" | 3058'10" | Dark gray shale |

| From | To | Fractures |
|---|---|---|
| 3006'8 1/2" | 3012'4" | Vertical, mineralized, open |
| 3021' | 3022'2" | Vertical, open |
| 3046'3" | 3047'2" | Vertical, open |
| 3049'10" | 3050'7" | Vertical, open |

Core #4 (3058'10" - 3117'8")

| From | To | Lithologic Description |
|---|---|---|
| 3058'10" | 3061'3" | Medium and dark gray banded shale, one calcareous layer near top |
| 3061'3" | 3062' | Medium gray shale |
| 3062' | 3063'1" | Dark gray shale |
| 3063'1" | 3064'2" | Medium and dark gray shale |
| 3064'2" | 3065'2 1/2" | Light gray calcareous shale |
| 3065'2 1/2" | 3065'7" | Dark gray shale |
| 3065'7" | 3065'9" | Light gray calcareous shale |
| 3065'9" | 3068'1" | Dark gray shale |
| 3068'1" | 3071'4" | Medium and dark gray banded shale, three calcareous zones |
| 3071'4" | 3073' | Light, medium and dark gray banded shale |
| 3073' | 3073'2" | Light gray calcareous shale |
| 3073'2" | 3075'6" | Light, medium and dark gray banded shale |
| 3075'6" | 3077'3" | Dark gray shale with some medium gray layers |
| 3077'3" | 3080'5" | Light to medium gray shale some 1/2" dark bands |
| 3080'5" | 3084'3" | Dark gray and medium gray banded shale |
| 3084'3" | 3087'6" | Medium gray shale, some dark bands to 1", basal calcareous zone |
| 3087'6" | 3088'1" | Light to medium gray shale with some dark bands, calcareous layers |
| 3088'1" | 3090'8" | Light to medium gray shale with several dark bands |
| 3090'8" | 3091'6" | Dark gray shale with medium gray bands |
| 3091'6" | 3098'4" | Light to medium and dark gray banded shale with two thin calcareous layers |
| 3098'4" | 3099'9" | Dark gray shale |
| 3099'9" | 3101'1" | Light to medium gray shale |
| 3101'1" | 3102'6" | Light, medium and dark gray banded shale |
| 3102'6" | 3103'9" | Light to medium gray shale with three calcareous layers |
| 3103'9" | 3104'8" | Light, medium and dark gray banded shale with several calcareous layers to 1" thick |
| 3104'8" | 3109'10" | Light and medium gray shale with several dark bands, two calcareous shale bands |
| 3109'10" | 3112'1" | Light and medium gray laminated shale |
| 3112'1" | 3115'2" | Dark gray shale with several light and medium gray bands |
| 3115'2" | 3117'8" | Dark and medium gray shale |

| From | To | Fractures | |
|---|---|---|---|
| 3059'8" | 3064'10" | Vertical, open | |
| 3065'10" | 3068'5" | Vertical, open | also rubble zone |
| 3069'10" | 3071'2" | Vertical, open | |
| 3095'4" | 3096'9" | Vertical, open | |
| 3098'2" | 3099'3" | Vertical, open | |
| 3100'10" | 3101'6" | Vertical, open | |
| 3112'2" | 3112'9" | Vertical, open | |

Core #5 (3298' - 3356'8")

| From | To | Lithologic Description |
|---|---|---|
| 3298' | 3305' | Medium gray shale, several dark bands up to 3/4", eight calcareous layers |
| 3305' | 3305'4" | Light gray banded calcareous and dark gray shale |
| 3305'4" | 3306' | Medium and dark gray banded shale |
| 3306' | 3319'2" | Black shale with a 1" calcareous zone |
| 3319'2" | 3325'10" | Medium gray shale, several black bands |
| 3325'10" | 3325'11" | Light gray calcareous shale |
| 3325'11" | 3341' | Medium gray shale, black bands up to 3" some calcareous shale zones |
| 3341' | 3347'10" | Medium gray and black banded shale |
| 3347'10" | 3356'8" | Black shale |

| From | To | Fractures |
|---|---|---|
| 3301' | 3301'8" | Vertical and open |
| 3302' | 3302'9" | Vertical and open |
| 3304'2" | 3305' | Vertical and open |
| 3307'5" | 3316'5" | Vertical and open |
| 3316'7" | 3317'10" | Vertical and open |
| 3318' | 3323'9" | Vertical and open |
| 3324'5" | 3325'6" | Vertical and open |
| 3326' | 3327' | Vertical and open |
| 3337'4" | 3339' | Vertical and open |
| 3343' | 3343'8" | Vertical and open |
| 3345'5" | 3346'7" | Vertical and open |
| 3347'5" | 3348'8" | Vertical and open |
| 3349' | 3356'8" | Vertical and open |

Core #6 (3356'8" - 3414')

| From | To | Lithologic Description |
|---|---|---|
| 3356' | 3357' | Black shale |
| 3357' | 3357'7" | Medium gray shale |
| 3357'7" | 3363'2" | Black shale |
| 3363'2" | 3365'3" | Black and medium gray banded shale |
| 3365'3" | 3367'6" | Medium gray shale, some black bands |
| 3367'6" | 3375'6" | Black shale, one large pyrite bleb |
| 3375'6" | 3376' | Medium gray shale |
| 3376' | 3379'11" | Black shale |
| 3379'11" | 3380'4" | Medium gray shale |
| 3380'4" | 3386'9" | Black shale |
| 3386'9" | 3388'10" | Medium gray shale |
| 3388'10" | 3389'5" | Black shale |
| 3389'5" | 3389'10" | Medium gray shale |
| 3389'10" | 3398'6" | Black shale, one 1/8" pyrite layer |
| 3398'6" | 3400' | Medium gray shale, one 2" siltstone bed |
| 3400' | 3400'4" | Black shale |
| 3400'4" | 3400'9" | Medium gray shale, one 1" light tan siltstone |
| 3400'9" | 3401' | Black shale |
| 3401' | 3406'9" | Light medium gray shale, two 1" calcareous bands, one 2" pyrite band |
| 3406'9" | 3409'5" | Black shale |
| 3409'5" | 3411'8" | Light-medium gray shale |
| 3411'8" | 3414' | Black shale |

| From | To | Fractures |
|---|---|---|
| 3356' | 3357' | Vertical, open |
| 3357'8" | 3363'5" | Vertical, open |
| 3364'4" | 3380' | Vertical, open |
| 3383'5" | 3385' | Vertical, open |
| 3390' | 3398'11" | Vertical, open |
| 3401'7" | 3401'11" | Slickensided surface |
| 3406'6" | 3407'7" | Vertical, open |
| 3409' | 3410'5" | Vertical, open |
| 3412' | 3414' | Vertical, open |

Core #7 (3414' - 3471'6")

| From | To | Lithologic Description |
|---|---|---|
| 3414' | 3416' | Black shale |
| 3416' | 3416'4" | Dark gray shale |
| 3416'4" | 3418' | Black shale, pyrite blebs |
| 3418' | 3419'2" | Dark gray shale |
| 3419'2" | 3419'8" | Black shale |
| 3419'8" | 3421'1" | Dark gray shale |
| 3421'1" | 3421'5" | Light gray calcareous siltstone |
| 3421'5" | 3422'9" | Medium and dark gray shale |
| 3422'9" | 3423'1 1/2" | Black shale |
| 3423'1 1/2" | 3424'1" | Medium gray shale, one 1 1/2" black band |
| 3424'1" | 3427'10" | Black shale |
| 3427'10" | 3428'5" | Black shale, 2 dark gray bands |
| 3428'5" | 3429'4" | Black shale |
| 3429'4" | 3431'4" | Medium gray shale, one 2" bed of very calcareous siltstone |
| 3431'4" | 3431'11" | Black shale |
| 3431'11" | 3434'6" | Medium gray shale |
| 3434'6" | 3434'7 1/2" | Light gray argillaceous limestone |
| 3434'7 1/2" | 3437'10" | Medium gray shale, one slightly calcareous 1" silt bed |
| 3437'10" | 3438'5" | Black shale |
| 3438'5" | 3439'4" | Medium gray shale |
| 3439'4" | 3439'8" | Light gray, slightly calcareous siltstone |
| 3439'8" | 3440'5" | Dark gray and black shale |
| 3440'5" | 3441'2" | Black shale |
| 3441'2" | 3442' | Medium gray and black shale (Turbidite layer) |
| 3442' | 3443'5" | Light gray, slightly calcareous, pyritic siltstone |
| 3443'5" | 3443'7" | Medium gray shale |
| 3443'7" | 3446' | Black shale, seven dark gray beds to 3" |
| 3446' | 3450'6" | Black shale, one large pyrite bleb |
| 3450'6" | 3450'11" | Very dark gray shale |
| 3450'11" | 3453'4" | Black shale |
| 3453'4" | 3455'9" | Banded dark gray and black shale |
| 3455'9" | 3458'6" | Medium gray shale |
| 3458'6" | 3462'3" | Black shale, numerous dark gray bands to 2" thick |
| 3462'3" | 3465'5" | Dark gray shale |
| 3465'5" | 3467'11" | Black shale |
| 3467'11" | 3468'1" | Medium gray shale |
| 3468'1" | 3471'4" | Black shale |

| From | To | Fractures |
|---|---|---|
| 3414' | 3416'5" | Vertical, open |
| 3416'6" | 3419'11" | Vertical, open |
| 3424' | 3430' | Vertical, open |

Core #7 (Cont'd)

| From | To | Fractures |
|---|---|---|
| 3434'6" | 3434'7 1/2" | Slickensided surface |
| 3437'10" | 3438' | Vertical, open |
| 3444'6" | 3445'5" | Vertical, open |
| 3453'2" | 3455'8" | Vertical, open |
| 3458'6" | 3459'6" | Vertical, open |
| 3461'6" | 3465'6" | Vertical, open |
| 3467'6" | 3471'4" | Vertical, open |

Core #8 (3471'6" - 3531'6")

| From | To | Lithologic Description |
|---|---|---|
| 3474' | 3477'2" | Black shale, one 2" medium gray shale band |
| 3477'2" | 3478'10" | Medium gray shale, three 1/2" black bands, one 1" black band |
| 3478'10" | 3479'7" | Black shale, one 1/2" medium gray shale band |
| 3479'7" | 3480'2" | Medium gray shale |
| 3480'2" | 3480'5" | Black shale with pyrite blebs |
| 3480'5" | 3481'10" | Medium gray shale with two pyritic black shale bands to 1" |
| 3481'10" | 3482'7" | Light to medium gray slightly calcareous shale |
| 3482'7" | 3486'7" | Medium gray calcareous shale with five 2-3" black bands |
| 3486'7" | 3486'9" | Light gray calcareous silty shale |
| 3486'9" | 3488'1" | Medium gray shale, three black shale bands 1" to 3" thick |
| 3488'1" | 3488'4" | Black shale |
| 3488'4" | 3488'9" | Medium gray shale |
| 3488'9" | 3490'5" | Medium gray and black banded shale |
| 3490'5" | 3499'8" | Black shale with several medium gray bands |
| 3499'8" | 3500'7" | Light to medium gray slightly calcareous silty shale, one black band |
| 3500'7" | 3500'11" | Black shale |
| 3500'11" | 3504'2" | Light to medium gray slightly calcareous silty shale with three pyritic black bands to 1 1/2" |
| 3504'2" | 3504'4" | Light gray calcareous siltstone |
| 3504'4" | 3505'5" | Black shale, two 1/4" medium gray bands |
| 3505'5" | 3505'8" | Medium gray shale |
| 3505'8" | 3505'11" | Light gray calcareous siltstone |
| 3505'11" | 3506'4" | Black and medium gray banded shale |
| 3506'4" | 3506'7" | Medium gray shale |
| 3506'7" | 3507'7" | Black and medium gray laminated shale (mostly black) |
| 3507'7" | 3515' | Black shale, four 1/4" medium gray bands, one 1/4" pyrite band |
| 3515' | 3515'3" | Light gray calcareous siltstone |
| 3515'3" | 3515'10" | Black shale with many medium gray bands |
| 3515'10" | 3516'3" | Medium gray slightly calcareous shale |
| 3516'3" | 3516'10" | Black and medium gray shale, (mostly black) |
| 3516'10" | 3517'2" | Medium gray and black banded shale, mostly medium gray |
| 3517'2" | 3518'9" | Black shale with some gray laminae |
| 3518'9" | 3519' | Medium gray shale, some black laminae |
| 3519' | 3525'6" | Black shale, some medium gray laminae and one 1/4" medium gray band |
| 3526'7" | 3527'7" | Black shale |
| 3527'7" | 3527'9" | Black and medium gray banded shale |
| 3527'9" | 3528'11" | Black shale, some pyrite blebs |
| 3528'11" | 3529' | Medium gray shale |

Core #8 (Cont'd)

| From | To | Lithologic Description |
|---|---|---|
| 3529' | 3529'5" | Black shale, some medium gray laminae |
| 3529'5" | 3530' | Light and medium gray banded slightly calcareous shale with one 1/4" black layer |
| 3530' | 3530'4" | Black shale |
| 3530'4" | 3531' | Light to medium gray banded shale (slightly calcareous), one 1/2" medium gray and black mottled shale band |
| 3531' | 3531'6" | Black shale |

| From | To | Fractures |
|---|---|---|
| 3470' | 3475'3" | Vertical, open |
| 3478'9" | 3480' | Vertical, open |
| 3480' | 3481'3" | Vertical, open |
| 3483' | 3485' | Vertical, open |
| 3487' | 3488' | Vertical, open |
| 3488'4" | 3492'7" | Vertical, open |
| 3492'7" | 3494'1" | Vertical, open |
| 3493'10" | 3495'9" | Vertical, open |
| 3495'8" | 3496'8" | Vertical, open |
| 3496'6" | 3497'7" | Vertical, open |
| 3501' | 3503'2" | Vertical, open |
| 3506' | 3509'7" | Vertical, open |
| 3509'11" | 3512' | Vertical, open |
| 3511'10" | 3515'3" | Vertical, open |
| 3517'7" | 3518'9" | Vertical, open |
| 3519' | 3523'8" | Vertical, open |

Core #9 (3531'6"-3591'3-1/2")

| From | To | Lithologic Description |
|---|---|---|
| 3531'6" | 3532'6" | Black shale |
| 3532'6" | 3532'9" | Light gray shale with dark gray laminae |
| 3532'9" | 3533'3" | Black shale |
| 3533'3" | 3533'7" | Light to medium gray slightly calcareous shale |
| 3533'7" | 3538'3" | Black shale with several dark gray laminae and pyrite blebs |
| 3538'3" | 3538'5" | Medium to dark gray shale with contorted bedding |
| 3538'5" | 3545'10" | Black shale, two 1-1/2" contorted beds |
| 3545'10" | 3546'5" | Medium gray shale with dark gray laminae |
| 3546'5" | 3546'10" | Medium and black laminated shale |
| 3546'10" | 3547'7" | Medium and dark gray laminated shale |
| 3547'7" | 3553'2" | Black shale with dark gray bands and pyrite blebs |
| 3553'2" | 3554'1" | Black shale with pyrite blebs |
| 3554'1" | 3554'5" | Light gray to gray-green calcareous shale contorted beds |
| 3554'5" | 3554'10" | Dark gray and black laminated shale |
| 3554'10" | 3555'6" | Medium and dark gray banded shale |
| 3555'6" | 3557'9" | Black shale with pyrite blebs, two dark gray bands |
| 3557'9" | 3558'6" | Medium and dark gray laminated shale |
| 3558'6" | 3559'1" | Black shale |
| 3559'1" | 3559'8" | Medium and dark gray laminated shale |
| 3559'8" | 3560'6" | Black shale with some dark gray bands and abundant pyrite |
| 3560'6" | 3561' | Medium and dark gray laminated shale |
| 3561' | 3561'11" | Black shale with dark gray laminae and pyrite blebs |
| 3561'11" | 3562'7" | Light and dark gray laminated shale |
| 3562'7" | 3565' | Black shale |
| 3565' | 3565'5" | Slightly calcareous medium gray shale |
| 3565'5" | 3565'10" | Black shale |
| 3565'10" | 3566'5" | Medium gray slightly calcareous shale |
| 3566'5" | 3570'4" | Black shale with dark gray laminae |
| 3570'4" | 3571' | Medium and dark gray laminated shale |
| 3571' | 3572'5" | Black shale with pyrite blebs |
| 3572'5" | 3574' | Medium gray and black banded shale |
| 3574' | 3576'4" | Black shale |
| 3576'4" | 3576'9" | Medium gray shale |
| 3576'9" | 3576'10" | Light gray calcareous shale |
| 3576'10" | 3579'5" | Black shale with pyrite blebs and dark gray laminae |
| 3579'5" | 3580'7" | Medium and dark gray shale with pyrite laminae |

Core #9 (Cont'd)

| From | To | Lithologic Description |
|---|---|---|
| 3580'7" | 3582'11" | Black shale with dark gray zones and pyrite laminae |
| 3582'11" | 3583'4" | Medium and dark gray laminated shale |
| 3583'4" | 3584'8" | Black shale with three 1-1/2" medium gray bands |
| 3584'8" | 3585' | Medium gray shale |
| 3585' | 3586' | Black shale with two medium gray bands |
| 3586'- | 3586'5" | Medium gray shale with one black band and one 1/8" pyrite seam at 30° to the bedding |
| 3586'5" | 3590'3-1/2" | Black shale with one 3" medium gray band, several dark gray laminae and blebs |

| From | To | Fractures |
|---|---|---|
| 3536'11" | 3538'4" | Vertical, open |
| 3549'4" | 3550'10" | Vertical, open |
| 3551'3" | 3552'8" | Vertical, open |
| 3559'7" | 3561'4" | Vertical, open |
| 3562'10" | 3565'2" | Vertical, open |
| 3566'8" | 3571' | Vertical, open |
| 3571' | 3572'9" | Vertical, open |
| 3573'6" | 3574'11" | Vertical, open |

Distinct Black Kerogen Layers

3533'11"
3551'

Core #10 (3892'-3950')

| From | To | Lithologic Description |
|---|---|---|
| 3892' | 3894'7" | Black shale with pyrite laminae and blebs |
| 3894'7" | 3895'2" | Medium and dark gray laminated shale with black shale and pyrite laminae |
| 3895'2" | 3897' | Black shale with three 3-4" bands of laminated shale |
| 3897' | 3899'5" | Black shale with pyrite blebs and laminae |
| 3899'5" | 3900' | Dark gray and black laminated shale with pyrite laminae |
| 3900' | 3903'10" | Black shale, some pyrite laminae and one bleb |
| 3903'10" | 3904'3" | Dark gray and black laminated shale with pyrite laminae |
| 3904'3" | 3907' | Black shale and pyrite laminae |
| 3907' | 3907'9" | Dark gray and black laminated shale, pyrite blebs |
| 3907'9" | 3911'6" | Black shale, many pyrite laminae, one 1" blebs |
| 3911'6" | 3912' | Medium gray shale with black laminae, one 2" pyrite bleb |
| 3912' | 3912'4" | Black shale |
| 3912'4" | 3915'. | Medium and dark gray calcareous shale, one 3" black band |
| 3915' | 3920' | Black shale with pyrite laminae |
| 3920' | 3920'8" | Dark gray and black laminated shale |
| 3920'8" | 3925'9" | Black shale with some pyrite blebs and laminae |
| 3925'9" | 3928'6" | Very dark gray shale with black pyritic bands |
| 3928'6" | 3931'8" | Dark gray and black banded shale with pyrite bands and blebs |
| 3931'8" | 3934'1" | Black shale, some dark gray laminae and pyrite laminae |
| 3934'1" | 3934'7" | Medium and dark gray laminated shale |
| 3934'7" | 3937' | Black shale, two 4" medium-dark bands, pyrite |
| 3937' | 3937'5" | Dark gray and black laminated shale |
| 3937'5" | 3937'8" | Black shale |
| 3937'8" | 3940'3" | Black and dark gray laminated shale, pyrite laminae |
| 3940'3" | 3942'2" | Black and green-gray shale with one 3" light gray calcareous siltstone |
| 3942'2" | 3943'10" | Dark gray and black calcareous laminated shale with pyrite blebs and laminae |
| 3943'10" | 3944'6" | Intraformational breccia with clasts of varying sizes, calcareous fillings |
| 3944'6" | 3946'1" | Dark gray and black laminated shale, abundant pyrite |
| 3946'1" | 3947'6" | Medium gray-green shale with one 2" medium gray band |

Core #10 (Cont'd)

| From | To | Lithologic Description |
|---|---|---|
| 3947'6" | 3949'3" | Dark gray, black and green-gray laminated shale with some pyrite laminae |
| 3949'3" | 3949'10" | Medium gray very calcareous shale with a 1" contorted zone with calcite filling |
| 3949'10" | 3950' | Black shale |

Fractures

| | |
|---|---|
| 3894'5" | Slickensided Surface |
| 3894'9" | Slickensided surface |
| 3898'3" | Slickensided surface |
| 3924' | Slickensided surface |
| 3924'11" | Slickensided surface |
| 3927'3" | Slickensided surface |
| 3929'8" | Slickensided surface |
| 3931'2" | Slickensided surface |
| 3934'6" | Slickensided surface |
| 3942'2" | Calcite healed surface, 70° dip |
| 3944'10" | Slickensided surface |
| 3949'2" | Slickensided surface |

Distinct Black Kerogen Layers

Observed at several depths in this core.

Core #11 (3950'-3977'10")

| From | To | Lithologic Description |
|---|---|---|
| 3950' | 3954'1" | Very dark gray shale with eight calcareous pyritic bands to 1/8" |
| 3954'1" | 3958'2" | Very dark gray-brown very calcareous shale |
| 3958'2" | 3963'11" | Very calcareous black shale |
| 3963'11" | 3973'11" | Black shale |
| 3973'11" | 3974'1/2" | Calcareous pyritic silty zone with biotite (meta-bentonite) |
| 3974'1/2" | 3976'9" | Medium gray fossiliferous limestone |

| From | To | Fractures |
|---|---|---|
| 3952'10" | 3953'6" | 45° slickensided surface with calcite |
| 3955'2" | 3956'5" | Several 45° slickensided surfaces |
| 3972'9" | 3972'10" | 45° slickensided surface |

Description of Cored Shale Intervals
from Well Number 20336, Martin Co., KY

Run #1 (2432-2491)

| From | To | Lithologic Description |
|---|---|---|
| 2432 | 2491 | Dark gray shale |

| From | To | Fractures |
|---|---|---|
| 2434.3 | 2434.7 | Vertical, parted |
| 2435.3 | 2435.9 | 70° inclined, parted |
| 2437.4 | 2438.4 | Nearly vertical, parted |
| 2438.6 | 2439.4 | Nearly vertical, parted |
| 2439.0 | 2439.4 | Vertical, parted |
| 2439.8 | 2440.8 | Vertical, parted |
| 2440.8 | 2442.6 | Vertical, parted |
| 2444.4 | 2445.3 | Vertical, parted |
| 2450.4 | 2451.2 | Vertical, parted |
| 2455.1 | 2460.6 | Vertical, parted |
| 2465.8 | 2465.5 | Vertical, parted |
| 2469.8 | 2470.5 | Vertical, parted |
| 2477.1 | 2477.9 | 70° inclined, parted |
| 2481.0 | 2482 | Nearly vertical, parted |

| From | To | Other Features |
|---|---|---|
| 2434 | 2434 | Thin calcareous seam |
| 2454.8 | 2455.1 | 2 thin calcareous seams |
| 2458 | 2458 | Thin calcareous seam |
| 2459.8 | 2459.8 | Thin calcareous seam |
| 2462.2 | 2462.7 | 4 thin calcareous seams |
| 2468.0 | 2468.5 | Numerous calcareous seams |
| 2469.5 | 2470 | Numerous calcareous seams |
| 2475.2 | 2475.3 | Numerous calcareous seams |
| 2476.6 | 2477.0 | 3 calcareous seams |
| 2478.0 | 2478.4 | 3 calcareous seams |
| 2479.1 | 2479.2 | Several calcareous seams |
| 2487.2 | 2487.4 | Calcareous zone |
| 2488.5 | 2490 | Scattered calcareous zones |

Run #2 (2491-2550)

| From | To | Lithologic Description |
|---|---|---|
| 2491 | 2502 | Dark gray shale |
| 2502 | 2509 | Medium dark gray shale |
| 2509 | 2510 | Medium gray and medium dark gray banded shale |
| 2510 | 2511 | Medium gray shale with dark gray bands |
| 2511 | 2518 | Medium gray shale |
| 2518 | 2519 | Medium gray and medium dark gray banded shale |
| 2519 | 2526.9 | Medium gray shale with dark gray bands |
| 2526.9 | 2527.1 | Medium gray siltstone |
| 2527.1 | 2528.0 | Medium dark gray shale |
| 2528.0 | 2528.2 | Medium gray siltstone |
| 2528.2 | 2529.5 | Medium gray shale with dark gray bands |
| 2529.5 | 2529.9 | Medium gray siltstone |
| 2529.9 | 2530.2 | Medium gray shale |
| 2530.2 | 2530.3 | Medium gray siltstone |
| 2530.3 | 2532.2 | Medium gray-green and dark gray banded shale |
| 2532.2 | 2533.0 | Medium gray-green shale |
| 2533.0 | 2534.5 | Medium gray-green shale with dark gray bands |
| 2534.5 | 2537.0 | Medium dark gray shale with medium gray green bands |
| 2537.0 | 2539.2 | Medium gray-green shale |
| 2539.2 | 2540.5 | Medium gray-green and dark gray banded shale |
| 2540.5 | 2541.6 | Dark gray shale |
| 2541.6 | 2545.7 | Medium gray-green shale with many silty bands up to .1' thick |
| 2545.7 | 2545.9 | Medium gray siltstone |
| 2545.9 | 2550.0 | Medium gray shale with three argillaceous siltstone bands |

| From | To | Fractures |
|---|---|---|
| 2505.0 | 2505.8 | Vertical fracture, parted |
| 2511.4 | 2512.5 | Vertical fracture, parted |
| 2513.1 | 2513.9 | Vertical fracture, parted |
| 2514.5 | 2515.6 | Vertical fracture, parted |
| 2520.3 | 2521.2 | Vertical fracture, parted |
| 2524.8 | 2526.8 | Vertical fracture, parted |
| 2527.2 | 2528.0 | Vertical fracture, parted |
| 2528.6 | 2529.2 | Vertical fracture, parted |
| 2530.5 | 2531.5 | Vertical fracture, parted |
| 2533.5 | 2534.6 | Vertical fracture, parted |
| 2536.8 | 2540.4 | Vertical fracture, parted |
| 2546.3 | 2546.8 | Vertical fracture, parted |

| From | To | Other Features |
|---|---|---|
| 2491.0 | 2520.0 | Numerous very thin light gray calcareous seams |
| 2524.8 | 2524.8 | Calcareous zone |
| 2534.8 | 2535.0 | Two thin calcareous seams |
| 2536.3 | 2536.3 | Thin calcareous seam |
| 2541.0 | 2541.0 | Thin calcareous seam |
| 2545.3 | 2545.6 | Vertical calcareous filling |
| 2523.7 | 2523.7 | Thin pyrite seam |
| 2524.8 | 2525.0 | Pyrite blebs |

Run #3 (2550-2588.3)

| From | To | Lithologic Description |
|---|---|---|
| 2550.0 | 2553.9 | Medium gray-green shale |
| 2553.9 | 2554.5 | Cross-bedded medium gray siltstone |
| 2554.5 | 2556.3 | Medium gray-green shale |
| 2556.3 | 2556.9 | Medium gray cross-bedded siltstone |
| 2556.9 | 2567.9 | Medium gray-green shale |
| 2567.9 | 2577.6 | Dark gray shale |
| 2577.6 | 2581.7 | Medium gray-green shale with some dark gray bands |
| 2581.7 | 2582.4 | Dark gray shale |
| 2582.4 | 2586.5 | Medium gray-green shale with dark gray bands |
| 2586.5 | 2586.9 | Dark gray shale |
| 2586.9 | 2587.4 | Medium gray-green shale |
| 2587.4 | 2588.0 | Dark gray shale |
| 2588.0 | 2588.3 | Medium gray-green shale |

| From | To | Fractures |
|---|---|---|
| 2551.5 | 2552.4 | Vertical, parted |
| 2557.0 | 2558.2 | Mineralized vertical fracture |
| 2558.5 | 2559.0 | Vertical fracture, parted |
| 2560.8 | 2561.8 | Vertical fracture, parted |
| 2562.4 | 2563.4 | Vertical fracture, parted |
| 2563.6 | 2564.8 | Vertical fracture, parted |
| 2564.8 | 2565.5 | Vertical fracture, parted |
| 2567.6 | 2568.5 | Vertical fracture, parted |
| 2570.0 | 2570.6 | Vertical fracture, parted |
| 2571.2 | 2572.8 | Vertical fracture, parted |
| 2577.9 | 2578.6 | Vertical fracture, parted |
| 2579.8 | 2580.7 | Vertical fracture, parted |
| 2583.3 | 2583.9 | Vertical fracture, parted |
| 2584.2 | 2586.0 | Vertical fracture, parted |
| 2586.7 | 2587.7 | Vertical fracture, parted |

| From | To | Other Features |
|---|---|---|
| 2573.3 | 2573.5 | Two calcareous bands |
| 2576.7 | 2576.7 | One calcareous band |
| 2586.4 | 2586.4 | One calcareous band |

Run #4 (2588.3 to 2646.3)

| From | To | Lithologic Description |
|---|---|---|
| 2588.3 | 2590.6 | Medium dark gray shale with dark gray bands |
| 2590.6 | 2591.4 | Dark gray shale |
| 2591.4 | 2594.3 | Medium dark gray shale |
| 2594.3 | 2595.1 | Dark gray shale |
| 2595.1 | 2595.6 | Medium gray shale |
| 2595.6 | 2596.6 | Medium dark gray shale |
| 2596.6 | 2600.6 | Medium dark gray shale with laminae and cross-beds of argillaceous silt |
| 2600.6 | 2605.8 | Medium gray-green shale |
| 2605.8 | 2607.1 | Dark gray shale |
| 2607.1 | 2608.9 | Medium gray-green shale with numerous dark gray bands |
| 2608.9 | 2612.3 | Dark gray shale |
| 2612.3 | 2613.6 | Medium gray-green shale |
| 2613.6 | 2614.1 | Dark gray shale |
| 2614.1 | 2617.3 | Medium gray-green shale with dark gray bands |
| 2617.3 | 2618.3 | Dark gray shale |
| 2618.3 | 2619.9 | Medium gray-green shale |
| 2619.9 | 2620.5 | Medium gray shale with light gray bands |
| 2620.5 | 2626.1 | Medium gray-green with medium gray bands |
| 2626.1 | 2626.4 | Medium gray, crossbedded, argillaceous siltstone |
| 2626.4 | 2641.3 | Medium gray-green shale with medium gray argillaceous siltstone bands up to .3' thick |
| 2641.3 | 2642.7 | Medium gray-green shale |
| 2642.7 | 2646.3 | Medium gray-green shale with numerous thin gray-green siltstone bands |

| From | To | Fractures |
|---|---|---|
| 2589.3 | 2590.3 | Vertical, parted |
| 2591.2 | 2593.1 | Vertical, parted |
| 2593.3 | 2593.9 | $70^{o}$ inclined, parted |
| 2594.3 | 2596.6 | Vertical, parted |
| 2603.1 | 2605.1 | Vertical, parted |
| 2605.2 | 2606.0 | Vertical, parted |
| 2607.0 | 2608.3 | Vertical, parted |
| 2608.8 | 2609.4 | Vertical, parted |
| 2610.7 | 2611.6 | Vertical, parted |
| 2612.0 | 2612.8 | Vertical, parted |
| 2613.5 | 2619.9 | Vertical, parted |
| 2621.1 | 2621.9 | Vertical, parted |
| 2622.0 | 2623.5 | Vertical, parted |
| 2623.0 | 2626.2 | Vertical, parted |
| 2626.5 | 2627.2 | Vertical, parted |
| 2629.3 | 2630.4 | Vertical, parted |
| 2640.7 | 2643.5 | Vertical, parted |
| 2645.0 | 2646.3 | Vertical, parted |

Run #5 (2646.3 to 2704.8)

| From | To | Lithologic Description |
|---|---|---|
| 2646.3 | 2652.3 | Medium gray-green shale with occasional medium dark gray laminae, and some argillaceous siltstone laminae |
| 2652.3 | 2654.2 | Black shale with argillaceous siltstone laminae |
| 2654.2 | 2654.9 | Medium gray-green shale |
| 2654.9 | 2658.0 | Black shale with several dark gray laminae |
| 2658.0 | 2659.1 | Black shale |
| 2659.1 | 2659.4 | Medium gray shale with one thin dark gray band |
| 2659.4 | 2670.7 | Black shale with numerous dark gray laminae |
| 2670.7 | 2671.6 | Medium gray-green shale with black laminae |
| 2671.6 | 2680.1 | Black shale with occasional medium to dark gray laminae |
| 2680.1 | 2680.4 | Medium gray-green shale with black laminae |
| 2680.4 | 2683.1 | Black shale |
| 2683.1 | 2683.3 | Medium dark gray shale with very fine pyrite laminae |
| 2683.3 | 2692.0 | Black shale with scattered medium gray laminae |
| 2692.0 | 2692.1 | Medium gray green shale |
| 2692.1 | 2698.5 | Black shale with occasional medium gray laminae |
| 2698.5 | 2698.6 | Medium gray green and black laminated shale |
| 2698.6 | 2704.8 | Black shale |

| From | To | Fractures |
|---|---|---|
| 2647.0 | 2649.0 | Vertical, parted |
| 2649.2 | 2650.7 | Vertical, parted |
| 2650.9 | 2651.7 | Vertical, parted |
| 2653.0 | 2656.0 | Vertical, parted |
| 2656.0 | 2657.5 | Vertical, parted |
| 2657.9 | 2660.7 | Vertical, parted |
| 2660.9 | 2661.6 | Vertical, parted |
| 2661.8 | 2662.7 | Vertical, parted |
| 2662.7 | 2664.4 | Vertical, parted |
| 2667.8 | 2668.5 | Vertical, parted |
| 2668.5 | 2671.5 | Vertical, parted |
| 2671.6 | 2674.3 | Vertical, parted |
| 2674.4 | 2677.7 | Vertical, parted |
| 2677.7 | 2677.7 | Slickensided horizontal plane |
| 2678.6 | 2680.9 | Slickensided horizontal plane |
| 2680.9 | 2681.9 | Slickensided horizontal plane |
| 2682.0 | 2683.9 | Slickensided horizontal plane |
| 2684.0 | 2686.6 | Slickensided horizontal plane |
| 2687.0 | 2687.9 | Slickensided horizontal plane |
| 2688.0 | 2688.9 | Slickensided horizontal plane |
| 2688.9 | 2691.7 | Slickensided horizontal plane |
| 2692.5 | 2693.3 | Slickensided horizontal plane |
| 2695.5 | 2697.6 | 3 nearly vertical, parted, overlapping fractures |
| 2698.3 | 2698.5 | Inclined slickensided surface |
| 2701.0 | 2704.3 | 5 nearly-vertical, curved parted surfaces |

Run #5 (Cont.) (2646.3 to 2704.8)

| From | To | Other Features |
|---|---|---|
| 2655.0 | 2670.0 | Scattered pyrite laminae and blebs |
| 2670.0 | 2685.0 | Occasional pyrite laminae |
| 2697.3 | 2697.3 | Large pyrite bleb |

Run #6 (2704.8-2762.8)

| From | To | Lithologic Description |
|---|---|---|
| 2704.8 | 2721.4 | Black shale |
| 2721.4 | 2728.7 | Medium dark gray shale with black laminae |
| 2728.7 | 2735.8 | Black shale |
| 2735.8 | 2741.7 | Medium dark gray shale with black laminae |
| 2741.7 | 2744.7 | Black shale with dark gray laminae |
| 2744.7 | 2749.2 | Black shale with several dark gray laminae |
| 2749.2 | 2762.8 | Black shale with numerous dark gray laminae |

| From | To | Fractures |
|---|---|---|
| 2704.8 | 2705.7 | Vertical, parted |
| 2708.5 | 2711.9 | Vertical, parted |
| 2711.9 | 2725.6 | Vertical, parted |
| 2725.6 | 2725.6 | Horizontal slickensided plane |
| 2725.6 | 2726.4 | Vertical, parted |
| 2727.4 | 2728.2 | Vertical, parted |
| 2728.1 | 2730.6 | Vertical, parted |
| 2730.7 | 2732.5 | Vertical, parted |
| 2733.2 | 2734.0 | Vertical, parted |
| 2734.1 | 2734.9 | Vertical, parted |
| 2736.2 | 2737.6 | Vertical, parted |
| 2738.0 | 2738.8 | Vertical, parted |
| 2740.1 | 2741.4 | Vertical, parted |
| 2741.5 | 2748.8 | Vertical, parted |
| 2762.0 | 2762.8 | Vertical, parted |

| From | To | Other Features |
|---|---|---|
| 2718.8 | 2719.0 | Pyrite blebs |

Run #7 (2762.8-2820.6)

| From | To | Lithologic Description |
|---|---|---|
| 2762.8 | 2773.5 | Black shale with medium dark gray laminae |
| 2773.5 | 2773.6 | Medium gray shale |
| 2773.6 | 2776.8 | Black shale |
| 2776.8 | 2777.0 | Medium gray shale |
| 2777.0 | 2780.2 | Black shale |
| 2780.2 | 2783.3 | Medium gray shale with dark gray laminae |
| 2783.3 | 2786.5 | Black shale with dark gray laminae |
| 2786.5 | 2786.8 | Medium dark gray shale |
| 2786.8 | 2792.4 | Black shale |
| 2792.4 | 2800.7 | Medium dark gray shale with black bands |
| 2800.7 | 2801.0 | Medium gray argillaceous siltstone |
| 2801.0 | 2802.9 | Medium dark gray shale |
| 2802.9 | 2803.2 | Medium gray silty shale |
| 2803.2 | 2803.5 | Medium dark gray shale |
| 2803.5 | 2804.3 | Medium gray shale |
| 2804.3 | 2804.4 | Medium gray silty shale |
| 2804.4 | 2805.1 | Medium dark gray shale |
| 2805.1 | 2805.3 | Medium gray silty shale |
| 2805.3 | 2809.7 | Medium dark gray shale with thin black layers |
| 2809.7 | 2810.2 | Medium gray shale |
| 2810.2 | 2810.4 | "Loading feature" dividing medium gray and medium dark gray shale |
| 2810.4 | 2811.7 | Medium dark gray shale with thin black layers |
| 2811.7 | 2812.2 | Medium gray silty shale |
| 2812.2 | 2817.3 | Medium dark gray shale with thin black and medium gray brown layers |
| 2817.3 | 2818.0 | Medium gray silty shale |
| 2818.0 | 2819.3 | Medium dark gray shale |
| 2819.3 | 2819.6 | Black shale |
| 2819.6 | 2820.0 | Medium gray slightly silty shale |
| 2820.0 | 2820.6 | Medium dark gray shale |

| From | To | Fractures |
|---|---|---|
| 2763.0 | 2768.2 | Vertical, parted |
| 2769.4 | 2770.7 | Vertical, parted |
| 2774.0 | 2775.7 | Vertical, parted |
| 2777.4 | 2778.5 | Vertical, parted |
| 2779.6 | 2782.1 | Vertical, parted |
| 2787.0 | 2788.9 | Vertical, parted |
| 2789.5 | 2790.3 | Vertical, parted |
| 2790.4 | 2795.1 | Vertical, parted |
| 2796.7 | 2797.3 | Vertical, parted |
| 2797.6 | 2799.3 | Vertical, parted |
| 2801.3 | 2802.9 | Vertical, parted |
| 2812.2 | 2813.5 | Vertical, parted |
| 2814.4 | 2816.4 | Vertical, parted |
| 2816.2 | 2817.0 | Vertical, parted |
| 2817.8 | 2819.8 | Vertical, parted |

Run #7 (Cont.) 2762.8-2820.6)

| From | To | Other Features |
|---|---|---|
| 2764.0 | 2772.0 | Pyrite laminae and one large bleb |
| 2797.0 | | Two pyrite laminae |

Run #8 (2820.6-2879.3)

| From | To | Lithologic Description |
|---|---|---|
| 2820.6 | 2823.6 | Medium dark gray shale with thin black bands |
| 2823.6 | 2824.3 | Black shale with medium dark gray laminae |
| 2824.3 | 2829.0 | Medium dark gray shale |
| 2829.0 | 2829.2 | Medium gray and medium dark gray laminated shale |
| 2829.2 | 2830.3 | Medium dark gray shale |
| 2830.3 | 2830.5 | Medium gray shale |
| 2830.5 | 2830.9 | Black shale with medium dark gray laminae |
| 2830.9 | 2831.9 | Medium dark gray shale with three medium dark to black bands |
| 2831.9 | 2833.5 | Medium dark gray shale |
| 2833.5 | 2833.7 | Medium gray silty shale |
| 2833.7 | 2834.1 | Medium dark gray shale |
| 2834.1 | 2834.4 | Medium gray shale with medium gray green laminae |
| 2834.4 | 2838.7 | Medium dark gray shale with several black bands |
| 2838.7 | 2839.0 | Medium gray shale |
| 2839.0 | 2840.8 | Medium dark gray shale |
| 2840.8 | 2840.9 | Medium gray silty shale |
| 2840.9 | 2841.4 | Medium dark gray shale |
| 2841.4 | 2841.5 | Medium gray silty shale |
| 2841.5 | 2841.9 | Medium dark gray shale |
| 2841.9 | 2842.2 | Medium gray silty shale |
| 2842.2 | 2843.1 | Medium dark gray shale |
| 2843.1 | 2843.5 | Black shale with medium dark gray laminae |
| 2843.5 | 2844.9 | Medium dark gray shale with black bands |
| 2844.9 | 2845.3 | Black shale |
| 2845.3 | 2845.7 | Medium dark gray shale |
| 2845.7 | 2846.2 | Black shale with medium gray laminae |
| 2846.2 | 2846.5 | Medium dark gray |
| 2846.5 | 2846.7 | Black shale |
| 2846.7 | 2847.1 | Medium dark gray shale |
| 2847.1 | 2847.4 | Black shale with medium dark gray laminae |
| 2847.4 | 2848.1 | Medium dark gray shale |
| 2848.1 | 2848.9 | Black shale with medium dark gray laminae |
| 2848.9 | 2849.7 | Medium dark gray shale |
| 2849.7 | 2850.0 | Medium dark gray and medium gray banded shale |
| 2850.0 | 2850.7 | Medium dark gray shale |
| 2850.7 | 2851.0 | Medium gray silty shale |
| 2851.0 | 2851.3 | Medium dark gray shale |
| 2851.3 | 2851.5 | Medium dark gray and dark gray laminated shale |
| 2851.5 | 2851.8 | Medium dark gray shale |
| 2851.8 | 2852.0 | Medium gray shale |
| 2852.0 | 2852.2 | Medium dark gray shale |
| 2852.2 | 2852.3 | Dark gray shale |
| 2852.3 | 2852.7 | Medium dark gray shale |
| 2852.7 | 2855.8 | Medium dark gray shale with dark gray and black bands |
| 2855.8 | 2856.9 | Dark gray and medium dark gray laminated shale |
| 2856.9 | 2857.9 | Medium dark gray shale with dark gray bands |
| 2857.9 | 2858.5 | Dark gray and medium dark gray laminated shale |
| 2858.5 | 2861.5 | Medium dark gray shale with dark gray bands |
| 2861.5 | 2862.6 | Dark gray shale with medium dark gray laminae |
| 2862.6 | 2862.9 | Medium dark gray shale |

Run #8 (Cont.) (2820.6-2879.3)

| From | To | Lithologic Description |
|---|---|---|
| 2862.9 | 2864.1 | Dark gray and medium dark gray laminated shale |
| 2864.1 | 2865.1 | Black shale |
| 2865.1 | 2866.5 | Medium dark gray shale |
| 2866.5 | 2867.5 | Black shale with medium dark gray laminae |
| 2867.5 | 2867.9 | Medium dark gray shale |
| 2867.9 | 2879.3 | Black shale with medium dark gray laminae |

| From | To | Fractures |
|---|---|---|
| 2820.6 | 2822.0 | Vertical, parted |
| 2821.8 | 2824.6 | Vertical, parted |
| 2824.7 | 2825.7 | Vertical, parted |
| 2825.7 | 2829.0 | Vertical, parted |
| 2829.0 | 2830.4 | Vertical, parted |
| 2831.9 | 2833.5 | Vertical, parted |
| 2834.2 | 2838.6 | Vertical, parted |
| 2839.2 | 2842.2 | Vertical, parted |
| 2842.2 | 2847.5 | Vertical, parted |
| 2847.9 | 2855.3 | Vertical, parted |
| 2855.4 | 2860.0 | Vertical, parted |
| 2859.9 | 2862.7 | Vertical, parted |
| 2863.6 | 2864.9 | Vertical, parted |
| 2865.1 | 2866.3 | Vertical, parted |
| 2867.8 | 2869.2 | Parted, curved, surface |
| 2869.2 | 2870.6 | Parted, curved, surface |
| 2871.0 | 2875.3 | Vertical, parted |
| 2876.0 | 2879.3 | Vertical, parted |

| From | To | Other Features |
|---|---|---|
| 2869.8 | 2869.8 | Pyrite bleb |
| 2866.3 | 2866.3 | Carbonate layer |

Run #9 (2879.3 to 2939.0)

| From | To | Lithologic Description |
|---|---|---|
| 2879.3 | 2893.6 | Black shale with medium and dark gray laminae |
| 2893.6 | 2893.8 | Medium gray shale |
| 2893.8 | 2894.6 | Black shale with medium and dark gray bands |
| 2894.6 | 2896.5 | Medium gray shale with dark gray and black bands |
| 2896.5 | 2898.3 | Black shale with dark gray bands |
| 2898.3 | 2899.1 | Medium dark gray shale |
| 2899.1 | 2899.5 | Black shale with medium dark gray laminae |
| 2899.5 | 2901.7 | Medium dark gray shale with occasional black bands |
| 2901.7 | 2902.1 | Black shale |
| 2902.1 | 2902.4 | Medium dark gray shale |
| 2902.4 | 2902.7 | Black shale |
| 2902.7 | 2903.3 | Black shale with medium dark gray laminae |
| 2903.3 | 2903.8 | Medium dark gray shale |
| 2903.8 | 2904.0 | Black shale |
| 2904.0 | 2904.3 | Medium dark gray shale |
| 2904.3 | 2904.5 | Black shale |
| 2904.5 | 2904.8 | Medium dark gray shale |
| 2904.8 | 2905.0 | Black shale |
| 2905.0 | 2906.0 | Medium dark gray shale |
| 2906.0 | 2906.1 | Dark gray shale |
| 2906.1 | 2906.5 | Medium dark gray shale |
| 2906.5 | 2906.9 | Dark gray shale |
| 2906.9 | 2907.1 | Medium dark gray shale |
| 2907.1 | 2907.3 | Dark gray shale |
| 2907.3 | 2908.3 | Medium dark gray shale with occasional dark gray bands |
| 2908.3 | 2920.5 | Black shale with medium dark gray laminae |
| 2920.5 | 2920.7 | Medium gray and black laminated shale divided by "loading structure" |
| 2920.7 | 2928.2 | Black with medium gray laminae |
| 2928.2 | 2934.7 | Medium dark gray shale with black bands and occasional slightly silty medium gray bands |
| 2934.7 | 2934.8 | Medium gray argillaceous siltstone |
| 2934.8 | 2936.7 | Medium dark gray shale with occasional black bands |
| 2936.7 | 2937.1 | Black shale |
| 2937.1 | 2939.0 | Medium dark gray shale with occasional black bands |

| From | To | Fractures |
|---|---|---|
| 2879.3 | 2880.1 | Vertical, parted |
| 2882.0 | 2883.4 | Vertical, parted |
| 2884.0 | 2886.8 | Vertical, parted |
| 2886.8 | 2886.8 | Mineralized horizontal fracture |
| 2886.8 | 2888.2 | Vertical, parted |
| 2888.4 | 2889.2 | Vertical, parted |
| 2889.6 | 2899.1 | Vertical, parted |
| 2901.4 | 2902.2 | Vertical, parted |

Run #9 (Cont.) (2879.3 to 2939.0)

| From | To | Fractures |
|---|---|---|
| 2902.4 | 2904.3 | Vertical, parted |
| 2904.3 | 2904.3 | Mineralized horizontal fracture |
| 2904.3 | 2905.7 | Vertical, parted |
| 2905.5 | 2906.3 | Vertical, parted |
| 2906.4 | 2909.3 | Vertical, parted |
| 2911.2 | 2913.5 | Vertical, parted |
| 2914.1 | 2918.9 | Vertical, parted |
| 2929.0 | 2930.2 | Vertical, parted |
| 2930.3 | 2932.4 | Vertical, parted |
| 2933.0 | 2934.0 | Vertical, parted |
| 2935.7 | 2939.0 | Vertical, parted |

| From | To | Other Features |
|---|---|---|
| 2894.0 | 2894.4 | Pyrite blebs and layers |
| 2900.8 | 2900.8 | Pyrite layer |
| 2913.5 | 2913.9 | Pyrite blebs |
| 2916.5 | 2916.5 | Pyrite blebs |
| 2919.7 | 2919.7 | Pyrite blebs |
| 2934.0 | 2934.0 | Pyrite blebs |

Run #10 (2939.0-2997.5)

| From | To | Lithologic Description |
|---|---|---|
| 2939.0 | 2940.0 | Medium dark gray shale with black bands |
| 2940.0 | 2940.8 | Black shale |
| 2940.8 | 2941.3 | Medium dark gray shale |
| 2941.3 | 2941.9 | Black shale |
| 2941.9 | 2942.2 | Medium dark gray shale |
| 2942.2 | 2943.1 | Black shale |
| 2943.1 | 2943.5 | Medium dark gray shale |
| 2943.5 | 2948.5 | Black shale with several medium gray and medium dark gray bands |
| 2948.5 | 2951.1 | Medium dark gray with several black bands |
| 2951.1 | 2951.8 | Black shale |
| 2951.8 | 2953.5 | Medium gray shale with black bands |
| 2953.5 | 2953.6 | Medium gray silty shale |
| 2953.6 | 2954.5 | Medium dark gray shale with several black bands |
| 2954.5 | 2954.6 | Medium gray silty shale |
| 2954.6 | 2955.9 | Medium dark gray with several dark bands |
| 2955.9 | 2956.0 | Medium gray silty shale |
| 2956.0 | 2958.0 | Medium dark gray shale with several black bands |
| 2958.0 | 2962.3 | Black shale |
| 2962.3 | 2962.4 | Medium dark gray shale |
| 2962.4 | 2976.7 | Black shale |
| 2976.7 | 2976.8 | Medium dark gray shale |
| 2976.8 | 2977.2 | Black shale |
| 2977.2 | 2977.5 | Medium dark gray shale with several distorted black laminae |
| 2977.5 | 2978.3 | Black shale |
| 2978.3 | 2980.0 | Alternating bands of black and medium dark gray shale (many at 70° to 80° from vertical) |
| 2980.0 | 2980.6 | Black shale |
| 2980.6 | 2981.4 | Medium dark gray shale with several distorted black laminae |
| 2981.4 | 2982.0 | Black shale |
| 2982.0 | 2982.6 | Medium dark gray shale |
| 2982.6 | 2982.7 | Black shale |
| 2982.7 | 2983.3 | Medium dark gray shale |
| 2983.3 | 2983.7 | Black shale |
| 2983.7 | 2984.7 | Medium dark gray shale |
| 2984.7 | 2985.4 | Black shale |
| 2985.4 | 2985.9 | Medium gray shale |
| 2985.9 | 2987.1 | Black shale |
| 2987.1 | 2987.2 | Medium dark gray shale |
| 2987.2 | 2990.4 | Black shale |
| 2990.4 | 2990.6 | Medium dark gray shale |
| 2990.6 | 2997.5 | Black shale |

| From | To | Fractures |
|---|---|---|
| 2939.0 | 2939.6 | Vertical, parted |
| 2941.0 | 2943.6 | Vertical, parted |
| 2946.6 | 2948.6 | Vertical, parted |

Run #10 (2939.0-2997.5) (Cont.)

| From | To | Fractures |
|---|---|---|
| 2948.6 | 2952.0 | Vertical, parted |
| 2954.6 | 2954.6 | Mineralized horizontal joint |
| 2957.0 | 2957.9 | Vertical, parted |
| 2958.4 | 2959.6 | Vertical, parted |
| 2963.0 | 2964.2 | Vertical, parted |
| 2966.8 | 2968.6 | Vertical, parted |
| 2968.6 | 2978.4 | Vertical, parted |
| 2978.3 | 2980.8 | Vertical, parted |
| 2980.8 | 2990.0 | 2 Slickensided 45$^{o}$ joints |
| 2981.0 | 2988.4 | 2 Slickensided 45$^{o}$ joints |
| 2988.2 | 2989.0 | 2 Slickensided 45$^{o}$ joints |
| 2989.0 | 2990.4 | 2 Slickensided 45$^{o}$ joints |
| 2991.5 | 2993.8 | 70$^{o}$ inclined, parted |
| 2993.6 | 2997.5 | 70$^{o}$ inclined, parted |

| From | To | Fractures |
|---|---|---|
| 2939.0 | 2942.0 | Abundant pyrite blebs |
| 2944.0 | 2948.0 | Scattered pyrite blebs |
| 2958.0 | 2978.0 | Pyrite blebs |
| 2978.5 | 2978.6 | Large pyrite nodule |
| 2981.5 | 2987.0 | Pyrite blebs in black shale zones |
| 2991.5 | 2997.0 | Large pyrite nodule and blebs |
| 2988.7 | 2988.7 | Discrete black organic substance |

Run #11 (2997.5-3047.8)

| From | To | Lithologic Description |
|---|---|---|
| 2997.5 | 3001.4 | Medium dark gray shale with medium gray and black bands |
| 3001.4 | 3002.2 | Black shale |
| 3002.2 | 3002.3 | Medium dark gray and black shale separated by "loading structure" |
| 3002.3 | 3002.8 | Medium dark gray shale |
| 3002.8 | 3004.2 | Medium gray shale |
| 3004.2 | 3004.7 | Black shale with medium dark gray laminae |
| 3004.7 | 3007.8 | Medium gray shale |
| 3007.8 | 3008.3 | Black shale |
| 3008.3 | 3009.0 | Medium dark gray and medium gray shale with "loading feature" |
| 3009.0 | 3009.3 | Medium dark gray shale |
| 3009.3 | 3011.6 | Very dark gray shale |
| 3011.6 | 3011.9 | Dark gray and medium dark gray shale with "loading structure" |
| 3011.9 | 3014.0 | Black shale |
| 3014.0 | 3014.1 | Medium gray shale |
| 3014.1 | 3016.3 | Black shale |
| 3016.3 | 3016.6 | Medium dark gray shale with dark gray and black bands showing loading structure |
| 3016.6 | 3017.1 | Black shale |
| 3017.1 | 3017.4 | Black shale with medium dark gray bands and "loading structure" |
| 3017.4 | 3018.2 | Black shale |
| 3018.2 | 3018.7 | Black shale with medium dark gray band showing "loading structure" |
| 3018.7 | 3019.4 | Black shale |
| 3019.4 | 3019.5 | Medium gray shale |
| 3019.5 | 3019.8 | Black shale |
| 3019.8 | 3020.5 | Medium dark gray shale with medium gray and black layers showing "loading structure" |
| 3020.5 | 3022.3 | Medium dark gray and black banded shale |
| 3022.3 | 3022.5 | Black and medium dark gray shale with "loading structure" |
| 3022.5 | 3022.8 | Black shale |
| 3022.8 | 3022.9 | Medium dark gray and black laminated shale |
| 3022.9 | 3024.0 | Black shale |
| 3024.0 | 3024.1 | Dark gray and black shale with contorted bedding |
| 3024.1 | 3025.2 | Black shale |
| 3025.2 | 3026.2 | Medium gray shale |
| 3026.2 | 3026.5 | Medium gray and dark gray shale with contorted bedding |
| 3026.5 | 3027.1 | Black shale |
| 3027.1 | 3029.6 | Medium gray shale |
| 3029.6 | 3029.8 | Medium dark gray and black banded shale |
| 3029.8 | 3030.5 | Black shale |
| 3030.5 | 3031.0 | Medium dark gray shale with several black bands |
| 3031.0 | 3031.5 | Black shale |
| 3031.5 | 3031.6 | Medium dark gray shale |
| 3031.6 | 3031.9 | Black shale |
| 3031.9 | 3032.3 | Medium gray shale |
| 3032.3 | 3032.4 | Black shale |

Run #11 (2997.8-3047.8) (Cont.)

| From | To | Lithologic Description |
|---|---|---|
| 3032.4 | 3033.1 | Medium gray shale |
| 3033.1 | 3033.3 | Black, medium gray, and medium dark gray banded shale with contorted bedding black bands at 60° to vertical |
| 3033.3 | 3034.2 | Medium gray and medium dark gray banded shale with fine black, irregular streaks, contorted bedding |
| 3034.2 | 3036.8 | Medium gray shale |
| 3036.8 | 3037.6 | Medium gray calcareous shale |
| 3037.6 | 3038.5 | Black shale |
| 3038.5 | 3038.9 | Medium dark gray shale |
| 3038.9 | 3039.2 | Black shale |
| 3039.2 | 3039.6 | Medium dark gray shale |
| 3039.6 | 3040.8 | Black shale |
| 3040.8 | 3040.9 | Medium dark gray shale |
| 3040.9 | 3043.2 | Black shale |
| 3043.2 | 3043.3 | Medium dark gray and black shale with contorted bedding |
| 3043.3 | 3047.8 | Black shale |

| From | To | Fractures |
|---|---|---|
| 2997.5 | 3000.0 | Vertical, parted |
| 3000.0 | 3000.8 | Vertical, parted |
| 3001.6 | 3007.5 | Vertical, parted |
| 3007.7 | 3008.9 | Vertical, parted |
| 3009.1 | 3014.7 | Vertical, parted |
| 3015.3 | 3019.8 | Vertical, parted |
| 3020.7 | 3026.1 | Vertical, parted |
| 3026.1 | 3027.2 | Vertical, parted |
| 3027.2 | 3036.3 | Vertical, parted |
| 3037.6 | 3047.8 | |

| From | To | Other Features |
|---|---|---|
| 3112.0 | 3114.0 | Pyrite blebs |
| 3120.4 | 3120.5 | Large pyrite nodule |
| 3122.8 | 3124.0 | Pyrite blebs |
| 3033.1 | 3033.3 | Pyrite blebs |
| 3041.3 | 3041.4 | Large pyrite nodule |
| 3036.8 | 3037.5 | Calcareous zone |

Run #12 (3047.8-3105.3)

| From | To | Lithologic Description |
|---|---|---|
| 3047.8 | 3049.4 | Black shale with medium dark gray laminae |
| 3049.4 | 3049.5 | Medium dark gray shale |
| 3049.5 | 3057.9 | Medium dark gray shale with black and medium gray laminae |
| 3057.9 | 3058.0 | Medium dark gray and dark gray shale with contorted bedding |
| 3058.0 | 3063.1 | Medium dark gray shale with black laminae |
| 3063.1 | 3064.9 | Black shale |
| 3064.9 | 3066.0 | Medium dark gray and black shale with contorted bedding |
| 3066.0 | 3067.7 | Black shale |
| 3067.7 | 3068.1 | Medium dark gray and dark gray shale with contorted bedding |
| 3068.1 | 3069.2 | Black shale with occasional gray laminae |
| 3069.2 | 3069.3 | Black and medium dark gray shale with contorted bedding |
| 3069.3 | 3075.7 | Black shale |
| 3075.7 | 3076.1 | Medium dark gray and dark gray laminated shale |
| 3076.1 | 3078.7 | Black shale |
| 3078.7 | 3080.4 | Medium gray shale with some dark gray bands |
| 3080.4 | 3080.6 | Medium dark gray shale |
| 3080.6 | 3083.1 | Medium dark gray and dark gray laminated shale |
| 3083.1 | 3084.2 | Black shale with dark gray laminae |
| 3084.2 | 3084.9 | Medium dark gray and dark gray laminated shale |
| 3084.9 | 3085.1 | Black shale |
| 3085.1 | 3085.7 | Medium dark gray and dark gray laminated shale |
| 3085.7 | 3088.3 | Black shale |
| 3088.3 | 3088.5 | Medium dark gray and black shale with contorted bedding |
| 3088.5 | 3088.9 | Black shale |
| 3088.9 | 3089.2 | Medium dark gray and dark gray laminated shale |
| 3089.2 | 3089.7 | Black shale |
| 3089.7 | 3089.9 | Medium dark gray shale |
| 3089.9 | 3090.7 | Black shale |
| 3090.7 | 3090.8 | Medium dark gray shale |
| 3090.8 | 3092.1 | Black shale |
| 3092.1 | 3092.3 | Medium dark gray and black shale with contorted bedding |
| 3092.3 | 3092.6 | Black shale |
| 3092.6 | 3092.8 | Medium dark gray and dark gray laminated shale |
| 3092.8 | 3101.7 | Black shale |
| 3101.7 | 3102.1 | Medium dark gray and dark gray laminated shale |
| 3102.1 | 3102.7 | Black shale with dark gray laminae |
| 3102.7 | 3102.9 | Medium dark and dark gray laminated shale |
| 3102.9 | 3105.3 | Black shale |

| From | To | Fractures |
| --- | --- | --- |
| 3047.8 | 3049.1 | Vertical, parted |
| 3049.7 | 3053.5 | Vertical, parted |
| 3053.9 | 3058.2 | Vertical, parted |
| 3058.3 | 3059.6 | Vertical, parted |
| 3063.6 | 3065.0 | Vertical, parted |
| 3065.3 | 3066.0 | Vertical, parted |
| 3066.0 | 3067.0 | Vertical, parted |
| 3068.8 | 3069.6 | Vertical, parted |
| 3070.0 | 3071.6 | Vertical, parted |
| 3071.8 | 3082.8 | Vertical, parted |
| 3083.1 | 3084.2 | Vertical, parted |
| 3085.7 | 3089.8 | Vertical, parted |
| 3090.0 | 3092.2 | Vertical, parted |
| 3092.8 | 3098.8 | Vertical, parted |
| 3100.7 | 3104.6 | Vertical, parted |

| From | To | Other Features |
| --- | --- | --- |
| 3047.8 | 3049.0 | Pyrite blebs |
| 3066.0 | 3067.3 | Pyrite blebs |
| 3068.4 | 3068.5 | Two pyrite laminae |
| 3070.5 | 3074.0 | Pyrite blebs |
| 3086.0 | 3087.8 | Pyrite blebs |
| 3094.1 | 3094.1 | Pyrite laminae |
| 3195.9 | 3095.9 | Pyrite blebs |
| 3097.4 | 3097.4 | Pyrite blebs |
| 3090.0 | | Calcareous band |

Run #13 (3105.3-3164.1

| From | To | Lithologic Description |
|---|---|---|
| 3105.3 | 3105.8 | Dark gray and medium dark gray laminated shale with contorted bedding |
| 3105.8 | 3118.6 | Black shale with several dark gray laminae |
| 3118.6 | 3119.0 | Medium gray green and dark gray laminated shale |
| 3119.0 | 3119.2 | Black and dark gray laminated shale |
| 3119.2 | 3120.1 | Medium gray-green and dark gray laminated shale |
| 3120.1 | 3120.8 | Black shale |
| 3120.8 | 3122.0 | Medium gray-green shale |
| 3122.0 | 3123.2 | Black shale |
| 3123.2 | 3130.2 | Medium gray-green shale with occasional dark gray laminae |
| 3130.2 | 3130.6 | Medium gray argillaceous siltstone |
| 3130.6 | 3135.9 | Medium gray-green shale with numerous dark group laminae |
| 3135.9 | 3136.2 | Black shale with some gray-green laminae |
| 3136.2 | 3149.0 | Medium dark gray-green shale with dark gray laminae |
| 3149.0 | 3151.5 | Medium gray argillaceous siltstone |
| 3151.5 | 3156.4 | Medium gray-green shale with dark gray laminae |
| 3156.4 | 3157.2 | Black shale |
| 3157.2 | 3158.7 | Medium dark gray-green shale with dark gray laminae |
| 3158.7 | 3159.9 | Medium gray-green slightly silty shale |
| 3159.9 | 3162.7 | Medium dark gray-green shale with dark gray laminae |
| 3162.7 | 3164.1 | Medium dark gray-green slightly silty shale |

| From | To | Fractures |
|---|---|---|
| 3105.8 | 3108.5 | Vertical, parted |
| 3108.4 | 3111.6 | Vertical, parted |
| 3112.0 | 3116.5 | Vertical, parted |
| 3116.5 | 3117.6 | Vertical, parted |
| 3117.6 | 3121.3 | Vertical, parted |
| 3119.8 | 3120.3 | Slickensided surface 40$^{o}$ from vertical |
| 3121.7 | 3123.7 | Vertical, parted |
| 3126.5 | 3129.2 | Vertical, parted |
| 3129.2 | 3140.2 | Vertical, parted |
| 3140.4 | 3141.6 | Vertical, parted |
| 3141.7 | 3142.5 | Vertical, parted |
| 3142.7 | 3143.5 | Vertical, parted |
| 3143.9 | 3144.5 | Vertical, parted |
| 3144.4 | 3147.3 | Vertical, parted |
| 3147.5 | 3150.4 | Vertical, parted |

Run #13 (3105.3-3164.1) cont'd.

| From | To | Fractures |
|---|---|---|
| 3150.8 | 3151.3 | Mineralized vertical fracture |
| 3151.7 | 3158.4 | Vertical, parted |
| 3159.6 | 3161.2 | Vertical, parted |
| 3161.5 | 3162.2 | Vertical, parted |

| From | To | Other Features |
|---|---|---|
| 3122.8 | 3122.9 | Calcareous horizontal filling |
| 3123.2 | 3130.2 | Slightly calcareous zone |
| 3149.0 | 3151.5 | Calcareous zone |
| 3106.0 | 3108.0 | Pyrite blebs |
| 3117.5 | 3117.5 | Pyrite nodule |
| 3158.4 | 3158.5 | Pyrite blebs |
| 3154.0 | 3154.0 | Discrete black organic layer |
| 3156.6 | 3156.6 | Discrete black organic layer |

Run #14 (3164.1-3221.0)

| From | To | Lithologic Description |
|---|---|---|
| 3164.1 | 3168.5 | Medium gray green with dark gray laminae |
| 3168.5 | 3169.0 | Dark gray shale |
| 3169.0 | 3172.1 | Medium gray green shale |
| 3172.1 | 3172.4 | Dark gray shale |
| 3172.4 | 3174.7 | Dark gray-green shale |
| 3174.7 | 3175.3 | Medium gray-green shale |
| 3175.3 | 3175.6 | Medium gray shale |
| 3175.6 | 3178.2 | Medium gray-green shale |
| 3178.2 | 3178.4 | Very dark gray shale |
| 3178.4 | 3183.0 | Medium gray-green shale |
| 3183.0 | 3186.2 | Light gray-green shale |
| 3186.2 | 3187.1 | Very dark gray shale |
| 3187.1 | 3188.4 | Medium gray-green shale |
| 3188.4 | 3188.7 | Light gray-green shale |
| 3188.7 | 3189.7 | Medium gray-green shale |
| 3189.7 | 3189.9 | Very dark gray shale |
| 3189.9 | 3192.4 | Medium gray-green shale |
| 3192.4 | 3192.5 | Very dark gray shale |
| 3192.5 | 3193.1 | Medium gray-green shale |
| 3193.1 | 3193.9 | Light gray-green shale |
| 3193.9 | 3197.1 | Medium gray-green shale |
| 3197.1 | 3198.5 | Medium gray-green shale with dark gray laminae |
| 3198.5 | 3198.9 | Medium gray-green shale |
| 3198.9 | 3199.1 | Very dark gray shale |
| 3199.1 | 3201.1 | Medium gray-green shale |
| 3201.1 | 3202.1 | Medium gray-green and dark gray laminated shale |
| 3202.1 | 3205.5 | Medium gray-green shale |
| 3205.5 | 3206.3 | Very dark gray shale |
| 3206.3 | 3208.8 | Medium gray-green shale |
| 3208.8 | 3208.9 | Very dark gray shale |
| 3208.9 | 3209.3 | Medium gray-green shale |
| 3209.3 | 3210.3 | Medium gray shale |
| 3210.3 | 3210.5 | Dark gray shale |
| 3210.5 | 3211.0 | Medium gray shale |
| 3211.0 | 3211.4 | Light gray argillaceous siltstone |
| 3211.4 | 3212.0 | Medium dark gray shale |
| 3212.0 | 3212.4 | Medium dark gray shale |
| 3212.4 | 3214.4 | Medium gray shale |
| 3214.4 | 3214.5 | Dark gray shale |
| 3214.5 | 3216.7 | Medium gray shale |
| 3216.7 | 3218.2 | Black shale |
| 3218.2 | 3221.0 | Medium gray shale |

| From | To | Fractures |
|---|---|---|
| 3181.7 | 3182.8 | Vertical, parted |
| 3183.8 | 3185.5 | Vertical, parted |
| 3186.0 | 3187.9 | Vertical, parted |

Run #14 (3164.1-3221.0) cont'd

| From | To | Fractures |
|---|---|---|
| 3194.7 | 3195.5 | Vertical, parted |
| 3195.7 | 3201.9 | Zone of closely-spaced, small inclined fractures |
| 3212.0 | 3217.0 | Zone of closely-spaced, small inclined fractures |
| 3217.5 | 3217.5 | Slickensided $60^{o}$ surface |

| From | To | Other Features |
|---|---|---|
| 3175.3 | 3175.4 | Very calcareous zone |
| 3181.3 | 3181.5 | Very calcareous zone |
| 3182.9 | 3183.0 | Very calcareous zone |
| 3183.7 | 3183.8 | Very calcareous zone |
| 3188.4 | 3188.6 | Very calcareous zone |
| 3193.1 | 3193.9 | Very calcareous zone |
| 3204.7 | 3204.7 | Very calcareous layer |
| 3207.3 | 3207.3 | Very calcareous layer |
| 3207.8 | 3207.8 | Very calcareous layer |
| 3211.0 | 3211.4 | Calcareous zone |
| 3211.8 | 3212.0 | Calcareous zone |
| 3213.3 | 3213.5 | Very calcareous zone |
| 3205.9 | 3205.9 | Pyrite nodule |
| 3218.0 | 3218.0 | Pyrite nodule |

Run #15 (3221-3280.5)

| From | To | Lithologic Description |
|---|---|---|
| 3221.0 | 3225.5 | Medium gray-green shale with many dark gray bands |
| 3225.5 | 3225.7 | Very dark gray shale |
| 3225.7 | 3225.8 | Medium gray-green shale |
| 3225.8 | 3226.7 | Very dark gray shale |
| 3226.7 | 3229.3 | Medium gray-green shale |
| 3229.3 | 3229.7 | Dark gray shale |
| 3229.7 | 3230.9 | Medium gray-green shale |
| 3230.9 | 3231.2 | Light gray-green shale |
| 3231.2 | 3233.1 | Dark gray and medium dark gray banded shale |
| 3233.1 | 3238.2 | Medium gray-green shale |
| 3238.2 | 3238.7 | Very dark gray shale |
| 3238.7 | 3239.8 | Medium gray-green shale |
| 3239.8 | 3239.9 | Light gray shale |
| 3239.9 | 3244.1 | Medium gray-green shale |
| 3244.1 | 3244.7 | Dark gray and medium gray-green banded shale |
| 3244.7 | 3248.2 | Medium gray-green shale |
| 3248.2 | 3249.4 | Very dark gray shale |
| 3249.4 | 3251.0 | Medium gray green shale |
| 3251.0 | 3252.0 | Medium gray-green and dark gray banded shale |
| 3252.0 | 3255.0 | Medium gray-green shale |
| 3255.0 | 3256.0 | Medium gray-green and dark gray banded |
| 3256.0 | 3261.0 | Medium gray-green shale |
| 3261.0 | 3261.6 | Dark gray shale |
| 3261.6 | 3265.8 | Medium gray-green shale |
| 3265.8 | 3266.5 | Dark gray shale |
| 3266.5 | 3270.3 | Medium gray green shale |
| 3270.3 | 3271.3 | Medium gray-green and dark gray banded |
| 3271.3 | 3271.8 | Dark gray shale |
| 3271.8 | 3273.3 | Medium gray-green shale |
| 3273.3 | 3274.9 | Medium gray-green and dark gray banded shale |
| 3274.9 | 3276.3 | Dark gray |
| 3276.3 | 3276.9 | Medium green-gray shale |
| 3276.9 | 3280.5 | Medium dark gray shale |

| From | To | Fractures |
|---|---|---|
| 3221.0 | 3226.4 | Small, closely spaced fractures |
| 3226.7 | 3228.1 | Vertical, parted |
| 3229.3 | 3230.1 | Vertical, parted |
| 3230.0 | 3230.8 | Vertical, parted |
| 3231.4 | 3234.5 | Small, closely spaced fractures |
| 3235.5 | 3240.3 | Vertical, parted |
| 3243.2 | 3244.2 | Vertical, parted |
| 3247.5 | 3248.2 | Vertical, parted |
| 3248.7 | 3249.8 | Vertical, parted |
| 3250.8 | 3251.7 | Vertical, parted |
| 3255.0 | 3256.0 | Vertical, parted |
| 3260.0 | 3261.6 | Vertical, parted |
| 3264.8 | 3265.5 | Vertical, parted |

Run #15 (3221-3280.5) cont'd

| From | To | |
|---|---|---|
| 3265.8 | 3267.0 | Vertical, parted |
| 3278.4 | 3279.6 | Vertical, parted |

| From | To | Other Features |
|---|---|---|
| 3230.9 | 3231.2 | Very calcareous layer |
| 3239.8 | 3239.9 | Very calcareous layer |
| 3267.4 | 3267.4 | Very calcareous layer |
| 3267.8 | 3267.8 | Very calcareous layer |
| 3278.3 | 3278.3 | Very calcareous layer |
| 3279.4 | 3279.4 | Very calcareous layer |

Run #16 (3280.5-3318.5)

| From | To | Lithologic Description |
|---|---|---|
| 3280.5 | 3281.2 | Medium gray-green shale |
| 3281.2 | 3281.5 | Very dark gray shale |
| 3281.5 | 3283.0 | Medium gray-green shale |
| 3283.0 | 3283.9 | Medium gray-green and dark gray laminated shale |
| 3283.9 | 3284.8 | Medium gray-green shale |
| 3284.8 | 3285.3 | Very dark gray and medium gray-green laminated shale |
| 3285.3 | 3285.7 | Very dark gray shale |
| 3285.7 | 3285.8 | Medium gray-green shale |
| 3285.8 | 3286.0 | Very dark gray shale |
| 3286.0 | 3287.2 | Medium gray-green shale |
| 3287/2 | 3288.1 | Very dark gray shale |
| 3288.1 | 3288.9 | Medium gray-green and very dark gray laminated shale |
| 3288.9 | 3289.9 | Very dark gray shale |
| 3289.9 | 3290.9 | Medium gray-green shale |
| 3290.9 | 3291.5 | Very dark gray shale |
| 3291.5 | 3294.9 | Medium gray-green shale |
| 3294.9 | 3295.3 | Very dark gray shale |
| 3295.3 | 3297.1 | Medium gray-green shale |
| 3297.1 | 3297.2 | Black shale |
| 3297.2 | 3298.5 | Medium gray-green shale |
| 3298.5 | 3299.6 | Dark gray-green shale |
| 3299.6 | 3300.1 | Very dark gray shale |
| 3300.1 | 3301.7 | Dark gray-green shale |
| 3301.7 | 3302.0 | Very dark gray shale |
| 3302.0 | 3302.8 | Medium gray-green shale |
| 3302.8 | 3304.6 | Dark gray-green shale |
| 3304.6 | 3304.9 | Very dark gray shale |
| 3304.9 | 3305.5 | Medium gray-green shale |
| 3305.5 | 3308.2 | Dark gray-green shale |
| 3308.2 | 3308.4 | Very dark gray shale |
| 3308.4 | 3309.0 | Dark gray-green shale |
| 3309.0 | 3309.3 | Very dark gray shale |
| 3309.3 | 3313.0 | Dark gray-green shale |
| 3313.0 | 3313.4 | Very dark gray shale |
| 3313.4 | 3315.0 | Dark gray-green shale |
| 3315.0 | 3315.2 | Very dark gray shale |
| 3315.2 | 3315.9 | Medium gray shale |
| 3315.9 | 3316.4 | Very dark gray shale |
| 3316.4 | 3317.0 | Medium gray shale |
| 3317.0 | 3317.4 | Very dark gray and black shale |
| 3317.4 | 3320.0 | Medium gray shale |

| From | To | Fractures |
|---|---|---|
| 3304.3 | 3305.9 | Vertical, parted |

Run #17 (3320.0-3379.1)

| From | To | Lithologic Description |
|---|---|---|
| 3320.0 | 3323.1 | Medium gray-green shale |
| 3323.1 | 3324.4 | Dark gray shale |
| 3324.4 | 3327.8 | Medium gray-green shale |
| 3327.8 | 3329.3 | Dark gray shale |
| 3329.3 | 3330.7 | Medium gray-green shale |
| 3330.7 | 3330.9 | Dark gray shale |
| 3330.9 | 3334.7 | Medium gray shale |
| 3334.7 | 3335.1 | Dark gray shale |
| 3335.1 | 3337.5 | Medium gray shale |
| 3337.5 | 3339.5 | Dark gray shale |
| 3339.5 | 3340.5 | Medium gray shale |
| 3340.5 | 3344.2 | Medium gray-green shale |
| 3344.2 | 3344.3 | Light gray argillaceous limestone |
| 3344.3 | 3344.4 | Dark gray-green shale |
| 3344.4 | 3346.5 | Dark gray shale |
| 3346.5 | 3348.5 | Dark gray-green shale |
| 3348.5 | 3349.0 | Medium gray-green shale |
| 3349.0 | 3350.0 | Medium gray shale |
| 3350.0 | 3350.4 | Dark gray-green shale |
| 3350.4 | 3351.6 | Medium and dark gray-green shale |
| 3351.6 | 3351.7 | Medium gray shale |
| 3351.7 | 3354.5 | Medium gray-green and dark gray laminated shale |
| 3354.5 | 3357.2 | Very dark gray and dark gray-green laminated shale |
| 3357.2 | 3357.3 | Medium gray shale |
| 3357.3 | 3360.9 | Very dark gray shale |
| 3360.9 | 3363.2 | Very dark gray to black shale |
| 3363.2 | 3364.5 | Very dark gray shale |
| 3364.5 | 3365.1 | Black shale |
| 3365.1 | 3366.5 | Very dark gray shale |
| 3366.5 | 3367.0 | Black shale |
| 3367.0 | 3368.8 | Very dark gray shale |
| 3368.8 | 3369.8 | Dark gray-green shale |
| 3369.8 | 3372.7 | Very dark gray to black shale |
| 3372.7 | 3373.2 | Very dark gray and medium gray laminated shale |
| 3373.2 | 3379.1 | Very dark gray to black shale |

| From | To | Fractures |
|---|---|---|
| 3320.5 | 3320.5 | Slickensided horizontal surface |
| 3322.7 | 3323.3 | Vertical, parted |
| 3323.4 | 3324.3 | Vertical, parted |
| 3324.3 | 3325.2 | Vertical, parted |
| 3326.7 | 3327.8 | Vertical, parted |
| 3330.5 | 3339.0 | Vertical, parted |
| 3339.4 | 3342.5 | Vertical, parted |

Run #18 (3379.1-3420.4)

| From | To | Lithologic Description |
|---|---|---|
| 3379.1 | 3390.9 | Very dark gray to black shale |
| 3390.9 | 3391.6 | Medium gray shale |
| 3391.6 | 3392.1 | Black shale |
| 3392.1 | 3393.5 | Very dark gray shale |
| 3393.5 | 3393.6 | Medium gray-green shale |
| 3393.6 | 3393.7 | Medium gray shale |
| 3393.7 | 3397.6 | Very dark gray shale |
| 3397.6 | 3397.9 | Dark gray-green shale |
| 3397.9 | 3399.2 | Very dark gray to black shale |
| 3399.2 | 3399.3 | Very dark gray shale |
| 3399.3 | 3403.6 | Black shale |
| 3403.6 | 3404.6 | Very dark gray to black argillaceous limestone |
| 3404.6 | 3405.1 | Medium gray argillaceous limestone |
| 3405.1 | 3407.1 | Very dark gray to black shale |
| 3407.1 | 3409.0 | Brownish black shale |
| 3409.0 | 3414.5 | Very dark gray to black shale |
| 3414.5 | 3420.4 | Light to medium gray limestone |

| From | To | Fractures |
|---|---|---|
| 3380.1 | 3382.3 | Vertical, parted |
| 3383.4 | 3385.1 | Vertical, parted |
| 3385.1 | 3387.1 | Vertical, parted |
| 3387.1 | 3387.6 | Inclined slickensided surface |
| 3388.5 | 3389.1 | Three intersecting slickensided surfaces |
| 3389.5 | 3390.0 | Inclined slickensided surface |
| 3389.6 | 3390.8 | Vertical, parted |
| 3390.2 | 3391.6 | Intersecting slickensided surfaces |
| 3391.6 | 3394.1 | Vertical, parted |
| 3395.7 | 3396.9 | Vertical, parted |
| 3401.0 | 3401.4 | Inclined slickensided surface |
| 3403.1 | 3403.9 | Vertical, parted |
| 3413.4 | 3413.4 | Horizontal slickensided surface |
| 3414.1 | 3414.1 | Horizontal slickensided surface |

| From | To | Other Features |
|---|---|---|
| 399.3 | 3399.4 | Very calcareous zone with calcite stringers |
| 3403.6 | 3405.1 | Very calcareous zone |
| 3414.5 | 3420.4 | Very calcareous zone |
| 3390.9 | 3390.9 | Pyrite lamina |
| 3397.7 | 3399.7 | Pyrite lamina |
| 3499.8 | 3400.8 | Pyrite blebs |
| 3403.1 | 3403.1 | Pyrite lamina |
| 3408.2 | 3408.5 | Pyrite laminae and blebs |

Description of Cored Shale Intervals
from Well Number 20,338, Wise Co., Va.

Run #1 (4870'-4928.6)

| From | To | Lithologic Description |
|---|---|---|
| 4870 | 4928.6 | Entire run represented by black shale |

| From | To | Fractures |
|---|---|---|
| 4885.2 | 4885.7 | Slickensided, near vertical, parted |
| 4894.2 | 4894.2 | Slickensided horizontal plane |
| 4896.2 | 4897.6 | 70° inclined, mineralized |
| 4905.7 | 4905.7 | Slickensided, horizontal plane |
| 4910.5 | 4910.5 | Slickensided, horizontal plane |
| 4914.0 | 4914.5 | 3 vertical mineralized fractures, horizontal slickensided surface |
| 4918.0 | 4918.0 | 3 near horizontal mineralized fractures, with a slickensided surface |

| From | To | Other Features |
|---|---|---|
| 4871.5 | 4871.7 | 3 anhydrite-carbonate layers |
| 4872.3 | 4872.3 | Anhydrite-carbonate layer, with 2 pyrite blebs |
| 4872.5 | 4873.3 | 3 anhydrite-carbonate layers |
| 4873.5 | 4874.2 | Numerous pyrite blebs |
| 4875.4 | 4875.6 | 3 anhydrite-carbonate layers |
| 4876.9 | 4877.1 | 3 anhydrite-carbonate layers |
| 4877.8 | 4877.8 | Anhydrite-carbonate layer |
| 4878.2 | 4878.5 | Numerous anhydrite-carbonate layers |
| 4879.4 | 4879.4 | 2 anhydrite-carbonate layers |
| 4882.2 | 4882.2 | 2 anhydrite-carbonate layers |
| 4882.6 | 4882.7 | 2 anhydrite-carbonate layers |
| 4884.2 | 4884.3 | 2 anhydrite-carbonate layers |
| 4884.8 | 4885.7 | Several anhydrite-carbonate layers |
| 4888.8 | 4888.8 | Anhydrite-carbonate layer |
| 4891.4 | 4891.4 | Anhydrite-carbonate layer |
| 4892.6 | 4892.6 | Anhydrite-carbonate layer |
| 4892.9 | 4892.9 | Anhydrite-carbonate layer |
| 4893.0 | 4893.0 | Anhydrite-carbonate layer |
| 4893.7 | 4893.7 | Pyrite filled layer |
| 4894.6 | 4894.8 | Numerous anhydrite-carbonate layers |
| 4897.0 | 4897.2 | Numerous anhydrite-carbonate layers |
| 4900.0 | 4900.0 | Anhydrite-carbonate layer |
| 4900.4 | 4900.4 | Anhydrite-carbonate layer |
| 4901.3 | 4901.3 | Anhydrite-carbonate layer |
| 4901.5 | 4901.5 | Anhydrite-carbonate layer |
| 4903.1 | 4903.1 | Anhydrite-carbonate layer with large pyrite bleb |
| 4903.3 | 4904.3 | 4 anhydrite-carbonate layers |
| 4904.5 | 4904.5 | Anhydrite-carbonate layer with large pyrite bleb |
| 4904.7 | 4904.7 | Anhydrite-carbonate layer |
| 4905.0 | 4905.0 | Anhydrite-carbonate layer with 2 pyrite blebs |
| 4905.5 | 4905.9 | 3 anhydrite-carbonate layers |
| 4907.0 | 4907.2 | Several anhydrite-carbonate layers |

Run #1 (Cont.) (4908.7-4928.0)

| From | To | Other Features |
|---|---|---|
| 4908.7 | 4908.8 | Anhydrite-carbonate layer with apparent fossil fragments |
| 4911.0 | 4911.0 | 2 pyrite layers |
| 4911.2 | 4911.5 | 2 anhydrite layers with 1 pyrite layer |
| 4914.6 | 4914.6 | Anhydrite-carbonate and pyrite layer |
| 4919.0 | 4919.2 | 3 anhydrite-carbonate layers |
| 4919.3 | 4919.3 | Large pyrite bleb |
| 4919.4 | 4928.0 | Numerous anhydrite-carbonate layers |

Gas bleeding throughout entire core

Run #2 (4928.6 - 4985.5)

| From | To | Lithologic Description |
|---|---|---|
| 4928.6 | 4943.6 | Black shale |
| 4943.6 | 4945.1 | Black shale with dark gray laminae |
| 4945.1 | 4945.9 | Medium dark gray shale |
| 4945.9 | 4946.9 | Medium dark gray and dark gray shale, banded and laminated |
| 4946.9 | 4948.1 | Dark gray shale with medium gray silty shale laminae |
| 4948.1 | 4948.3 | Medium dark gray shale |
| 4948.3 | 4948.5 | Medium dark gray shale with medium gray silty shale laminated in bedding or loading feature |
| 4948.5 | 4950.2 | Medium dark gray shale and dark gray bands laminae |
| 4950.2 | 4951.1 | Medium dark gray and black liminated shale with numerous silt laminae and loading feature pyrite blebs |
| 4951.1 | 4951.8 | Medium gray shale with medium dark to dark gray bands, loading features |
| 4951.8 | 4955.3 | Medium gray shale with dark gray and medium dark gray bands, silt laminae |
| 4955.3 | 4955.8 | Dark gray shale with medium dark gray laminae, with numerous siltstone |
| 4955.8 | 4956.6 | Medium gray shale with dark gray band |
| 4956.6 | 4956.9 | Medium gray silt shale |
| 4956.9 | 4957.7 | Medium gray shale with 2.5' dark and medium gray shale and silty laminae |
| 4957.7 | 4958.5 | Medium gray shale to black shale, silty laminae showing loading features |
| 4958.5 | 4958.9 | Medium gray shale |
| 4958.9 | 4960.7 | Medium dark gray shale with medium gray black shale, light gray laminae |
| 4960.7 | 4961.9 | Medium gray shale with medium dark gray laminae and some light gray laminae |
| 4961.9 | 4962.5 | Medium dark gray shale |
| 4962.5 | 4963.4 | Medium gray with occasional medium dark gray laminae |
| 4963.4 | 4963.6 | Light gray shale with slightly silty band |
| 4963.6 | 4963.9 | Medium gray shale |
| 4963.9 | 4964.4 | Light gray to medium gray shale with light gray silty laminae |
| 4964.4 | 4964.9 | Medium gray shale with a .15' light gray shale band |
| 4964.9 | 4965.3 | Light gray shale and medium gray shale cross bedded. |
| 4965.3 | 4969.7 | Medium gray shale with occasional light gray shale laminae |
| 4969.7 | 4970.1 | Medium gray shale |
| 4970.1 | 4971.3 | Light gray silty shale with medium dark gray laminae crossbedded |
| 4971.3 | 4971.8 | Medium gray shale |
| 4971.8 | 4972.4 | Light gray silty shale with medium gray laminae crossbedding |
| 4972.4 | 4973.0 | Medium gray shale with light gray laminated bands |
| 4973.0 | 4980.8 | Medium gray shale with sparse medium dark gray shale laminae and some light gray laminae |
| 4980.8 | 4982.0 | Medium gray with numerous medium dark gray bands, some light gray silty laminae with loading features |
| 4982.0 | 4982.5 | Medium gray shale |

Run #2 (Cont.) (4982.5 - 4985.5)

| From | To | Lithologic Description |
|---|---|---|
| 4982.5 | 4982.9 | Black and medium gray shale laminae with light gray shale laminae |
| 4982.9 | 4984.4 | Medium gray shale with two .05 black shale bands |
| 4984.4 | 4985.5 | Medium dark gray and black laminated shale with light gray shale laminae |

| From | To | Fractures |
|---|---|---|
| 4930.0 | 4930 | Slickensided, horizontal plane, parted |
| 4931.5 | 4931.5 | Slickensided, horizontal plane, parted |
| 4934.4 | 4934.4 | Slickensided, horizontal plane, parted |
| 4934.8 | 4934.8 | Slickensided, horizontal plane, parted |
| 4934.8 | 4935.2 | 4 near vertical, parted |
| 4935.2 | 4935.2 | Slickensided, horizontal plane, parted |
| 4935.4 | 4935.4 | Horizontal plane, mineralized |
| 4935.7 | 4935.7 | Slickensided, horizontal plane, parted |
| 4937.7 | 4937.7 | Slickensided, horizontal plane, parted |
| 4939.5 | 4939.5 | Slickensided, horizontal plane, parted |
| 4940.5 | 4940.5 | Slickensided, horizontal plane, parted |
| 4941.7 | 4941.7 | Slickensided, horizontal plane, parted |
| 4942.2 | 4942.7 | 3 slickensided, horizontal planes, parted |
| 4943.8 | 4945.0 | 3 slickensided, horizontal planes, parted |
| 4946.3 | 4947.7 | 3 slickensided, horizontal planes, parted |
| 4950.6 | 4950.6 | Slickensided, horizontal plane, parted |
| 4961.5 | 4961.5 | Slickensided, horizontal plane, parted |
| 4972.6 | 4972.6 | Slickensided, horizontal plane, parted |
| 4973.0 | 4973.7 | 2 $60^{o}$ inclined, slickensided, parted |
| 4974.3 | 4974.3 | Slickensided, horizontal plane, parted |
| 4977.0 | 4977.4 | 4 slickensided, horizontal planes, parted |
| 4978.4 | 4978.4 | Slickensided, horizontal plane, parted |
| 4980.5 | 4980.5 | Slickensided, horizontal plane, parted |
| 4981.7 | 4981.7 | Slickensided, horizontal plane, parted |
| 4984.2 | 4985.5 | 3 slickensided, horizontal planes, parted |

| From | To | Other Features |
|---|---|---|
| 4929.0 | 4929.0 | 2 anhydrite - carbonate layers |
| 4929.8 | 4930.0 | 3 anhydrite - carbonate layers |
| 4931.2 | 4932.0 | 7 anhydrite - carbonate layers |
| 4932.8 | 4932.8 | Pyrite filled layer |
| 4933.2 | 4935.3 | 6 anhydrite - carbonate layers |
| 4937.2 | 4937.2 | Large pyrite bleb |
| 4938.5 | 4939.5 | Numerous anhydrite - carbonate layers |
| 4940.0 | 4940.3 | 3 anhydrite - carbonate layers |
| 4943.7 | 4944.9 | 4 anhydrite - carbonate layers |
| 4949.0 | 4950.6 | 5 pyrite blebs |
| 4952.2 | 4955.0 | Several pyrite blebs and layers |
| 4960.2 | 4960.5 | Large pyrite bleb with several filled layers |

Run #2 (Cont.) (4962.2 - 4982.7)

| From | To | Other Features |
|---|---|---|
| 4962.2 | 4962.4 | Several pyrite blebs and filled layers |
| 4964.0 | 4964.0 | 2 pyrite filled layers |
| 4965.0 | 4965.4 | 2 slightly anhydrite - carbonate layers |
| 4982.7 | 4982.7 | 2 pyrite blebs |

Slickensides in all directions but mostly horizontal for entire length of core.

Run #3 (5210-5220)

| From | To | Lithologic Description |
|---|---|---|
| 5210 | 5220 | Entire core cross-bedded medium dark gray shale with black shale bands and some silty laminae |

| From | To | Fractures |
|---|---|---|
| 5211.4 | 5215.0 | Slickensided, vertical, parted |
| 5212.6 | 5212.6 | Slickensided, horizontal plane, parted |
| 5212.6 | 5214.2 | Slickensided, near vertical, parted |
| 5213.0 | 5213.0 | Slickensided, horizontal plane, parted |
| 5215.0 | 5215.8 | $50^{o}$ inclined, slickensided, parted |
| 5216.0 | 5217.7 | $70^{o}$ inclined, slickensided, parted |
| 5218.0 | 5218.0 | Slickensided plane, parted |
| 5219.1 | 5219.8 | $80^{o}$ inclined, parted |

| From | To | Other Features |
|---|---|---|
| 5210.0 | 5210.8 | Numerous anhydrite - carbonate layers |
| 5213.6 | 5214.0 | 5 anhydrite - carbonate layers |
| 5215.1 | 5217.6 | 5 anhydrite - carbonate layers |
| 5218.6 | 5218.8 | 3 anhydrite - carbonate layers |

Run #4 (5220-5251)

| From | To | Lithologic Description |
|---|---|---|
| 5220.0 | 5236.0 | Medium dark gray shale with some black shale bands and laminae. Occasional silty streaks |
| 5236.0 | 5236.3 | Light gray silty zone |
| 5236.3 | 5237.0 | Medium dark gray shale with black shale bands |
| 5237.0 | 5237.3 | Light gray silty zone |
| 5237.3 | 5249.2 | Medium dark gray shale with black shale bands |
| 5249.2 | 5251.0 | Primarily black shale with some black shale bands |

| From | To | Fractures |
|---|---|---|
| 5222.0 | 5223.0 | Vertical, parted |
| 5222.4 | 5222.4 | Slickensided, horizontal plane, parted |
| 5223.8 | 5224.4 | $45^{o}$ inclined, slickensided, parted |
| 5245.6 | 5246.4 | Near vertical, parted |
| 5246.2 | 5246.2 | Slickensided, horizontal plane, parted |
| 5247.0 | 5248.5 | Vertical, parted |
| 5249.2 | 5250.2 | Vertical, parted |

| From | To | Other Features |
|---|---|---|
| 5247.2 | 5247.2 | Pyrite bleb |
| 5247.7 | 5247.7 | Pyrite bleb |
| 5248.4 | 5248.4 | Pyrite bleb |
| 5248.9 | 5248.9 | Pyrite bleb |

Run #5 (5251-5310)

| From | To | Lithologic Description |
|---|---|---|
| 5251.0 | 5255.4 | Black shale with medium dark gray and dark gray shale laminae and bands, numerous anhydrite stringers |
| 5255.4 | 5258.2 | Dark gray shale and black shale layers with some worm burrows |
| 5258.2 | 5260.7 | Black shale and dark gray laminated shale |
| 5260.7 | 5264.4 | Medium dark gray shale with black shale bands and laminae, pyritized worm burrows near top |
| 5264.4 | 5267.8 | Black shale with medium dark gray shale bands and laminae |
| 5267.8 | 5268.7 | Black shale |
| 5268.7 | 5272.2 | Black shale with medium dark gray shale bands and laminae |
| 5272.2 | 5273.4 | Medium dark gray shale |
| 5273.4 | 5278.9 | Black shale with medium dark gray shale bands and laminae |
| 5278.9 | 5280.5 | Mostly medium dark gray shale with some dark gray and black shale bands and laminae |
| 5280.5 | 5286.9 | Black shale with dark gray shale bands and laminae and a few anhydrite seams |
| 5286.9 | 5287.7 | Medium dark gray shale with one .1' black shale band |
| 5287.7 | 5292.3 | Black shale with dark gray shale bands and laminae |
| 5292.3 | 5292.7 | Medium dark gray shale |
| 5292.7 | 5310.0 | Black shale with dark gray shale laminae and bands |

| From | To | Fractures |
|---|---|---|
| 5253.3 | 5253.3 | Slickensided, horizontal plane, parted |
| 5263.5 | 5263.5 | Slickensided, horizontal plane, parted |
| 5266.4 | 5266.4 | Slickensided, horizontal plane, parted |
| 5268.8 | 5268.8 | Slickensided, horizontal plane, parted |
| 5270.0 | 5270.0 | Slickensided, horizontal plane, parted |
| 5274.6 | 5274.6 | Slickensided, horizontal plane, parted |
| 5275.2 | 5275.2 | Slickensided, horizontal plane, parted |
| 5285.2 | 5286.0 | Near vertical to 70$^{o}$ incline |
| 5292.1 | 5292.1 | Slickensided, horizontal plane, parted |
| 5305.0 | 5307.0 | Vertical, irregular surface, parted |
| 5307.5 | 5308.4 | Vertical, irregular surface, parted |

| From | To | Other Features |
|---|---|---|
| 5251.0 | 5254.8 | Numerous anhydrite stringers |
| 5258.3 | 5258.5 | 3 anhydrite - carbonate layers |
| 5264.4 | 5264.4 | Anhydrite - carbonate layer |
| 5265.2 | 5266.0 | 5 anhydrite - carbonate layers |
| 5267.3 | 5267.3 | Anhydrite - carbonate layer |
| 5268.5 | 5268.5 | Anhydrite - carbonate layer |
| 5271.7 | 5271.7 | Anhydrite - carbonate layer |
| 5272.8 | 5272.8 | Anhydrite - carbonate layer |

Run #5 (Cont.) 5274.7 - 5307.8

| From | To | Other Features |
|---|---|---|
| 5274.7 | 5274.7 | Anhydrite - carbonate layer |
| 5276.0 | 5277.0 | Numerous anhydrite - carbonate layers |
| 5277.3 | 5277.3 | Anhydrite - carbonate layer |
| 5278.0 | 5278.0 | Anhydrite - carbonate layer |
| 5278.4 | 5278.4 | Anhydrite - carbonate layer |
| 5279.0 | 5279.2 | 2 anhydrite - carbonate layers |
| 5282.8 | 5282.8 | Anhydrite - carbonate layer |
| 5284.7 | 5284.7 | Anhydrite - carbonate layer |
| 5285.0 | 5285.2 | 2 anhydrite - carbonate layers |
| 5285.4 | 5285.4 | 2 anhydrite - carbonate layers |
| 5292.8 | 5292.8 | Anhydrite - carbonate layer |
| 5299.1 | 5299.4 | 2 anhydrite - carbonate layers |
| 5299.8 | 5299.9 | Several thin anhydrite - carbonate layers |
| 5301.6 | 5301.6 | Anhydrite - carbonate layer |
| 5303.8 | 5303.8 | Anhydrite - carbonate layer |
| 5305.0 | 5305.0 | Anhydrite - carbonate layer |
| 5307.8 | 5307.8 | Anhydrite - carbonate layer |

Gas leaking along most of core.

Run #6 (5310-5345)

| From | To | Lithologic Description |
|---|---|---|
| 5310.0 | 5313.8 | Black shale |
| 5313.8 | 5314.0 | Medium dark gray shale |
| 5314.0 | 5314.3 | Black shale |
| 5314.3 | 5314.5 | Medium dark gray shale |
| 5314.5 | 5318.2 | Black shale |
| 5318.2 | 5318.5 | Medium dark gray shale |
| 5318.5 | 5325.7 | Black shale |
| 5325.7 | 5327.7 | Medium dark gray shale with black shale bands |
| 5327.7 | 5329.0 | Black shale with one band of medium dark to light gray shale .2' long |
| 5329.0 | 5332.9 | Medium dark gray shale with 2 black shale bands. One calcareous band at top and a few pyrite worm burrows |
| 5332.9 | 5335.0 | Black shale |
| 5335.0 | 5337.5 | Medium dark gray shale with 3 black shale bands .1' to .2' in width |
| 5337.5 | 5339.0 | Black shale |
| 5339.0 | 5339.5 | Medium dark gray shale |
| 5339.5 | 5341.1 | Black shale |
| 5341.1 | 5341.3 | Medium dark gray band |
| 5341.3 | 5345.0 | Black shale |

| From | To | Fractures |
|---|---|---|
| 5311.5 | 5312.6 | 9 slickensided, horizontal plane |
| 5314.2 | 5314.2 | Horizontal plane |
| 5319.2 | 5319.2 | Slickensided, horizontal plane, parted |
| 5320.0 | 5320.0 | Slickensided, horizontal plane, parted |
| 5321.3 | 5321.3 | 2 slickensided, horizontal planes, parted |
| 5322.4 | 5322.4 | Slickensided, horizontal plane, parted |
| 5334.2 | 5334.2 | Slickensided, horizontal plane, parted |
| 5336.0 | 5336.0 | Slickensided, horizontal plane, parted |
| 5336.9 | 5337.4 | 3 slickensided, horizontal planes, parted |
| 5338.0 | 5338.4 | 4 slickensided, horizontal planes, parted |
| 5339.6 | 5339.6 | Slickensided, horizontal plane, parted |
| 5340.3 | 5340.3 | Slickensided, horizontal plane, parted |
| 5341.3 | 5341.3 | Slickensided, horizontal plane, parted |

| From | To | Other Features |
|---|---|---|
| 5310.8 | 5310.8 | Anhydrite - carbonate layer |
| 5311.5 | 5312.4 | 4 anhydrite - carbonate layers |
| 5313.0 | 5313.0 | Anhydrite - carbonate layer |
| 5318.2 | 5318.2 | Anhydrite - carbonate layer |
| 5319.9 | 5319.9 | Anhydrite - carbonate layer |
| 5321.5 | 5321.5 | Anhydrite - carbonate layer |
| 5322.8 | 5322.8 | Anhydrite - carbonate layer |
| 5329.9 | 5329.9 | Pyrite bleb |
| 5330.3 | 5330.3 | Pyrite bleb |
| 5330.8 | 5330.8 | Pyrite bleb |

Run #6 (Cont'd) (5331.4-5337.0)

| From | To | Other Features |
|---|---|---|
| 5331.4 | 5331.4 | Pyrite bleb |
| 5332.4 | 5332.4 | Pyrite bleb |
| 5335.6 | 5335.6 | Pyrite bleb |
| 5336.1 | 5336.1 | Pyrite bleb |
| 5337.0 | 5337.0 | Pyrite bleb |

Considerable gas bleeding along core.

Run #7 (5345-5360)

| From | To | Lithologic Description |
|---|---|---|
| 5345.0 | 5345.9 | Black shale |
| 5345.9 | 5347.9 | Half black shale and half dark gray shale |
| 5347.9 | 5351.0 | Black shale |
| 5351.0 | 5351.3 | Medium dark gray shale |
| 5351.3 | 5354.0 | Black shale |
| 5354.0 | 5354.5 | Medium dark gray shale |
| 5354.5 | 5354.9 | Black shale |
| 5354.9 | 5355.2 | Medium dark gray shale |
| 5355.2 | 5357.3 | Black shale |
| 5357.3 | 5357.5 | Medium dark gray shale |
| 5357.5 | 5360.0 | Black shale |

| From | To | Fractures |
|---|---|---|
| 5352.2 | 5352.3 | 2 slickensided, horizontal planes, parted |
| 5352.5 | 5352.8 | 3 slickensided, horizontal planes, parted |
| 5354.0 | 5354.0 | Slickensided, horizontal plane, parted |
| 5354.5 | 5354.5 | Slickensided, horizontal plane, parted |
| 5354.7 | 5354.7 | Slickensided, horizontal plane, parted |
| 5355.0 | 5355.8 | 7 slickensided, horizontal planes, parted |
| 5356.2 | 5356.2 | Slickensided, horizontal plane, parted |
| 5356.4 | 5356.4 | Slickensided, horizontal plane, parted |
| 5357.7 | 5357.7 | Slickensided, horizontal plane, parted |
| 5358.2 | 5358.2 | Slickensided, horizontal plane, parted |
| 5359.1 | 5360.0 | 9 slickensided, horizontal planes, parted |

Slickensides at 20$^{0}$ from horizontal

| From | To | Other Features |
|---|---|---|
| 5346.9 | 5346.9 | Anhydrite - carbonate layer |
| 5351.4 | 5351.4 | Anhydrite - carbonate layer |
| 5352.7 | 5352.7 | 2 anhydrite - carbonate layers |
| 5354.2 | 5354.2 | Anhydrite - carbonate layer |
| 5354.7 | 5354.7 | Anhydrite - carbonate layer |
| 5355.8 | 5355.8 | Anhydrite - carbonate layer |
| 5356.2 | 5356.2 | 2 anhydrite - carbonate layers |

Run #8 (5360-5392)

| From | To | Lithologic Description |
|---|---|---|
| 5360.0 | 5380.9 | Black shale |
| 5380.9 | 5382.3 | Medium gray shale |
| 5382.3 | 5383.1 | Black shale |
| 5383.1 | 5383.7 | Medium dark gray shale |
| 5383.7 | 5384.2 | Black shale |
| 5384.2 | 5384.6 | Dark gray shale |
| 5384.6 | 5385.3 | Black shale |
| 5385.3 | 5385.8 | Dark gray shale |
| 5385.8 | 5388.0 | Black shale |
| 5388.0 | 5388.2 | Medium dark gray shale |
| 5388.2 | 5389.6 | Black shale |
| 5389.6 | 5392.0 | Medium gray shale |

| From | To | Fractures |
|---|---|---|
| 5360.4 | 5360.6 | 3 slickensided, horizontal planes, parted |
| 5361.4 | 5361.4 | Slickensided, horizontal plane, parted |
| 5361.8 | 5361.8 | Slickensided, horizontal plane, parted |
| 5362.5 | 5362.5 | Slickensided, horizontal plane, parted |
| 5363.1 | 5363.1 | Slickensided, horizontal plane, parted |
| 5367.6 | 5367.6 | Slickensided, horizontal plane, parted |
| 5368.0 | 5368.0 | Slickensided, horizontal plane, parted |
| 5370.8 | 5370.8 | Slickensided, horizontal plane, parted |
| 5371.2 | 5371.2 | Slickensided, horizontal plane, parted |
| 5373.3 | 5373.8 | 3 Slickensided, horizontal planes, parted |
| 5375.4 | 5375.6 | 2 slickensided, horizontal planes, parted |
| 5376.0 | 5378.0 | 12 slickensided, horizontal planes, parted |
| 5378.5 | 5378.5 | Slickensided, horizontal plane, parted |
| 5379.0 | 5379.0 | Slickensided, horizontal plane, parted |
| 5379.3 | 5379.3 | Slickensided, horizontal plane, parted |
| 5379.6 | 5379.6 | Slickensided, horizontal plane, parted |
| 5380.9 | 5380.9 | Slickensided, horizontal plane, parted |
| 5381.4 | 5381.4 | Slickensided, horizontal plane, parted |
| 5381.8 | 5381.8 | Slickensided, horizontal plane, parted |
| 5382.0 | 5382.0 | Slickensided, horizontal plane, parted |
| 5383.3 | 5383.3 | Slickensided, horizontal plane, parted |
| 5384.1 | 5384.1 | Slickensided, horizontal plane, parted |
| 5384.5 | 5384.5 | Slickensided, horizontal plane, parted |
| 5384.7 | 5384.7 | Slickensided, horizontal plane, parted |
| 5387.0 | 5387.0 | Slickensided, horizontal plane, parted |
| 5388.0 | 5388.0 | Slickensided, horizontal plane, parted |
| 5388.2 | 5388.2 | Slickensided, horizontal plane, parted |
| 5389.1 | 5390.1 | 6 slickensided, horizontal planes, parted |

| From | To | Other Features |
|---|---|---|
| 5362.9 | 5362.9 | Anhydrite - carbonate layer |
| 5380.6 | 5380.6 | Large pyrite bleb |
| 5386.6 | 5386.6 | Pyrite bleb |

Run #8 (Cont'd) (5388.5-5389.6)

| From | To | Other Features |
|---|---|---|
| 5388.5 | 5388.5 | Pyrite layer |
| 5389.0 | 5389.0 | Pyrite layer |
| 5389.6 | 5389.6 | Pyrite layer |

Gas bleeding profusely through entire core.

Run #9 (5392-5455)

| From | To | Lithologic Description |
|---|---|---|
| 5392.0 | 5393.0 | Medium gray shale with numerous $45^{0}$ filled hair-line fractures |
| 5393.0 | 5397.6 | Medium dark gray shale with worm burrows near base |
| 5397.6 | 5399.3 | Black shale |
| 5399.3 | 5399.6 | Medium dark gray shale and black shale with worm burrows |
| 5399.6 | 5402.5 | Black shale with some very dark gray shale |
| 5402.5 | 5405.0 | Medium dark gray shale with some black shale bands and laminae |
| 5405.0 | 5406.7 | Black shale with medium dark gray shale bands |
| 5406.7 | 5410.3 | Medium dark gray shale with 3 black shale bands approximately .25' - .41' wide |
| 5410.3 | 5411.6 | Black shale with a few dark gray shale laminae |
| 5411.6 | 5413.0 | Medium dark gray shale with one .3' wide black shale band with some worm burrows |
| 5413.0 | 5413.7 | Black shale |
| 5413.7 | 5414.1 | Medium dark gray shale band |
| 5414.1 | 5418.4 | Black shale with olive black shale layers |
| 5418.4 | 5420.5 | Black shale with olive black shale bands |
| 5420.5 | 5422.4 | Olive black shale with dark gray shale and black shale bands |
| 5422.4 | 5428.3 | Black shale |
| 5428.3 | 5429.8 | Black shale with dark gray shale bands |
| 5429.8 | 5430.7 | Black shale |
| 5430.7 | 5431.1 | Black shale and dark gray shale |
| 5431.1 | 5434.4 | Black shale |
| 5434.4 | 5435.0 | Black shale and dark gray shale with worm burrows |
| 5435.0 | 5437.7 | Black shale |
| 5437.7 | 5438.0 | Dark gray shale and black shale with worm burrows |
| 5438.0 | 5439.5 | Black shale |
| 5439.5 | 5440.2 | Dark gray shale and black shale with worm burrows |
| 5440.2 | 5445.0 | Black shale |

| From | To | Fractures |
|---|---|---|
| 5393.0 | 5395.5 | 18 slickensided fractures, at $70^{0}$ parted |
| 5396.0 | 5396.5 | 5 slickensided, horizontal planes, parted |
| 5396.8 | 5396.8 | Slickensided, horizontal plane, parted |
| 5397.2 | 5397.5 | 3 slickensided, horizontal planes, parted |
| 5397.8 | 5398.2 | 4 slickensided, horizontal planes, parted |
| 5398.6 | 5398.6 | Slickensided, horizontal plane, parted |
| 5399.6 | 5399.6 | Slickensided, horizontal plane, parted |
| 5400.0 | 5400.6 | Near vertical |
| 5401.0 | 5402.0 | Near vertical |
| 5402.4 | 5402.4 | Slickensided, horizontal plane, parted |
| 5404.4 | 5404.4 | Slickensided, horizontal plane, parted |
| 5405.0 | 5405.2 | 3 slickensided, horizontal planes, parted |
| 5410.2 | 5410.2 | Slickensided, horizontal plane, parted |

Run #9 (Cont'd) (5411.3-5444.4)

| From | To | Fractures |
|---|---|---|
| 5411.3 | 5411.3 | Slickensided, horizontal plane, parted |
| 5414.5 | 5414.5 | Slickensided, horizontal plane, parted |
| 5416.4 | 5416.4 | Slickensided, horizontal plane, parted |
| 5416.9 | 5416.9 | Slickensided, horizontal plane, parted |
| 5417.3 | 5417.3 | Slickensided, horizontal plane, parted |
| 5417.4 | 5418.0 | Near vertical |
| 5428.0 | 5428.9 | Near vertical |
| 5432.6 | 5432.8 | 2 slickensided, horizontal planes, parted |
| 5433.9 | 5434.0 | 2 slickensided, horizontal planes, parted |
| 5434.4 | 5434.4 | Slickensided, horizontal plane, parted |
| 5434.7 | 5434.7 | Slickensided, horizontal plane, parted |
| 5435.0 | 5435.1 | 2 slickensided, horizontal planes, parted |
| 5435.3 | 5435.5 | 3 slickensided, horizontal planes, parted |
| 5435.7 | 5435.7 | Slickensided, horizontal plane, parted |
| 5435.9 | 5435.9 | Slickensided, horizontal plane, parted |
| 5436.1 | 5436.5 | 5 slickensided, horizontal planes, parted |
| 5436.7 | 5437.4 | 5 slickensided, horizontal planes, parted |
| 5437.8 | 5437.8 | Slickensided, horizontal plane, parted |
| 5438.0 | 5438.0 | Slickensided, horizontal plane, parted |
| 5438.9 | 5438.9 | Slickensided, horizontal plane, parted |
| 5439.4 | 5439.4 | Slickensided, horizontal plane, parted |
| 5442.0 | 5442.0 | Slickensided, horizontal plane, parted |
| 5442.5 | 5442.5 | Slickensided, horizontal plane, parted |
| 5444.4 | 5444.4 | Slickensided, horizontal plane, parted |

| From | To | Other Features |
|---|---|---|
| 5398.0 | 5398.0 | 2 pyrite blebs |
| 5399.0 | 5399.0 | Large pyrite bleb |
| 5400.0 | 5400.0 | Pyrite bleb |
| 5406.4 | 5406.4 | Anhydrite - carbonate layer |
| 5417.4 | 5417.5 | Large pyrite bleb |
| 5418.3 | 5418.3 | Pyrite bleb |
| 5419.0 | 5419.0 | Large pyrite bleb |
| 5420.0 | 5420.0 | Distinct black kerogen layer |
| 5420.1 | 5420.1 | Pyrite bleb |
| 5421.5 | 5421.5 | Pyrite bleb |
| 5423.4 | 5423.4 | Pyrite bleb |
| 5426.2 | 5426.2 | Pyrite bleb |
| 5428.3 | 5428.3 | Pyrite bleb |
| 5432.7 | 5432.7 | Pyrite layer |
| 5438.2 | 5438.2 | 2 pyrite blebs |
| 5438.4 | 5438.4 | Pyrite bleb |

# APPENDIX IV

# TERRA TEK REPORTS

# IN SITU STRESS DETERMINATION IN THE DEVONIAN SHALE (IRA McCOY 20402) WITHIN THE ROME BASIN

By

A. S. Abou-Sayed
C. E. Brechtel
R. J. Clifton

Submitted to

Columbia Gas System Service Corporation
1600 Dublin Road
Columbus, Ohio 43215

Attention: Mr. Eric Smith

TR 77-89
October 1977

## RECOMMENDATIONS

1. The nature (direction, size and frequency) of the small-scale natural fracture system in the Devonian shale should be investigated. The intent in any MHF treatment is that the induced fracture will intersect the existing natural channel (fractures) available for gas flow. Hence, the proximity, at least at the wellbore, of the directions of both the natural fractures and the hydraulically induced one should be considered when a full-scale stimulation job is planned.

2. Difference in magnitudes of the minimum horizontal *in situ* stresses acting within the various layers in any stimulated well represent one of the most important parameters in fracture containment within the pay zone. Achievement of deeply penetrating fractures in the pay formation, which is associated with minimum excursion into the barrier layers, depends on controlling the BHTP in accordance with the difference in *in situ* stresses. Therefore, until better understanding of the factors affecting the *in situ* stress field is achieved, it is imperative to continue the present effort in measuring the *in situ* stresses in the pertinent formation prior to any MHF treatment.

## SUMMARY

The hydrofracturing technique has been used to determine the naturally occurring horizontal *in situ* stress field in the Upper Gray zone of the Devonian shales. The field experiment was performed at a depth of 2745 ft. (837m) in Ira McCoy #20402 well. The bearing of the induced fracture at the wellbore has been determined using an impression packer. Laboratory tests have been performed on core samples from the same formation to determine the rock resistance to fracturing.

Logging data and laboratory observations of core samples reveal the existance of small-scale ($\sim$0.25 - 0.5 in.) vertical cracks oriented at N 50° E to N 60° E. This direction corresponds with the direction of fracture propagation indicated by the impression packer. Furthermore, it appears to be aligned with the direction of the projection of the Rome Trough in the test region.

Analysis of all the available field and laboratory data along with the geologic considerations gives the following values and estimates of the *in situ* stress field:

Overburden Stress = 3210 psi (22.1 MPa)

Minimum Horizontal Stress = 2360 psi (16.3 MPa)

Maximum Horizontal Stress = 4390 psi (30.3 MPa) - estimated

Bearing of Induced Fracture = N 45° E to N 55° E

Hence, the induced fracture tends to align itself at the wellbore with the small-scale natural fracture system in that zone.

## ABSTRACT

The *in situ* stress field was determined at a depth of 837 m (2,745 feet) in Devonian Shale ("gray" shale) within the Rome Basin in West Virginia. Logging data and laboratory observations of core samples reveal vertical cracks oriented at N $50^{0}$ - $60^{0}$ E. Because of these cracks and their preferred orientation, a new approach based on fracture mechanics concepts is used to evaluate the *in situ* stresses from the field and laboratory data. The resulting prediction of the maximum horizontal stress ($\sigma_{HMAX}$) is compared to that predicted by Haimson and Fairhurst's [1967] method; the latter method appears to overestimate the value of this stress component because the effect of loading the faces of any pre-existing crack is neglected.

# TABLE OF CONTENTS

# LIST OF FIGURES

# LIST OF TABLES

# INTRODUCTION

Recent attempts to stimulate natural gas production in low-permeability sandstones in the Western United States by massive hydraulic fracturing (MHF) have resulted in increases of flow of up to 8 times (J. Wroble, unpublished data 1976). However, many attempts have been unsuccessful, probably owing to certain unfavorable characteristics of the pay formations, such as permeability and deformation moduli [Randolph, 1976], all of which are affected by the magnitude of the *in situ* stress. Thus, knowledge of the stress state in the pay and surrounding formations is essential in the simulation of *in situ* conditions during laboratory experiments designed to measure the true subsurface characteristics. These measurements, in turn, make the analysis of phenomena such as containment of the fracture within the pay zone and *in situ* permeability more reliable. In addition, determination of the *in situ* state of stress at depth gives insight into what the breakdown pressure, extension pressure, and the direction of fracture will be during MHF. The difference in horizontal principal stresses is of particular interest because the direction of a hydraulic fracture will be determined by the prevailing direction of the minimum principal stress, provided that the difference in principal stresses is significantly greater than local fluctuations in principal stresses. Furthermore, knowledge of the direction of the minimum *in situ* principal stress and/or the preferred orientation of natural fracture systems is needed in deviated well technology (Komar, unpublished data, 1976a). In this technology the well bore is drilled at a pre-determined inclination with its horizontal projection aligned with either the direction of minimum *in situ* principal stress or orthogonal to the direction of the natural fracture system.

Field techniques to determine the magnitudes and directions of *in situ* principal stresses include, among others, hydrofracturing. The method is a by-product of the hydraulic fracture stimulation technique. The conventional analysis of the results of hydrofracturing involves computation of the *in situ* stresses from the elasticity solution for a pressurized, smooth well bore in an isotropic, homogeneous elastic medium.

During a hydrofracturing experiment to determine *in situ* stresses in the Devonian Shales within the Rome Basin of West Virginia, it was observed that the natural fractures in the core samples from the test well (Ira McCoy 20402) violated the assumptions used in the conventional methods of calculating the *in situ* stress field [cf. Haimson and Fairhurst, 1967]. The problem was, therefore, approached using the principles of linear elastic fracture mechanics; and the results of this analysis suggest that the conventional analysis is incorrect in the determination of the maximum principal stress $\sigma_{HMAX}$. The error occurs because the mechanics of fracture initiation and fracture extension are ignored in the conventional method of calculating maximum compressive *in situ* stress from an elasticity solution for a pressurized cylindrical cavity.

The present report has been divided into two distinct sections. The first section deals with the conventional approach as applied to this particular experiment; a proposed new approach is presented in the second section. The differences between the two approaches for computing the maximum *in situ* stress are examined and found to be due mainly to neglect of crack geometry and the loading of pre-existing cracks by the pressurized fluid in the former approach. From fracture mechanics principles, these factors have a marked effect on crack extension and should, therefore, be considered in the determination of $\sigma_{HMAX}$.

## THE OPEN-HOLE FIELD TESTS AND RESULTS

### Background

In hydrofracturing experiments designed to measure *in situ* stresses the hole is left open so that the orientation of the fracture can be determined after the formation has been broken down. The section of the hole to be tested is isolated by lowering "straddle packers" into position and then pressurizing the sealing components at each end of the device (see Figure 1). The "fracturing fluid" is then injected into the section between the upper and lower seals. Surface and, if possible, downhole recorders are used for continuously monitoring the fluid pressure. The pressure is raised slowly until the breakdown pressure ($P_b$) is reached, i.e., the pressure at which the rock surrounding the hole fractures. If the flow rate remains constant after the breakdown pressure has been reached, the pressure will drop to a constant level, known as the extension pressure ($P_f$) at which the fracture propagates. If the fluid flow is stopped, crack extension ceases and the pressure drops to an equilibrium value called the shut-in pressure ($P_s$). Finally, to determine the orientation of the fracture, an impression packer is lowered into the test section and a trace is formed on the packer by extruding a soft rubber membrane into the fracture. A photograph of a downhole compass is taken and then correlated with a reference mark on the outside of the packer. For a more complete description, see Haimson [1968].

Applications of hydrofracturing are potentially unlimited in depth (except for unavailability of pumping equipment suitable for the necessary high pressure needed for great depths) and do not depend on the determination of load-deformation response, as in the case of overcoring techniques. Since its inception, it has undergone theoretical development [cf. Hubbert and Willis; 1957, Scheidegger, 1960; Kehle, 1964; Haimson and Fairhurst, 1967] and has been applied in both laboratory experiments [Lamont and Jensen, 1963; Haimson and Fairhurst, 1967] and field experiments (cf. Raleigh, *et al.* [1972], Haimson, *et al.* [1973] and Bredenhoeft, *et al.* [1976]).

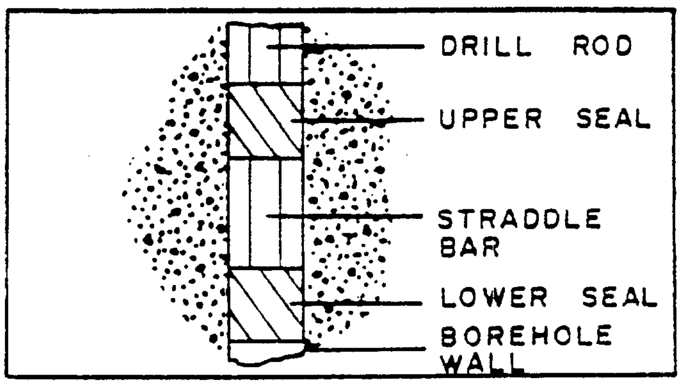


Figure 1. Configuration of a typical straddle packer

The Open-Hole Test

The open-hole test was conducted in the Upper Gray Zone of the Devonian Shales using a standard Lynes straddle packer for a 22.2cm (8-3/4 inch) hole. The straddle length was roughly 4.27m (14 ft.) and its center was located at a depth of 837m (2745 ft.). The packer and drill stem were then filled with a low-viscosity fluid (a combination of KCl, Macobar Drispak and water) that was used to drill the well. The packers were then pressurized to 10.5 MPa (1520 psi, downhole gage).

After the packer had been pressure-set, the formation was pressurized until the breakdown pressure was reached (see Figure 2). Both the pressure and flow rates were monitored at the surface and a downhole pressure monitor

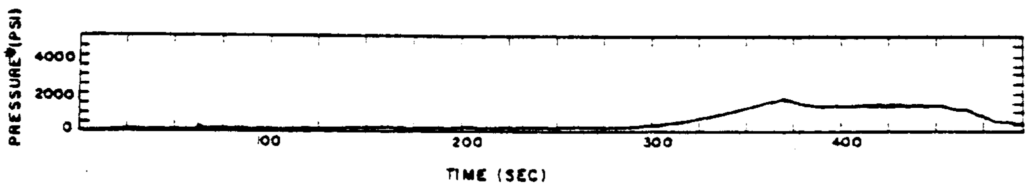


Figure 2. Test record indicating breakdown pressure and extension pressure

* Add hydrostatic head equal to 8.4 MPa (1220 psi)

installed in the straddle bar confirmed the surface measurements. Figure 3 indicates the breakdown of the formation and the initial extension of the fracture in more detail. It was not possible to record the instantaneous shut-in pressure after breakdown because a pressure fitting at the top of the drill stem started leaking.

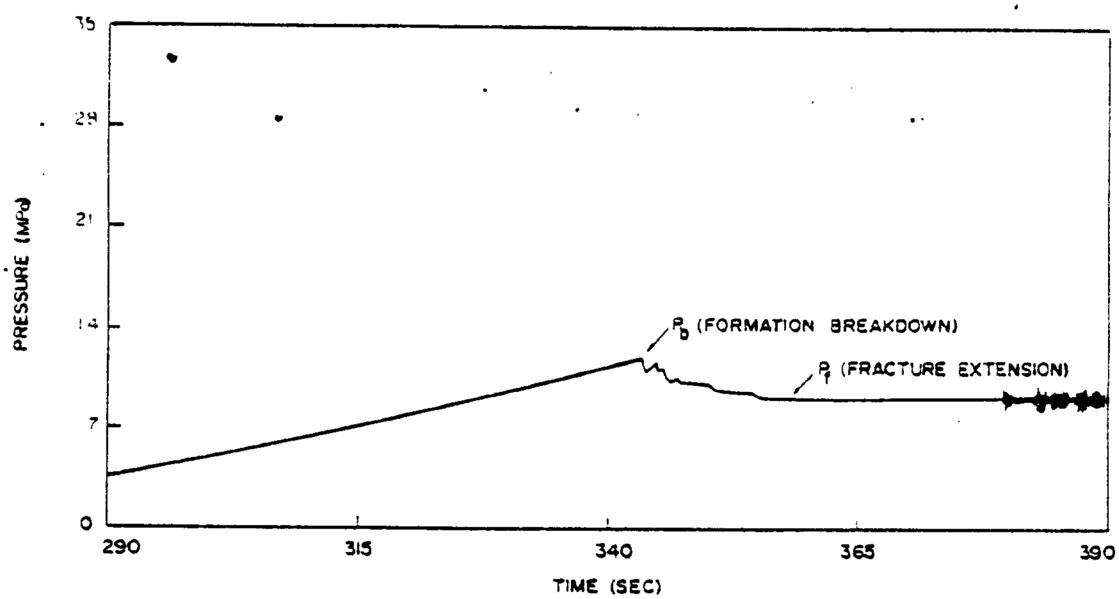


Figure 3. Test record indicating breakdown pressure and extension pressure.

* Add hydrostatic head equal to 8.4 MPa (1220 psi)

The pressure fitting was replaced and the shut-in pressure was measured on the three successive runs, two of which are shown in Figures 4 and 5.

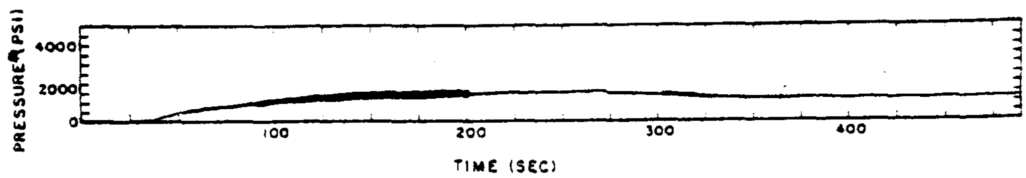


Figure 4. Fracture extension and shut-in Number 1.
* Add hydrostatic head equal to 8.4 MPa (1220 psi)

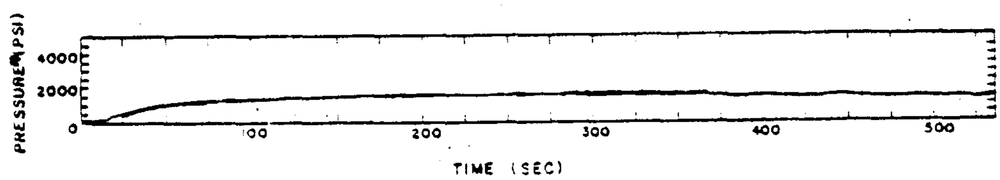


Figure 5. Fracture extension and shut-in Number 2.
* Add hydrostatic head equal to 8.4 MPa (1220 psi)

The numerical results of the open-hole test are presented in Table I. Maximum variation between the successive measurements of the shut-in pressure was within ± 6 percent.

TABLE I

Results of the Open-Hole Test

| Pressure Run | Breakdown Pressure ($P_b$) Mpa (psi) | Shut-in Pressure ($P_s$) Mpa (psi) |
|---|---|---|
| 1 | 20.2 (2930) | --- |
| 2 | --- | 16.4 (2380) |
| 3 | --- | 17.3 (2470) |
| 4 | --- | 15.3 (2215) |

The straddle packer was removed from the hole and a Lynes impression packer was lowered to map the fracture that had been formed. The bottom of the impression was at 839m (2752 ft.); it extended 3.66m (12 ft.) with an 0.61m (2 ft.) blank in the middle. The impression packer indicated the formation of a very narrow (approximately 0.02 in.) vertical fracture over its entire length. The bearing of the fracture trace at the borehole surface was determined to be N 45° E to N 50° E using an Eastman Whipstock single-shot downhole camera.

Evaluation of the *In Situ* Stress Field

Determination of the complete *in situ* stress field can be achieved if the three principal stresses and their directions can be calculated. In general, several hydrofracturing experiments in non-coplanar boreholes are required to obtain the necessary information. This method was used to measure the *in situ* stress at the Nevada Test Site [Haimson, *et. al.* 1973]. If, however, the direction and magnitude of one of the principal stresses are known, the complexity of the experimental work needed to determine the other two principal stresses is reduced substantially. This situation is not uncommon since the vertical (overburden) stress is usually a principal stress and, except at very shallow depth, will generally exceed the minimum *in situ* principal stress.

If the rock is viewed as a homogeneous, isotropic, elastic medium with an isotropic failure criterion, it is easily shown that a crack propagating in this medium, due to fluid pressure acting on its face, will grow along the path of least resistance (i.e., it will extend in the plane perpendicular to the least compressive *in situ* principal stress). For a moderately long crack, the pressure required to hold the crack open, but not extend it, will be slightly greater than the far-field stress acting normal to the fracture. Therefore, it follows that the shut-in pressure is approximately equal to the minimum horizontal compressive stress.

In this case, if the rock is assumed to fail when a critical tensile stress is reached, then the principal stress field can be calculated by applying Equations (1), (2) and (3).

$$\sigma_{HMAX} = T_o + 3P_s - P_b - P_o \quad (1)$$

$$\sigma_{OB} = \rho H \quad (2)$$

$$\sigma_{HMIN} = P_s \quad (3)$$

$\sigma_{HMAX}$ = total maximum horizontal compressive stress.

$\sigma_{HMIN}$ = total minimum horizontal compressive stress.

$\sigma_{OB}$ = total vertical principal stress due to overburden.

$\rho$ = specific weight of rock (kPa/m or Psi/ft)

$H$ = depth of the test zone (m or ft)

$P_o$ = formation pore pressure

$T_o$ = tensile strength of the rock

$P_s$ = shut-in pressure

$P_b$ = breakdown pressure

This solution, based on the elasticity solution for a pressurized cylindrical cavity in an infinite isotropic elastic continuum, was first proposed by Hubbert and Willis [1957] and Haimson and Fairhurst [1967]. It should be noted that Equations (1) and (3) are valid only for the case where the fracturing fluid does not penetrate the matrix of the formation material. Due to the low permeability of the Devonian Shales of the Rome Basin, neglect of fracturing-fluid penetration should not introduce major errors into the analysis. Equations (1), (2) and (3) are not applicable if the vertical stress is less than the smallest horizontal stress, in which case a horizontal fracture will form and determination of the horizontal *in situ* principal stresses is not possible using conventional hydrofracturing techniques.

In addition to the magnitude of the *in situ* principal stresses obtained from the measured pressures and Equations (1) and (3), the impression packer provides the direction of the cracks that have formed at the borehole wall. If the material is isotropic, these cracks should be normal to the direction of the minimum principal stress.

Results of the Laboratory Experiments

Laboratory tests conducted in this study were used to supply the material properties necessary to obtain the *in situ* stresses from the field test. A series of six hollow-cylinder burst tests were conducted on oriented core samples recovered from the Gray Shale section at a depth of 823m (2699 ft.) to 845m (2770 ft.). These tests, when interpreted in terms of a critical tensile stress required for fracture, provided the tensile strength ($T_0$) of the shale. A description of the experimental techniques used in these tests can be found elsewhere [Haimson and Fairhurst, 1967].

Briefly, the test consists of internal pressurization of a thick-walled cylindrical sample until failure occurs. The failure pressure, $P_i$, is measured and is related to the tensile strength of the rock, $T_0$, through the equation

$$T_0 = P_i \left( \frac{W^2 + 1}{W^2 - 1} \right) \qquad (4)$$

where w is the ratio of the outer radius b to the inner radius a of the hollow cylinder. The tests reported here were carried out with a = 9.27mm (0.365 in.) and b = 96.5mm (3.80 in.).

In spite of the visual competence of the shale from the test section, nearly all of the core samples developed extensive horizontal fractures during transportation to the Terra Tek facility. The fractures are apparently due to bedding plane separation caused by the removal of the overburden stress. These fractures limited the length of the burst test specimens to less than 63mm (2.5 in). The results of these laboratory tests are shown in Table II.

TABLE II
Results of Unjacketed Burst Tests

| Sample Depth m (ft.) | b/a = w | $P_i$ Failure Pressure MPa (psi) | Remarks |
|---|---|---|---|
| 823 (2699) | 10.7 | 22.3 (3230) | Very competent sample, few fractures. |
| 831 (2724) | 10.7 | 7.7 (1120) | Failed on pre-existing fractures. |
| 836 (2741) | 10.7 | 11.3 (1640) | Failed on pre-existing fractures. |
| 836.3 (2742) | 10.7 | 2.3 (340) | Failed along a bedding-plane fracture. |
| 842 (2761) | 10.7 | 5.9 (850) | Failed along a bedding-plane fracture. |
| 845 (2770) | 10.7 | 19.2 (2790) | Very competent sample, very few fractures. |

It is obvious that the results from the unjacketed burst tests can be grouped into two classes. Samples at 823m and 845m levels have an average tensile strength which is over twice as great as for samples at the 831m and 836m levels. Samples from depths of 823m and 845m had considerably fewer natural fractures than the samples from the 831m and 836m levels.

Both of the samples that failed at the lower pressures (831m and 836m) had groups of small, tight vertical fractures with the same directional trend, and the failure plane induced during the test was parallel to the pre-existing fractures. The orientation of pre-existing cracks was generally N 45-55° E, which agrees reasonably well with the bearing of the fracture trace at the well bore.

## Calculation of *In Situ* Stress Based on a Critical Tensile Strength Hypothesis

A comparison of the densities obtained from the Birdwell 3-D ultrasonic log and the density measurements done by Terra Tek indicates excellent agreement. Therefore, the log densities were averaged and used to calculate the overburden stress. The calculated value for the overburden stress $\sigma_{OB}$ is 22.1 MPa (3210 psi).

The tensile strength used in the calculation of the maximum horizontal stress is taken from the results of the unjacketed burst of a core from the field test section that did not fail because of bedding plane fractures. The three measurements of the shut-in pressure were averaged to determine the value of the minimum horizontal stress, $\sigma_{HMIN}$. The pore pressure term in Equation (1) is estimated from a downhole-pressure-build-up test to be 1.7 MPa (250 psi) (<u>Smith</u>, unpublished data, 1976). A tabulation of the measured and calculated data at the mid-position of the fractured section (837m) is presented in Table III.

TABLE III

Calculation of *In Situ* Stress at 837m (2745 feet) for Isotropic Medium

| Depth m(feet) | $P_b$ MPa(psi) | $P_o$ MPa(psi) | $P_s$ MPa(psi) | $T_{oavg}$ MPa(psi) | $\rho$ k Pa/m(psi/ft) | $\sigma_{OB}=\rho H$ MPa(psi) | $\sigma_{HMAX}=T_o+3P_s-P_b-P_o$ MPa(psi) | $\sigma_{HMIN}=P_s$ MPa(psi) | Direction of $\sigma_{HMAX}$ |
|---|---|---|---|---|---|---|---|---|---|
| 837 (2745) | 20.2 (2930) | 1.7 (250) | 16.3 (2360) | 11.3 (1640) | 25.4 (1.17) | 22.1 (3210) | 38.3 (5550) | 16.3 (2360) | N45°-50°E |

As a result of the scatter observed in the laboratory burst tests, the error bounds for the maximum horizontal stress are quite large. If, for example, the material in the test section between the packers were isotropic and homogeneous with a tensile strength of 21.1 MPa (3060 psi), corresponding to the average burst pressure of the very competent samples at 823m and 845m, then a maximum horizontal stress of 48.1 MPa (6980 psi) would be obtained. On the other hand, if the tensile strength of the rock were 7.7 MPa (1120 psi), corresponding to the minimum burst pressure when bedding plane fracture does not occur, then the maximum horizontal stress would be 34.7 MPa (5020 psi).

The wide range of measured burst pressures coupled with the effect of the known existing fractures observed in the recovered cores indicate that the shale medium has pronounced anisotropy with respect to its tensile strength. Figure 6 shows that the induced failure plane is parallel to the group of existing vertical fractures in the sample at the 831m (2726

Figure 6. Burst sample from 831m (2724 ft.)
[$P_i$ = 7.7 MPa (1120 psi)]

ft.) level. Furthermore, examination of the fracture density logs from Ira McCoy well 20403 indicates a consistent set of vertical fractures through the entire cored section (see Figure 7). Azimuths of these fractures are within ± 10 degrees of the direction of the fracture created during the hydrofracturing test. Hence, the assumptions of a crack-free well bore and a critical-tensile-strength failure criterion do not appear to be appropriate.

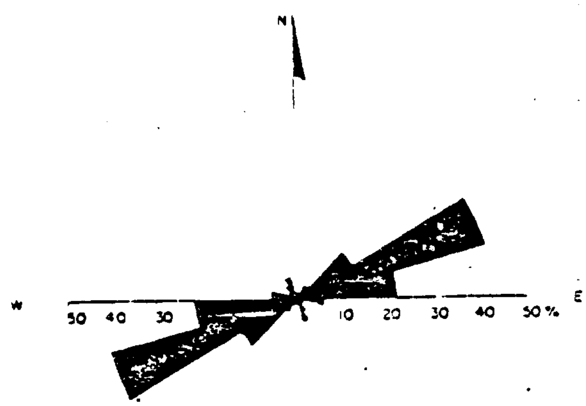


Figure 7. Histogram of the strikes of 605 vertical extension fractures mapped in Devonian Shale recovered from well No. 20403 (from Swolfs, *et al.*, 1976).

In order to account for the existence of the developed fracture system in the field test, the problem has been reanalyzed by applying the methods of linear elastic fracture mechanics. The effect of preferred crack orientation on fracture growth and the initiation of fracture are accounted for in the calculation of the *in situ* stress. The calculated stress state will be found to differ from the estimates obtained using the conventional formulation [Haimson and Fairhurst, 1967].

# FRACTURE MECHANICS ANALYSIS OF THE HYDROFRACTURING TEST

Growth of a crack inclined to the directions of the far-field *in situ* stresses and subjected to pressure on its faces can be analyzed by using fracture mechanics concepts in which linear elasticity is assumed and attention is given to the elevation of stresses near the crack tip. While large stresses around the crack tip are usually accompanied by some plasticity, linear elastic fracture mechanics properly forms the basis for analyses when plastic deformation and other non-linear effects near the crack tip are confined to a small region within a linear elastic field. The near-tip stress state in such a field is characterized by a single parameter. Irwin [1960] introduced the stress-intensity factor K as one such parameter--others include the J-integral [Rice, 1968] and the specific energy-release rate, G [Irwin, 1957]. These parameters, which are equivalent in linear elastic fracture mechanics, measure the intensity of the local stress field at the crack tip. They are determined by the applied loading, the crack configuration, and the geometry of the body. Cracks are expected to advance if the values of these parameters reach critical values characterisitic of the material considered. On the other hand, if the loads acting on the body and its geometry are such that the value of K, J, or G is less than this characteristic material property, then the crack is expected to remain stationary.

## Effect of Preferred Crack Orientation on Crack Growth in Hydraulic Fracturing

Consider a pressurized crack oriented at an arbitrary angle $\alpha$ relative to the direction of minimum principal stress $\sigma_3$ of the far-field stress system, illustrated in Figure 8. If the crack faces of length 2L are subjected to a pressure p, the stress-intensity factors $K_I$ (for the opening mode)

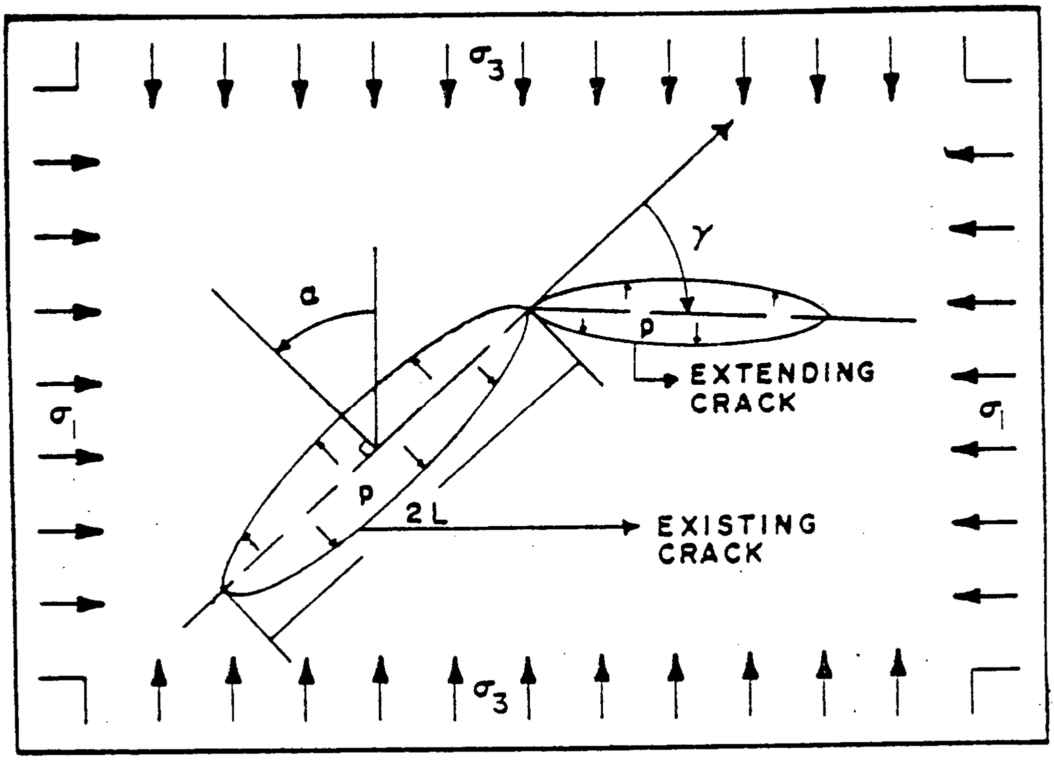


Figure 8. Skewed crack under far-field stress and internal pressure

and $K_{II}$ (for in-plane shearing mode) for the existing crack are given by (cf. Rice, 1970, eq. 97):

$$K_I = \sqrt{\pi L}\ \{p - \sigma_1 \sin^2\alpha - \sigma_3 \cos^2\alpha\} \qquad (5)$$

$$K_{II} = \sqrt{\pi L}\ \{\tfrac{1}{2}(\sigma_1 - \sigma_3)\sin 2\alpha\} \qquad (6)$$

where $\sigma_1$ and $\sigma_3$ denote, respectively, the maximum and minimum compressive far-field horizontal principal stresses.

If the existing crack extends in an arbitrary direction, as shown in Figure 8, then the energy-release rate $\Gamma(\gamma)$ associated with extension in the direction $\gamma$ will be given by the following equation [Hussain, *et al.*, 1974]

$$\Gamma(\gamma) = \frac{4(1-\nu^2)}{E} \left(\frac{1}{3+\cos^2\gamma}\right)\left(\frac{\pi-\gamma}{\pi+\gamma}\right)^{\gamma/\pi} \Big[(1+3\cos^2\gamma)K_I{}^2 + 8\sin\gamma\cos\gamma K_I K_{II} + (9-5\cos^2\gamma)K_{II}{}^2\Big] \qquad (7)$$

where $K_I$ and $K_{II}$ are given by Equations (5) and (6), and E and $\nu$ denote the Young's modulus and Poisson's ratio of the material, respectively. If the crack is assumed to advance in the direction, $\gamma_{max}$, for which $\Gamma(\gamma)$ is a maximum, then the relationship between the direction of crack advance, $\gamma_{max}$ and the ratio, $(K_{II}/K_I)$, is given by Figure 9 [Clifton, 1973; Palaniswamy and Knauss, 1972].

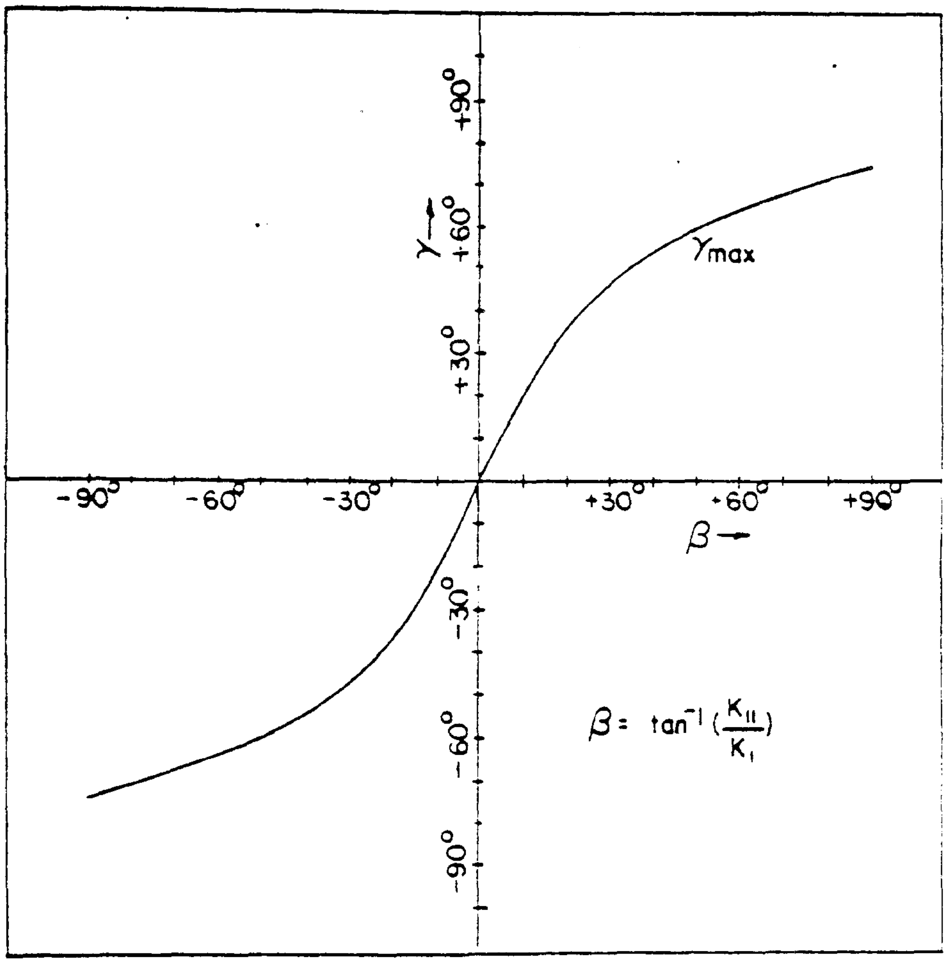


Figure 9. Orientation of propagating crack which maximizes energy-release rate (Clifton, 1974).

The energy release rate $\Gamma(\gamma)$ is a positive definite function of $K_I$ and $K_{II}$. Furthermore, substitution of (5) and (6) into (7) reveals that $\Gamma(\gamma)$ is proportional to the crack length. Therefore, if cracks advance for a prescribed finite value of $\Gamma(\gamma_{max})$, the only way a sufficiently long open crack cannot advance is for $K_I$ and $K_{II}$ to be equal to zero. From (5) and (6) the conditions $K_I = 0$ and $K_{II} = 0$ are satisfied for

$$p = \sigma_1 \sin^2\alpha + \sigma_3 \cos^2\alpha \tag{8a}$$

and

$$(\sigma_1 - \sigma_3)\sin 2\alpha = 0 \tag{8b}$$

In the former case, $\alpha = 0$, Equation (8a) requires that the pressure p equals the minimum horizontal compressive stress, $\sigma_3$, whereas, in the latter case, $\alpha = \pi/2$, the pressure p equals the maximum horizontal compressive stress $\sigma_1$. That is, sufficiently long open cracks can be stationary only if they are parallel to principal stress directions and if the pressure p is equal to the principal stress perpendicular to the crack face.

Whether the case $\alpha = \pi/2$ or $\alpha = 0$ is more likely to occur can be determined by noting whether an arbitrarily oriented crack tends to rotate to become perpendicular to $\sigma_1$ or $\sigma_3$. From Figure 9, a crack tending to open due to internal pressure (i.e., a crack with $K_I>0$) will have a maximum energy release rate if it extends in the direction of positive $\gamma$ for $K_{II}>0$ and negative $\gamma$ for $K_{II}<0$. Then, for $(\sigma_1 - \sigma_3)>0$, equation (6) indicates that for $\alpha$ in the interval $(0,\pi/2)$ the predicted inclination $\gamma$ of the extending crack is positive whereas $\gamma$ is negative for $\alpha$ in the interval $(-\pi/2,0)$. In other words, the maximum energy release rate hypothesis predicts that the crack tends to extend in a direction which is more nearly perpendicular to the direction of minimum compressive stress than was the existing crack as long as $(\sigma_1 - \sigma_3)$ is not zero. This prediction is consistent with laboratory results [Brace and Bombolakis, 1963; Ingraffea and Heuze, 1976].

Thus, for long cracks the angle $\alpha$ approaches zero so that, from (8a), the shut-in pressure, $P_s$, is given by

$$P_s = \sigma_3 = \sigma_{HMIN} \qquad (9)$$

That is, for sufficiently long cracks the static pressure at which crack advance is imminent is independent of the crack length and the mechanical properties of the rock. The minimum crack length necessary for (9) to provide a good approximation of $\sigma_{HMIN}$ can be estimated from (5) and an assumed critical value, $K_{Ic}$, of the stress-intensity factor at which crack advance occurs. For $K_{Ic} = 40 \mathrm{MPa}(\mathrm{mm})^{1/2}$ (See Table A1), the difference $(P_s - \sigma_3)$ is less than 0.5 MPa (73 psi) for crack lengths greater than 2 meters. The injected volume of fluid in hydrofracturing experiments is sufficiently large that crack lengths are expected to be considerably greater than 2 meters. Hence, Equation (9) or (3), should allow reasonably accurate determination of the minimum *in situ* stress from the measured shut-in pressure.

Crack Initiation with a Pre-Existing Crack of Prescribed Orientation

An estimate of the maximum horizontal *in situ* stress, $\sigma_{HMAX} = \sigma_1$, can be obtained by considering the initial advance of an existing crack which intersects the bore hole at a prescribed orientation. A cylindrical hole with two radially opposed cracks subjected to an internal pressure p and the far-field stress state $\sigma_1$ and $\sigma_3$ is shown in Figure 10. The stress-intensity factor, $K_I$, at the crack tip for the case when the pressure p acts on the bore and the crack faces is given by [Johnson, *et. al.*, 1973, Eq. 49].

$$K_I = p\sqrt{L\pi}\,F(L/a) - (\sigma_1 \cos^2\alpha + \sigma_3 \sin^2\alpha)\,F(L/a)\,\sqrt{L\pi}$$
$$+ (\sigma_1 \cos 2\alpha - \sigma_3 \cos 2\alpha)\,G(L/a)\,\sqrt{L\pi} \qquad (10)$$

where F(L/a) and G(L/a) are given in Table A2 [cf., Paris and Sih, 1965].

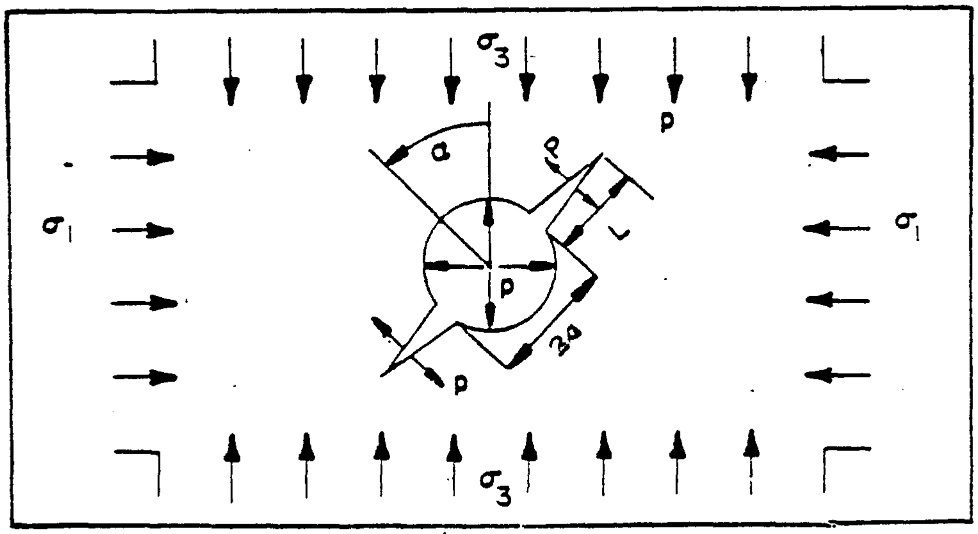


Figure 10. Crack in a borehole wall under far-field stress and internal pressure

In order to determine $\sigma_1$ from (10) it is necessary to know the minimum compressive stress $\sigma_3$, the initial crack length L, and the breakdown pressure $p = P_b$ at which the stress-intensity factor $K_I$ is equal to the critical value $K_{Ic}$, required for crack advance. Now $\sigma_3$ can be determined from measurement of the shut-in pressure, $P_s$ (see Equation (9)), and $K_{Ic}$ can be determined from fracture toughness tests (see Appendix). Estimates of L can be obtained from visual inspection of cores. For given values of $K_{Ic}$, $P_b$ and L, Equation (10) becomes a relation between $\sigma_1$ and $\alpha$. This relation can be written in the more useful form

$$-I(\alpha)(\sigma_1 - \sigma_3) = \sigma_3 - P_b + \frac{K_{Ic}}{F(L/a)\sqrt{L\pi}} \qquad (11)$$

where

$$I(\alpha) = \cos^2\alpha - \frac{G(L/a)}{F(L/a)}\cos 2\alpha \qquad (12)$$

The function $I(\alpha)$ is shown in Figure 11 for various values of the ratio $L/a$. Because $I(\alpha)$ is near zero only for a limited range of values of $\alpha$, it appears that (11) can usually be solved uniquely for $(\sigma_1 - \sigma_3)$ when $\alpha$ is known.

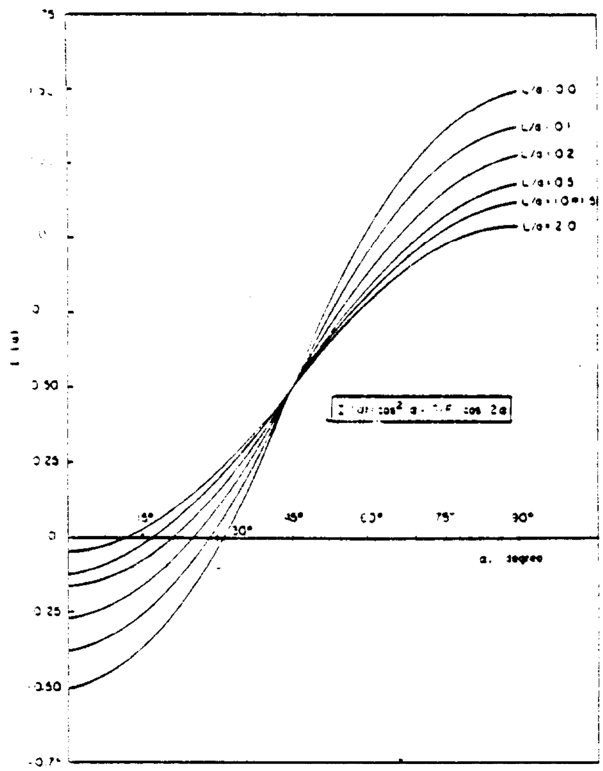


Figure 11. $I(\alpha)$ as a function of $\alpha$ for different ratios of $(L/a)$

If $\sigma_1 = \sigma_3$, then the value of $\alpha$ is irrelevant and the principal stresses in the horizontal plane are

$$\sigma_1 = \sigma_3 = P_b - \frac{K_{Ic}}{F(L/a)\sqrt{L\pi}} \tag{13}$$

On the other hand, the condition $\sigma_3 < \sigma_1$ requires that $\sigma_3$ and $\alpha$ satisfy the inequalities

$$\sigma_3 < P_b - \frac{K_{Ic}}{F(L/a)\sqrt{L\pi}} \qquad \text{for } \alpha > \alpha_c \tag{14a}$$

$$\sigma_3 > P_b - \frac{K_{Ic}}{F(L/a)\sqrt{L\pi}} \qquad \text{for } \alpha < \alpha_c \tag{14b}$$

where $\alpha_c$ is the solution of the equation

$$I(\alpha) = 0. \tag{15}$$

Values of $\alpha_c$ for a wide range of values of $(L/a)$ (i.e., $0 \leq L/a \leq 2$) lie in the interval $15^\circ < \alpha_c < 30^\circ$. For known values of $\sigma_3$, $P_b$, $K_{Ic}$ and L, inequalities (14) limit the possible range of the values of $\alpha$. Unfortunately, however, L is generally not known with much certainty and allowable variations in the value for L may lead to satisfaction of either (14a) or (14b). Such uncertainty could be removed if a dominant crack of known length L could be introduced in the field test.

While it appears that there is no unambiguous way of determining $\sigma_1$ without additional information, there are a number of observations that can be made. First, if cracks of known length L could be artificially introduced before hydraulic fracturing of a well bore at two different depths within nominally the same formation, then the principal stress $\sigma_1$ could be determined without *a priori* determination of $\alpha$. This would be accomplished by introducing the cracks at orientations differing by $\pi/2$ and making use of the identity $I(\alpha) + I(\alpha + \pi/2) = 1 - G/F$. Then, from (11)

$$\sigma_1 = \{P_b^{\alpha} + P_b^{\alpha+\pi/2}\} - \sigma_3 - \frac{2K_{Ic}}{F(L/a)\sqrt{L\pi}} \tag{16}$$

where $P_b^{\alpha}$ and $P_b^{\alpha+\pi/2}$ are the breakdown pressures in the sections with cracks oriented at angles $\alpha$ and $\alpha+\pi/2$, respectively. Once $\sigma_1$ is obtained from (16), the angle $\alpha$ can be obtained from application of (11) to the results of each field test. Comparison of the two values of $\alpha$ obtained in this way would serve as a check on the validity of the procedure for determining $\sigma_1$ and $\alpha$.

If results from only a single hydrofracturing test are available, then an additional assumption must be introduced in order to estimate $\sigma_1$, unless the principal stress directions can be determined from an independent measurement of the hydraulic fracture orientation at large distances from the well bore. In the latter case, measurement of crack orientation at the well bore by means of an impression packer suffices for the determination of $\alpha$. If there is no preferred orientation of existing flaws, then the expected value for $\alpha$ is $\alpha = 0$ because $K_I$ is a maximum for $\alpha = 0$. On the other hand, even if there is a preferred orientation of existing cracks, the development of these cracks may be such that their orientation will be near $\alpha = 0$. Such orientation would result if the paleostresses are still dominant and the cracks are due to extensional failure, i.e., lie in the principal plane of the greatest and intermediate stress [Swolfs, *et al.*, 1976]. In the Devonian Shale core samples the existing vertical cracks are not planar and do not contain pulverized material which would suggest their formation or subsequent sliding in a shear mode. Thus, it appears plausible that initial crack extension in the hydraulic fracturing experiment occurs in a direction near $\alpha = 0$. Furthermore, Equation (14b), measured values of $P_s$, $P_b$, $K_{Ic}$ and laboratory values for L suggest that $\alpha$ satisfies $\alpha < \alpha_c$. Consequently, in what follows, the orientation of the crack at the well bore will be assumed to be $\alpha = 0$. This assumption is the same as the one used in the conventional method for determining $\sigma_{HMAX}$ discussed previously. Use of the same assumption here facilitates direct comparison of the two approaches.

If one assumes that during a hydrofracturing test the initial crack intersects the borehole in a radial plane perpendicular to the minimum *in situ* compressive stress, then from (11) and (9) one obtains

$$\sigma_1 = \frac{K_{Ic}}{\sqrt{\pi L}(G-F)} - \frac{F}{(G-F)} P_b + \frac{G}{(G-F)} P_s \qquad (17)$$

where G and F are to be evaluated for appropriate values of L/a.

The critical stress-intensity factor $K_{Ic}$ in (17) is obtained from the results of jacketed pre-notched burst tests as discussed in the Appendix. However, the values of $K_{Ic}$ reported for these tests (Table II) are applicable for fracture from an initial state of zero confining pressure, whereas, the pre-fracture state in the field involves substantial confining pressures. Recent experiments on the fracture toughness of Indiana Limestone [Schmidt and Huddle, 1976 and Abou-Sayed, 1977] indicate that the critical stress-intensity factor at which crack extends increases significantly with the increasing confining pressure. Although the dependence of $K_{Ic}$ on confining pressure has not been measured for Devonian Shale, it appears likely that the value of $K_{Ic}$ for shale will be considerably larger under the *in situ* confining pressure than measured in the unconfined laboratory tests. In the absence of data on the effects of confining pressure on $K_{Ic}$ for shale from the test section, it appears reasonable to assume that $K_{Ic}$ increases by a factor of 1.6--the fractional increase of $K_{Ic}$ reported for Indiana Limestone under a confining pressure of 24 MPa (3500 psi) corresponding to the mean *in situ* normal stress at the test section.

The crack length L in (17) is taken to be 8mm. This length corresponds to the length of most pre-existing vertical cracks observed in the test cores (see Figure 6). This choice appears reasonable because many such cracks can be expected to intersect the 22.2 cm hole and it is likely that for at least one of these cracks the depth is essentially equal to the initial length of the crack.

The dimensionless stress-intensity factors F and G should be reduced because the cracks are not plane-strain cracks. The extent of the reduction is difficult to assess, but comparison of plane-strain-crack solutions with solutions for a circular crack in an infinite medium, [Sneddon, 1946], and elliptical crack in a plate, [Rice and Levy, 1970] or hollow cylinder [Underwood, 1972] suggests that the stress-intensity factor could be reduced by approximately 40 percent from the value for a plane-strain crack of the same depth. The functions F and G should decrease similarly so that quotients F/(G-F) and G/(G-F) should be essentially the same as for plane-strain conditions. The quantity (G-F) in the first term of (17) can be expected to be approximately 60 percent of the value for the plane-strain conditions.

Incorporating these considerations in the application of (17) one finds that the maximum horizontal compressive stress $\sigma_{HMAX}=\sigma_1$ is approximately

$$\sigma_1 \approx \frac{38.2 \times 1.6}{\sqrt{\pi 8}(2.93 - 2.06)\ .60} - \frac{2.06}{.87}(20.2) + \frac{2.93}{.87}(16.3)$$

or

$$\sigma_1 \approx + 23.2 - 47.8 + 54.9$$

or

$$\sigma_{HMAX} = \sigma_1 \approx 30.3 \text{ MPa (4390 psi).} \qquad (18)$$

The intermediate steps are shown in order to indicate the relative magnitude of the terms. The accuracy in the computed value of $\sigma_{HMAX}$ is reduced because the computation involves differences in terms of comparable magnitude. However, the two large terms are regarded as known with quite good certainty (say ± 5 percent) and the larger percent error (say ± 50 percent) occurs in the smallest term. As a result, the probable error in the computed value of $\sigma_{HMAX}$ is regarded as about 40 percent. The calculated values of the principal *in situ* stresses based on a linear elastic fracture mechanics analysis are summarized in Table IV along with other relevant parameters.

TABLE IV

The *In Situ* Stress at 837m (2745 feet) Based on Linear Elastic Fracture Mechanics

| Depth (h) m (feet) | $P_b$ MPa (psi) | $P_s$ MPa (psi) | L mm (in.) | $\sigma_{OB}$ (Vertical) MPa (psi) | $\sigma_{HMAX}$ MPa (psi) | $\sigma_{HMIN}$ MPa (psi) | Direction of $\sigma_{HMAX}$ |
|---|---|---|---|---|---|---|---|
| 837 (2745) | 20.2 (2930) | 16.3 (2360) | 8 | 22.1 (3210) | 30.3 (4390) | 16.3 (2360) | N45°-50°E |

In order for the computations shown in (18) to be consistent with a model of breakdown based on (10) it is necessary for the entire length of the dominant well bore crack to be subjected to the breakdown pressure $P_b$. For tight natural cracks of the type observed in the cores, pressurization of the crack faces will probably not occur unless the crack is opened by circumferential tensile stress at the wall of the bore. From (1), this circumferential tensile stress is given by

$$\sigma_{\theta\theta}\big|_{r=a} = \sigma_{HMAX} - 3P_s + P_b + P_o$$

which for the values given in Table IV, yields $\sigma_{\theta\theta}\big|_{r=a} = 3.3$ MPa (480 psi).

Because the crack faces cannot support a tensile stress, the faces should separate and allow the low viscosity pressurizing fluid to penetrate. Once the fluid begins to penetrate, the crack should open further and allow the fluid to advance until the fluid pressure acts over essentially the entire surface area of the crack. In view of the combination of slow pressure build-up and low fluid viscosity, the effects of fluid flow on breakdown [Zoback and Pollard, 1977] are not expected to be significant in this case.

The primary uncertainties in the calculation of $\sigma_{HMAX}$ are associated with the geometry of the dominant well bore crack and with the value of $K_{Ic}$ for the loading conditions of the field test. The uncertainty regarding the crack geometry can largely be removed by cutting vertical cracks of known depth L as discussed in connection with Equation (16). Uncertainty associated with the value of $K_{Ic}$ can be reduced by employing laboratory fracture toughness experiments which simulate the stress state existing in the field. Such experiments can be conducted employing the configuration shown in the Appendix with independent control of axial stress, confining pressure, and internal pressure. Also, the influence of errors in $K_{Ic}$ on the computed value of $\sigma_{HMAX}$ can be reduced by an optional choice of L such that the first term in (17) and (18), i.e., the term that depends on $K_{Ic}$ is made as small as possible.

The latter concept of reducing the relative significance of terms related to rock strength is similar to the concept [Bredehoeft, *et al.*, 1976] of employing cyclic pressurization of the well bore to determine the maximum compressive stress $\sigma_{HMAX}$. In this approach the first cycle of pressurization to breakdown is assumed to propagate a vertical crack in the direction perpendicular to the minimum compressive stress $\sigma_3$ so that breakdown in subsequent cycles of pressurization is associated with re-opening the induced crack. Then the *in situ* stress $\sigma_{HMAX}$ is computed from (1) with $T = 0$ and $P_b$ equal to the breakdown pressure for the second and later cycles of pressurization. The cyclic pressurization technique has the obvious advantages of simplicity and accuracy through elimination of rock strength parameters that are the least well-known terms in (1) and (17). This technique holds considerable promise, provided that breakdown on subsequent pressurization cycles can be related unambiguously to the opening of induced cracks perpendicular to the minimum compressive stress.

Comparison of Two Methods for Computing $\sigma_{HMAX}$

So far, two methods for computing $\sigma_{HMAX}$ have been discussed. The first, based on a critical tensile stress fracture criterion and neglect of consideration of cracks in the wall of the laboratory specimen and the field well, gives [from (1) and (4)]

$$\sigma^{t}_{HMAX} = 3P_s - P_b + \left(\frac{w^2+1}{w^2-1}\right) P_i - P_o. \tag{19}$$

The second, based on linear elastic fracture mechanics gives

$$\sigma^{f}_{HMAX} = \frac{G}{(G-F)} P_s - \frac{F}{(G-F)} P_b + \frac{K_{Ic}}{0.6(G-F)\sqrt{\pi L}} \tag{20}$$

For both (19) and (20) failure is assumed to occur on the radial plane perpendicular to the minimum *in situ* compressive stress.

If L/a is much less than unity, say less than 0.1, then G is approximately 1.5 F and G-F is approximately unity so that (20) reduces to

$$\sigma^{f}_{HMAX} = 3P_s - 2P_b + \frac{K_{Ic}}{\sqrt{\pi L}\,(0.6)} \tag{21}$$

Comparison of (19) and (21) reveals the primary differences between the two methods for computing $\sigma_{HMAX}$. The term in (21) related to the breakdown pressure $P_b$ is twice the corresponding term in (19). This doubling of the effect of the bore pressure $P_b$ is due to the fact that, according to linear elastic fracture mechanics, the stress-intensity factor for a shallow, pressurized, radial crack in the wall of a cylindrical cavity is obtained from the addition of two equal effects: (i) the circumferential tensile stress $P_b$ due to internal pressure acting on the well bore and (ii) the pressure $P_b$ acting on the crack face. Superposition, locally, of a uniform tensile stress $P_b$ removes the compressive stress on the crack face and causes the region containing the shallow crack to be subjected to an effective tensile stress $P_b$, in addition to the tensile stress $P_b$ due to (i). The effect (ii) of pressure acting on the faces of the well bore crack is not included in (19).

The second difference between (19) and (21) is in the treatment of rock strength. In (21) the rock strength is characterized by the size L of the dominant crack and by the critical stress-intensity factor $K_{Ic}$ necessary for crack advance. In (19) the rock strength is characterized by the nominal tensile stress in the wall of a thick-walled cylinder that bursts under an internal pressure $P_i$. Because $P_i$ and $P_b$ are generally not equal, the influence of pressure acting on bore hole cracks is not incorporated consistently when (19) is used. Also, Equation (19) does not incorporate the size effect associated with the probability that the dominant crack intersecting the well bore will be larger than the largest crack intersecting the bore of the laboratory specimen.

Finally, use of (19) requires the value of the pore pressure $P_o$ at breakdown. On the other hand, the pore pressure does not appear in (21) but is incorporated directly because, according to linear elastic fracture mechanics, the stress-intensity factor for a given geometry and loading is unaffected by superposition of a uniform hydrostatic pressure. Thus, if the total stress $\sigma^f_{HMAX}$, $P_s$, and $P_b$ in (21) are replaced by $\tilde{\sigma}^f_{HMAX} + P_o$, $\tilde{P}_s + P_o$, $\tilde{P}_b + P_o$, where $\tilde{\sigma}^f_{HMAX}$, $\tilde{P}_s$, and $\tilde{P}_b$ denote effective stresses, then (21) is changed only by the replacement of total stresses by effective stresses and pore pressure does not appear explicitly. The pore pressure is required in (19) in order for a similar substitution to lead to a relationship between effective stresses and rock strength that is independent of pore pressure.

## CONCLUDING REMARKS

A fracture mechanics analysis of hydrofracturing indicates that, if the principal stresses are not equal, fractures will tend to become oriented normal to the minimum *in situ* compressive stress as the crack length increases. For crack lengths of several meters the crack should be quite nearly perpendicular to the minimum compressive stress and the shut-in pressure $P_s$ should provide an accurate estimate of the minimum principal stress. These conclusions are consistent with previous interpretations of hydrofracturing tests.

The fracture mechanics approach provides helpful insight into the more difficult problem of determining the principal stress directions and the maximum principal stress. This approach suggests that more accurate determination of the maximum principal stress can be achieved if better information is obtained on the size and shape of the dominant well bore crack and on the value of $K_{Ic}$ under field conditions. The analysis suggests that uncertainties associated with crack geometry can be reduced greatly by modifying hydrofracturing tests to include the cutting of narrow notches of known depth. If these notches are made deeper than all cracks in the cores, then the hydrofracturing test should become comparable to that of the laboratory test used for determining $K_{Ic}$. Also, by notching two different sections in two known orthogonal directions it should be possible to determine $\sigma_{HMAX}$ and the principal stress directions with reasonable certainty (See Equation (16) and the discussion following it). Improved values of $K_{Ic}$ under field conditions should be attainable by conducting fracture toughness tests under confining pressure as discussed by Abou-Sayed [1977].

The measured principal stress directions agree well with the prevailing geological structure in the region and with the principal stress directions reported by Overbey [1976] from a series of measurements in West Virginia. A basement structure map of the region in which the reported test was conducted is shown in Figure 12. The map, adapted from Harris (USGS Map I-919 D, 1975) by Overbey [1976], shows a projection of the Rome Trough through the northwestern edge of West Virginia. Schumaker [1976] describes the Rome Trough as a graben bounded by high-angle, normal faults. This structure lies within an area which is a junction of three distinct geological provinces [Werner, 1976].

1) Central Appalachian Fold Belt
2) Southern Appalachian Thrust Fault Belt
3) Appalachian Plateau with Basement Faults

Although it is not known whether or not the basement faults penetrate into the Devonian Shales in this area, Overbey's measurements [1976] suggest a correlation of principal stress directions with the basement structure. At locations which fall outside the projection of the Rome Trough, the measured direction of $\sigma_{HMAX}$ are oriented generally E-W and are normal to the predominately N-S strike of the thrust faults and foldings of the Appalachian Mountains. Measured directions of $\sigma_{HMAX}$ which fall within the projection of the Rome Trough trend N 45° E to N 50° E, or parallel to the strike of the basement faults and in agreement with the directions reported here.

For the relative magnitudes of the principal stresses to be consistent with the expected state in a region bounded by normal faults [Hubbert and Willis, 1957] the vertical stress should be the maximum principal stress. The minimum principal stress direction should be normal to the strike of the

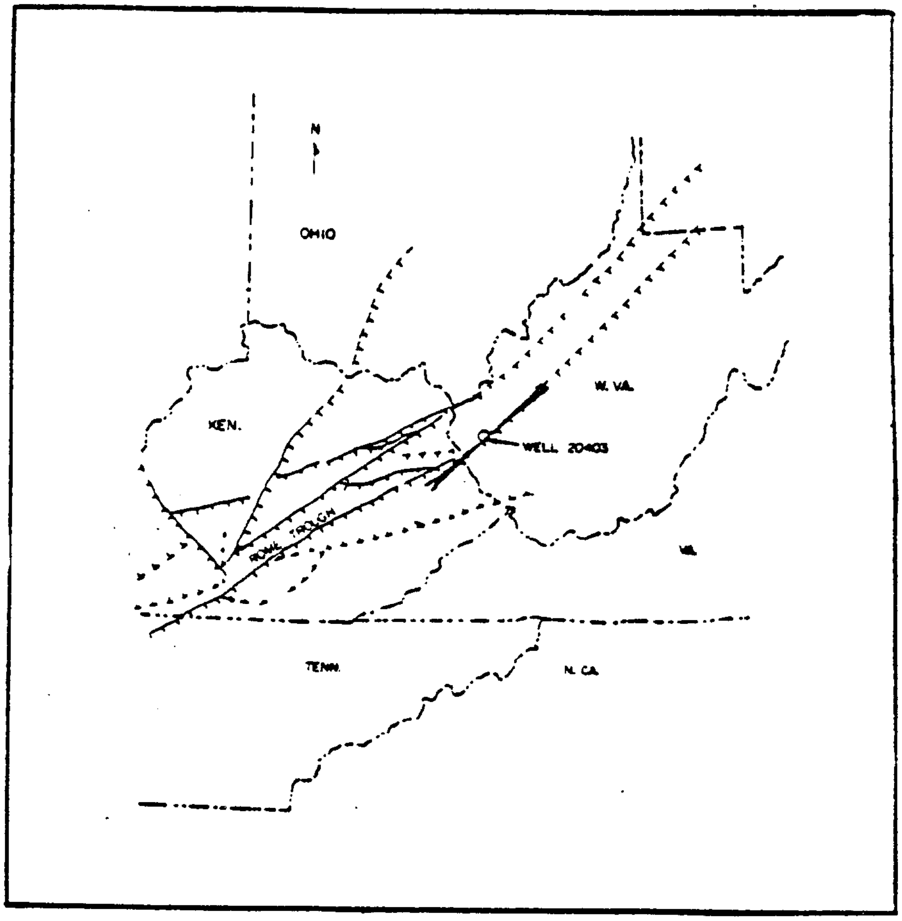


Figure 12. Basement Structure of Kentucky-West Virginia Adapted from Overbey [1976] with the Direction of Maximum Horizontal Stress at Well 20403

normal faults and the intermediate principal stress direction should be parallel to the strike of the faults. In order for the *in situ* stresses reported here to conform with such an orientation of principal stress directions it would be necessary to reduce the estimated value of $\sigma_{HMAX}$ to a value between $\sigma_{HMIN}$ and $\sigma_{OB}$. According to linear elastic fracture mechanics such a revision in the computed value of $\sigma_{HMAX}$ would require (i) an initially open well bore crack that could accept the fracturing fluid at a pressure $P_b$ for which the nominal circumferential stress at the well bore is compressive and (ii) an appreciably larger crack length and/or smaller $K_{Ic}$ so that the first term in (18) can be reduced by roughly a factor of two. Although this combination of circumstances is clearly possible, it is believed to be more likely that the maximum principal stress is horizontal as reported in Table III and Table IV.

In summary, the complex geological structure in this region does appear to be related to the measured orientation of the stress field. It is not yet clear why stresses relating to the large scale deformation and mountain building during the Paleozoic Era should still remain a controlling factor in this region. However, the evident influence of ancient structural features on present-day measurements should discredit attempts to smooth these measurements across distinct structural boundaries.

# APPENDIX

## Description of Laboratory Tests

### Fracture-Toughness Tests

The experiment used to determine a materials resistance to fracture extension consists of subjecting a prenotched, thick-walled cylinder to an internal pressure that loads the wall at the inner radius but does not load the faces of the notch. This type of test has been proposed by Clifton, *et al.*, [1976] to measure the critical stress-intensity factor $K_{Ic}$, of geologic materials. The experimental configuration is shown in Figure A1. The test specimen is a thick-walled cylinder with an outer-to-inner-diameter ratio of 10 or more and an outer diameter of 96.5mm. Two radially opposed prenotches are cut into the inner bore and penetrate one tenth of the wall thickness along the full length of the specimen. Prenotching is accomplished using a diamond-impregnated copper wire, 0.2 mm (0.008 in.) in diameter. A soft impermeable jacket of urethane tubing with a thickness of 0.15mm (0.060 in.) prevents the fluid pressure from loading the crack faces and the fluid from permeating the rock matrix. The jacket extends into steel end caps that are attached to each end of the sample. The seal for the pressurizing fluid is made in the steel end caps as shown in Figure A1. A cone shaped rubber plug forms a seal between the inside of the urethane jacket and the fluid port when a small axial force is applied to the system. The seal pressure is varied by changing the amount of interference between the steel end cap and the compression rod. A small steel tube in the upper rubber end seal allows fluid to communicate between the inner bore and the high pressure line.

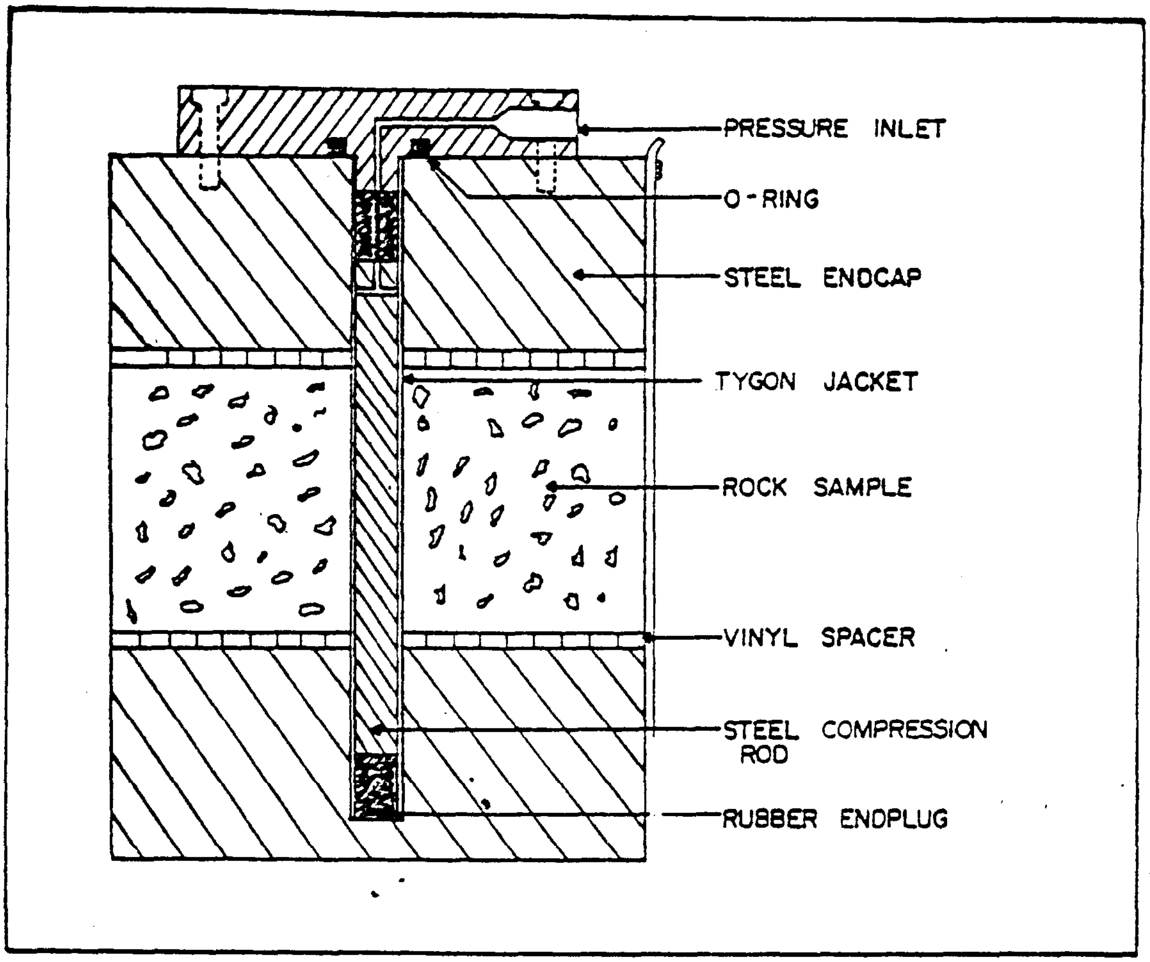


Figure A1. Cross-section of a typical specimen for fracture-toughness-burst test.

To evaluate $K_{Ic}$ for a given sample material the internal pressure is increased slowly and recorded until a crack is observed to propagate. As predicted by the analysis of this configuration [Bowie and Freese, 1970] the first phase of crack propagation is stable for wall-thickness ratio greater than 10. Further increase of the internal pressure initiates unstable crack growth and results in catastrophic failure of the cylindrical specimen. The maximum internal pressure ($P_m$) that can be applied to the inner wall is related to the critical stress-intensity factor, $K_{Ic}$, of the tested material and the geometry of the sample, by the following equation:

$$K_{Ic} = K^*_{Ic} \left(P_m \sqrt{\pi a_o}\right)$$

where $a_o$ is the internal radius and $K^*_{Ic}$ corresponds to the local minimum value of the numerically calculated function $K^*_I$ shown in Figures A2 and A3 for different wall thickness ratios, w, and crack geometry. For example, for a wall thickness ratio of 10, $K^*_{Ic}$ is given by 0.245 or 0.42 depending on whether the sample has single or double radial cracks, respectively.

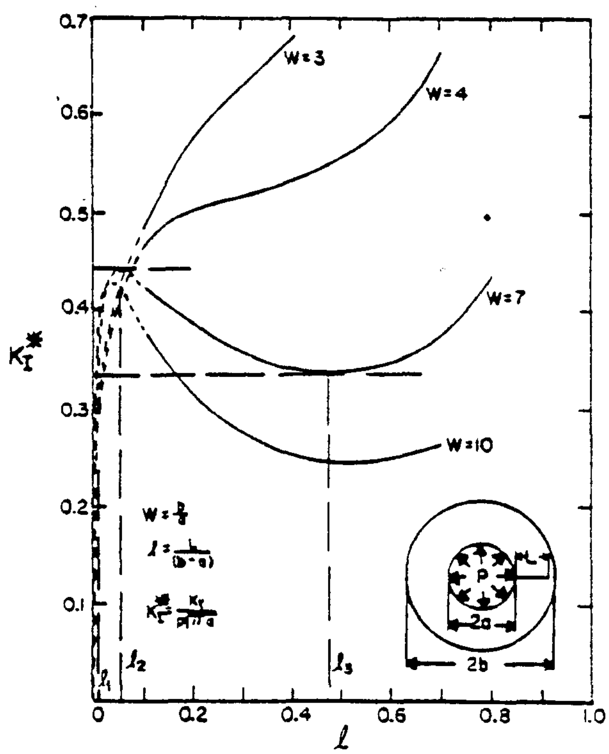

Figure A2. Stress-intensity factor for jacketed cylinder with one radial crack (from Bowie and Freese, 1972).

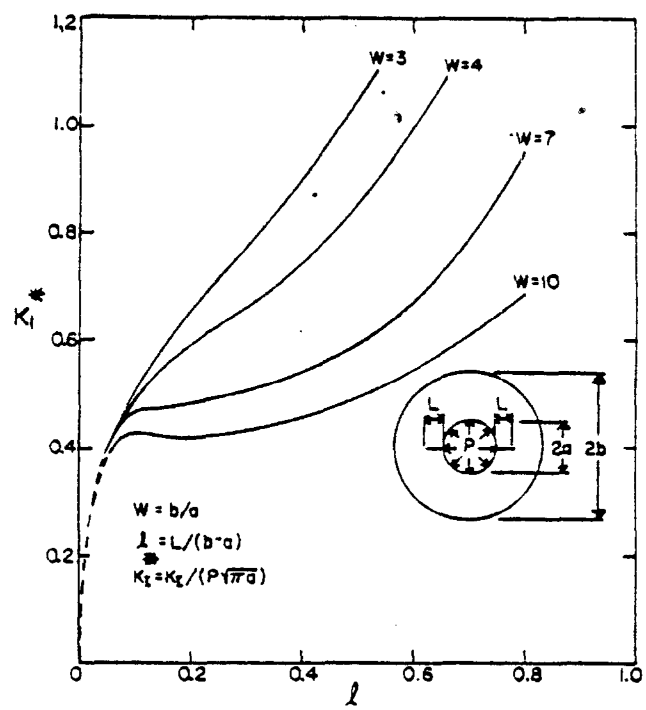

Figure A3. Stress-intensity factor for jacketed cylinder with two radial cracks (from Bowie and Freese, 1972).

## Results of Fracture Toughness Tests

The results of the fracture toughness tests are further evidence of the anisotropic nature of this shale (see Table A1). Figures A4 and A5 are photographs of the two samples that were pre-notched and pressurized with impermeable membranes. In Figure A4 the failure plane originated at the tips of the pre-notch but turned the moment it intersected a natural fracture. The failure plane in Figure A5 began in three places, at one pre-notch and at radially opposed points along a natural fracture, however, catastrophic failure occurred along the natural fracture.

TABLE A1

Results of Fracture Toughness Tests

| Sample Depth m (ft.) | $b_o/a_o$ w | $P_m$ Failure Pressure MPa (psi) | $K_{Ic}$* | $K_{Ic}$ MPa$\sqrt{m}$ (psi$\sqrt{in}$) | Remarks |
|---|---|---|---|---|---|
| 826.5 (2711) | 10.47 | 19.5 (2825) | 0.4 | 42.4 (1220) | Failure initiated along notch then turned along pre-existing fracture |
| 839 (2761) | 10.47 | 26.21 (3800) | 0.25 | 38.2 (1100) | Failure ignored notch and occurred on a pre-existing fracture |

TABLE A2

Tabulation of Functions F and G [Paris and Sih, 1965]

| L/a | One Radial Crack F(L/a) | One Radial Crack G(L/a) | Two Radial Cracks F(L/a) | Two Radial Cracks G(L/a) |
|---|---|---|---|---|
| 0.00 | 2.26 | 3.39 | 2.26 | 3.39 |
| 0.10 | 1.98 | 2.73 | 2.06 | 2.93 |
| 0.20 | 1.82 | 2.30 | 1.83 | 2.41 |
| 0.30 | 1.69 | 2.04 | 1.70 | 2.15 |
| 0.40 | 1.58 | 1.86 | 1.61 | 1.96 |
| 0.50 | 1.49 | 1.73 | 1.57 | 1.83 |
| 0.60 | 1.42 | 1.64 | 1.52 | 1.71 |
| 0.80 | 1.32 | 1.47 | 1.43 | 1.58 |
| 1.00 | 1.22 | 1.37 | 1.38 | 1.45 |
| 1.50 | 1.06 | 1.18 | 1.26 | 1.29 |
| 2.00 | 1.01 | 1.06 | 1.20 | 1.21 |
| 3.00 | 0.93 | 0.94 | 1.13 | 1.14 |
| 5.00 | 0.81 | 0.81 | 1.06 | 1.07 |
| 10.00 | 0.75 | 0.75 | 1.03 | 1.03 |
| ∞ | 0.707 | 0.707 | 1.00 | 1.00 |

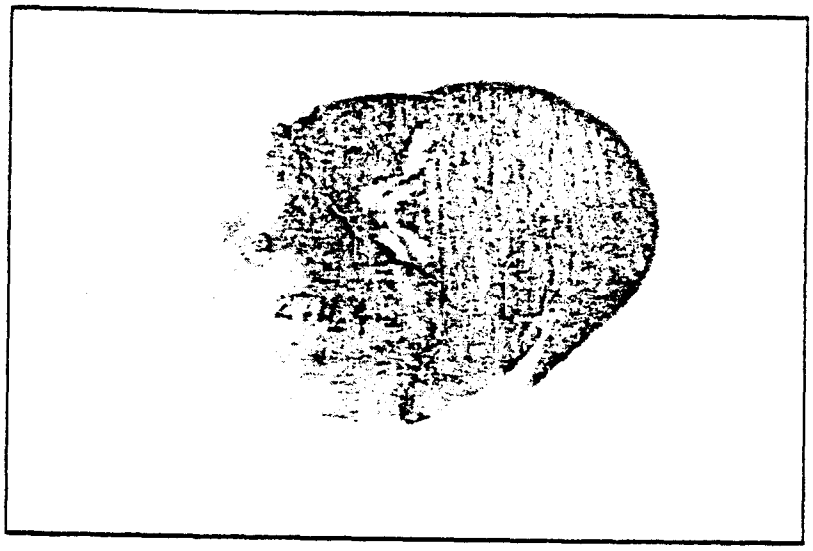

Figure A4. Fracture toughness sample from 826.5 m (2711 ft.)

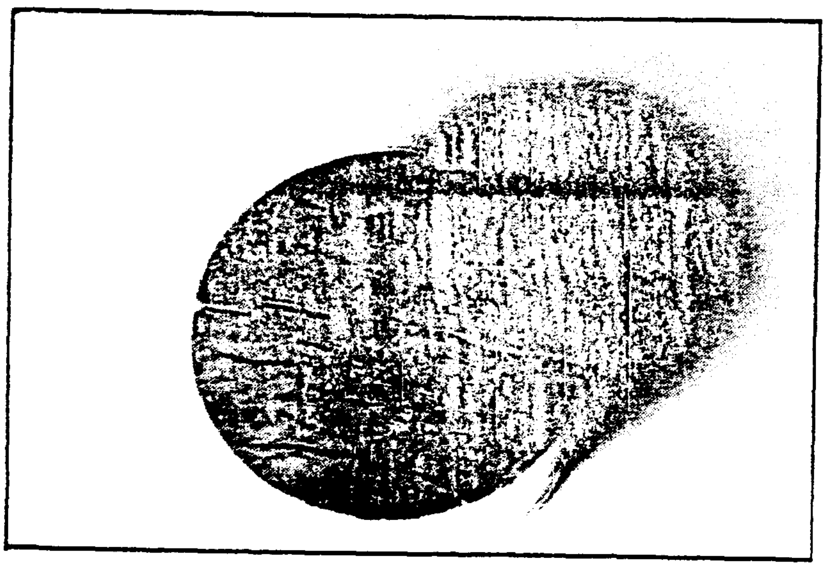

Figure A5. Fracture toughness sample from 829 m (2761 ft.)

ACKNOWLEDGEMENT

The authors would like to acknowledge the help of Dr. B. C. Haimson, of the University of Wisconsin, Madison, in supervising the field experiment. Professor J. Handin of Texas A & M and Dr. H. Swolfs of Terra Tek have pointed out the effects of the nearby garben on the nature of the lithological stress in the field experiment. Helpful discussions with Dr. A. H. Jones and Dr. E. R. Simonson of Terra Tek, and pertinent comments and criticism of many individuals from the oil and gas industry with regard to the first draft of this report made it possible to have the work in its present form. Acknowledgment is also extended to the anonymous reviewers for their helpful suggestions.

REFERENCES

Abou-Sayed, A. S., "Fracture toughness $K_{IC}$ of triaxially loaded Indiana Limestone," in *Energy Resources and Excavation Technology*, Proc. of 18th U.S. Symposium on Rock Mechanics, Keystone, Colorado, June, 1977.

Bowie, O. L. and Freese, D. E.,"Elastic analysis for radial crack in a circular ring," *Eng. Fracture Mech.*, vol. 4,pp. 315-320, 1972.

Bredehoeft, J. D., Wolff, R. G., Keys, W. S. and Shuter, E., "Hydraulic fracturing to determine the regional in situ stress field, Piceance Basin, Colorado," Geological Society of America, vol. 87, pp.250-258, 1976.

Clifton, R. J., Simonson, E. R., Jones, A. H. and Green, S. J., "Determination of the critical stress intensity factor $K_{IC}$ in a circular ring," *Experimental Mechanics*, vol. 16, pp. 233-238, 1976.

Clifton, R. J., "Some recent developments in fracture mechanics," *Terra Tek Report* TR 73-70, November, 1974.

Haimson, B. and Fairhurst, C., "Initiation and extension of hydraulic fractures in rocks," *Society of Petroleum Engineers Journal*, vol. 7, pp. 310-318, 1967.

Haimson, B., "Hydraulic fracture in porous and nonporous rock and its potential for determing in situ stress at great depth," *Ph.D Thesis*, University of Minnesota, July, 1968.

Haimson, B., LaComb, J., Jones, A. H. and Green, S. J., "Deep stress measurements in tuff at the Nevada test site," *Terra Tek Report* TR 74-11, January, 1974.

Hussain, M. A., Pu, S. L. and Underwood, J., "Strain-energy release rate for a crack under combined mode I and Mode II," *Fracture Analysis*, Proc. of the 1973 National Symposium on Fracture Mechanics, Part II, ASTM, STP 560, 1974.

Hubbert, M. K. and Willis, B. G., "Mechanics of hydraulic fracturing," *Trans - AIME* , vol. 210, pp. 153-166, 1957.

Ingraffea, A. R. and Heuze, F. E., "Fracture propagation in rock: laboratory tests and finite element analysis," *Site Characterization*, Proc. of the 17th U. S. Symposium on Rock Mechanics, paper 5C4, 1976.

Irwin, G. R., "Analysis of stresses and strains near the end of a crack transversing a plate," *J. Appl. Mech.*, vol. 24, pp. 361-364, 1957.

Irwin, G. R., "Fracture mechanics," in *Structural Mechanics*, J. N. Goodier and N. J. Hoff Editors, pp. 557-594, Pergamon Press, N.Y., 1960.

Johnson, J. N., Clifton, R. J., Simonson, E. R. and Green, S. J., "Analysis of fracture for hollow cylindrical and spherical rock specimens subjected to internal pressure with applications to underground nuclear containment," *Terra Tek Report* TR 73-50, September, 1973.

Kehle, R. O., "The determination of tectonic stresses through analysis of hydraulic well-fracturing," *J. Geophys. Res.*, vol. 69, pp. 259-273, 1964.

Knauss, W. G., "Propagation of a crack under general, inplane tension," *Int. Journal Fracture Mech.*, vol. 8, pp. 114-117, 1972.

Lamont, N. and Jessen, R. W., "The effects of existing fractures in rock on the extension of hydraulic fractures," *J. of Petr. Tech.*, vol. 15, pp. 203-209, 1963.

Overbey, W. K., "Effect of in situ stress on induced fractures," Proc. of the Seventh Appalachian Petroleum Geology Symposium, Morgantown, pp. 182-211, 1976.

Palaniswamy, K. and Knauss, W. G., "Propagation of a crack under general, inplane tension," *Int. Journal Fracture Mech.*, vol. 8, pp. 114-117, 1972.

Paris, P.C. and Sih, G.C., "Stress analysis of cracks," in *Fracture Toughness Testing and Its Application*, ASTM, STP 381, 1965.

Randolph, P.L., "MHF Research in Green River Basin," Proc. of the Symposium on Stimulation of Low Permeability Reservoirs, Colorado School of Mines, February, 1976.

Raleigh, C. B., Healy, J. H. and Bredehoeft, J. D., "Faulting and crustal stress at Rangely, Colorado, "Flow and fracture of rock, *The Griggs Volume, Geophysical Monograph Series of the American Geophysical Union*, Washington, D. C., p. 275, 1972.

Rice, J. R. and Levy, N., "The part-through surface crack in an elastic plate," *Brown University Technical Report* No. NASA NGL 40-002-Q8013 to the National Aeronautics and Space Administration, 1970.

Rice, J. R., "Mathematical analysis in the mechanics of fracture," in *Treatise on Fracture*, vol. II, Ch. 3, H. Liebowitz editor, Academic Press, pp. 191-311, 1968.

Scheidegger. A. E., "On the connection between tectonic stresses and well fracturing data," *Geofis. Pura Appl.*, vol. 46, pp. 66-76, 1960.

Schmidt, R. A., and Huddle, C. W., "Effect of confining pressure on fracture toughness of Indiana Limestone," in *Site Characterization*, Proc. of 17th U.S. Symposium on Rock Mechanics, Snowbird, Utah, August, 1976.

Schumaker, R. C., "A digest of Appalachians structural geology," Proc. of the Seventh Appalachian Petroleum Geology Symposium, Morgantown, pp. 75-93, 1976.

Sneddon, I. N., "The distribution of stress in the neighborhood of a crack in an elastic solid," Proc., *Royal Soc. London A,* vol. 187, pp. 229-260, 1946.

Swolfs, H., Lingle, R. and Thomas, J., "Strain relaxation tests on selected cores from Columbia Gas System Service Corporation Well No. 20402, Lincoln County, West Virginia," *Terra Tek Technical Report* TR 76-60, November, 1976.

Underwood, J. H., "Stress-Intensity factors for internally pressurized thick-walled cylinders," *Special Technical Publication 513, American Society of Testing and Materials,* p. 59, 1972.

Werner, E., "Remote sensing studies in the Appalachian plateau for application to fossil fuel extractions," Proc. of the ERDA Symposium on Enhanced Oil and Gas Recovery," Tulsa, vol. 2, C-2, 1976.

Zoback, M. D. and Pollard, D. D., "Hydraulic fracture propagation and the interpretation of pressure time records for in situ stress determination," Preprint of a paper submitted to *J. of Geophys.* for publication.

Open File No. 199
Volume 2 - Appendices

# TERRA TEK REPORT

# DETERMINATION OF THE STRAIN RELAXATION AND THEIR RELATION TO SUBSURFACE STRESSES IN THE DEVONIAN SHALE

# FINAL REPORT
# TASK II

# DETERMINATION OF THE STRAIN RELAXATION AND THEIR RELATION TO SUBSURFACE STRESSES IN THE DEVONIAN SHALE

By

H. S. Swolfs
R. Lingle
J. M. Thomas

Submitted to

Columbia Gas System Service Corporation
1600 Dublin Road
Columbus, Ohio 43215

Attention: Eric C. Smith

Submitted by

Terra Tek, Inc.
University Research Park
420 Wakara Way
Salt Lake City, Utah 84108

TR 77-12(F)
February 1977

TABLE OF CONTENTS

## LIST OF TABLES

# SUMMARY OF TASK II

## DETERMINATION OF THE STRAIN RELAXATION AND THEIR RELATION TO SUBSURFACE STRESSES IN THE DEVONIAN SHALE

Strain-relaxation tests were performed on twenty-four specimens of Devonian Shale obtained from the Columbia Well No. 20402, Lincoln County, West Virginia, for the overall purpose of identifying, among the gas-bearing shales, the prime zones for stimulation (MHF) treatment within the Devonian Shale sequence.

The results of this work provide information on the strains and stresses in only three shale zones - Upper Gray Shale, Middle Gray Shale and Middle Brown Shale - and yield the following interpretations:

1. The rate of strain relaxation is 2 to 2.5 times higher in the Middle Brown Shale zone than in the overlying Gray Shale zones, which suggest that
2. The minimum horizontal matrix-stress in the Middle Brown Shale zone could be up to 30 percent lower than the minimum horizontal matrix-stress in the upper Gray Shale zones.

From these measurements alone it appears that the upper Gray Shale zones may act as an effective barrier which prevents upward fracture propagation, thereby promoting larger lateral extension of a fracture initiated within the Middle Brown Shale, a prime gas-bearing zone.

## INTRODUCTION

The question addressed in this report is as follows: Can an inexpensive but reliable core-analysis technique be developed to provide useful information on the present-day stress distribution in subsurface reservoirs and aid in the identification and selection of prime gas-bearing zones for stimulation by massive-hydraulic-fracture (MHF)?

To provide answers to this question we have begun to use a technique that very accurately measures the small dimensional changes (strain relief) of Devonian Shale samples after they are cored and brought to the surface. The smallest dimensional change (strain) that can be detected by this technique is of the order of several micro-inches*. For example, a four-inch diameter shale sample that strained or relaxed ten micro-inches ($\Delta$ 1/1 = $10 \times 10^{-6}$) changed dimensions by 0.00004 inch.

Basically, the idea is that as a sample of any kind of rock is cored and taken from its subsurface environment, it will experience a rapid change in stresses and consequently relax and change dimensions. The amount of relaxation over a period of time after coring is related to the magnitude of the subsurface stresses or, more specifically, the magnitude of the difference between the greatest (overburden) stress and the least (minimum-horizontal) stress in the formation from which the sample was obtained.

From these relaxation measurements, however, we can only develop a qualitative estimate of the distribution of the subsurface minimum-horizontal stress-gradient and determine the relative changes, if any, in the gradient distribution from formation to formation. Nevertheless, this kind of information is useful and important because it can lead to an early recognition of anomalies in the subsurface stress gradients (usually assumed

* One micro-inch = one inch per one million inches = $10^{-6}$.

to increase linearly with depth) and the identification of prime zones for stimulation and fracture-treatment.

In this report we will briefly outline the important aspects of the well-site technique of strain relaxation and its limitations. These will be followed by the description of the strain-relaxation results obtained in samples from the upper Gray Shale and Middle Brown Shale zones in Columbia Well No. 20402. Next, attention will be focused on how these results can be interpreted to provide new and useful information and, finally, how they can be applied and lead to improvements in the results of a fracture treatment program.

# WELL-SITE TECHNIQUES

## Strain Relaxation

The technique used at the well-site consisted of selecting small pieces of rock as soon as they were removed from the core barrel and laid out for initial geologic identification and description. The rock was slabbed with a rock saw to provide two flat, parallel surfaces and result in a test specimen two inches thick and four inches in diameter. The top surface was air dried and then washed with acetone to dissolve whatever moisture was retained at the surface of the sample. A 45-degree strain-rosette was fastened in the central part of the top surface using a quick-setting epoxy (Figure 1). Gage No. 2 (center gage) in each rosette was aligned with the reference (orientation) groove of the sample. The principle of operation of a 45-degree strain rosette is outlined in Appendix I.

Figure 1. Core sample instrumented with 45-degree strain rosette. Gages 1, 2 and 3 are seen from left to right. The sample is Dakota sandstone cored in a western gas well.

Each of the three strain gages in the 45-degree rosette were wired into a switching unit and a strain indicator. The switching unit allowed the concurrent measurement of strain changes in as many as 12 specimens. Data were recorded manually every half-hour for the first day and every hour for all subsequent days. Three strain-time curves were drawn for each specimen to provide the basic data from which to calculate the rates and magnitudes of strain relaxation.

The limitations in reliably measuring the strain relaxation in rock samples should be clearly recognized. They are listed as follows:

1. The rock sample must be representative of the subsurface formation.
2. The rock samples must be maintained under constant moisture and temperature conditions. A change in temperature of 1°F, for example, will result in an apparent strain of about $6 \times 10^{-6}$ or 6 micro-inches.
3. The rock samples should be oriented geographically to determine the directions of the major axes of strain relaxation.
4. The rock sample should be instrumented soon after removal of the subsurface stresses to assure maximum accuracy of measurement.
5. The elastic strain-relaxation, which occurs instantaneously upon coring down-hole, is not detected by this technique.

Velocity Measurements

Longitudinal (P) wave measurements were made on rock samples as soon as possible after the coring of Columbia Well No. 20402. These measurements were made in conjunction with, and with the same objective as, the strain relaxation measurements.

Figure 2 shows the technique used to obtain the transit times of the ultrasonic wave through the rock sample. A DC pulse generator was used to

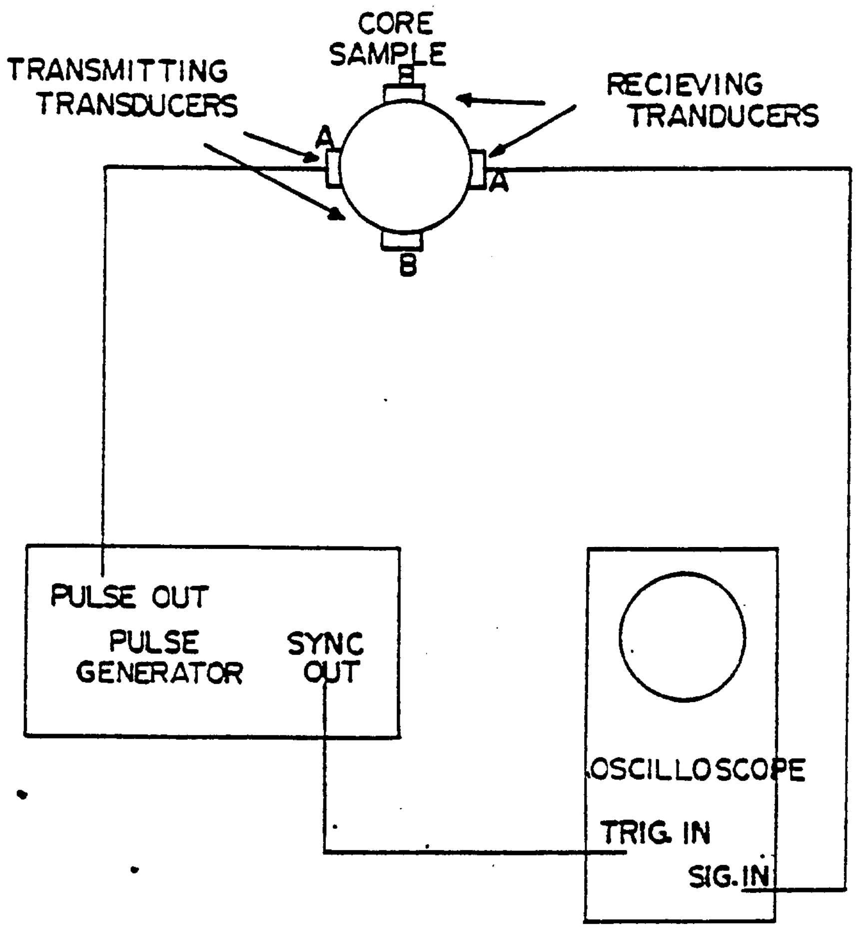


Figure 2. Schematic diagram of field equipment used to measure changes in P-wave velocity along two horizontal directions in a relaxing core.

excite the transmitting transducer and the same time to initiate the sweep on an oscilloscope. The signal produced by the receiving transducer was displayed as a vertical deflection on the oscilloscope trace. The travel times were obtained directly from the calibrated sweep speed of the trace. The accuracy of the time measurements was of the order of three percent.

The transit times were determined in two planes across the rock sample. In order to eliminate the effects of changes in the transducer to sample bonding the transducer assembly (Figure 3) was firmly attached to the rock,

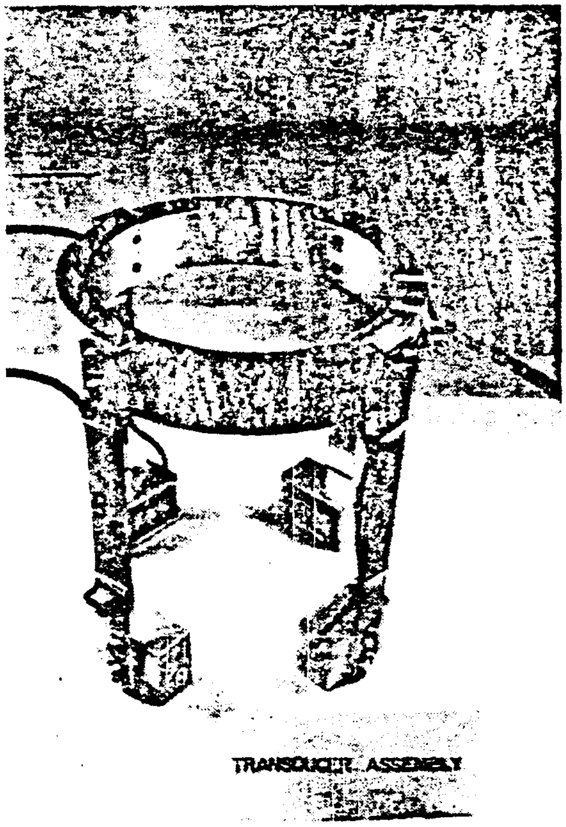


Figure 3. Photograph of sonic-transducer assembly.

and remained so for the duration of the test. The transducer elements were made from PZT-5 material and were cut to resonate at a natural frequency of 200 kilohertz.

It should be emphasized, however, that significant changes in velocity across the rock sample will occur only if the strain relaxation in the rock sample exceeds a certain minimum value, thereby causing significant changes in the elastic moduli of the rock sample. In some sandstones, for example, the lower limit of strain relaxation is about 500 micro-inches ($5 \times 10^{-4}$) beyond which velocity changes can be observed.

## RESULTS

### Strain Relaxation

The strain-time plots (Figures A1 through A21, Appendix II, form the basic data and consist of three curves. Each curve represents each strain gage in the 45-degree rosette applied to the rock surface (Figure 1). Because of the large, daily temperature variations at the well site during the measurement period, each curve has been corrected for temperature using a correction factor of $10 \times 10^{-6}/°C$ ($6 \times 10^{-6}/°F$).

The data indicates that the very small strain changes with time are nearly uniform in all directions. There were a few exceptions, however. Samples No. 1 (Figure A1) showed maximum horizontal, relaxation of about $240 \times 10^{-6}$ along a direction (N 10° W) almost perpendicular to the predominant fracture trend (N 70° E) in the Devonian Shale. The most dramatic strain changes were observed in Sample No. 7 (Figure A4). The overall relaxation, nearly uniform in the horizontal plane ($\varepsilon_{max} = 400 \times 10^{-6}$; $\varepsilon_{min} = 350 \times 10^{-6}$), is due to the formation of a sub-horizontal fracture about 1.5 inches below the top of the specimen during the time of measurement. Velocity measurements (Table I, 2768 feet), made below the fracture, indicated no measureable changes in P-wave velocity with time.

Nearly uniform or isotropic strain-relaxation was typical in the remainder of the shale specimens. Table I summarizes this information and also lists the relaxation rates (micro-inches per hour) for each specimen. Because at least three specimens were sampled from the bottom portion of the well, the relaxation rates in each group of samples were averaged and plotted against depth in Figure 4. This plot clearly shows that the relaxation rates are 2 to 2.5 times higher in the Middle Brown Shale (about 4 to $5 \times 10^{-6}$/hour) than those measured in the Upper and Middle Gray Shales (about $2 \times 10^{-6}$/hour).

Velocity Measurements

Ultrasonic measurements were made on a total of twelve core segments. The transducer assembly was mounted to the samples as soon as possible after coring, without interfering with the strain gaging operation. Table II is a listing of the changes in transit times at various intervals after the initial readings. The changes in transit time in all of the samples are very slight and are not considered in the discussion that follows.

TABLE I

Strain Relaxation Tests

| Sample (#) | Depth (feet) | Strain Relaxation Gage 1 ($\times 10^{-6}$) | 2 | 3 | Elapsed Time (hours) | Average Relaxation per Sample ($\times 10^{-6}$) | Average Relaxation Rate per Sample ($\times 10^{-6}$/hour) | Average Relaxation Rate per Core Run ($\times 10^{-6}$/hour)* |
|---|---|---|---|---|---|---|---|---|
| 3 | 2709 | 40 | 50 | 60 | 14 | 50 | 3.6 | 1.8 |
| 6 | 2703 | 0 | 0 | 0 | 14 | 0 | 0 | |
| 8 | 2759 | 30 | 0 | 0 | 15 | 10 | 0.7 | 2.1 |
| 9 | 2746 | 110 | 20 | 30 | 15 | 53 | 3.5 | |
| 10 | 3058 | 50 | 10 | 25 | 40 | 28 | 0.7 | 2.0 |
| 11 | 3057 | 150 | 200 | 150 | 40 | 167 | 4.2 | |
| 12 | 3049 | 50 | 50 | 35 | 40 | 45 | 1.1 | |
| 13 | 3117 | 25 | 15 | 10 | 24 | 17 | 0.7 | 1.2 |
| 14 | 3116 | 0 | 25 | 30 | 24 | 18 | 0.8 | |
| 15 | 3114 | 75 | 50 | 35 | 24 | 53 | 2.2 | |
| 16 | 3348 | 175 | 165 | 130 | 30 | 157 | 5.2 | 4.0 |
| 17 | 3343 | 40 | 110 | 120 | 30 | 90 | 3.0 | |
| 18 | 3340 | 85 | 130 | 135 | 30 | 117 | 3.9 | |
| 19 | 3403 | 150 | 110 | 60 | 32 | 107 | 3.3 | 4.0 |
| 21 | 3399 | 140 | 170 | 150 | 32 | 153 | 4.8 | |
| 22 | 3458 | 80 | 130 | 90 | 16 | 100 | 6.3 | 5.7 |
| 23 | 3457 | 90 | 110 | 100 | 16 | 100 | 6.3 | |
| 24 | 3435 | 70 | 60 | 80 | 16 | 70 | 4.4 | |

* This column is plotted against depth in Figure 25.

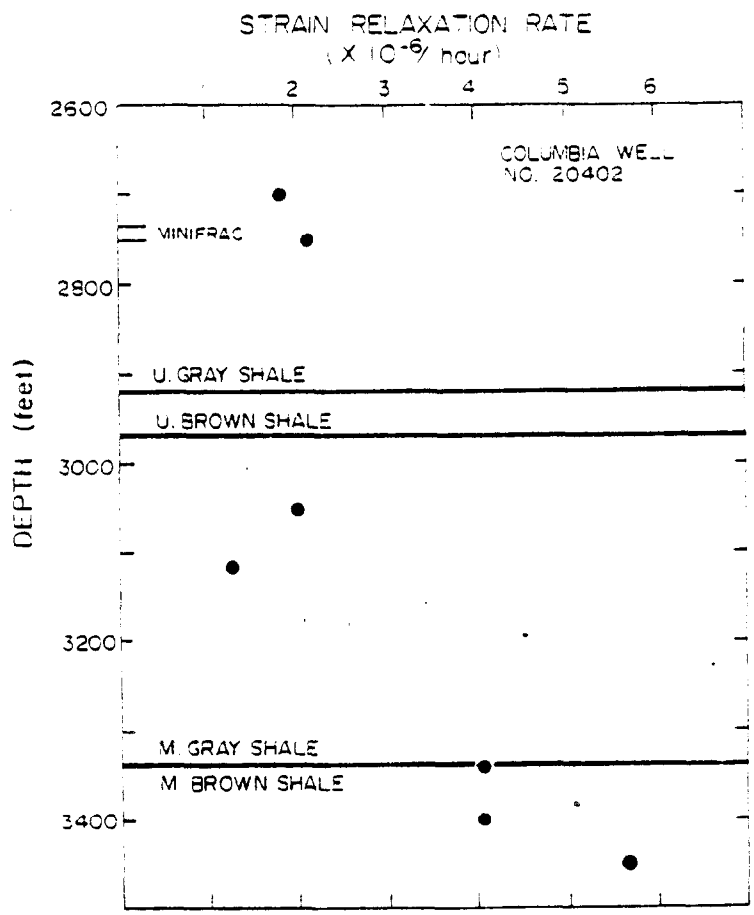


Figure 4. Plot of strain-relaxation rate against depth in Columbia Well No. 20402.

TABLE II

Change in P-Wave Transit Times with Elapsed Time on Cores Retrieved from Columbia Well #20402

| Sample Depth (ft) | Elapsed Time | | Normalized Transit Time (t/to) | |
|---|---|---|---|---|
| | Hrs. | Min. | "A" | "B" |
| 2686 | | 30 | 0.97 | 1.00 |
| 2686 | 14 | 10 | 0.97 | 0.98 |
| 2686 | 16 | 25 | 1.00 | 0.98 |
| 2698 | | 30 | 1.00 | 1.00 |
| 2709 | | 15 | 1.00 | 1.00 |
| 2709 | 11 | 30 | 1.02 | 1.00 |
| 2768 | | 20 | 1.00 | 1.00 |
| 2768 | | 50 | 1.00 | 1.00 |
| 2768 | 3 | 50 | 1.01 | 1.00 |
| 2768 | 26 | 20 | 1.01 | 1.00 |
| 3049 | | 15 | 1.00 | 1.00 |
| 3049 | | 35 | 1.00 | 1.00 |
| 3049 | 1 | | 1.00 | 1.00 |
| 3049 | 13 | 50 | 0.98 | 1.00 |
| 3114 | | 20 | 1.01 | 0.98 |
| 3114 | | 40 | 1.03 | 0.98 |
| 3114 | 1 | 30 | 1.03 | 0.98 |
| 3114 | 24 | 10 | 1.01 | 0.98 |
| 3117 | | 20 | 1.00 | 0.99 |
| 3117 | | 50 | 1.00 | 0.97 |
| 3117 | 1 | 35 | 1.00 | 0.97 |
| 3117 | 24 | 20 | 0.97 | 0.97 |
| 3340 | | 10 | 1.00 | 1.00 |
| 3340 | | 40 | 1.01 | 1.01 |
| 3340 | 1 | | 1.03 | 1.03 |
| 3340 | 2 | 10 | 0.99 | 0.99 |
| 3340 | 10 | 10 | 0.99 | 0.97 |
| 3344 | | 25 | 1.00 | ---- |
| 3344 | 10 | 50 | 1.00 | ---- |
| 3400 | | 20 | 0.97 | 1.00 |
| 3400 | 1 | | 0.96 | 0.99 |
| 3435 | | 15 | 1.00 | 1.02 |
| 3435 | | 45 | 0.99 | 1.00 |
| 3435 | 1 | 30 | 0.99 | 1.00 |
| 3459 | | 35 | 1.01 | 1.01 |
| 3459 | 1 | | 1.00 | 1.01 |
| 3459 | 1 | 45 | 1.01 | 1.03 |

# DISCUSSION

The subsurface stresses in sedimentary rocks are generally thought to increase linearly with depth: the vertical stress due to the overburden weight increases at about 1 psi per foot and the minimum-horizontal stress, on the average, increases at about 0.7 psi per foot (Figure 5).

The overburden stress-gradient of 1 psi per foot is generally accepted, although in geologically more recent environments (i.e., the Gulf Coast) this gradient is slightly less at 0.9 psi per foot. On the other hand, evidence is accumulating rapidly to suggest that the minimum-horizontal stress-gradient varies with rock type. For example, in hard rocks such as granites and quartzites the minimum stress-gradient can be as low as 0.5 psi per foot, in low-porosity sandstones it varies between 0.6 and 0.7 psi per foot and in weak shales and salt it can be as high as 0.9 psi per foot. It appears that the minimum stress-gradient decreases with increasing rock strength, but the underlying reason for this phenomenon is little understood.

The well-bore pressure gradient, required to induce and extend fractures in subsurface formations, is primarily dependent on the minimum stress-gradient and partially dependent on the overburden stress-gradient and formation pore-pressure gradient. It appears, therefore, that a good stimulation or fracture-treatment of a potential gas reservoir will, among other equally important variables, depend on the proper estimation or measurement of the stratigraphic distribution of the subsurface stress-gradients.

## Estimation of Devonian Shale Stress Gradients

Within the essentially monolithic Devonian Shale sequence, is it possible to determine whether or not significant variations in the minimum stress-

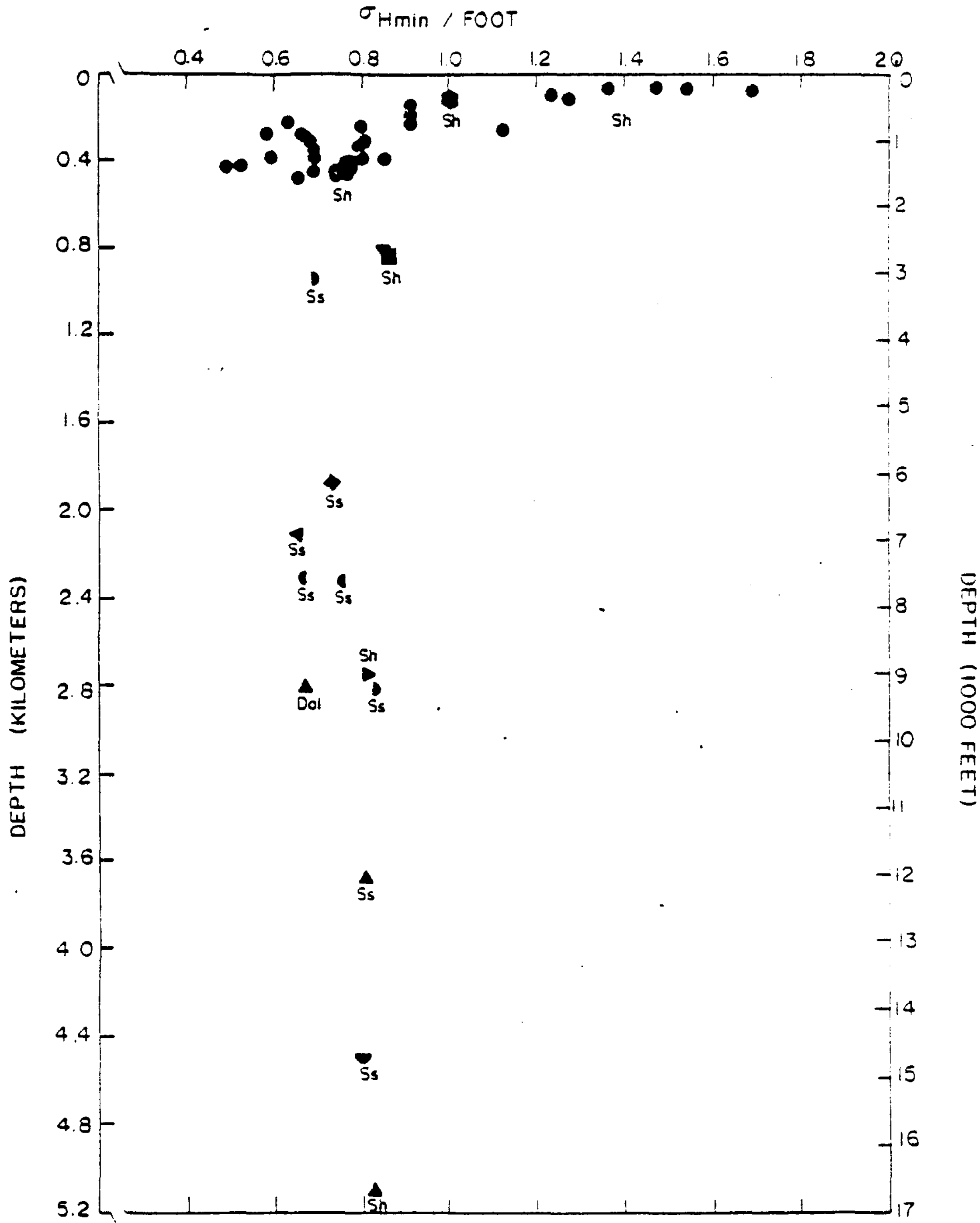


Figure 5. Vertical distribution of the minimum-horizontal-stress gradient (psi/ft) in sedimentary basins. Below a depth of 1000 feet the stress gradient is 0.7 psi/ft and increases slowly to 0.8 psi/ft at 17,000 feet. Ss - sandstone, Dol - dolomite and Sh - Shale.

gradients exist among the major shale zones and to predict whether or not the fracture-treatment of prime shale zones will be successful? A partial answer to this question is suggested by the strain-relaxation tests on cored samples from three major shale zones in the Devonian Shale.

Among the many variables that affect strain-relaxation in rock samples, the two that follow are the most influential:

- Rock type; i.e., soft versus hard rock, and
- Magnitude of local, subsurface stresses.

All of the samples were obtained from the Devonian Shale which is finely stratified and almost entirely composed of micaceous minerals (Figure 6). The compositional differences between the major shale zones are, if any, very slight and do not significantly affect the strain-relaxation results.

The limited information that is available on the behavior of rock samples under load indicates that strain-relaxation rates increase markedly, but not necessarily linearly, when higher loads are removed from the samples. An important variable in this context is the magnitude of the maximum stress difference. In the subsurface, the maximum stress difference is that between the overburden stress and the minimum horizontal stress ($\sigma_{O.B.} - \sigma_{Hmin}$).

The results of the strain-relaxation tests (Figure 4) show that samples from the Middle Brown Shale (MBs) zone relaxed at a rate 2 to 2.5 times greater than those representative of the upper Gray Shale (uGs) zones. Because the relaxation rates ($\dot{\varepsilon}$) are proportional to the local, subsurface, maximum stress differences ($\sigma_{O.B.} - \sigma_{Hmin}$), we can write for each shale zone:

$$\dot{\varepsilon}_{MBs} \propto (\sigma_{O.B.} - \sigma_{Hmin})$$

and (1)

$$\dot{\varepsilon}_{uGs} \propto (\sigma_{O.B.} - \sigma_{Hmin})$$

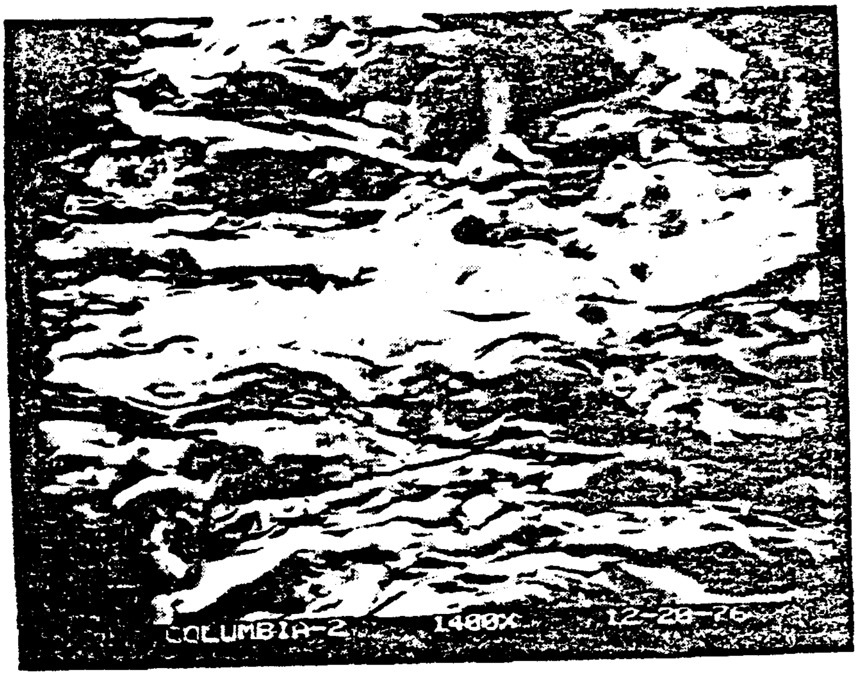


Figure 6. Scanning-electron micrograph of Middle Gray Shale (3056 ft) showing compacted clay particles. Scale: 1 cm = 20 microns.

The relaxation rates on the left of the proportionality can be written in terms of stress by multiplying $\dot{\varepsilon}$ by the Young's modulus (E) and an arbitrary time interval (t) and we get:

$$(E)\ (\dot{\varepsilon}_{MBs})(t) \propto (\sigma_{O.B.} - \sigma_{Hmin})$$

and (2)

$$(E)\ (\dot{\varepsilon}_{uGs})(t) \propto (\sigma_{O.B.} - \sigma_{Hmin})$$

Both sides of the proportionality are now in psi units, but the stresses on either side are not exactly equal to each other because the left-hand term refers to a stress in the sample and the right-hand term refers to the stress difference in the respective subsurface shale zones. We can now normalize proportionality (2) by dividing both sides by $\sigma_{O.B.}$ or, what amounts to the same thing since $\sigma_{O.B.}$ increases by 1 psi/foot, by depth (feet):

$$(E)(\dot{\varepsilon}_{MBs})(t)/ft \propto (1 - \sigma_{Hmin}/ft)$$

and (3)

$$(E)(\dot{\varepsilon}_{uGs})(t)/ft \propto (1 - \sigma_{Hmin}/ft)$$

The relaxation rates are now proportional to the minimum-horizontal stress-gradients in each of the shale zones. For the time being we assume that the Young's moduli (E) in both shale zones are equal to 4 x $10^6$ psi* and that (t) is equal to 100 hours. The relaxation rates in the Middle Brown Shale zone and in the upper Gray Shale zones are 4 x $10^{-6}$/hour and 2 x $10^{-6}$/hour, respectively (Figure 4). Upon inserting and multiplying these values on the left side of proportionality (3), reversing sides and rearranging, we get:

$$(\sigma_{Hmin}/ft)_{MBs} \propto (1 - 1600/ft)$$

and (4)

$$(\sigma_{Hmin}/ft)_{uGs} \propto (1 - 800/ft)$$

From well logs, the contact or boundary between the Gray Shale zone and the Middle Brown Shale zone in Columbia Well No. 20402 is at a depth of about 3340 feet. Upon dividing the numbers on the right side by 3340, we observe that the minimum stress-gradient in the Middle Brown Shale zone is proportional to (1 - 0.48) = 0.52 psi/ft and in the overlying Gray Shale the minimum stress-gradient is proportional to (1 - 0.24) = 0.76 psi/ft. The minimum stress-gradient in the Middle Brown Shale increases to 0.64 psi/ft if the Young's modulus (E) is reduced from 4 x $10^6$ to 3 x $10^6$ psi* (Figure 7).

It should be understood, at this point, that the values of the minimum stress-gradients just obtained are only estimates; they do not equal the actual subsurface stress gradients. However, these estimates serve an

* The values for Young's modulus (E) were taken from Terra Tek Progress Report No. 3 and 4.

important purpose. They suggest that the minimum stress-gradient is higher (by as much as 30 percent) in the Gray Shales than in the Middle Brown Shale. This, in turn, suggests that an artificial fracture could be induced and extended at lower bottom-hole pressures in the Middle Brown Shale and, furthermore, if the bottom-hole treating-pressure can be kept below a peak-pressure level (1600 - 1700 psi at the well-head*), the fracture propagating into the Middle Brown Shale can be contained and prevented from propagating upward into the Gray Shale zone because of the higher stress levels in this upper zone.

Comparison with Well-Bore Data

The discussion above may appear as so much conjecture. It is necessary, therefore, to compare the results and conclusions obtained from core-analysis (strain-relaxation) work with direct down-hole measurements.

The results of the Schlumberger Synergetic Log are abstracted in Figure 7A. It appears that the fracture-pressure-gradient profile of the Devonian Shale clearly identifies shale zones in which fractures can be induced and extended at lower bottom-hole pressures; i.e., the Lower Brown Shale (Marcellus) and the Middle Brown Shale. Although stresses do not appear explicitly in the calculation of the fracture-pressure-gradient profile, the log is an estimate of the minimum stress-gradients. The correlation between the subsurface data and the core-analysis (strain-relaxation) results is remarkably good (Figures 7A and B).

The result of the minifrac experiment performed by Terra Tek is also plotted in Figure 7A. The point represents the down-hole instantaneous shut-in pressure divided by the depth at which the measurement was made (2360 psi/2745 feet = 0.86). The agreement between the minifrac result

*This upper limit in pressure is equal to the breakdown pressure plus the difference in the horizontal stresses between the upper Gray Shales and the Middle Brown Shale.

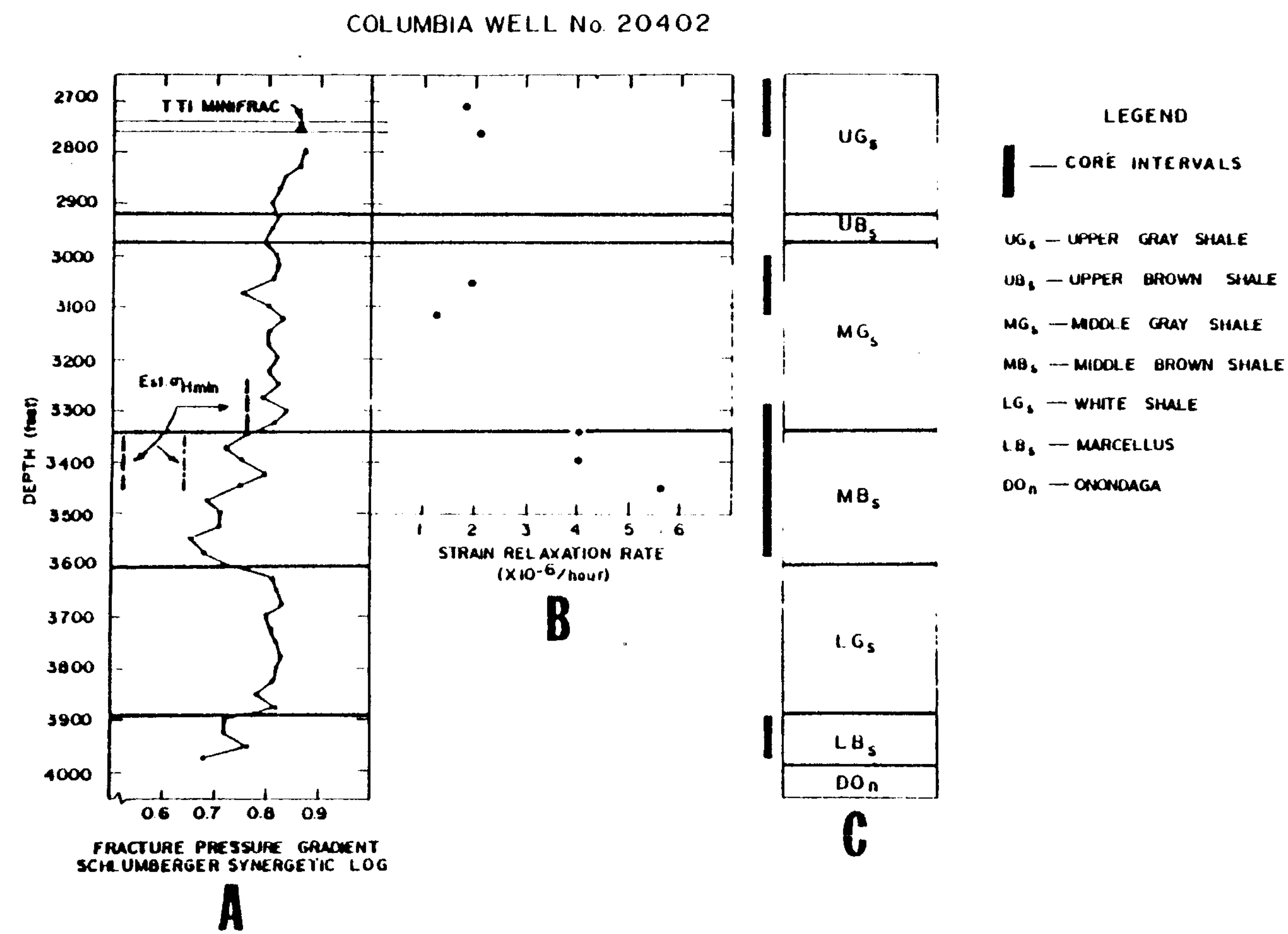


Figure 7. A. Correlation between the minimum-horizontal-stress estimates (--- for $E = 4 \times 10^6$ psi and -·-·- for $E = 3 \times 10^6$ psi) and the fracture-pressure-gradient profile and the instantaneous shut-in pressure gradient determined down-hole.
B. Same as Figure 25.
C. Stratigraphic column of Devonian Shale in Columbia Well No. 20402.

and the Synergetic Log which starts just below the minifrac interval is quite good. It confirms the inference that high subsurface stress-gradients are proportional to low strain-relaxation rates in cored samples.

# RECOMMENDATIONS

## FOR COLUMBIA WELL NO. 20402

1. The prime, gas-bearing, candidate shale zones for fracture (MHF) treatment in Columbia Well No. 20402 which is presently shut-in are:

   The Middle Brown Shale and

   The Marcellus.

2. Fracture treatment should be confined to these two shales only, if the object is to contain the induced fractures within these shale zones and increase gas production.

3. The higher stresses in the Gray Shales and White Slate will aid in the containment of the induced fracture within the Middle Brown Shale and in the Marcellus, prevent them from propagating either upward or downward into the barrier zones, and promote the lateral extension of the fracture.

4. The bottom-hole treating-pressure (BHTP) should not be greater by 400 to 800 psi above the bottom-hole breakdown pressure, which is about 800 to 900 psi at the well-head for the Middle Brown Shale. If BHTP greatly exceeds this peak pressure the barrier zones (Gray Shale and White Slate) may breakdown as well.

5. These recommendations, based only on the strain-relaxation tests and a single minifrac test, should be carefully checked against previous MHF experience in Wells No. 20401 and 20403, in which the potential barrier zones were perforated and fractured.

6. Unsolved, but pertinent problems remaining are, among others:

   - Exact fracture-density variation among zones
   - Secondary-porosity prediction
   - Prediction of formation breakdown-pressure.

# BIBLIOGRAPHY

Many of the concepts and ideas used in the development of the well-site technique and in the writing of this final report have been abstracted and modified from the following partial list of published papers and reports:

Brechtel, C. E., A. S. Abou-Sayed, R. J. Clifton and B. C. Haimson, 1976, *In Situ* Stress Determination in the Devonian Shales (Ira McCoy 20402) within the Rome Basin; TerraTek Report TR 76-36.

Bredehoeft, J. D., R. G. Wolff, W. S. Keys and E. Shuter, 1976, Hydraulic Fracturing to Determine the Regional State of Tectonic Stress, Piceance Basin, Colorado; Geol. Soc. America Bull., Vol. 87, p. 250-258.

Emery, C. L., 1964, Strain Energy in Rocks; *In:* W. R. Judd (Editor), State of Stress in the Earth's Crust, American Elsevier, New York, p. 234-279.

Friedman, M., 1972, Residual Elastic Strain in Rocks; Tectonophysics, Vol. 15, p. 297-330.

Friedman, M. and J. M. Logan, 1970, Influence of Residual Elastic Strain on the Orientation of Experimental Fractures in Three Quartzose Sandstones; Jour. Geophys. Res., Vol. 75, No. 2, p. 387-405.

Friedman, M. and H. C. Heard, 1974, Principal Stress Ratios in Cretaceous Limestones from Texas Gulf Coast; Am. Assoc. Petroleum Geologists Bull., Vol. 58, No. 1, p. 71-78.

Friedman, M. and T. R. Bur, 1974, Investigations of the Relations among Residual Strain, Fabric, Fracture and Ultrasonic Attenuation and Velocity in Rocks; Int. J. Rock Mech. Min. Sci. & Geomech. Abstr., Vol. 11, p. 221-234.

Haimson, B. C., 1976, The Hydraulic Fracturing Technique for Stress Measurement; Preprint, ISRM Symp. Advances in Stress Measurement, Sydney, Australia.

Hubbert, M. K., 1972, Natural and Induced Fracture Orientation; Am. Assoc. Petroleum Geologists Memoir 18, p. 235-238.

Hubbert, M. K. and D. G. Willis, 1957, Mechanics of Hydraulic Fracturing; Am. Inst. Mining Engineers Trans., Vol. 210, p. 153-168.

Hubbert, M. K. and D. G. Willis, 1972, Mechanics of Hydraulic Fracturing; Am. Assoc. Petroleum Geologists Memoir 18, p. 239-257.

Jaeger, J. C. and N. G. W. Cook, 1969, Fundamentals of Rock Mechanics: Methuen & Co. Ltd., London.

Komar, G. A., W. K. Overbey and R. J. Watts, 1976, Prediction of Fracture Orientation from Oriented Cores and Aerial Photos in Sand Draw Field, Wyoming; MERC/TPR-76/4, 12 pp.

McWilliams, J. R., 1966, TheRole of Microstructure in the Physical Properties of Rock; *In:* Testing Techniques of Rock Mechanics, ASTM-STP 402, p. 175-189.

Min, K. D., 1974, Analytical and Petrofabric Studies of Experimental Faulted Drape-Folds in Layered Rock Specimens; Ph.D. Dissertation, Texas A & M University.

Nichols, T. C. and Savage, W. Z., 1976, Rock Strain Recovery - Factor in Foundation Design; unpublished report, U.S.G.S., Denver, Colorado.

Overbey, W. K., 1976, Effect of *In Situ* Stress on Induced Fractures; *In:* Devonian Shale Production and Potential, Proc. 7th Appalachian Petroleum Geol. Symp., Morgantown, p. 182-211.

Power, D. V., C. L. Schuster, R. Hay and J. Twombly, 1975, Detection of Hydraulic Fracture Orientation and Dimensions in Cased Wells; Paper SPE 5626, 50th Annual Fall Meeting SPE-AIME, Dallas.

Price, N. J., 1974, The Development of Stress Systems and Fracture Patterns in Undeformed Sediments; *In:* Advances in Rock Mechanics, Proc. 3rd Cong. ISRM, Vol. I, Part A, p. 487-496.

Secor, D. T. J. and D. D. Pollard, 1975, On the Stability of Open Hydraulic Fractures in the Earth's Crust; Geophys. Res. Letters, Vol. 2, No. 11, p. 510-513.

Simonson, E. R., A. S. Abou-Sayed and R. J. Clifton, 1976, Containment of Massive Hydraulic Fractures; Paper SPE 6089, 51st Annual Fall Meeting SPE-AIME, New Orleands.

Smith, M. B., G. B. Holman, C. R. Fast and R. J. Covlin, 1976, The Azimuth of Deep, Penetrating Fractures in the Wattenberg Field; Paper SPE 6092, 51st Annual Fall Meeting SPE-AIME, New Orleands.

Stearns, D. W., 1971, Mechanism of Drape Folding in the Wyoming Province; 23rd Annual Field Conf. Guidebook, Wyo. Geol. Assoc., p. 125-143.

Swolfs, H. S., 1975, Determination of *In Situ* Stress Orientation in a Deep Gas Well by Strain Relief Techniques; Terra Tek Report 75-43, 47 pp.

Swolfs, H. S., R. Lingle and J. M. Thomas, 1976, Strain-Relaxation Tests on Selected Cores from El Paso Natural Gas Company Canyon Largo No. 288; Terra Tek Report 76-50, 23 pp.

Varnes, D. J. and F. T. Lee, 1972, Hypothesis of Mobilization of Residual Stress in Rock; Geol. Soc. America Bull., Vol. 83, p. 2863-2866.

# APPENDIX I

## DATA ANALYSIS FOR STRAIN ROSETTES

The stress in a solid material (rock) subjected to uniaxial stress can be determined experimentally by attaching a strain gage oriented in the direction of the applied stress. The stress (S) is then computed, in terms of the measured strain ($\varepsilon$), from $S = E\varepsilon$, where E is the elastic Young's Modulus of the material. The strain is generally small (a few parts in 1000000); hence sensitive instruments are required for measuring it. Originally, strain gages were mechanical or optical, but these have now been almost completely replaced by electrical gages. This type of gage contains a wire element whose electrical resistance varies with its deformation. The gage is cemented to the test specimen, the strain in the specimen being measured as a function of the change in the electrical resistance of the wire element.

A single strain gage oriented in the direction of a uniaxially applied stress is sufficient for computing the stress in the test specimen. For biaxial stress, one might suppose that two strain gages would be sufficient; this would be true if the directions of the principal stresses were known, but this is not usually the case. To determine the direction of the principal stresses in addition to their magnitudes, three values of strain are required. As a matter of practical convenience, the linear strains are obtained by using a combination of three resistance gages: three gages set with their axes at 45° to each other (central figure in Figure 8). This combination is known as a strain rosette. The three gages are electrically insulated from each other and are used to determine the strain at the surface of a specimen to which they are attached.

For a 45° strain rosette, the principal strains are

$$\varepsilon_{\substack{max \\ min}} = \frac{\varepsilon_a+\varepsilon_c}{2} \pm 0.71\left[(\varepsilon_a-\varepsilon_b)^2 + (\varepsilon_b-\varepsilon_c)^2\right]^{1/2}$$

and the direction of the maximum principal strain is defined by

$$\tan 2\Theta = \frac{\varepsilon_a+\varepsilon_c-2\varepsilon_b}{\varepsilon_a-\varepsilon_c} .$$

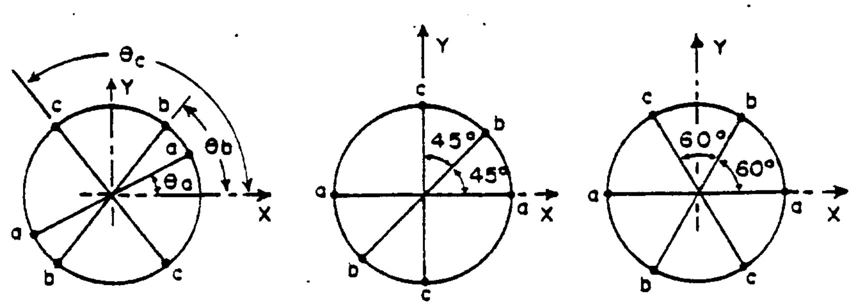


Figure 8. Strain Rosettes.

# APPENDIX II

## STRAIN TIME PLOTS.

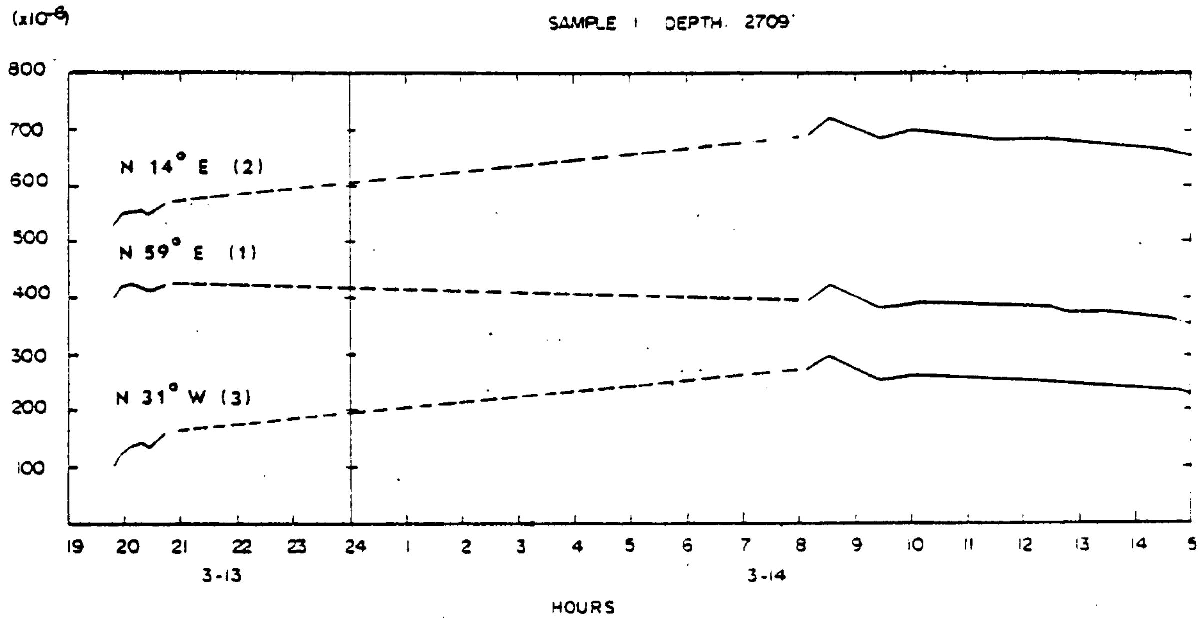


Figure A1. Strain-relaxation-time plots of Devonian Shale.

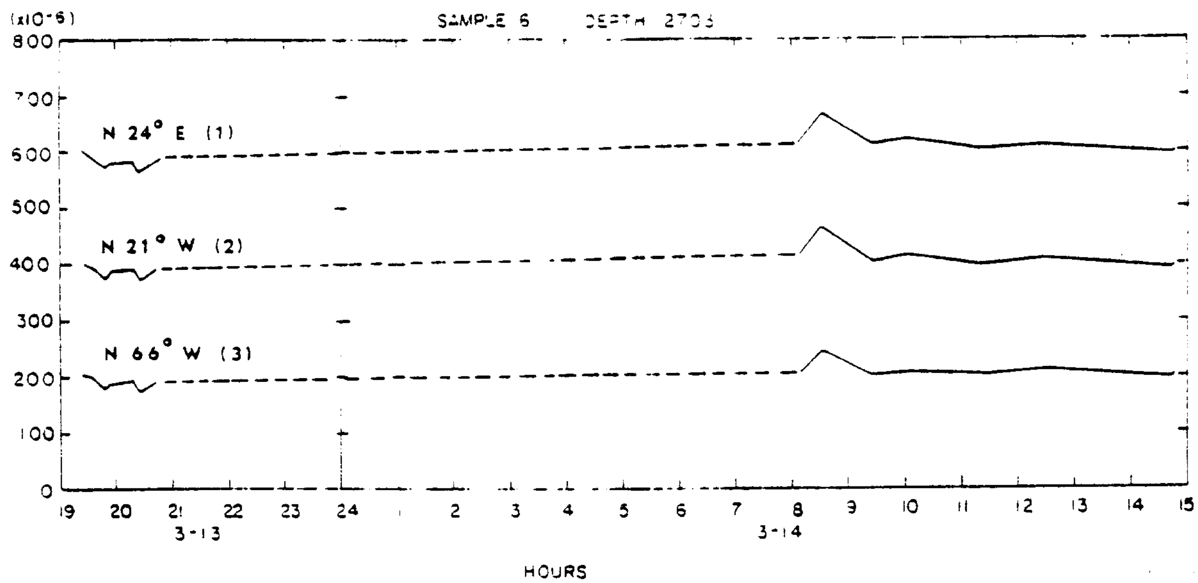


Figure A2. Strain-relaxation-time plots of Devonian Shale.

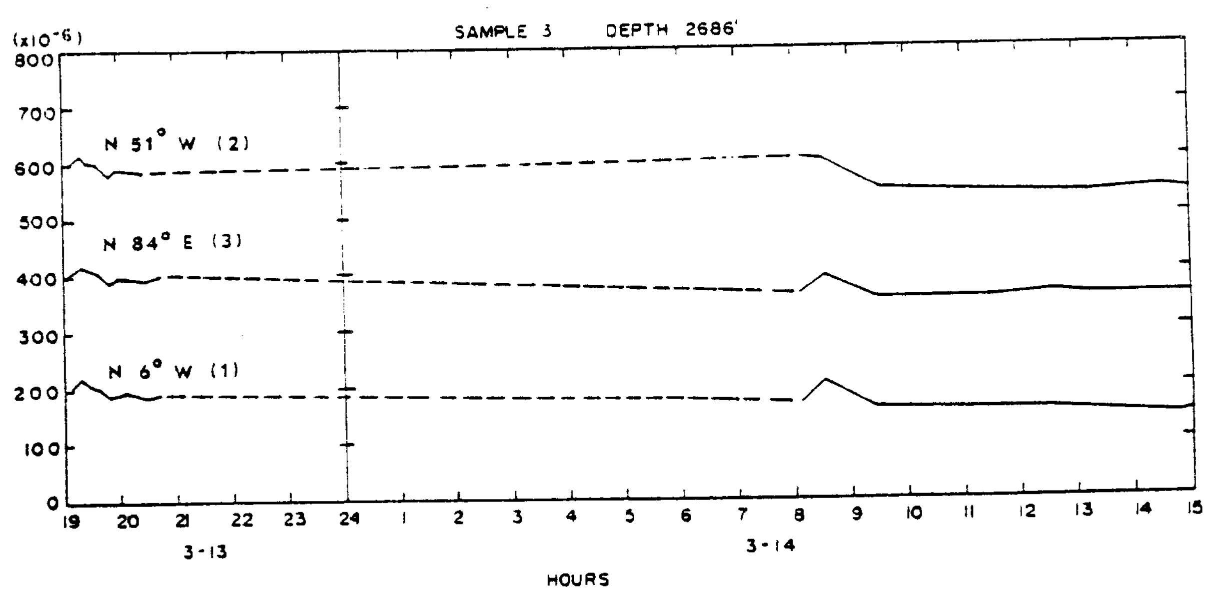


Figure A3. Strain-relaxation-time plots of Devonian Shale.

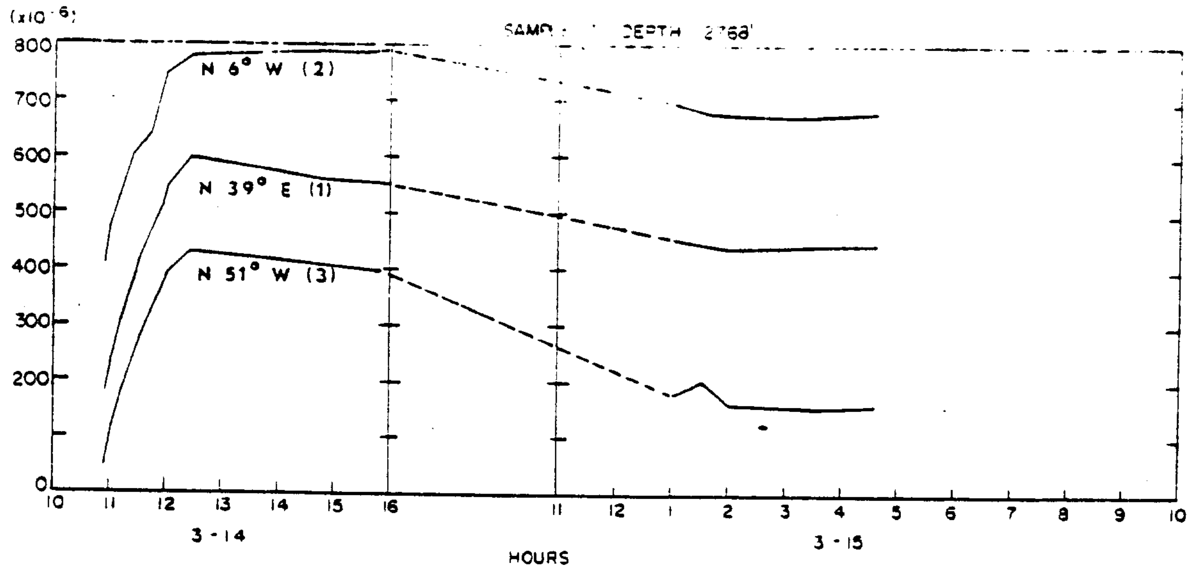


Figure A4. Strain-relaxation-time plots of Devonian Shale.

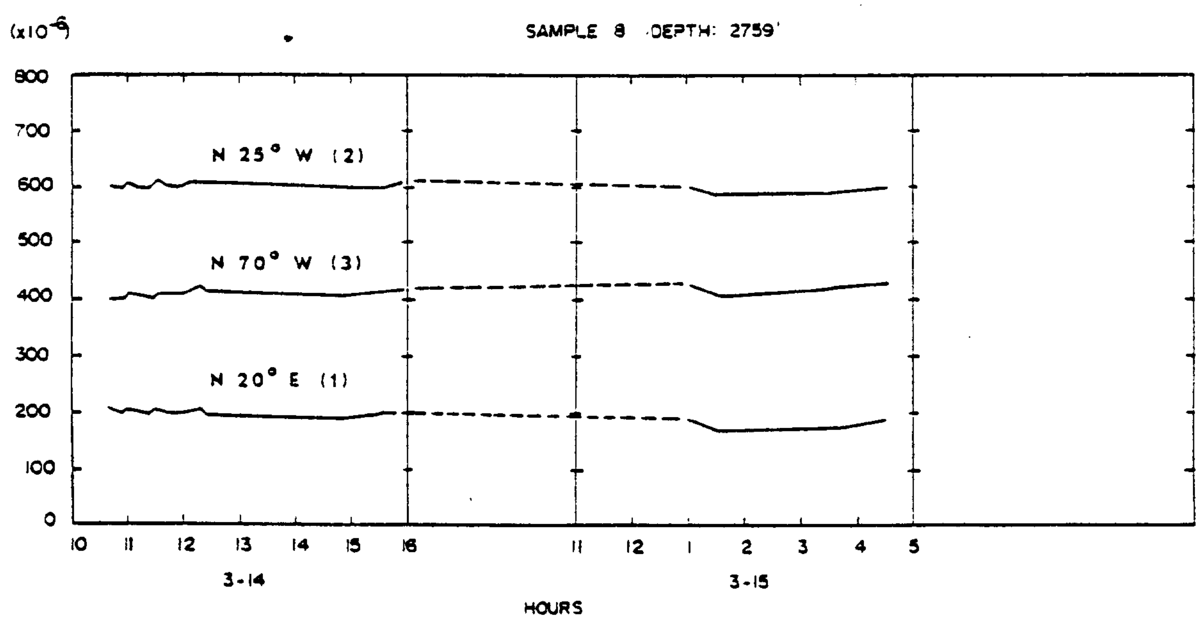


Figure A5. Strain-relaxation-time plots of Devonian Shale.

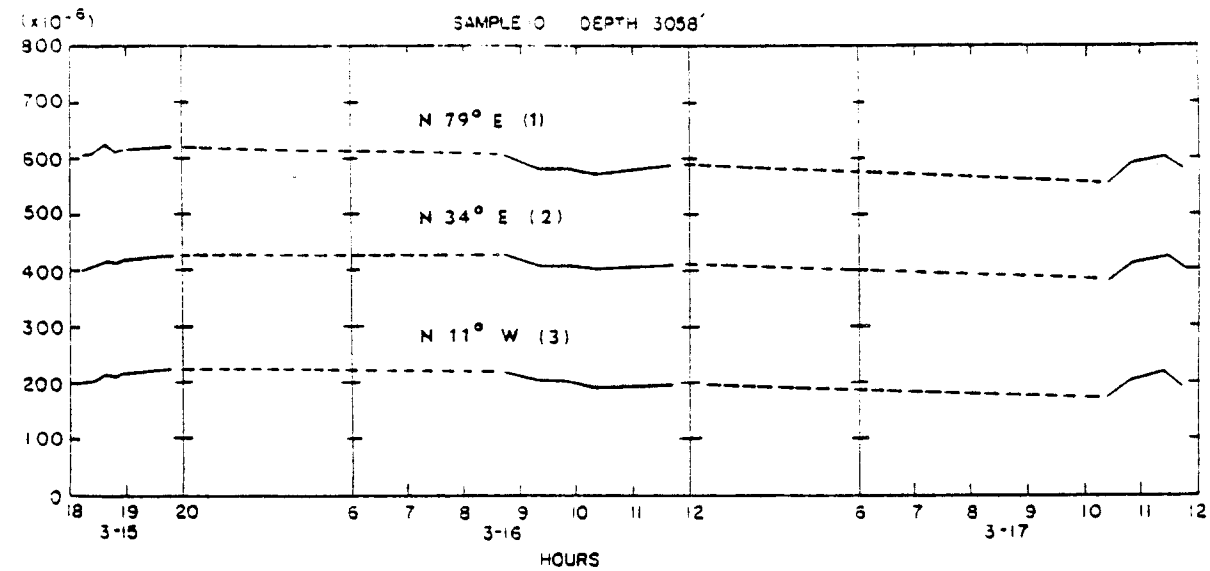


Figure A6. Strain-relaxation-time plots of Devonian Shale.

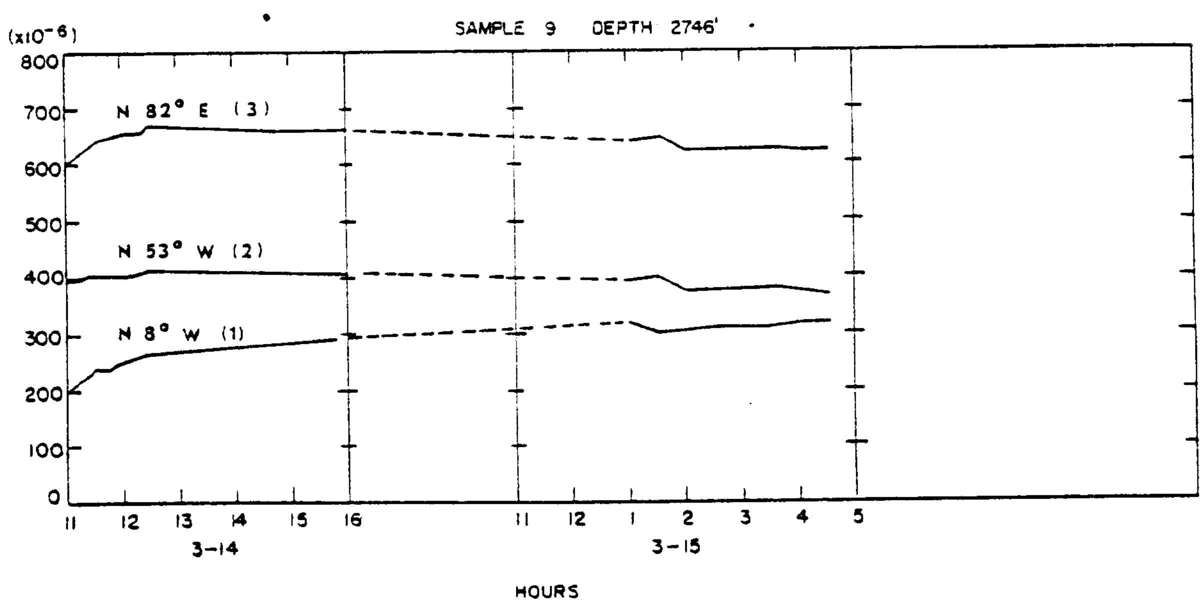


Figure A7. Strain-relaxation-time plots of Devonian Shale.

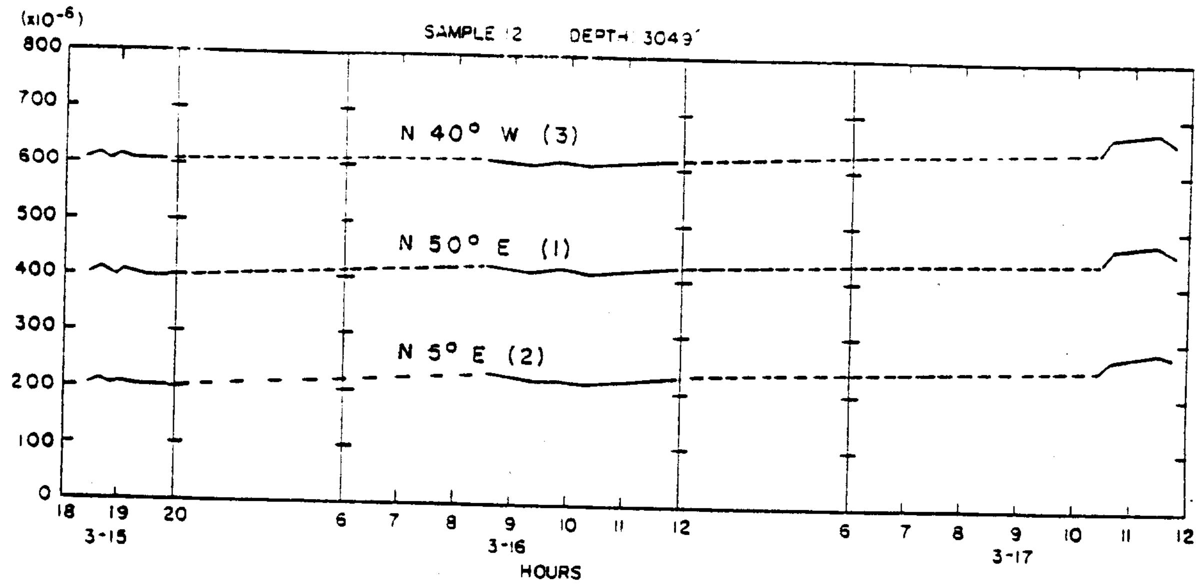


Figure A8. Strain-relaxation-time plots of Devonian Shale.

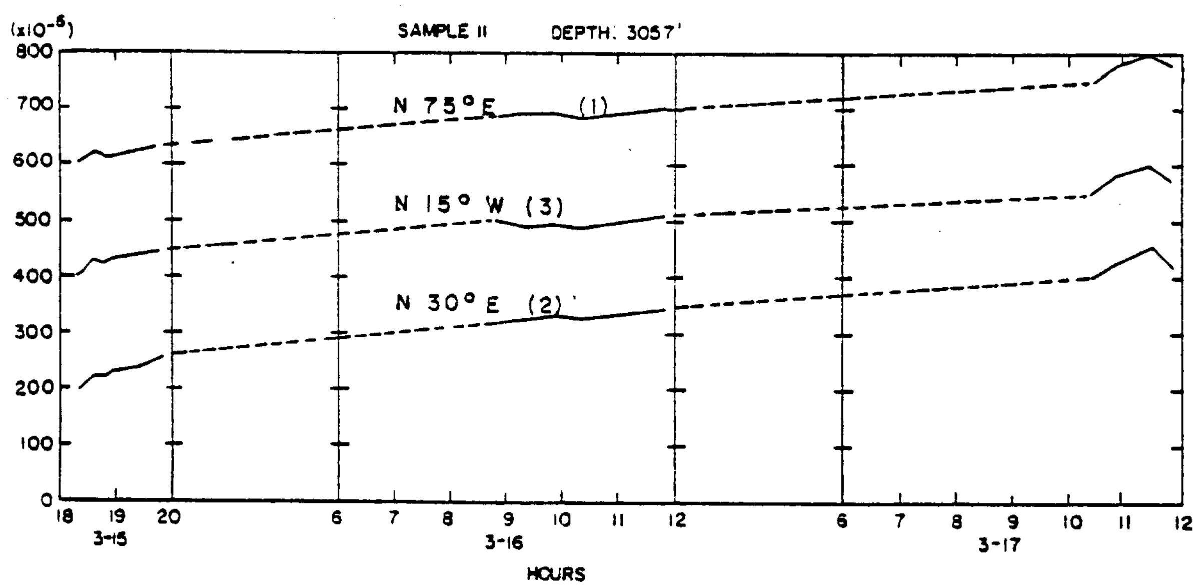


Figure A9. Strain-relaxation-time plots of Devonian Shale.

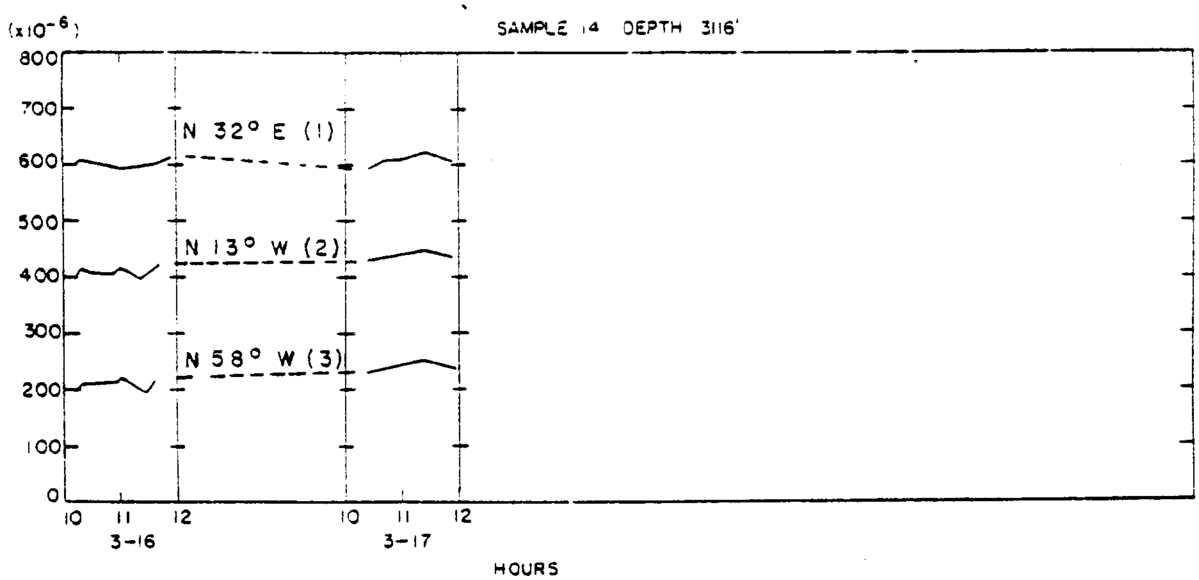


Figure A10. Strain-relaxation-time plots of Devonian Shale.

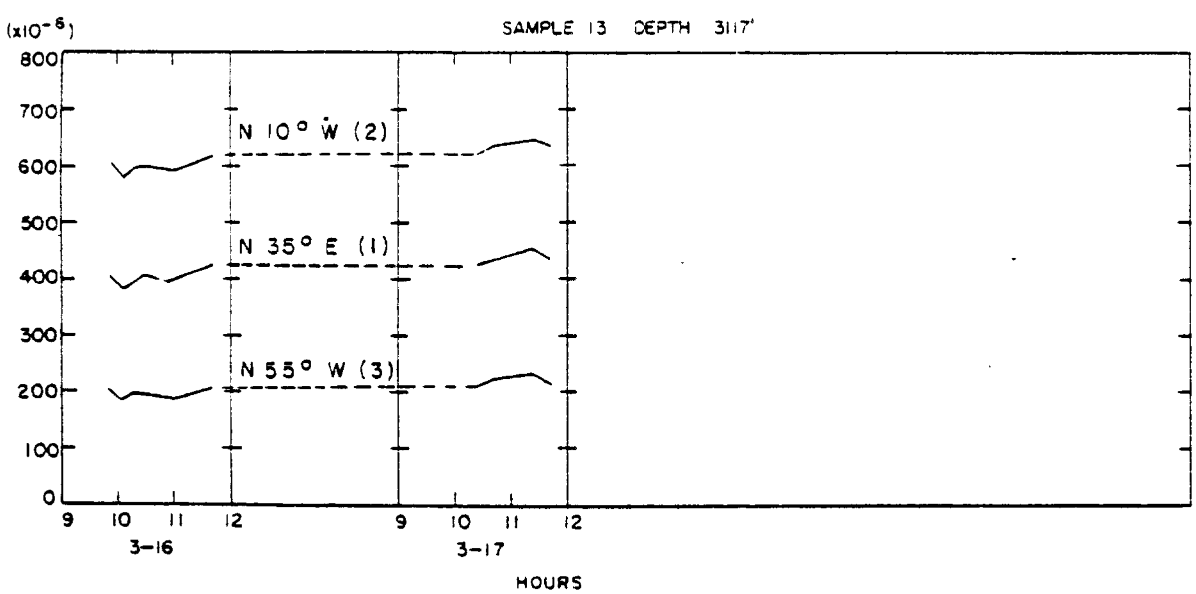


Figure A11. Strain-relaxation-time plots of Devonian Shale.

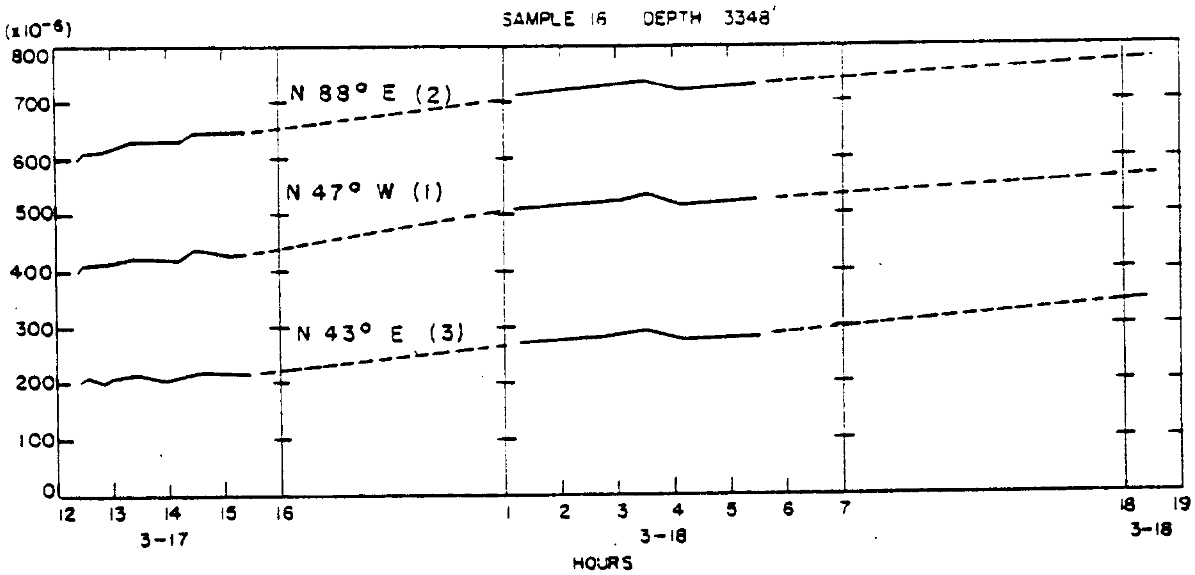


Figure A12. Strain-relaxation-time plots of Devonian Shale.

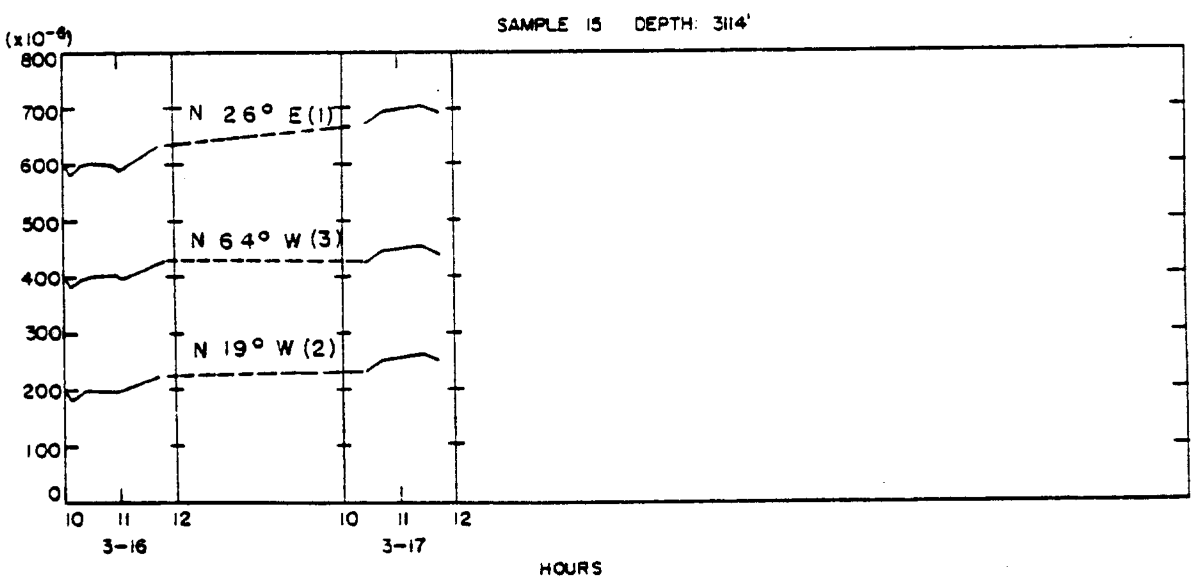


Figure A13. Strain-relaxation-time plots of Devonian Shale.

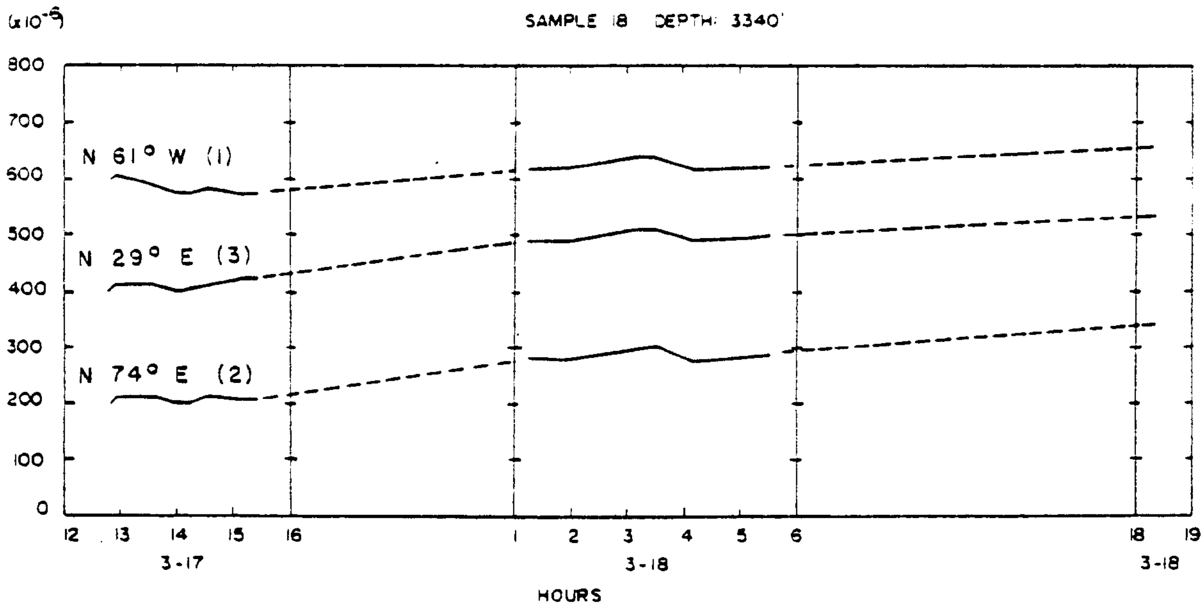


Figure A14. Strain-relaxation-time plots of Devonian Shale.

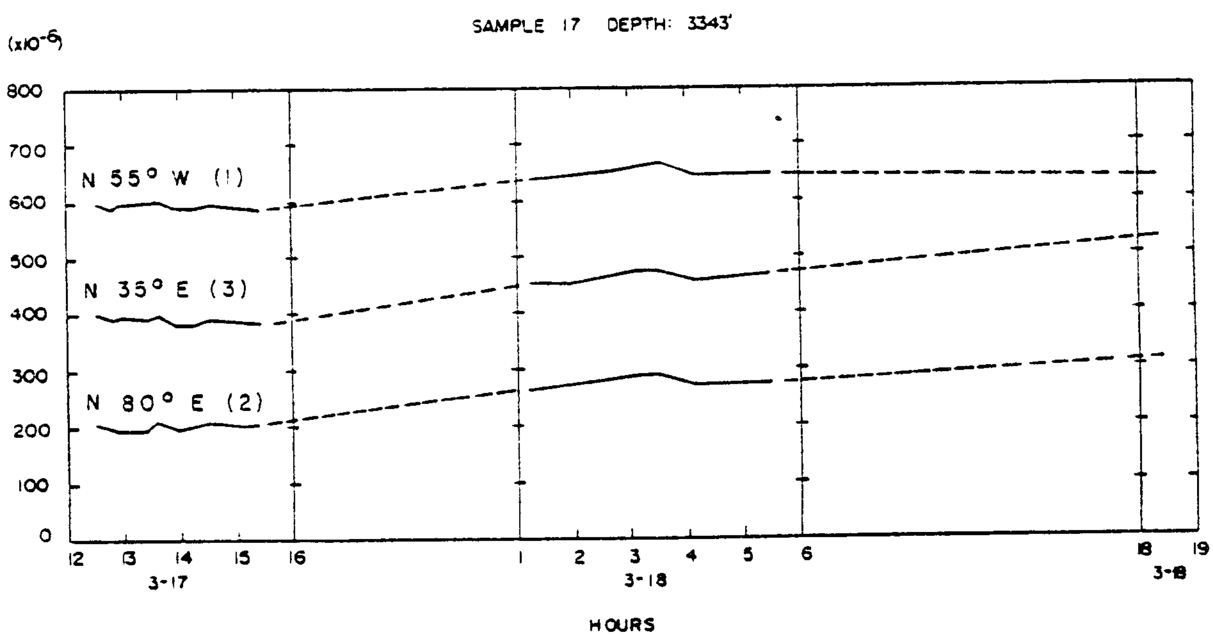


Figure A15. Strain-relaxation-time plots of Devonian Shale.

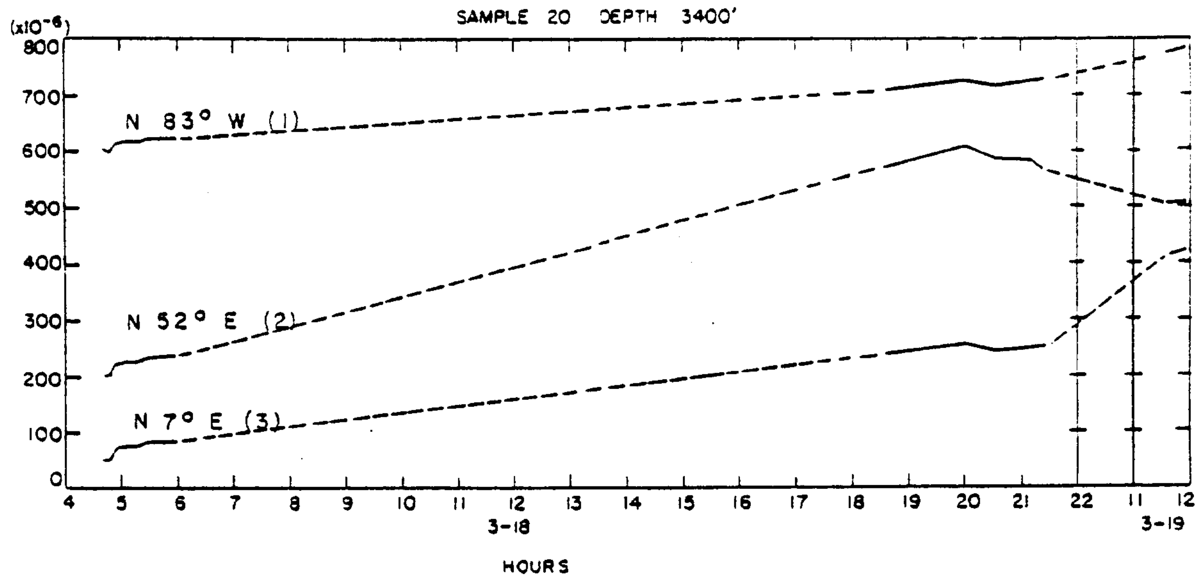


Figure A16. Strain-relaxation-time plots of Devonian Shale.

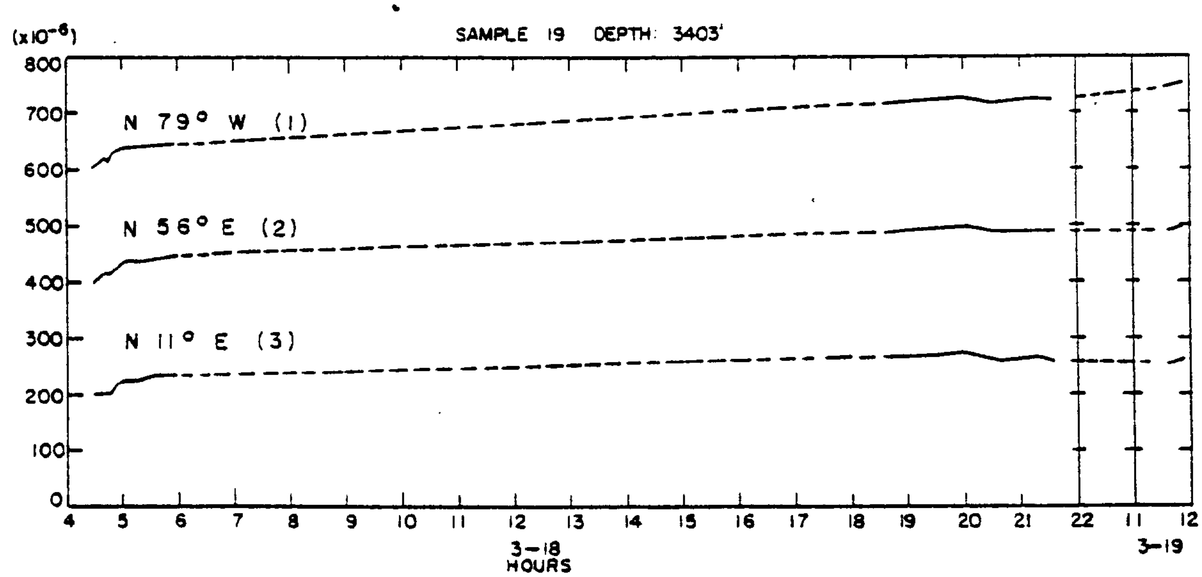


Figure A17. Strain-relaxation-time plots of Devonian Shale.

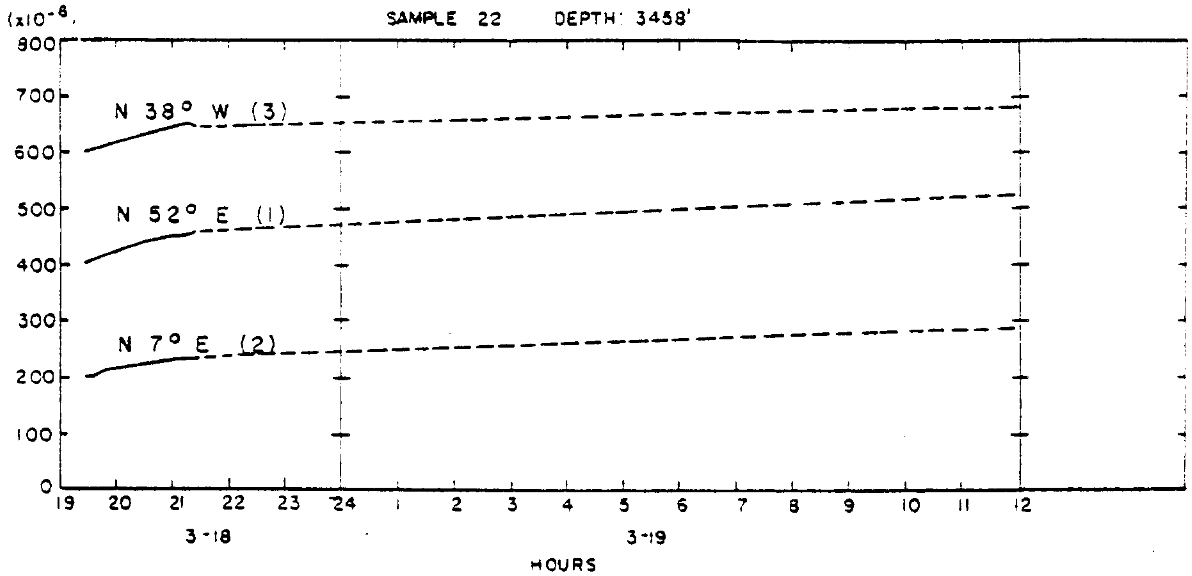


Figure A18. Strain-relaxation-time plots of Devonian Shale.

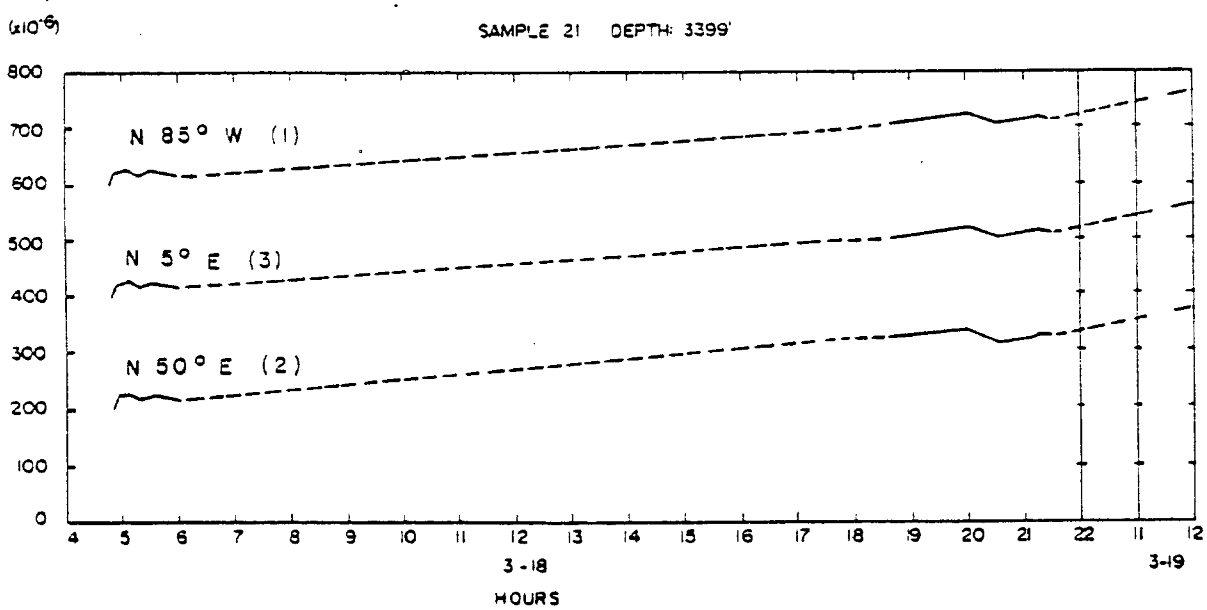


Figure A19. Strain-relaxation-time plots of Devonian Shale.

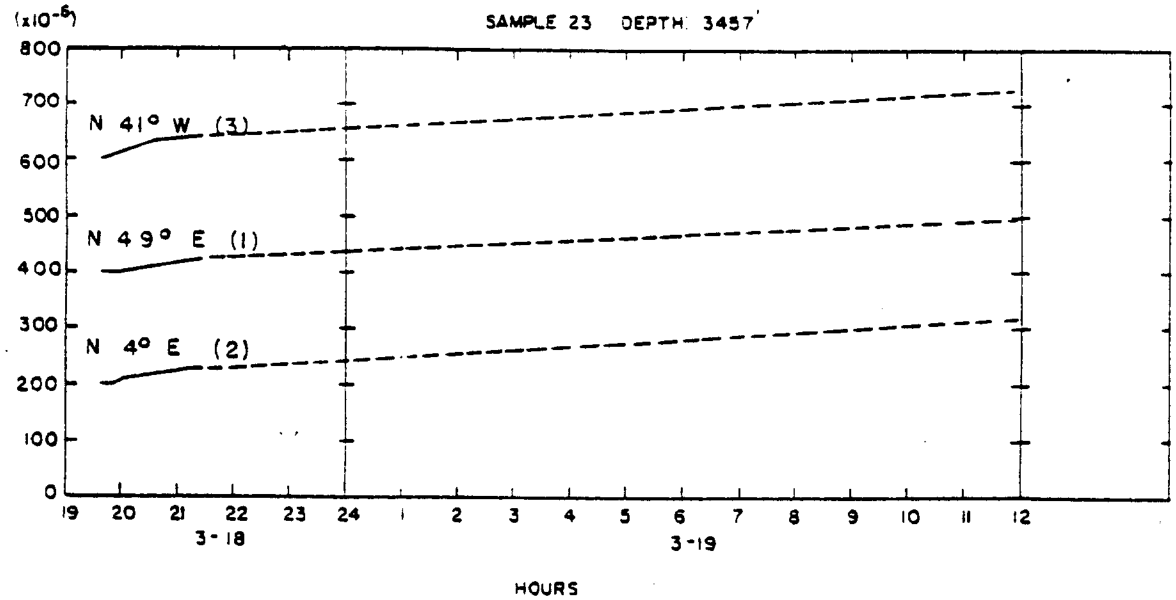


Figure A20. Strain-relaxation-time plots of Devonian Shale.

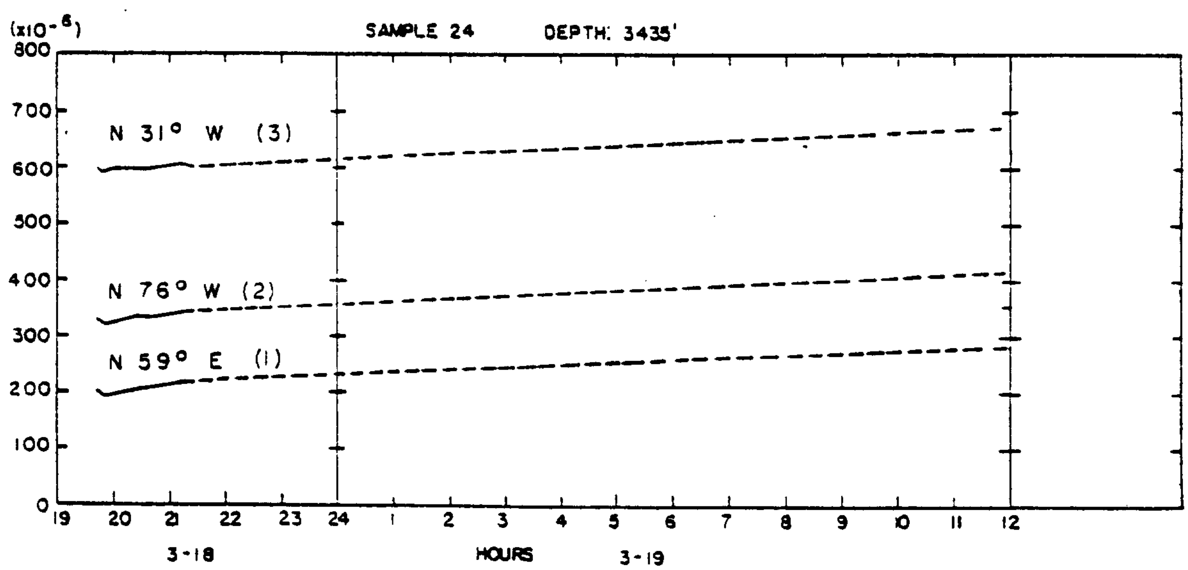


Figure A21. Strain-relaxation-time plots of Devonian Shale.

Open File No. 199
Volume 2 - Appendices

# TERRA TEK REPORT

# ROCK MECHANICS STUDIES RELATED TO MHF OF EASTERN UNITED STATES DEVONIAN SHALES

# ROCK MECHANICS STUDIES RELATED TO MASSIVE HYDRAULIC FRACTURING OF EASTERN UNITED STATES DEVONIAN SHALES

## FINAL CORE ANALYSIS REPORT

WORK COMPLETED FOR
COLUMBIA GAS SYSTEM SERVICE CORPORATION
UNDER PRIME CONTRACT NO. E(46-1)-8014

By .

A. H. Jones
A. S. Abou-Sayed
L. M. Buchholdt
R. Lingle
L. A. Rogers

Submitted to

Columbia Gas System Service Corporation
1600 Dublin Road
Columbus, Ohio 53215

Attention: Eric C. Smith

Submitted by

Terra Tek, Inc.
University Research Park
420 Wakara Way
Salt Lake City, Utah 84108

TR 77-16
March 1977

# SUMMARY

Ultrasonic velocities and elastic moduli were determined for cores taken from several layers in wells #20402 and #20403. The effect of *in situ* conditions (pressure and temperature) on the measured velocities was very small; a change on the order of 2 percent or less for pressures ranging from atmospheric to 4,000 psi and temperatures up to 100°F. Laboratory-measured densities and p-wave velocities are in good agreement with log-measured values. However, the log-measured shear wave velocities had to be interpreted as surface wave velocities in order to obtain good agreement with the corresponding laboratory-measured values. Dynamic Young's moduli have been calculated using the log-derived bulk densities, p-wave and s-wave (after correction) velocities. The static moduli were determined from triaxial compression tests on the Upper Brown and Lower Gray Shales. The static moduli are lower than the dynamic moduli; for the samples tested, the difference is 20 to 30 percent.

Critical stress-intensity factors were determined experimentally for the gray shales. Permeability of shale samples as well as a flow conductivity through propped and unpropped fractured specimens have been determined under simulated downhole stress conditions. Both the permeability and the unpropped-fracture conductivity are strongly affected by the confining pressure. On the other hand, conductivity of the propped fracture shows insignificant reduction with application of confining pressure to simulated *in situ* conditions.

## RECOMMENDATIONS

Fracture containment analysis indicates that the gray shales and Onondaga Limestone will act as barriers to fracture growth in the brown shales. The Onondaga Limestone forms a strong barrier to fractures in the Lower Brown Shale. The gray shales are not strong barriers, however, and can also be broken down if fluid pressure is too high. The brown shales will not form barriers to fractures in the gray shales. The following are recommendations to optimize MHF treatments in this test area.

1. For the Upper Brown Shale, the Upper Gray and Middle Gray Shales will form weak barriers and a treatment pressure within the formation (FTP) of no more than 200 psi in excess of the minimum horizontal stress for the Upper Brown Shale, plus any expected drop in pressure across the perforations, will be required for fracture containment.

2. In treating the Middle Brown Shale, the fracture will propagate into both the Middle Gray and Lower Gray Shales. There is the possibility that later fractures initiated in the Upper Brown and Lower Brown Shales will interact with the earlier fracture created in the Middle Brown Shale. Therefore, in a multi-stage MHF it is important that the Middle Brown Shale formation, having the best gas potential, should be fractured first.

3. Penetration of a fracture which is initiated in the Middle Brown Shale into the Middle Gray Shale can be minimized to 50 feet or less by maintaining the FTP during hydraulic fracturing of the Middle Brown Shale layer within 400 psi in excess of the minimum horizontal stress in that zone, plus any expected drop in pressure across the perforations.

4. Corresponding considerations for the Lower Brown and Lower Gray Shales leads to a FTP of at most 250 psi in excess of the minimum horizontal stress for the Lower Brown Shale, plus any expected drop in pressure across the perforations.

## ABSTRACT

Laboratory core analyses were performed on cores taken from Columbia Gas System Service Corpoation wells #20402 and #20403, located in Lincoln County, West Virginia. Physical and mechanical properties, determined at simulated *in situ* conditions (where applicable), were compared directly with the Birdwell (3-D) and Schlumberger logs. Densities compare favorably; compressional and shear wave comparisons are complicated by anisotropic material behavior and discrepancy in field-measured shear wave velocities. Good correlation is obtained for compression and shear wave velocities parallel to the wellbore provided the log-determined shear wave velocity is assumed to be the surface wave velocity. Measured physical and mechanical properties are combined with theoretical models to assess possible fracture containment. The anlaysis indicates that for successsful massive hydraulic fracture in the Middle Brown Shale the formation treatment pressure (FTP) to extend the fracture should not be greater than 400 psi above the minimum *in situ* stress in order to prevent deep excursion of the fracture into the barrier layers. For fracturing treatment of the Upper Brown Shale and the Lower Brown Shale, the corresponding treating pressure should be limited to 200 psi and 250 psi, respectively, in excess of the minimum horizontal stress in the respective zone. The Middle Brown Shale should be the first formation treated. Fracture conductivities at simulated *in situ* conditions for an unpropped fracture and for fractures propped with 0.56 lb/ft$^2$ of 100 mesh and 1.44 lb/ft$^2$ of 20/40 sand were found to be 1 md-cm, 1100 md-cm and 8000 md-cm, respectively, for the Lower Brown Shale.

# TABLE OF CONTENTS

# LIST OF FIGURES

# LIST OF TABLES

# APPENDIX IV: REPORTS ON ROCK MECHANICS RESEARCH BY TERRA TEK

# BACKGROUND

Under contract E(46-1)-8014 from the Energy Research and Development Administration, Columbia Gas System Service Corporation was to:

1. Determine the technical and economic feasibility of hydraulic fracturing of the Devonian shales, and
2. Identify the fracture distribution, gas distribution, and ways to achieve economical production by application of stimulation research findings.

Three wells were drilled in Lincoln County, West Virginia. Different fracture treatments were planned for each well to optimize the stimulation treatment. Terra Tek, under subcontract from Columbia Gas System Service Corporation, was to determine the physical characteristics of the formations to better design and interpret the results of the massive hydraulic fracture (MHF) tests. This work was performed through three tasks:

1. Core Analysis: Evaluate physical and mechanical properties to determine fracture containment and pumping schedule.
2. Strain Relaxation on Recovered Cores: Estimate the *in situ* principal stresses in principal shale zones. Results were to be used to determine fracture containment, pumping shedule and fracture direction.
3. Open Hole Tests: Determine *in situ* stresses and their directions.

The present report describes the results and implications to massive hydraulic fracture design from core analyses.

Laboratory test data gathered in support of log interpretation, MHF design and reservoir engineering are briefly summarized. This consists of physical and mechanical properties data on cores retrieved from wells #20402 and #20403. Since the subsurface bedding is very nearly horizontal in the area of these wells and there is no major tectonic displacements between them, the shale layers are expected to be similar in the three wells, #20401, #20402 and #20403. Figure 1 is a schematic that summarizes all geological findings for the wells.

Except for density determination, all tests were performed at simulated "down-hole" pressure conditions. These include sonic wave velocities, triaxial extension and compression, fracture toughness, rock permeability and fracture permeability for the propped and unpropped conditions. The test data is then used to assess fracture containment. A fracturing analysis is presented along with a recommended treatment pressure limitations.

# SUMMARY OF GEOLOGICAL FINDINGS
## (COLUMBIA MHF WELLS, Lincoln Co., W. Va.)

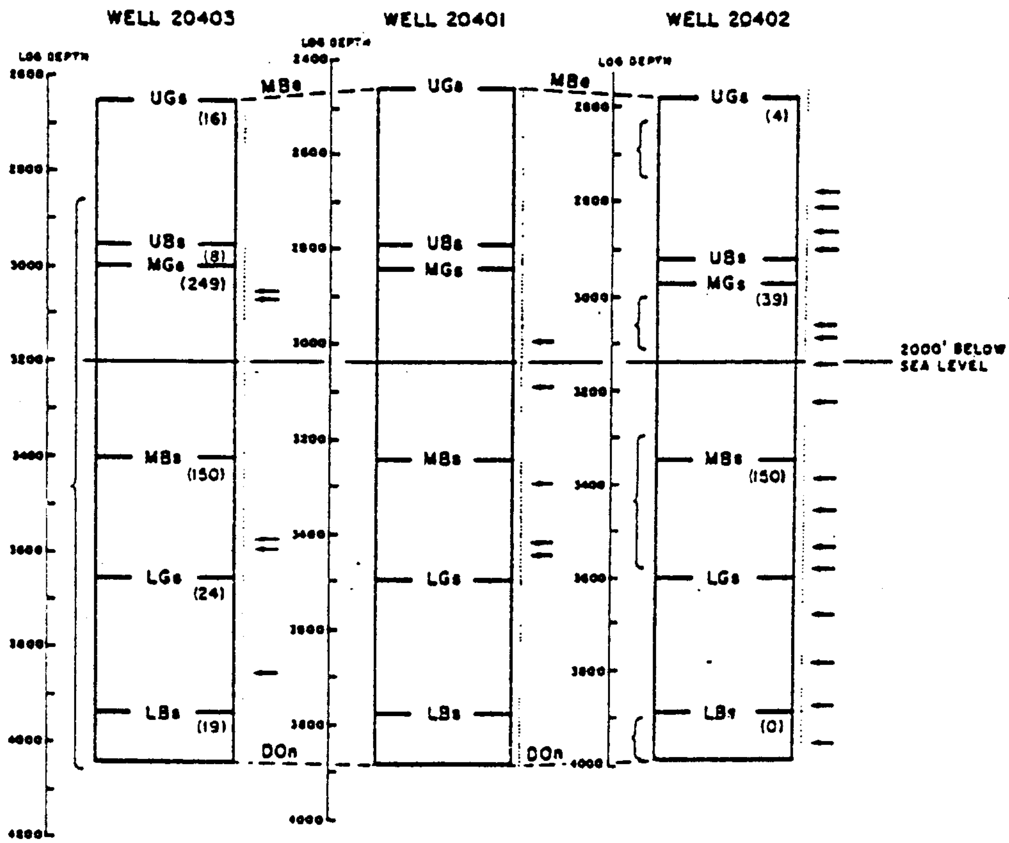


**LEGEND**

MBe - BASE OF BEREA SANDSTONE
UGs - TOP OF UPPER GRAY SHALE AND SILTSTONE
UBs - TOP OF UPPER BROWN SHALE
MGs - TOP OF MIDDLE GRAY SHALE
MBs - TOP OF MIDDLE BROWN SHALE
LGs - TOP OF LOWER GRAY SHALE
LBs - TOP OF LOWER BROWN SHALE
DOn - TOP OF CORNIFEROUS (ONONDAGA) LIMESTONE
— - GAS SHOW FROM SIBILATION LOG
! - PROBABLE PERMEABLE INTERVAL FROM RESISTIVITY CROSS PLOTS
(5) - FEET OF OBSERVED VERTICAL FRACTURES
{ - CORED INTERVAL

Figure 1. Summary of geological findings (from Ranostaj, 1976).

LABORATORY MEASUREMENTS OF PHYSICAL PROPERTIES AND ULTRASONIC VELOCITIES

Physical properties and ultrasonic velocities have been determined in the laboratory on cores recovered from wells #20402 and #20403. Bulk dry density, grain density and porosity measurements have been carried out on samples obtained from depths of 2980, 3446, 3760 and 3996 feet. Three specimens frcm each depth have been used for measurement. To determine the bulk dry density, the samples are dried at 110°F, weighed, then the total volume is measured in a mercury porometer. Grain density is measured using crushed or puverized specimen. The percent porosity is determined from the bulk dry density, $\rho_D$, and the grain density, $\rho_g$, by the following equation

$$\text{Percent Porosity} = 100\left(1 - \frac{\rho_D}{\rho_g}\right)$$

Results of the physical property measurements are given in Table I.

Both the compression wave and shear wave velocities were measured on samples subjected to simulated *in situ* conditions. Measurements were performed both in the axial (normal to bedding) and the horizontal (parallel to bedding) directions. This data, along with the measured bulk density, has been used to calculate the dynamic elastic moduli of the materials. The measured moduli were used to establish the validity of comparable data obtained for sonic logs. The comparison of log-derived and laboratory-measured data is illustrated in Figures 2 and 3, and in further detail in Appendices A and B.

The findings are summarized as follows:

1. The laboratory bulk density measurements show good agreement with the wireline log measurements.

2. The laboratory compression wave velocities measured in the vertical direction are in good agreement with the wireline log data.

3. The laboratory shear wave velocity measurements, taken in the same direction as the log measurements, are consistently higher.

4. Laboratory-measured Poisson's ratios in the different directions are only slightly different (same ratio of P-wave to S-wave velocities).

5. Young's modulus and the bulk modulus in the horizontal plane, derived assuming isotropy of the Devonian shales, are vastly different from those moduli in the vertical direction.

Since the elastic properties in the horizontal plane are pertinent to containment analysis of massive hydraulic fractures and not the vertical velocities usually measured by a wireline sonic log, care should be exercised when interpreting the log data for containment analysis. When the horizontal and vertical velocities are different, the most that can be obtained from a wireline elastic properties log is a close approximation of Poisson's ratios. This approximation is only possible if the ratio of the compression wave velocity to the shear wave velocity remains nearly constant in different directions, as is the case for the Devonian shales.

At the present time, there is an unaccountable discrepancy between the laboratory-determined and log-measured shear wave velocities. A possible explanation for the discrepancy is that the wireline logs were detecting the arrival of a surface wave instead of the shear wave. If the log shear wave velocities are recalculated based on the assumption that the log-measured wave was really a surface wave, then (see Figure 4) the corrected log velcities (denoted by •) are in very good agreement with the laboratory data (denoted by x). This is discussed in more detail in Appendix A.

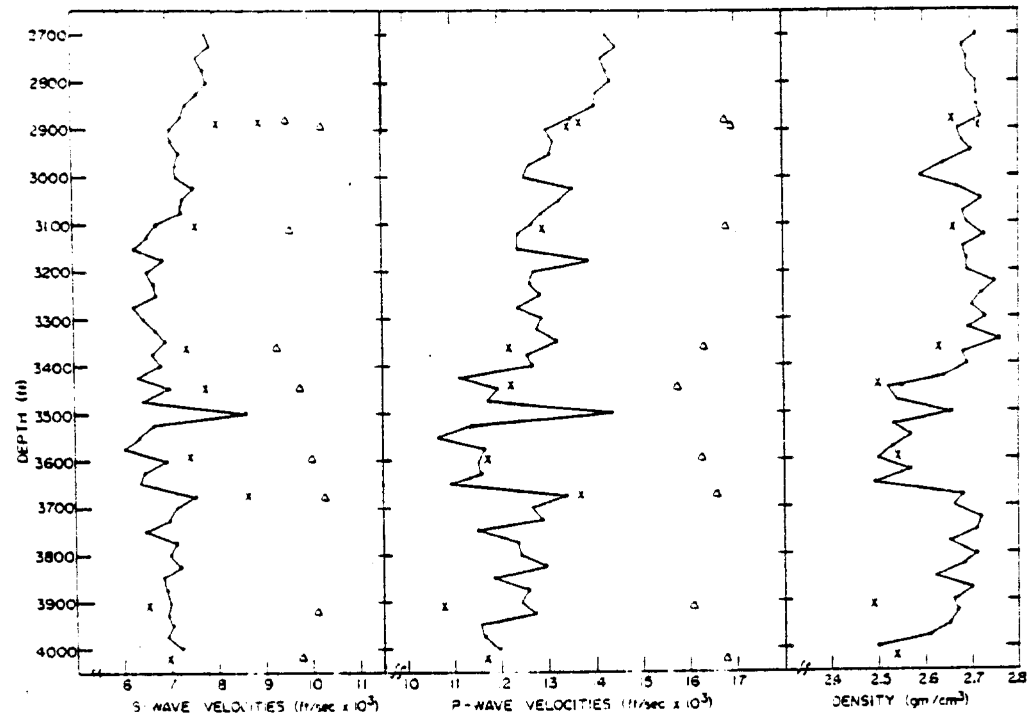


Figure 2. Comparison of laboratory data (Terra Tek, Inc.) with data from a Schlumberger experimental s-wave logging tool on Columbia Gas System Service Corporation well #20403. "X" indicates sample orientation parallel to borehole, "Δ" - perpendicular.

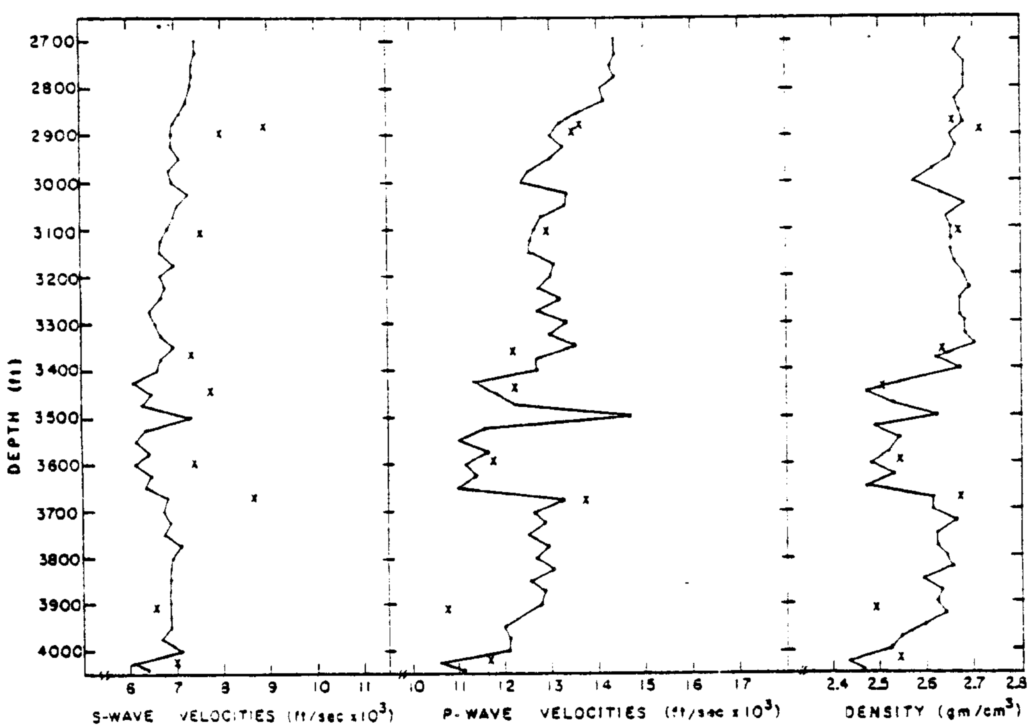


Figure 3. Comparison of laboratory data (Terra Tek, Inc.) with data from the Birdwell (3-D) log on Columbia Gas System Service Corporation well #20403. "X" indicates sample orientation parallel to borehole

TABLE I

Physical Property Measurements
for Samples from the #20403 Well

IDENT = Sample Identification
W DEN = Wet Bulk Density (gm/cc)
D DEN = Dry Bulk Density (gm/cc)
G DEN = Grain Density (gm/cc)
% WAT = Moisture (by wet wt.)
% POR = Percent Total Porosity
% SAT = Percent Saturation
% A V = Percent Calc. Air Voids

| | | | | | | | |
|---|---|---|---|---|---|---|---|
| UBS 2980 A | 2.500 | 2.484 | 2.600 | 0.629 | 4.451 | 35.349 | 2.878 |
| 2980 B | 2.450 | 2.433 | 2.630 | 0.689 | 7.486 | 22.553 | 5.798 |
| 2980 C | 2.640 | 2.623 | 2.680 | 0.636 | 2.119 | 79.210 | 0.441 |
| MBS 3446 A | 2.470 | 2.459 | 2.580 | 0.452 | 4.697 | 23.787 | 3.579 |
| 3446 B | 2.480 | 2.468 | 2.550 | 0.486 | 3.210 | 37.444 | 2.013 |
| 3446 C | 2.450 | 2.437 | 2.620 | 0.526 | 6.981 | 18.465 | 5,692 |
| LGS 3760 A | 2.650 | 2.635 | 2.780 | 0.561 | 5.211 | 18.547 | 3.724 |
| 3760 B | 2.630 | 2.617 | 2.870 | 0.495 | 8.816 | 14.770 | 7,514 |
| 3760 C | 2.640 | 2.624 | 2.860 | 0.600 | 8.246 | 19.200 | 6.663 |
| LBS 3996 A | 2.690 | 2.680 | 2.750 | 0.364 | 2.538 | 38.573 | 1.559 |
| 3996 B | 2.690 | 2.678 | 2.870 | 0.439 | 6.683 | 17.677 | 5.502 |
| 3996 C | 2.680 | 2.667 | 2.710 | 0.472 | 1.574 | 80.353 | 0.309 |

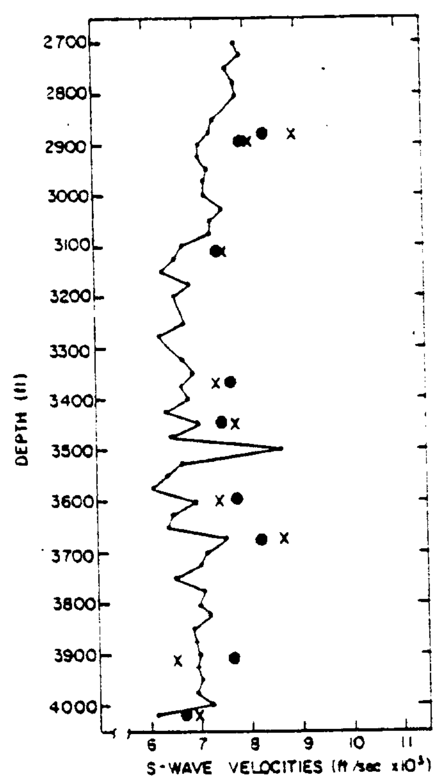


Figure 4. Comparison of log data, laboratory data (x) and calculated s-wave velocities from log data (•), assuming that the log detected the Rayleigh surface wave.

# MECHANICAL PROPERTIES TESTS

Samples from four selected zones of the Devonian shale in well #20403 were used in the mechanical and physical properties tests. The zones are the 2981-2982 ft. interval in the Upper Gray shale, the 3446-3447 ft. interval in the Middle Brown shale, the 3821-2823 ft. interval in the Lower Gray shale and the 3996-3997 ft. interval in the Lower Brown shale. Samples used in the triaxial compression and extension tests were cylinders 0.75 inch in diameter by 1.5 inches in length and were obtained perpendicular to the core axis, i.e., parallel to the bedding plane. Table II lists the results of the measurements and the confining pressures at which the tests were run. The elastic moduli were determined from the initial slopes of the stress-strain curves. The results of these extension tests indicate that the four formations have nearly identical static elastic moduli in extension.

Triaxial compression tests were also carried out to determine the static elastic moduli at simulated downhole conditions. Samples were again taken perpendicular to the core axis and tested under confining pressures adjusted to 1.0 psi/ft. to approximate the overburden stress. A summary of the test data is given in Table III. The unusually high Young's moduli reported for the Lower Brown shale are not believed to be representative of the bulk property of the entire zone. The values are correct for a thin zone from which the samples were extracted but, in this case, do not indicate the average property as do the logs. This was verified by wave velocities measurements on different samples.

As expected, the static moduli are appreciably lower than the moduli derived from sonic velocities.

TABLE II

Triaxial Extension Test Data for
Samples from the #20403 Well

| Nomenclature | Depth (ft) | Test Density ($g/cm^3$) | Confining Pressure (psi) | Young's Modulus ($10^6$ psi) | Poisson's Ratio |
|---|---|---|---|---|---|
| Upper Brown Shale | 2981 | 2.62 | 2981 | 3.43 | .27 |
| | | 2.58 | 2981 | 3.00 | .13 |
| | | 2.57 | 2981 | 3.00 | .11 |
| Middle Brown Shale | 3446 | 2.51 | 3446 | 4.00 | .20 |
| | | 2.50 | 3446 | 3.33 | .20 |
| | | 2.49 | 3446 | 3.43 | .14 |
| Lower Gray Shale | 3821 | 2.66 | 3821 | 3.00 | .20 |
| | | 2.67 | 3821 | 3.15 | .23 |
| | | 2.66 | 3821 | 2.86 | .17 |
| Lower Brown Shale | 3996 | 2.68 | 3996 | 4.00 | .20 |
| | | 2.69 | 3996 | 3.19 | .20 |
| | | 2.68 | 3996 | 3.61 | .20 |

TABLE III

Triaxial Compression Test Data for
Samples from the #20403 Well

| Nomenclature | Depth (ft) | Test Density ($g/cm^3$) | Confining Pressure (psi) | Young's Modulus ($10^6$ psi) | Poisson's Ratio |
|---|---|---|---|---|---|
| Upper Brown Shale | 2981 | 2.59 | 2981 | 3.75 | .11 |
| | | 2.60 | 2981 | 4.80 | .28 |
| | | 2.58 | 2981 | 4.29 | .23 |
| Middle Brown Shale | 3446 | 2.49 | 3446 | 5.25 | .17 |
| | | 2.47 | 3446 | 4.50 | .20 |
| | | 2.48 | 3446 | 4.62 | .23 |
| Lower Gray Shale | 3821 | 2.65 | 3821 | 7.20 | .35 |
| | | 2.68 | 3821 | 5.00 | .23 |
| | | 2.67 | 3821 | 3.60 | .14 |
| | | 2.66 | 3821 | 3.80 | .27 |
| Lower Brown Shale | 3996 | 2.68 | 3996 | 7.50 | .41 |
| | | 2.68 | 3996 | 8.00 | .41 |
| | | 2.68 | 3996 | 8.50 | .23 |

## FRACTURE TOUGHNESS TESTS

Fracture toughness measurements were carried out on cylinderical samples using the burst technique developed by Clifton, *et al.*, (1976). In this technique a core sample about three inches long is used. A small hole is drilled along the axis of the specimen and two opposite prenotches are placed at the internal walls to specify the fracture initiation points. A bladder is placed in the hole to prevent fluid from entering the sample or the notches and then pressure is applied in the bladder until the sample bursts. Table IV lists the results of these tests.

TABLE IV

Results of Fracture Toughness Tests

| | Sample Depth (ft) | Radii Ratio b/a | Failure Pressure (psi) | $K_{Ic}$ (psi$\sqrt{in}$) | Remarks |
|---|---|---|---|---|---|
| Upper Gray Shale | 2711 | 10.47 | 2825 | 1220 | Failure initiated along notch then turned along pre-existing fracture. |
| | 2761 | 10.47 | 3800 | 1100 | Failure ignored notch and occurred on a pre-existing fracture. |
| Middle Gray Shale | 3365 | 10.50 | 2313 | 737 | Fractured as expected. |
| Lower Gray Shale | 3760 | 10.50 | 3375 | 1075 | Fractured as expected. |

## PERMEABILITY MEASUREMENTS

Permeability measurements were made on three samples from Well #20403 using the pressure transient technique (Appendix C). In this technique a step pressure of a few psi is applied to one side of a sample by a gas (nitrogen) contained in a small reservoir connected with the sample. As the gas penetrates the sample, the pressure in the reservoir declines. The permeability is calculated from the rate of pressure decline. This technique is well suited for permeabilities in the microdarcy range. The results are given in Table V.

TABLE V

Permeability Measurements on Samples from the #20403 Well

| | Sample Depth (feet) | Confining Pressure (psi) | Pore Pressure (psi) | Permeability (microdarcies) | Comments |
|---|---|---|---|---|---|
| Middle Brown Shale | 3626 | 1000 | 600 | 8.7 | |
| | | 4000 | 600 | 2.8 | |
| | | 4000 | 350 | 2.7 | |
| Lower Gray Shale | 3675 | 500 | 350 | < 0.1 | Permeability was below the resolution of the equipment. |
| Lower Brown Shale | 3965 | 500 | 350 | 15 | Sample had visible fractures running the length of the flow path. |

Pore pressures of 350 psi were selected to represent the actual downhole pressures. The tests were performed before an accurate measurement of the formation pore pressure was available. Later, however, the actual formation pore pressure was determined by well testing to be 250 psi. The difference between the test pore pressure and the actual formation pressure should have an insignificant effect on the measured permeability.

FLOW CAPACITY TESTS

A shale sample from the 4,020 foot depth (Lower Brown Shale) in well #20403 was fractured by the "Brazallian" method and fitted back together for the test. Tests were performed on the following arrangements:

1. A fractured sample fitted back together without any proppant. This test was to simulate the part of a hydraulic fracture which was cracked open by the fluid but did not receive any proppant.
2. A one-inch-thick layer of 20/40 sand. This width was selected on the basis of Halliburton's calculation for fracture width for the foam treatment. This test would simulate the part of the fracture that achieved the calculated width and had a sand bed settled in it.
3. A sample propped with 1.44 lb/ft$^2$ of 20/40 sand to simulate the condition of perfect transport where the suspended sand remained in place while the fracture closed.
4. A sample propped with 0.56 lb/ft$^2$ of 100 mesh sand to simulate a spearhead of fine sand in the fracture which would behave mostly like a fluid-loss material.

These tests were made at several confining pressures in order to bracket the actual *in situ* closure pressures. The sand, sent to Terra Tek by Halliburton, was a sample of the material used in the hydraulic fracture treatment in Well #20403. A description of the experimental procedure is given in Appendix D. The results are summarized as follows:

1. Unpropped Fracture. Flow capacities were dependent on both the closure stress on the rock faces and the pressure of the gas used for the measurements. For downhole closure stresses between about 1,000 and 4,000 psi, and dry nitrogen pressures between about zero and 100 psi the flow capacities ranged from about 1 md-cm to about 300 md-cm. Visual examination of the faces of the samples after the test found only small contact marks. There was no visible plastic flow or imbedment. An approximate calculation (Appendix D) of the effective open fracture width is 0.001 to .03 cm for downhole closure stress conditions.
2. Fracture Propped with 0.56 $lb/ft^2$ of 100-mesh sand. Again, the flow capacities were dependent on closure stress and gas pressure. Measurements at simulated downhole closure stress, but low gas pressure yielded flow capacity measurements of about 1100 md-cm.
3. One-inch-thick Layer of 20/40 Sand. The sand did not crush under the simulated downhole stresses so the measurements were essentially those for compacted sand. The permeability to dry nitrogen measured at pressures near atmospheric pressure was in the range to 6,000 to 10,000 md-cm, and there was only a small decrease in permeability with increasing confining stress.
4. Fracture Propped with 1.44 $lb/ft^2$ of 20/40 Sand. Flow capacities were dependent on both the closure stress

and the gas pressure. Plots of flow capacity versus reciprocal pressure did not always show a linear relationship as expected from the Klinkenberg theory. For downhole conditions of pressure and closure stress the flow capacity is approximately 8,000 md-cm.

Figure 5 is a plot showing the results for the unpropped fracture and for the fracture propped with 0.56 $lb/ft^2$ of 100 mesh sand and 1.44 $lb/ft^2$ of 20/40 mesh sand. Because of the pressure and flow rate dependency, the plots are indicated as bands with trends rather than definite lines.

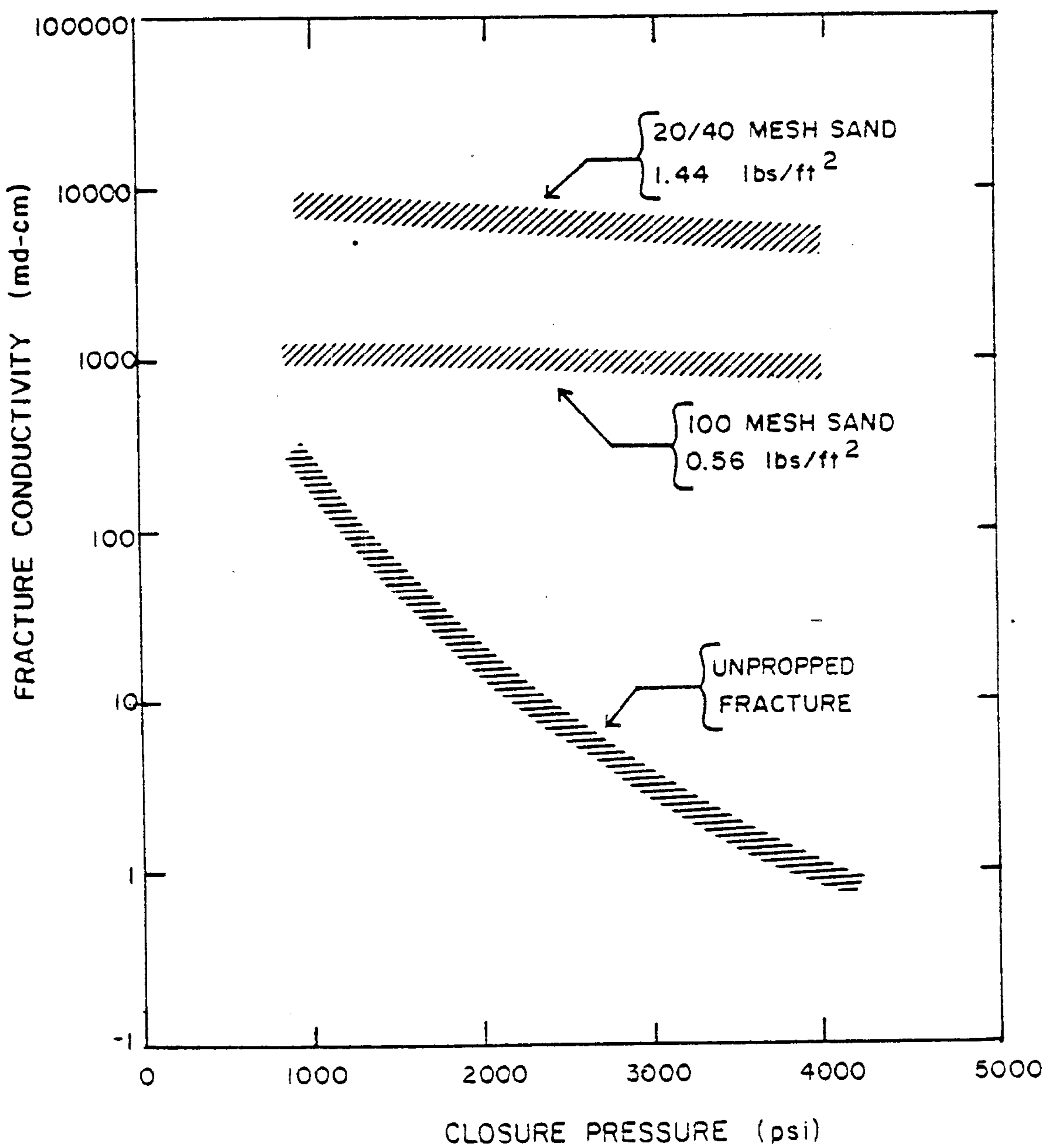


Figure 5. Fracture conductivity for unpropped and propped fracture in Lower Brown Shale.

## DATA INTERPRETATION AND CONCLUDING REMARKS

### BACKGROUND

The Devonian shale in the area of the three-well test program consists of several layers of brown and gray shales, as shown in Figure 1. Natural gas is found in all of the layers with the Middle and Lower Brown Shale layers having the best potentials. Since the bedding is nearly horizontal and there are no major tectonic displacements in the area of the test program, the shale layers are expected to be similar in the 20401, 20402 and 20403 wells. Data from all three wells are thus combined to form a composite picture of the area.

In hydraulic fracturing of reservoir rock formations, the rock is subject to:

1) The fracturing fluid pressure which tends to open the crack, and
2) The far field *in situ* stresses acting to close the crack.

During a hydraulic fracture treatment, the forces from the fracturing fluid need to overcome both the *in situ* stress and the fracture toughness of the rocks, a material property similar to the tensile strength that represents the resistance of rock to fracturing. In a layered subsurface formation such as the Devonian shale, the separate layers may have different fracture toughness, and/or elastic moduli along with different naturally occurring stresses in the ground. Fracture containment analysis is accomplished by evaluating these factors as they apply to the particular zone of the gas reservoir being stimulated. To determine whether a layer is a barrier or not, it is thus necessary to evaluate its properties in relation to the adjacent layers. A particular layer may be a barrier in some instances and not a barrier in other instances, depending on the relative relationships of the stresses and mechanical properties.

## CONTAINMENT CRITERIA

When a fracture is initiated in rock, the fracture will extend when the stress-intensity factor at its tip reaches a critical value. Whether a fracture moves up, down or out depends on the relative values of the critical stress-intensity factors for the various materials as well as along the fracture perimeter as generated by the loading conditions and fracture geometry. Hence, a fracture analysis requires the determination of the stress-intensity values around the crack periphery and then their comparison to the critical values for the different formations [Simonson, *et al.*, 1975]. The following data is used in such analysis:

1) The elastic moduli in the pay zone and bounding layers
2) The *in situ* stress field and, in particular, the minimum principal stresses in the pay zone and bounding layers above and below the pay zone
3) The fracture toughness or critical stress-intensity factors for the pay zone and bounding layers
4) The physical properties of the fracturing fluid and the pumping schedule.

Knowledge of the elastic moduli and *in situ* stresses for the pay zone and both of the bounding layers is needed to determine whether or not the bounding layers are barriers to crack extension outside the pay zone.

Hydraulic fracture analysis is inherently a three-dimensional problem; the mathematical solutions of which are extremely complicated. The present work will be limited to treating two-dimensional cracks. Such a simplified analysis provides considerable insight into understanding the parameters and conditions which influence hydraulic fracture propagation [Simonson, *et al.*, 1976].

The basic concept of containment analysis is illustrated in Figure 6. The fluid is moving such that the pressure near the wellbore is higher than the pressure near the tip. Estimates of the stress-intensity factor at the edges and tip of the propagating fracture can be made if the pressure profile, *in situ* stresses and elastic moduli along the crack shape are known. These estimates are then compared to the critical stress intensities. The fracture will propagate when the stress-intensity factors reach the critical values. In the special case where the stress-intensity factor would be equal to the critical value at all points of the perimeter around the crack, the fracture would propagate in all directions at the same time. On the other hand, if the stress-intensity factor reaches a critical value only at the tip and not at the upper and lower edges, the fracture is then confined to the pay zone.

For this discussion we will consider an infinitely long, narrow crack in layered media. This model is representative of a hydraulic

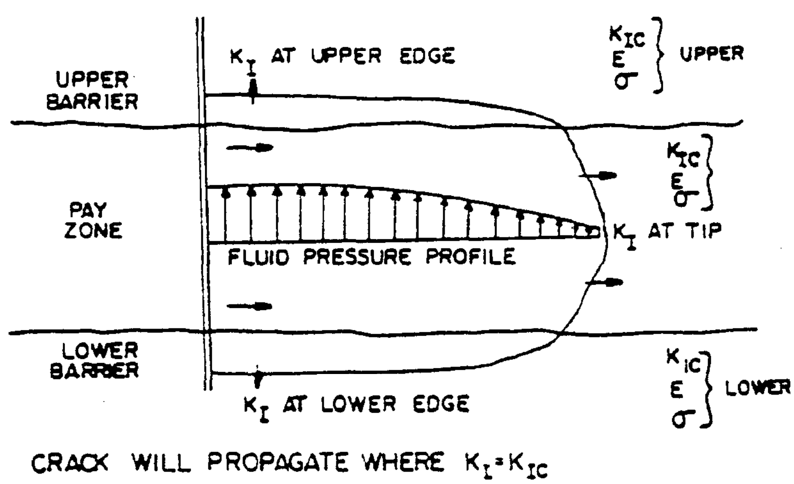


Figure 6. Schematic diagram to illustrate fracture containment analysis

fracture with a short height and a long length. The plane-strain mathematical model gives the following equation for the stress-intensity factor at the upper crack edge

$$K_I = \frac{1}{\sqrt{\pi \ell}} \int_{-\ell}^{+\ell} \left(P_y - S_y\right) \sqrt{\frac{\ell + y}{\ell - y}}\, dy$$

where

$P_y$ = Pressure profile in crack

$S_y$ = Far-field horizontal stress profile

$y$ = Position along crack

$\ell$ = Height from the crack center to the tip

$S_y$ represents the minimum principal *in situ* stress since fracture will be normal to this stress. Note in this equation that the stress-intensity factor is dependent upon the profile of the stress difference between the pressure inside the fracture and native *in situ* stresses across the fracture. Different combinations of fluid pressures and *in situ* stresses will give different values of $K_I$ and, in turn, different results for a prediction of the final fracture geometry.

(i) Influence of Elastic Moduli

The above equation for $K_I$ is for the hypothetical case where the elastic moduli of the pay zone and the bounding layer are equal. If the elastic moduli of the several layers were different, then there is an additional influence on the stress-intensity factor as a result of the difference in the moduli. Figure 7 illustrates the qualitative behavior of the stress-intensity factor for a crack that moves perpendicular to an interface between two materials with different moduli when plane-strain conditions prevail. If the elastic modulus in the pay zone is higher than that of the bounding layer, then as a fracture propagates toward the boundary, the stress-intensity factor increases such that it will reach the critical value and the fracture will "snap" into the bounding layer. On the other hand, if the modulus in the pay zone is lower than the moduli in the bounding layers, then a fracture which is propagating from the pay zone toward the bounding layers will find the stress-intensity at its tip nearest the interface decreasing as the boundaries are approached such that the critical value is not reached and the fracture is contained within the pay zone.

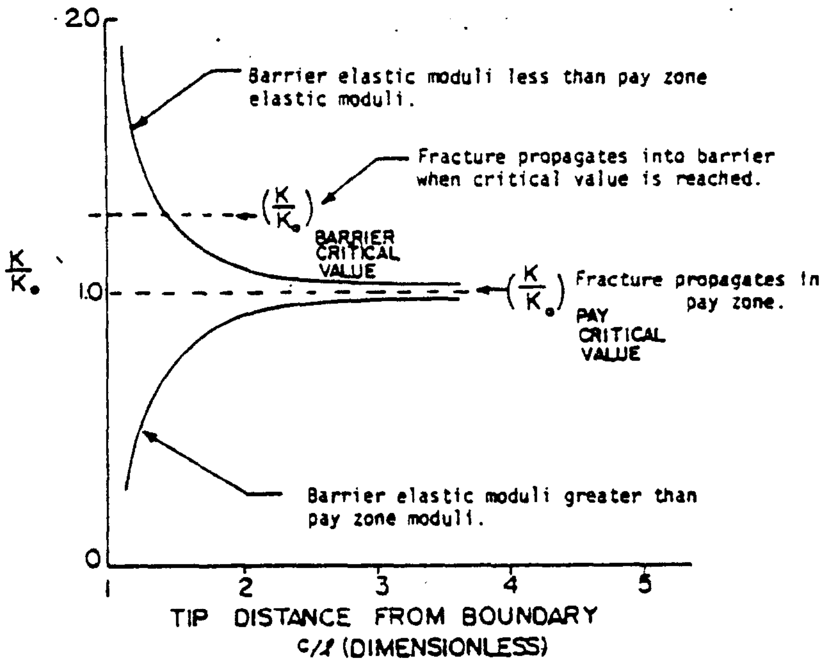


Figure 7. Qualitative behavior of the stress-intensity factor as a crack of length 2a approaches the boundary of an adjacent layer with different elastic moduli (c is the distance from fracture center to boundary)

(ii) Influence of *In Situ* Stress

Difference in *in situ* stresses between the pay zone and the barrier layers have a distinct influence on fracture propagation. Consider the hypothetical case, shown in Figure 8 in which a hydraulic fracture has extended by some mechanism or other into adjacent layers with similar

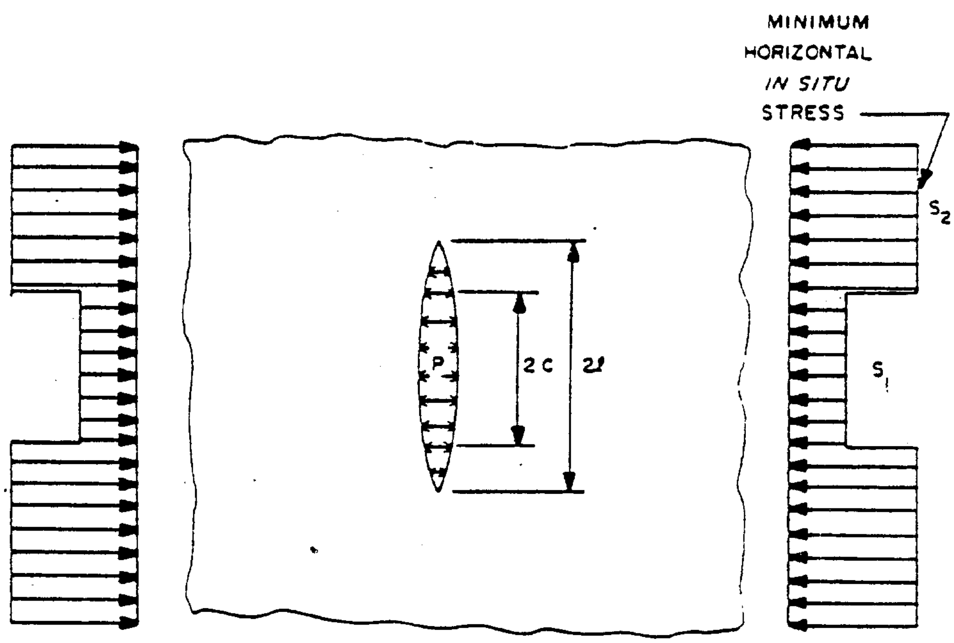


Figure 8. Vertical hydraulic fracture loaded under uniform pressure (P) with differing minimum horizontal stress in pay zone and barriers

elastic moduli but different *in situ* stresses. Figure 9 shows a plot of the distance the crack will advance into the region of high stress (the barrier layers) in terms of the pressure, P, within the fracture and $P_o$, the fracture fluid pressure required for the fracture to reach the interface. The curves in this figure are for a crack height of 200 feet, a fracture toughness of 1,000 psi$\sqrt{\text{in}}$ and for parametric values of the *in situ* stress difference $S_2$ - $S_1$. For a stress difference of 1,000 psi, for example, an over pressure of 500 psi would be expected if the fracture were to propagate a distance of 100 feet into the region of higher *in situ* stress. Finally, if the *in situ* stress in the barrier layers ($S_2$) were less than the *in situ* stress in the pay zone ($S_1$), a situation would exist where it requires less pressure to propagate the fracture in the barrier than in the pay zone.

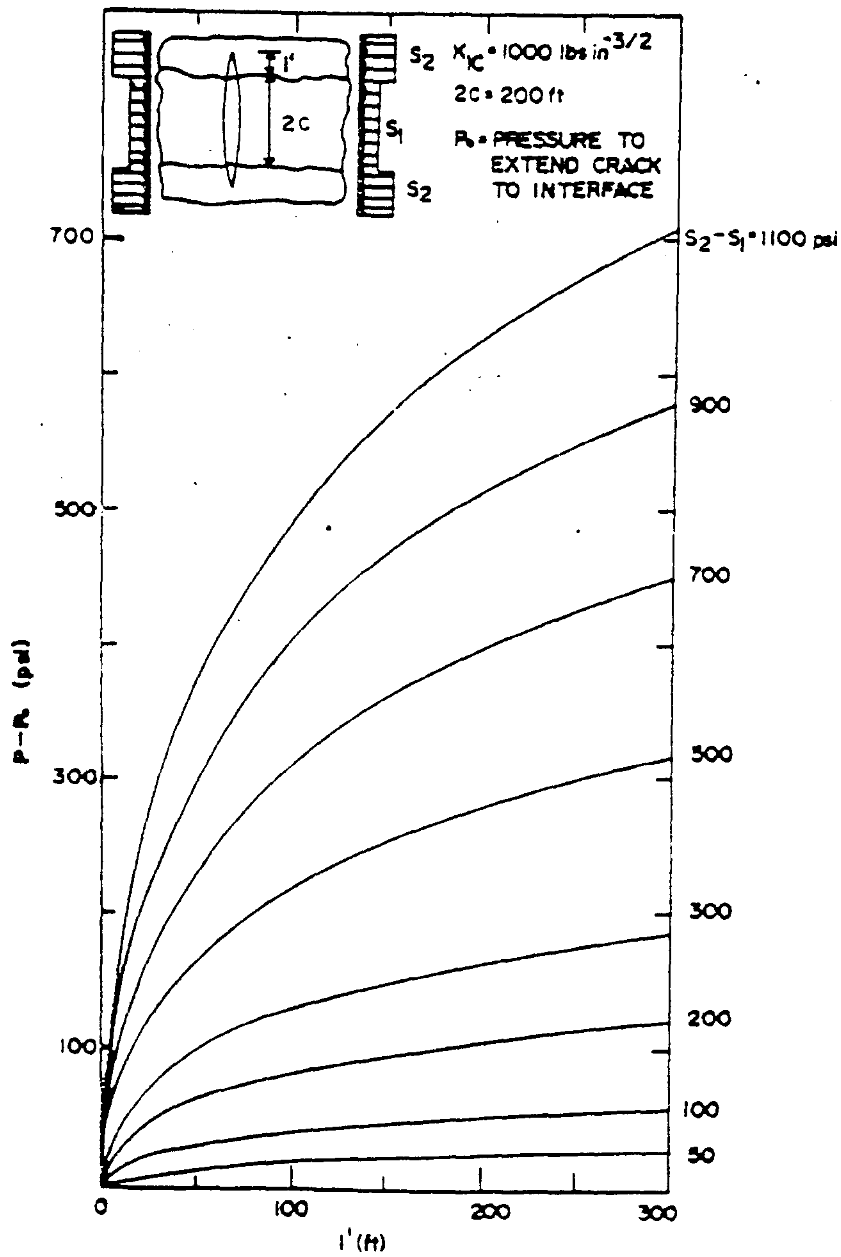


Figure 9. Estimate of fracture migration into the barrier layers [from Simonson, *et al.*, 1976]

SUMMARY OF ROCK MECHANICS DATA

Young's moduli have been calculated using the measured bulk densities. P-wave velocities and the revised S-wave velocities as an incomplete set of triaxial data is available. For the purpose of these calculations, the material was assumed isotropic and homogeneous. Figure 10 illustrates the general trend of the data. Also shown are static moduli from triaxial compression of the Upper Brown and Lower Gray Shales. As expected, the static moduli are lower than the sonic moduli; for the sample tested, the difference is on the order of 20 to 30 percent. Figure 10 summarizes the results of critical stress-intensity tests for the Gray Shales.

*In situ* stresses, especially the difference in *in situ* stresses between the pay and barrier formations, are the most critical parameters to MHF containment. Unfortunately, this is the parameter for which the least amount of data is available. A single mini-hydraulic fracturing test was performed by Terra Tek at the 2745 foot level (Upper Gray Shale) in well #20402 [Abou-Sayed, *et al.*, 1977]. These results were as follows:

| | |
|---|---|
| Minimum Horizontal Stress | 2360 psi, N 35° W to N 45° W |
| Maximum Horizontal Stress | 4390 psi, N 45° E to N 55° E |
| Overburden Stress | 3210 psi |
| Pore Pressure | $\sim$ 250 psi |

The measured principal stress directions agree well with the prevailing geological structure in the region and with the principal stress directions reported by Overbey (1976) from a series of measurements in West Virginia. A basement structure map of the region in which the reported tests were conducted is shown in Figure 11. The map, adapted from Harris (USGS Map I-919D, 1975) by Overbey (1976), shows a projection of the Rome Trough the projection of the Rome Trough are N 45° E to N 50° E, i.e., parallel to the strike or the basement faults and in agreement with the directions reported here.

An estimate of the minimum horizontal stresses in the other shale layers was made on the basis of elastic theory. Data from the Upper Gray Shale was analyzed for determination of applied boundary displacements in both horizontal directions as might be imposed-through normal faulting on the boundaries of the Rome Trough. These same displacements were applied to the other shale layers and the resulting minimum *in situ* stress in these layers was estimated using moduli derived from corrected logs. Figure 10c shows a plot of the estimated minimum horizontal principal stresses in the different formations. These estimates correlate with two independent observations. Swolfs, *et al.*, (1977), based on strain relaxation data, estimated the minimum *in situ* stress gradients from the surface of 0.52 psi per foot for the Middle Brown Shale and 0.76 psi per foot for the overlying Middle Gray Shale. These stress gradients coincide with the data shown in FIgure 10c at the Middle Gray/Middle Brown Shales interface. Field engineers contend that either the Lower Gray or the Lower Brown Shale will break down under a hydrostatic head of water. The estimated minimum *in situ* stress shown in Figure 10c for the Lower Brown Shale would also predict this behavior.

DATA INTERPRETATION

Although the tests were minimal, sufficient data was gleaned from available information to perform a containment analysis. Both Figure 10a and 10c indicate that the gray shales and Onondaga Limestone will act as barriers to the fracture growth in the brown shales. The gray shales are not strong barriers (moduli contrast is less than 30 percent and the largest *in situ* stress difference is less than 800 psi), however, and can also be broken down if fluid pressures are too high. The brown shales will not form barriers to fractures in the gray shales. This interpretation correlates with field results reported by McKetta (1977). A fracture initiated in the Lower Gray Shale in well #20403 propagated upward into the Middle Brown Shale. Communication was noted on perforating and breaking down the Middle Brown Shale.

A significant factor in successful completion of MHF treatment in reservoirs with marginal barrier formations is the control of fracturing fluid flow rate and the maximum allowable bottomhole treatment pressure (BHTP). There are other factors, besides containment of the induced fracture, that might impose certain bounds on both flow rate and BHTP. These are proppant transport, created crack width, strength of casing, location of perforation and the like. However, the calculated value of BHTP that would prevent the fracture penetration into barrier zones would prove instrumental in achieving a contained fracture geometry. An estimate of the maximum BHTP for a given treatment can be obtained following the arguments presented earlier. For a pay formation height of 2c and a pumping pressure of P, the fracture will extend a length $\ell'$ into the barrier layer such that [Simonson, *et al.*, 1976]:

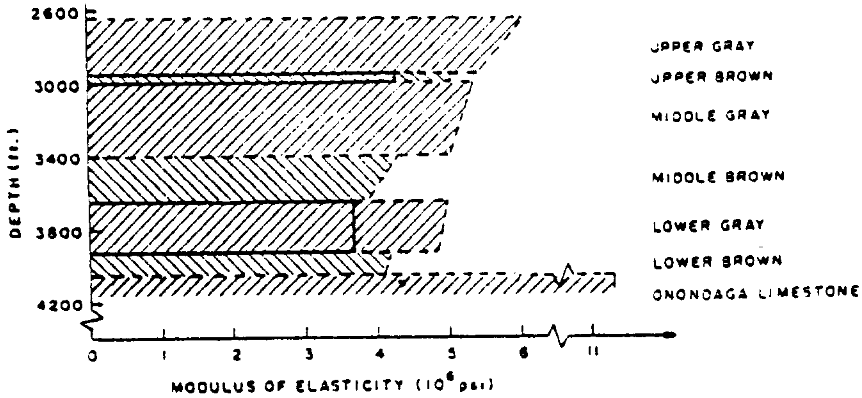


Figure 10a. Log-derived (dotted lines) and laboratory-measured (solid lines) modulus of elasticity

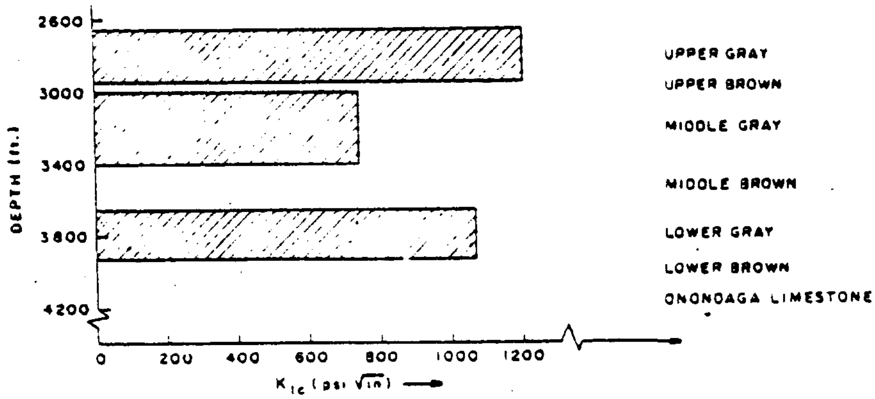


Figure 10b. Critical stress-intensity factor for the barrier shales only

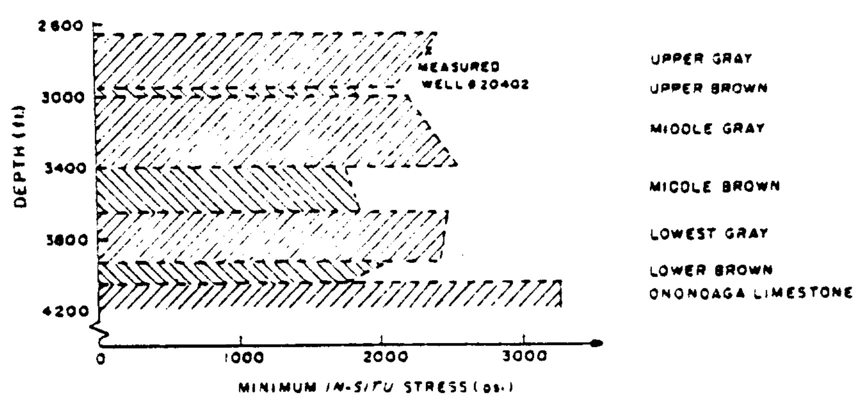


Figure 10c. Derived minimum *in situ* stresses correlated to measured stresses (x) at 2745 ft. in Well #20402

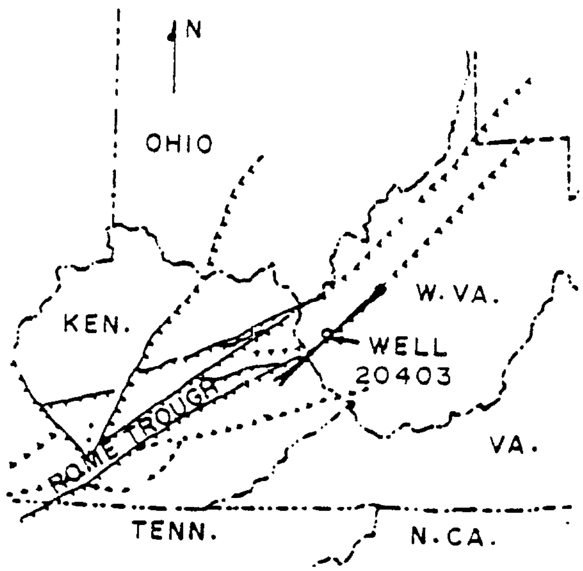


Figure 11. Basement structure of Kentucky-West Virginia adapted from Overbey (1976) with the direction of maximum horizontal stress at well #20403

through the northwestern edge of West Virginia. Schumaker (1976) describes the Rome Trough as a graben bounded by high-angle, normal faults. This structure lies within an area which is a junction of three distinct geological provinces [Werner, 1976]:

1) Central Appalachian Fold Belt,
2) Southern Appalachian Thrust-Fold Belt, and
3) Appalachian Plateau with Basement Faults.

Although it is not known whether or not basement faults penetrate into the Devonian shales in this area, Overbey's measurements (1976) suggest a correlation of principal stress directions with the basement structure. At locations which fall outside the projection of the Rome Trough, the measured directions of $\sigma_{HMAX}$ are oriented generally east-west and are normal to the predominantly north-south strike of the thrust faults and folds of the Appalachian Mountains. Measured directions of $\sigma_{HMAX}$ which fall within

$$P - S_1 = \frac{1}{\sqrt{\pi(c+\ell')}} \left[ K_{Ic} - \frac{2(S_2-S_1)(c+\ell')\cos^{-1}\left(\frac{c}{c+\ell'}\right)}{\sqrt{\pi(c+\ell')}} \right]$$

where $K_{Ic}$ is the critical stress-intensity factor for the barrier layer and $S_1$ and $S_2$ are the minimum *in situ* stresses for the pay and barrier zones, respectively. Penetration of a fracture which initiated in the Middle Brown Shale into the Middle Gray Shale is shown in Figure 12. For excess pumping pressure in the fracture ($P-S_1$) less than 400 psi, the penetration is kept within 50 feet. To maintain fracture intrusion into the Middle Gray Shale within this limit, the bottomhole treatment pressure during hydraulic fracturing of the Middle Brown Shale layer should not exceed the minimum horizontal stress in that zone by more than 400 psi, plus any expected drop in pressure across the perforation. Corresponding considerations for the Lower Brown and Lower Gray Shales (the Onondaga Limestone forms a strong barrier due to its large elastic moduli) leads to a treating pressure within the formation of 250 psi in excess of the minimum horizontal stress for the Lower Brown Shale. For the Upper Brown Shale, the Upper Gray and Middle Gray Shales will form weak barriers. Following similar considerations as outlined above, this leads to an in formation treating pressure of 200 psi in excess of the minimum horizontal stress for fracturing the Upper Brown Shale.

In treating the Middle Brown Shale first, the fracture will propagate into both the Middle Gray and Lower Gray Shales. There is, therefore, the possibility that later fractures initiated in the Upper Brown and in the Lower Brown Shales will interact with the earlier fracture created in the Middle Brown Shale. In a multi-stage MHF it is important that the better reservoir formation be fractured first.

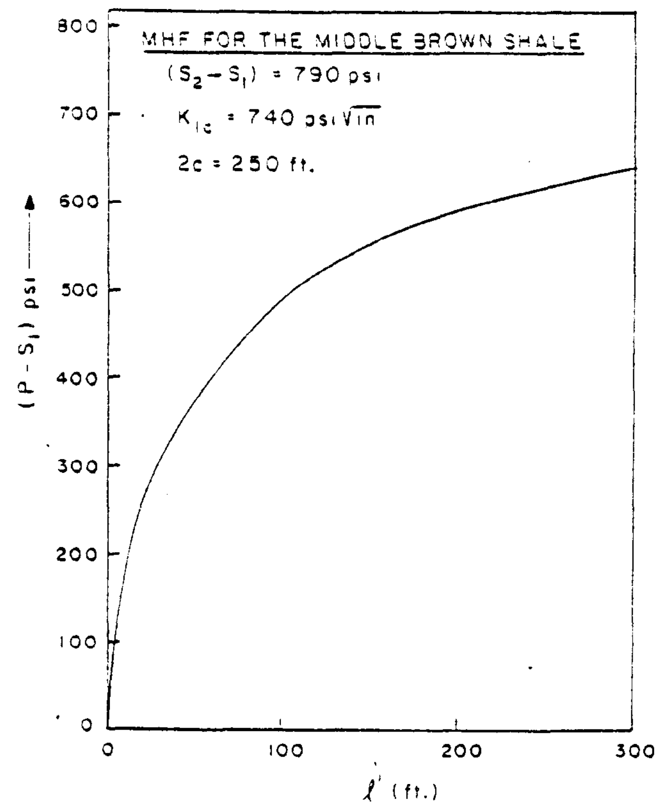


Figure 12. Fracture penetration into the Middle Gray Shale for fracture in the Middle Brown Shale

## REFERENCES

Abou-Sayed, A. S., C. E. Brechtel and R. J. Clifton; "*In Situ* Stress Determination by Hydrofracturing - A Fracture Mechanics Approach," *Journal of Geophysical Research,* 1977, in press.

Brechtel, C. E., A. S. Abou-Sayed, and R. J. Clifton; "*In Situ* Stress Determination in the Devonian Shales (Ira McCoy 20402) within the Rome Basin," *Terra Tek Report,* TR 76-36, July 1976.

Clifton, R. J., E. R. Simonson, A. H. Jones and S. J. Green; "Determination of the Critical Stress-Intensity Factor $K_{Ic}$ in a Circular Ring," *Experimental Mechanics,* Vol. 16, pp. 233-238, June, 1976.

Lingle, R. and A. S. Abou-Sayed; "Comparison of Log with Laboratory Measured Data for Columbia Gas System Service Corporation Well #20403," Fourth Progress Report, *Terra Tek Report,* TR 76-45, September 1976.

Lingle, R. and A. H. Jones; "Comparison of Log and Laboratory Measured P-Wave and S-Wave Velocities," *Terra Tek Report,* TR 77-19, Published in *Proceedings of the Eighteenth Annual Logging Symposium,* Houston, 1977.

McKetta, S. F.: "Massive Hydraulic Fracturing of the Devonian Shale in Lincoln County, West Virginia," *Proceedings of ERDA Enhanced Oil, Gas Recovery, and Improved Drilling Methods Symposium,* Tulsa, Oklahoma, Vol. 2, p. G-7, August 30-31, September 1, 1977.

Overbey, W. K.; "Effect of *In Situ* Stress on Induced Fractures," *Proc. of Seventh Appalachian Petroleum Geology Symposium,* USERDA, Morgantown, MERC/SP-76-2, March 1-4, pp. 182-211, 1976.

Ranostaj, E. J.; "Massive Hydraulic Fracturing Eastern Devonian Shales," *ERDA Symposium on Enhanced Oil, Gas Recovery,* Tulsa, Oklahoma, Vol. 2, p. C-3, September 9-10, 1976.

Shumaker, R. C.; "A Digest of Appalachians Structural Geology," *Proceedings of Seventh Appalchian Petroleum Geology Symposium,* USERDA, Morgantown, MERC/SP/76-2, March 1-4, pp. 75-93, 1976.

Simonson, E. R., A. H. Jones and A. S. Abou-Sayed, "Experimental and Theoretical Considerations of Massive Hydraulic Fracturing," *Terra Tek Report,* TR 75-39, December 1975.

Simonson, E. R., A. S. Abou-Sayed and R. J. Clifton; "Containment of Massive Hydraulic Fracture," *Society of Petroleum Engineers Journal*, 1977, in press.

Swolfs, H. S., R. Lingle and J. M. Thomas; "Determination of the Strain Relaxation and their Relation to Subsurface Stresses in Devonian Shale," *Terra Tek Report*, TR 77-12, February 1977.

Werner, E.; "Remote Sensing Studies in the Appalachian Plateau for Applications to Fossil Fuel Extractions," *Proceedings of ERDA Symposium on Enhanced Oil, Gas Recovery*, Tulsa, Oklahoma, Vol. 2, p. C-2, September 9-10, 1976.

# APPENDIX A

## COMPARISON OF LOG AND LABORATORY MEASURED P-WAVE AND S-WAVE VELOCITIES

Terra Tek, Inc.
Report TR 77-19

Accepted for presentation at the
Eighteenth Annual Logging Symposium

# COMPARISON OF LOG AND LABORATORY MEASURED P-WAVE AND S-WAVE VELOCITIES

by

R. Lingle
A. H. Jones

Terra Tek, Inc.
420 Wakara Way
Salt Lake City, Utah 84108

## ABSTRACT

Longitudinal (p-wave) velocity, shear (s-wave) velocity, and density measurements were made in the laboratory under simulated *in situ* conditions, on Devonian shale core samples. These values and calculated elastic moduli are compared with data obtained from wire-line logs. The densities and p-wave velocities are in good agreement; however, the laboratory s-wave velocities are consistently higher (10 to 15 percent) than the log measurements. These discrepancies are greatly magnified in the derived elastic moduli. Hypothesizing that the log-detected s-wave is in reality the Rayleigh wave, the calculated s-wave velocities agree as well as the p-wave velocities with the corresponding lab-measured values.

## INTRODUCTION

Many engineering applications now require knowledge of *in situ* formation elastic properties. Well completion, production scheduling in fields with weak formations, fluid injections to increase recovery, and massive hydraulic fractures are a few of the applications. Since the elastic moduli can be calculated from material density, p-wave velocity ($V_p$), and s-wave velocity ($V_s$), this work was directed toward the comparison of these data obtained from wire-line logs and simulated *in situ* laboratory measurements. The measurements were made on Devonian shale cores obtained from Columbia Gas System Service Corporation well #20403 located in Lincoln County, West Virginia. This well was logged with both the Schlumberger experimental tool and the Birdwell 3-D tool.

In general, the data from the logs agreed with each other and both agreed with the laboratory density and p-wave velocity measurements. However, the s-wave velocities obtained on the laboratory samples were consistently higher (10 to 15 percent) than those obtained from the logs. Errors in the derived elastic moduli are greatly magnified. For example, a 10 percent difference in the s-wave velocity would produce over a 30 percent change in the calculated Poisson's ratio.

The reason for the difference in the s-wave velocities is not known. However, the consistent offset in the s-wave data along with the good agreement of the p-wave velocities introduces a question as to what was actually being measured by the logs. It is hypothesized that the log measured s-wave is in reality the Rayleigh wave.

## LABORATORY TECHNIQUES

The laboratory test samples were prepared by coring parallel to the original core. They were 1 inch in diameter and typically 1.5 inches long, the ends were ground flat and parallel to within .001 inch. A urethane jacket sealed to the end cap was used to prevent confining fluid contact with the rock. The sample was mounted to the removable base plug and the entire assembly inserted into the pressure vessel, which was subsequently filled with fluid and pressurized. Feedthrough were provided to enable electrical contact with the ultrasonic transducers. The test configuration is shown in Figure 1.

A through-transmission technique similar to that introduced by Mattaboni and Schreiber (1967) was used in the laboratory to obtain the velocities. A single transmitting transducer (1 MHz) was used to produce both a p-wave and an s-wave. Separate receivers detect the arrival of each signal. The accuracy of this technique is better than 0.5 percent.

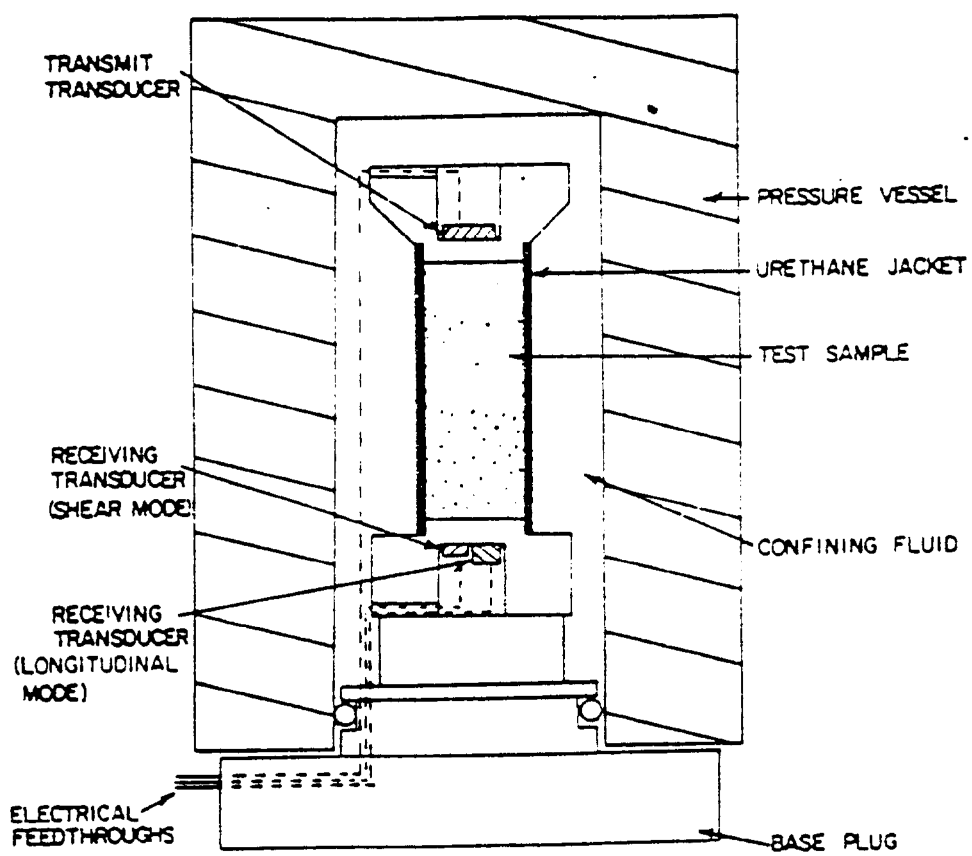


Figure 1. Test configuration for laboratory ultrasonic measurements.

Certain precautions were taken to insure the validity of comparing laboratory and log data. For example, all velocity measurements were made in the same plane and with the same s-wave polarization as the logs, this avoided complications resulting from material anisotropy. Also all measurements were performed at simulated *in situ* stresses. Based on the measured *in situ* stresses, [Brechtel, et al. (1976)] hydrostatic conditions are a close approximation of the measured stress, with a gradient of 1 psi/foot.

The effect of confining pressure on the measured velocities was very small, as indicated by Figure 2. The sample from 3,365 feet indicates the greatest change but even for this sample the p-wave velocity varied less than 6.5 percent for a 4000 psi change in confining pressure. The corresponding change in s-wave velocity is slightly more than 3.5 percent for the same change in pressure.

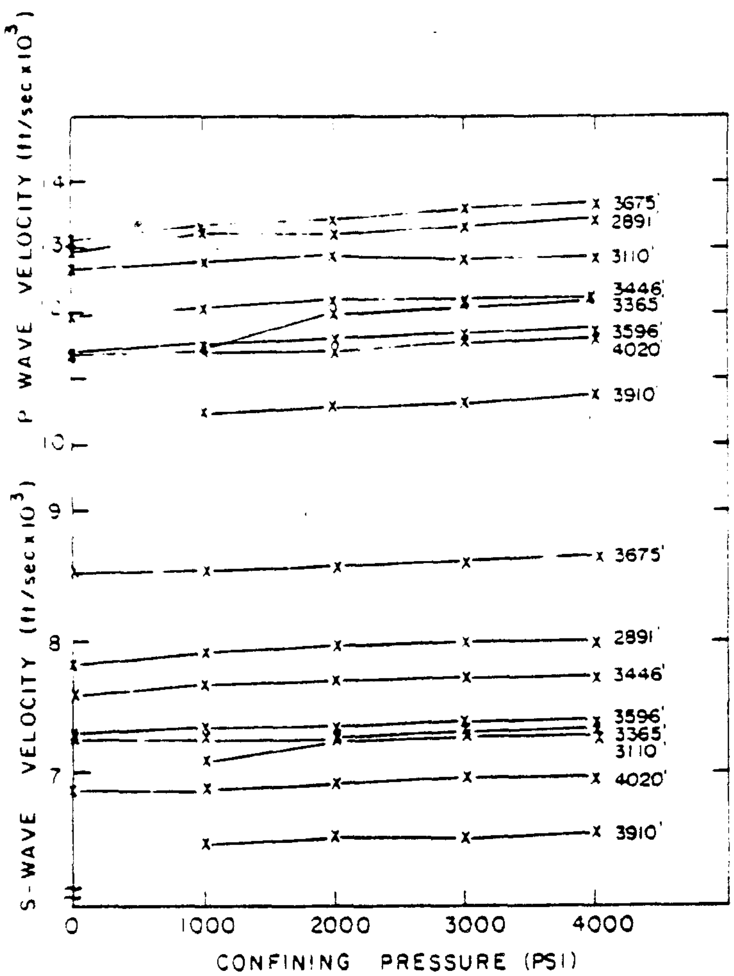


Figure 2. P-wave and s-wave velocities as functions of hydrostatic confining pressure on Devonian shale samples from various depths.

Preliminary measurements showed very little velocity change with temperature over the range encountered in this well (~100°F). The change in the p-wave velocity was less than one percent and the s-wave velocity was within the accuracy of the measuring system. This is consistent with reported velocity versus temperature data on geological materials, c.f. Timur (1976). Therefore, all laboratory velocity data reported here were taken at room temperature.

Densities were obtained from the measured dimensions and weight of the prepared test samples. The accuracy of these measurements were within one percent. The measured change in the density with applied confining pressure up to 4000 psi was no more than 0.2 percent. Because of this small change, the data was not corrected for change in density with pressure.

## COMPARISON OF DATA

Figures 3 and 4 shows the comparison of laboratory data with that obtained from the logs. The p-wave velocities and densities are, in general, in good agreement, with the exception of the sample from 3910 feet. The laboratory s-wave velocities are consistently 10 to 15 percent higher than the log values at identical depths. Young's modulus, Poisson's ratio, and the bulk modulus have been calculated, using the measured bulk densities, p-wave velocities, and the s-wave velocities. For the purpose of these calculations, the material was assumed isotropic and homogeneous. The equations that were used are presented in Appendix A1. The comparison of these data are shown in Tables I and II. As anticipated the discrepancy in s-wave velocities are greatly magnified in the elastic moduli.

With the geometry of a sonic log in a borehole, it is physically possible to generate, by mode conversion at the fluid-rock interface, a Rayleigh wave (surface wave) in addition to the p- and s-wave. This is shown in Figure 5. One possible explanation for the discrepancy between the laboratory and log s-wave velocities is that the logs were detecting the arrival of the Rayleigh wave ($V_r$) and not the s-wave. If this assumption is made then it is possible to calculate the s-wave velocities using the established relationships found in the open literature, c.f. Fung, Chap. 7, p. 180 (1965). Because of the difficulties in solving the equation directly for the Rayleigh wave velocity, a plot relating the velocity ratios was made and is presented in Figure 6.

The revised s-wave velocities, calculated from the Schlumberger log data, are shown in Table III. The comparison of the revised data, original log data, and the laboratory data is shown in Figure 7. With the exception of the 3910 foot samples, the revised s-wave velocity values agree very well (within 0.5 percent on the average) with those obtained from laboratory measurements.

## CONCLUSIONS

The close agreement obtained on the measured p-wave velocities and densities is a good indication that the laboratory samples were representative of the material encountered by the logs. The data strongly indicates that the logs measured the arrival of the Rayleigh wave and not the s-wave. It is obvious that more work is needed in this area in order to properly assess the

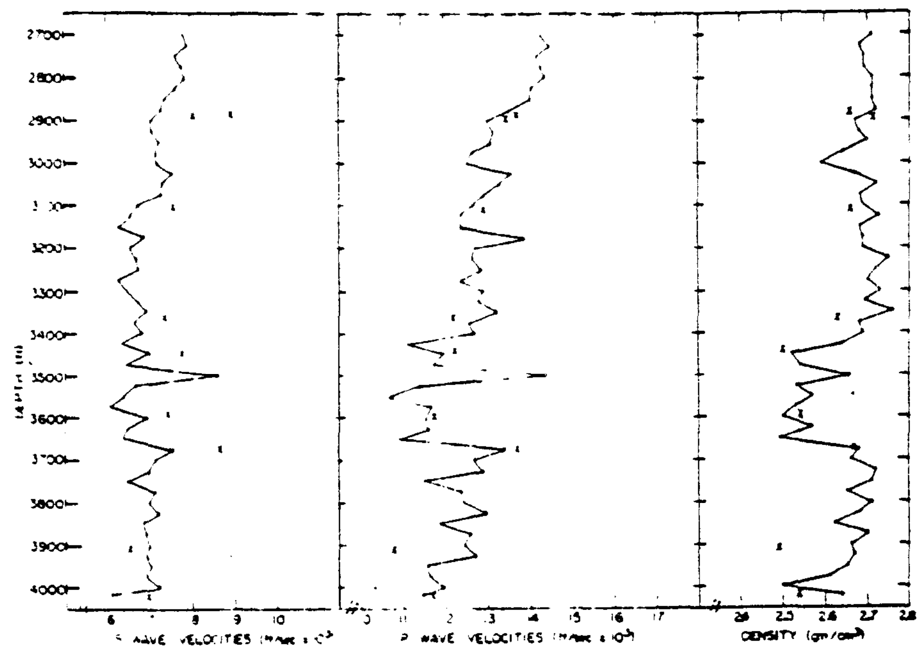


Figure 3. Comparison of laboratory data (X) with data from a Schlumberger experimental s-wave logging tool.

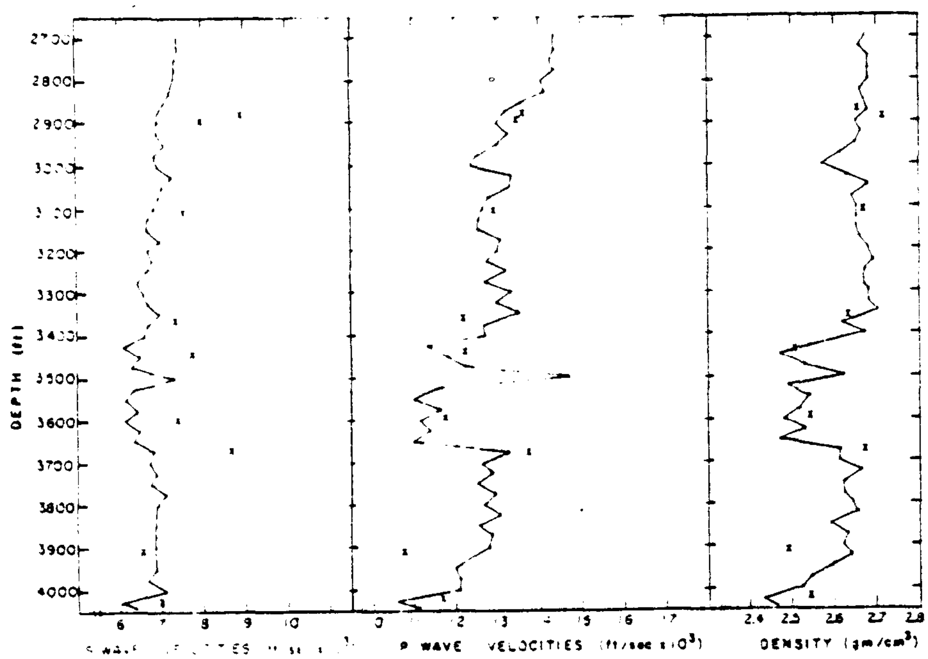


Figure 4. Comparison of laboratory data (X) with data from the Birdwell (3-D) log.

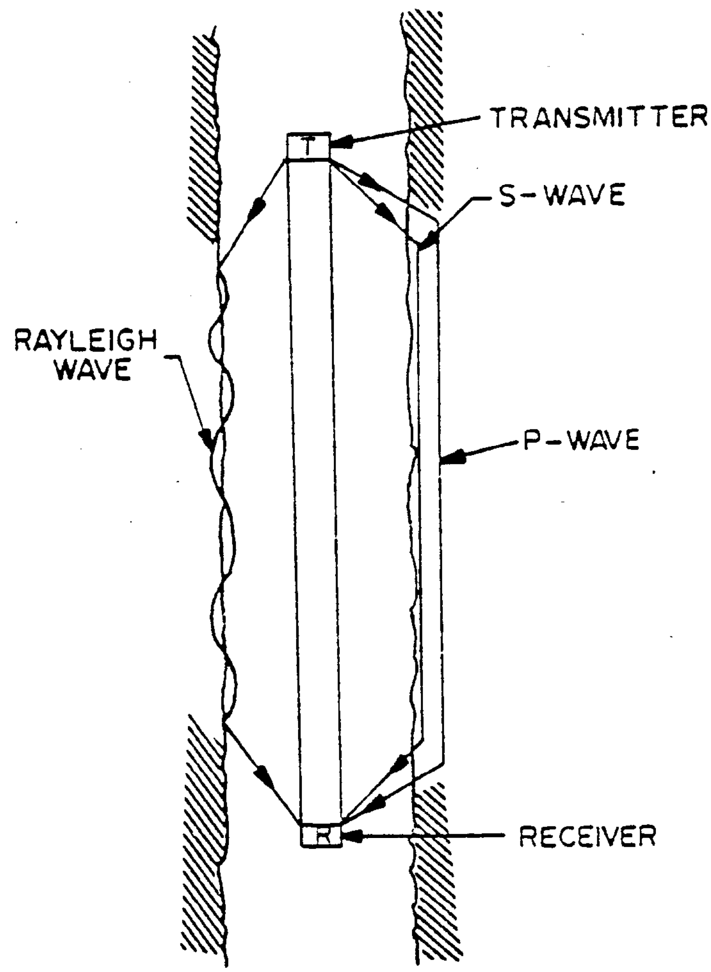


Figure 5. Ray paths for elastic wave produced by a sonic tool in a fluid-filled borehole.

## TABLE I

Laboratory Data (Terra Tek, Inc.) and Log Data (Birdwell)
on Columbia Gas System Service Corp., Well #20403 (Devonian Shale)

| DEPTH (FT.) | VELOCITIES | | | | MODULI | | | | | | POISSON'S RATIO $\nu$ | | DENSITY $\rho$ GM/CM$^3$ | |
|---|---|---|---|---|---|---|---|---|---|---|---|---|---|---|
| | P-WAVE (FT/SEC) | | S-WAVE (FT/SEC) | | YOUNG'S E(PSI x $10^6$) | | BULK K(PSI x $10^6$) | | SHEAR G(PSI x $10^6$) | | | | | |
| | LOG | LAB | LOG | LAB | LOG | LAB | LOG | LAB | LOG | LAB | LOG | LAB | LOG | LAB |
| 2880 | 13420 | 13640 | 7180 | 8950 | 4.31 | 6.43 | 4.00 | 2.34 | 1.85 | 2.86 | .300 | .122 | 2.67 | 2.66 |
| 2891 | 13460 | 13450 | 7270 | 8030 | 4.90 | 5.75 | 3.96 | 3.46 | 1.89 | 2.35 | .294 | .223 | 2.66 | 2.71 |
| 3110 | 12490 | 12300 | 6830 | 7560 | 4.27 | 5.06 | 3.34 | 3.23 | 1.66 | 2.04 | .287 | .239 | 2.64 | 2.66 |
| 3365 | 11650 | 12170 | 6670 | 7340 | 3.89 | 4.63 | 2.66 | 2.70 | 1.55 | 1.91 | .257 | .214 | 2.58 | 2.63 |
| 3446 | 12040 | 12230 | 6330 | 7740 | 3.56 | 4.69 | 3.10 | 2.35 | 1.36 | 2.01 | .309 | .167 | 2.52 | 2.50 |
| 3596 | 11200 | 11740 | 6080 | 7400 | 3.19 | 4.39 | 2.55 | 2.22 | 1.24 | 1.87 | .291 | .170 | 2.48 | 2.54 |
| 3675 | 13250 | 13710 | 6800 | 8660 | 4.31 | 6.30 | 4.01 | 3.15 | 1.63 | 2.70 | .321 | .168 | 2.61 | 2.67 |
| 3910 | 12280 | 10780 | 6760 | 6540 | 4.16 | 3.47 | 3.19 | 1.99 | 1.52 | 1.44 | .283 | .209 | 2.63 | 2.49 |
| 4020 | 11880 | 11670 | 6600 | 6970 | 3.85 | 4.07 | 2.87 | 2.45 | 1.51 | 1.66 | .276 | .223 | 2.57 | 2.54 |

## TABLE II

Laboratory Data (Terra Tek, Inc.) and Log Data (Schlumberger)
on Columbia Gas System Service Corp., Well #20403 (Devonian Shale)

| DEPTH (FT.) | VELOCITIES | | | | MODULI | | | | | | POISSON'S RATIO $\nu$ | | DENSITY $\rho$ GM/CM$^3$ | |
|---|---|---|---|---|---|---|---|---|---|---|---|---|---|---|
| | P-WAVE (FT/SEC) | | S-WAVE (FT/SEC) | | YOUNG'S E(PSI x $10^5$) | | BULK K(PSI x $10^5$) | | SHEAR G(PSI x $10^5$) | | | | | |
| | LOG | LAB | LOG | LAB | LOG | LAB | LOG | LAB | LOG | LAB | LOG | LAB | LOG | LAB |
| 2880 | 13560 | 13640 | 7630 | 8950 | 5.39 | 6.43 | 3.88 | 2.84 | 2.13 | 2.36 | .268 | .122 | 2.71 | 2.66 |
| 2891 | 13330 | 13450 | 7260 | 8030 | 4.91 | 5.75 | 3.88 | 3.46 | 1.90 | 2.35 | .289 | .223 | 2.68 | 2.71 |
| 3110 | 12580 | 12900 | 6800 | 7560 | 4.32 | 5.06 | 3.49 | 3.23 | 1.67 | 2.04 | .293 | .239 | 2.68 | 2.66 |
| 3365 | 11430 | 12170 | 6870 | 7340 | 4.07 | 4.63 | 2.40 | 2.70 | 1.67 | 1.91 | .217 | .214 | 2.63 | 2.63 |
| 3446 | 11300 | 12230 | 6730 | 7740 | 3.86 | 4.69 | 2.34 | 2.35 | 1.57 | 2.01 | .225 | .167 | 2.58 | 2.50 |
| 3596 | 11380 | 11740 | 6900 | 7400 | 3.91 | 4.39 | 2.24 | 2.22 | 1.62 | 1.87 | .209 | .170 | 2.52 | 2.54 |
| 3675 | 13400 | 13710 | 7510 | 8650 | 5.18 | 6.30 | 3.77 | 3.16 | 2.04 | 2.70 | .271 | .168 | 2.68 | 2.67 |
| 3910 | 12200 | 10780 | 6940 | 6540 | 4.32 | 3.47 | 3.01 | 1.99 | 1.71 | 1.44 | .251 | .209 | 2.64 | 2.49 |
| 4020 | 11490 | 11670 | 6100 | 6970 | 3.45 | 4.07 | 2.93 | 2.45 | 1.32 | 1.66 | .304 | .223 | 2.64 | 2.54 |

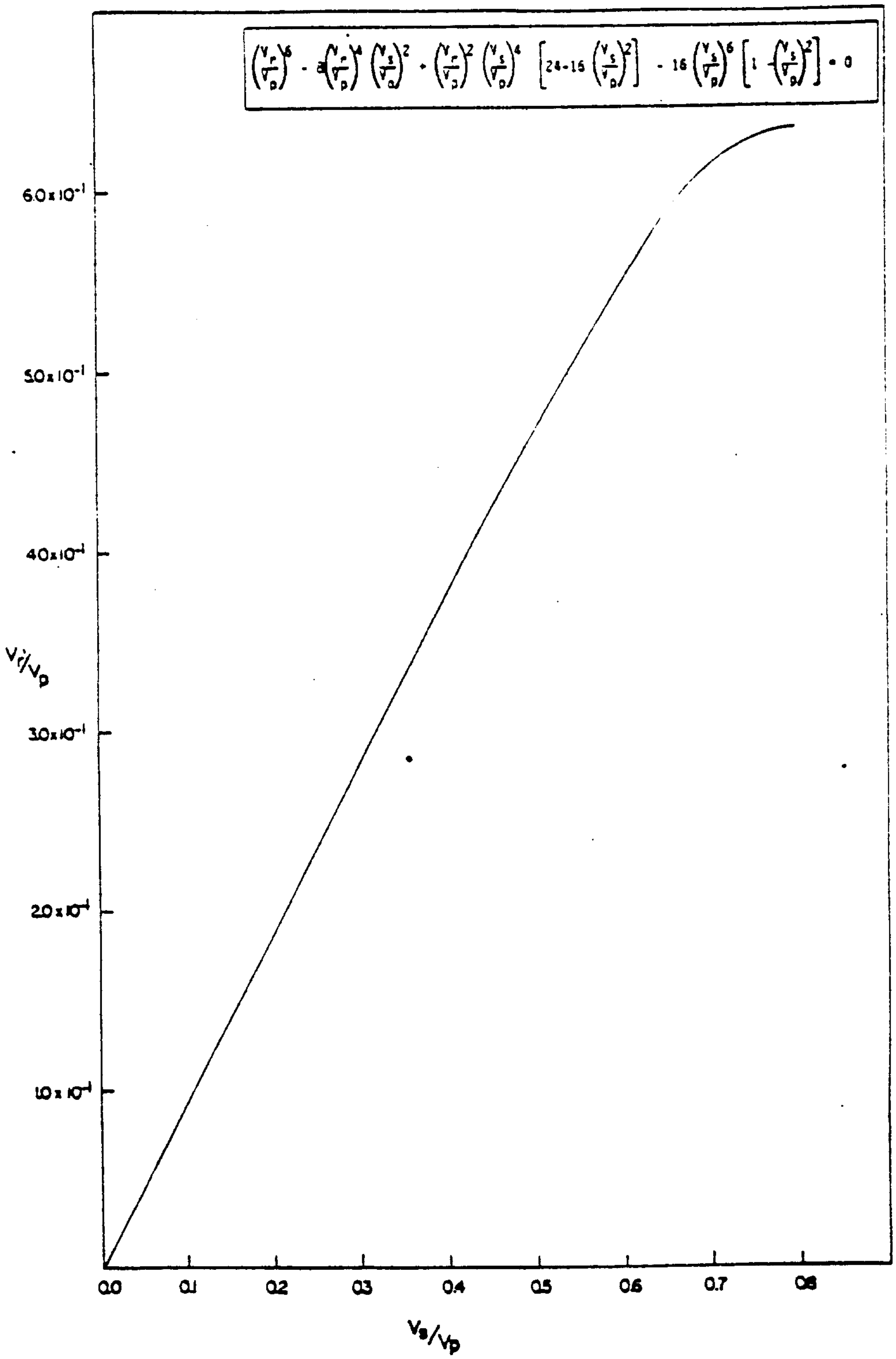


Figure 6. Plot of ratio of the Rayleigh wave ($V_r$) velocity to the p-wave ($V_p$) velocity as a function of the ratio of the s-wave ($V_s$) velocity to the p-wave velocity.

TABLE III

P-wave, Rayleigh wave, and calculated s-wave taking the log s-wave data as the Rayleigh wave. From a Schlumberger experimental log.

| Depth (ft) | Velocity (ft/sec) | | |
|---|---|---|---|
| | Log $V_p$ | Log $V_r$ | Derived $V_s$ |
| 2880 | 13560 | 7630 | 8330 |
| 2891 | 13320 | 7260 | 7870 |
| 3110 | 12580 | 6800 | 7380 |
| 3365 | 11430 | 6870 | 7640 |
| 3446 | 11300 | 6730 | 7450 |
| 3596 | 13380 | 6900 | 7710 |
| 3675 | 13400 | 7510 | 8200 |
| 3910 | 12200 | 6940 | 7611 |
| 4020 | 11490 | 6100 | 6630 |

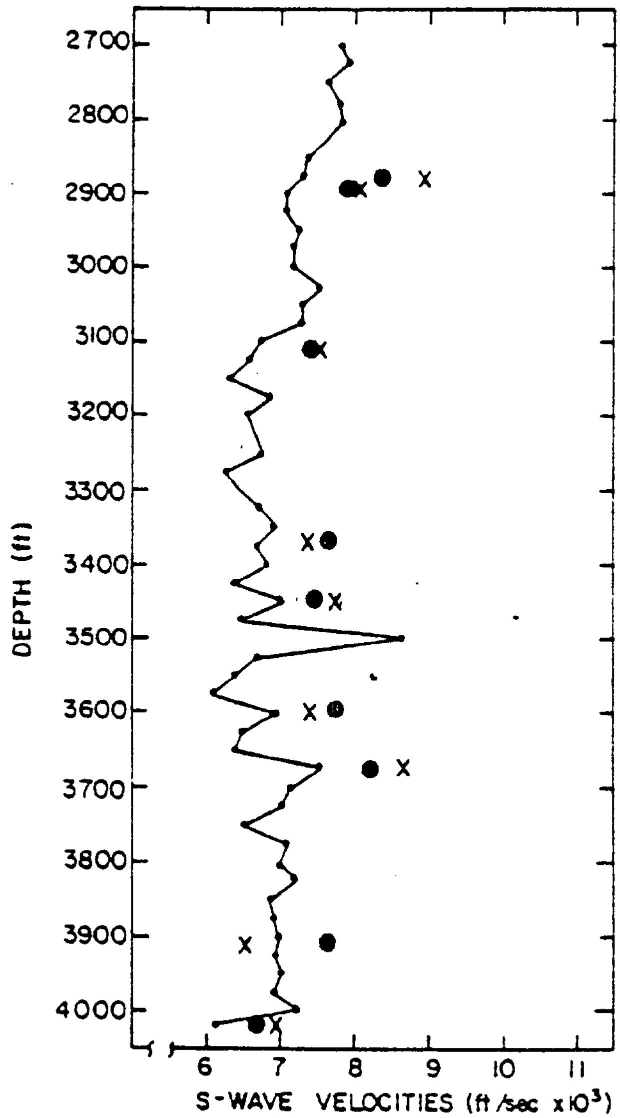


Figure 7. Comparison of log data, laboratory data (x) and calculated s-wave velocities from log data (•), assuming that the log detected the Rayleigh surface wave.

capabilities and limitations of a sonic logging tool as an elastic properties tool. Another project is presently under way to make similar comparisons on a well with considerably different lithology, in the Rocky Mountain area.

## ACKNOWLEDGMENTS

This work was done by Terra Tek, Inc. in conjunction with Columbia Gas System Service Corporation under a U.S. Energy Research and Development Administration contract no. E(46-1)-8016. The authors wish to acknowledge the cooperation received from Dr. D. Rader, Schlumberger-Doll Research, who first pointed out the possibility of the logs detecting the Rayleigh wave. Appreciation is also expressed for the support received by Dr. A. Abou-Sayed, H. Morales, and K. Bradshaw of Terra Tek, Inc.

## REFERENCES

Brechtel, C., et al., "Second Progress Report, Columbia Gas System Service Corporation, Prime Contract No. E(46-1)-8016 ," Terra Tek Report TR 76-36, July 1976.

Fung, Y. C., Foundations of Solid Mechanics, Prentice-Hall Inc., Englewood Cliffs, New Jersey, Chap. 7, p. 180, 1965.

Mattaboni, P., Schreiber, E., "Methods of Pulse Transmission Measurements for Determining Sound Velocities," Journal of Geophysical Research, Vol. 70, No. 20, pp. 5160-5163, 1967.

Timur, A., "Temperature Dependence of Compressional and Shear Wave Velocities in Rocks," Transactions of the SPWLA Seventeenth Annual Logging Symposium, June 1976.

## APPENDIX A-1

### ELASTIC MODULI FROM THE THEORY OF ELASTICITY FOR HOMOGENEOUS, ISOTROPIC SOLIDS

The elastic moduli and Poisson's ratio are obtained from the longitudinal velocity ($V_p$), shear velocity ($V_s$) and density ($\rho$) of homogeneous, isotropic solids as follows:

$$\text{Poisson's Ratio, } \nu = \frac{V_p^2 - 2V_s^2}{2(V_p^2 - V_s^2)} ,$$

$$\text{Shear Modulus, } G = \rho\, V_s^2 ,$$

$$\text{Young's Modulus, } E = 3G \left[ \frac{V_p^2 - 4/3\, V_s^2}{V_p^2 - V_s^2} \right] ,$$

$$\text{Bulk Modulus, } K = \rho(V_p^2 - 4/3\, V_s^2) .$$

# APPENDIX B

# COMPARISON OF LABORATORY AND LOG DATA

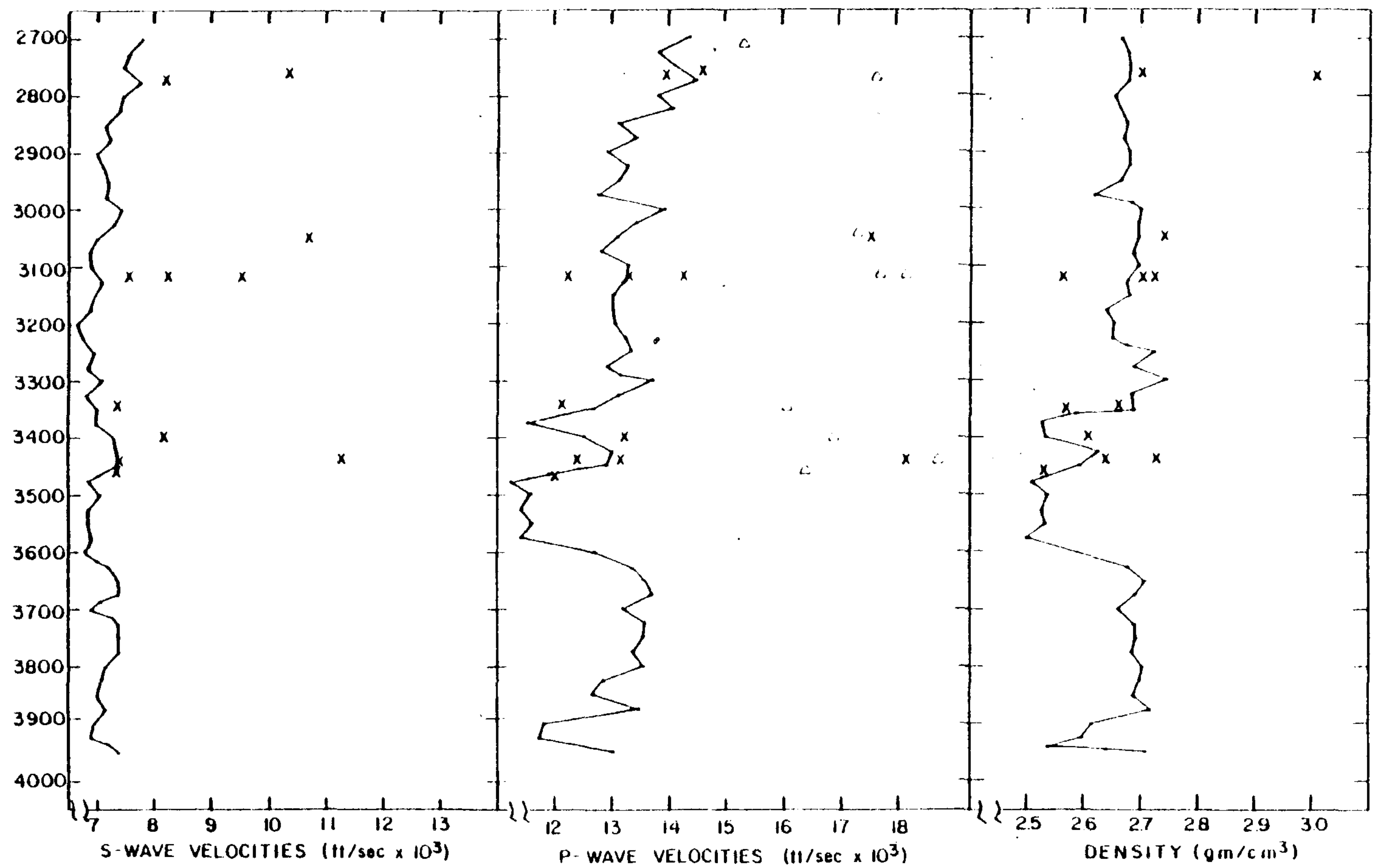


Figure B-1. Comparison of laboratory data with data from the Birdwell (3-D) log on Columbia Gas System Service Corp., well #20402 ("Δ" signifies velocity measurement made in a plane perpendicular to the borehole).

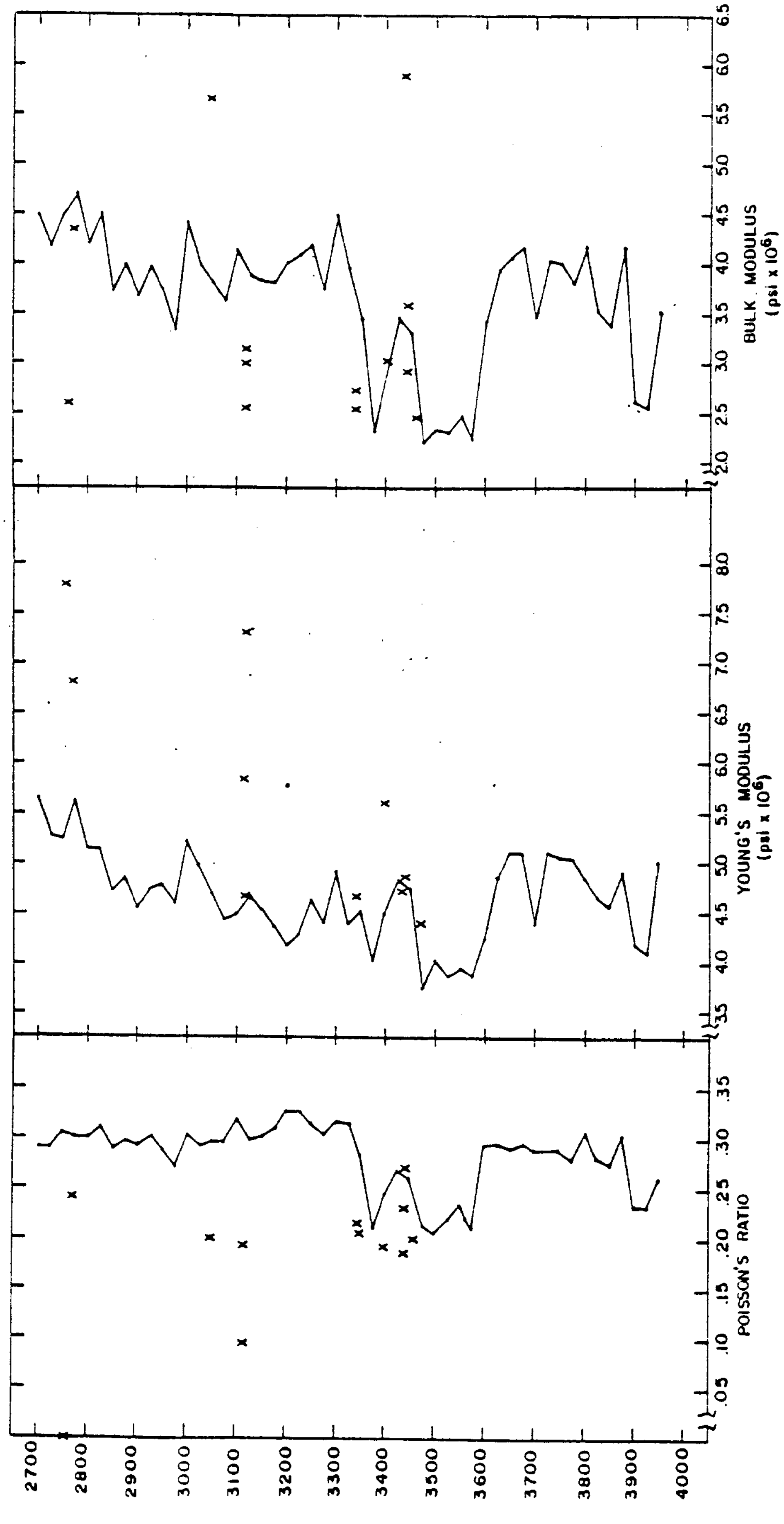


Figure B-2 Comparison of elastic properties obtained from laboratory and Birdwell (3-D) log data on Columbia Gas System Service Corp., well #20402.

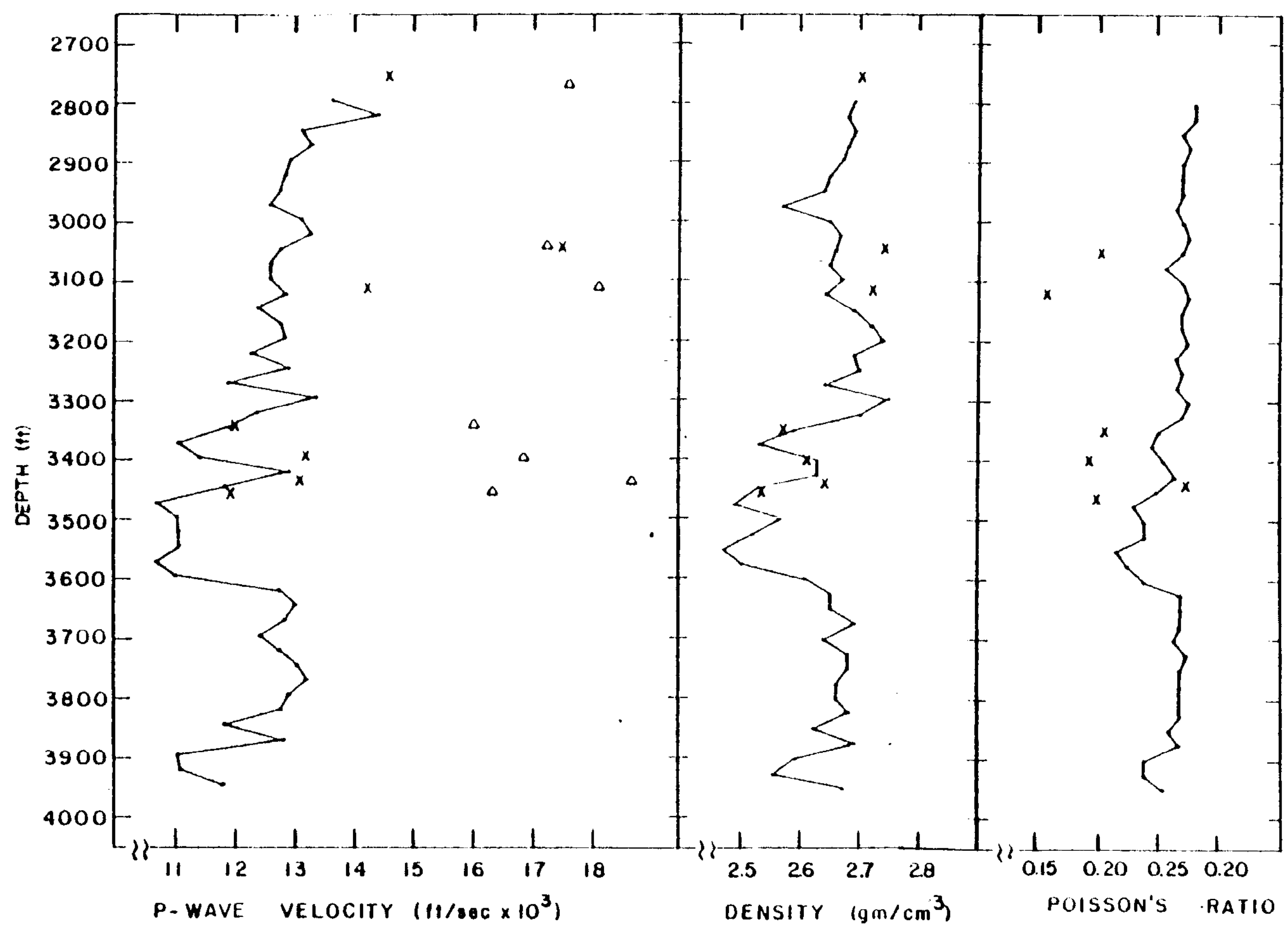


Figure B-3 Comparison of laboratory data with data from Schlumberger logs on Columbia Gas System Service Corp., well #20402. ("Δ" signifies velocity measurements made in a plane perpendicular to the borehole).

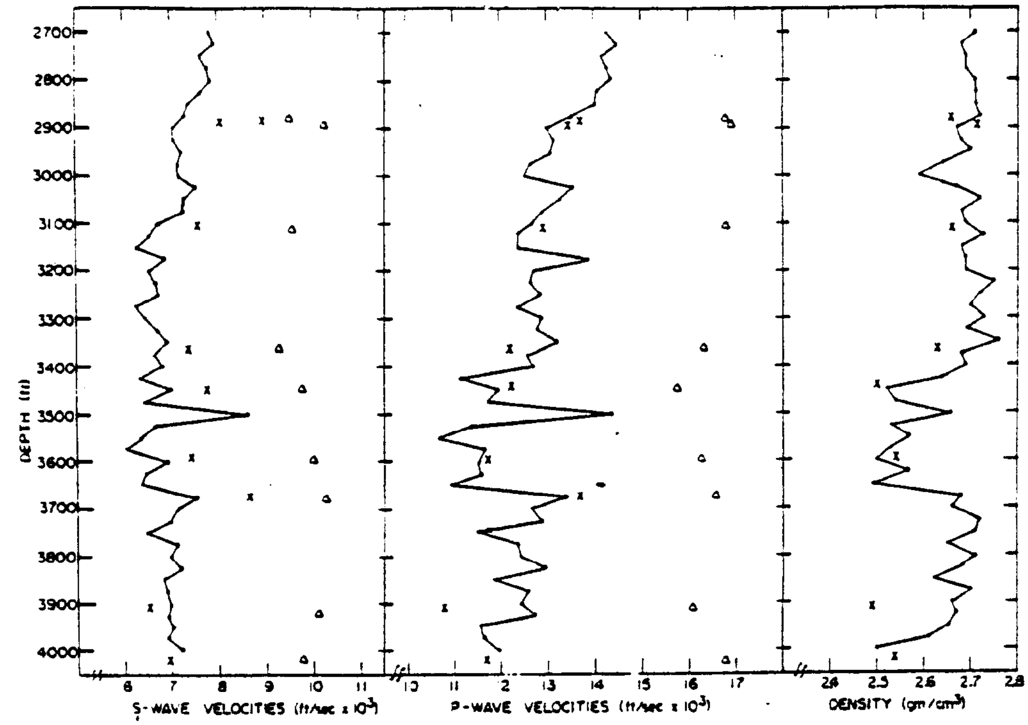


Figure B-4 Comparison of laboratory data (Terra Tek, Inc.) with data from a Schlumberger experimental s-wave logging tool on Columbia Gas System Service Corporation, well #20403. "X" indicates sample orientation parallel to borehole, "Δ" - perpendicular.

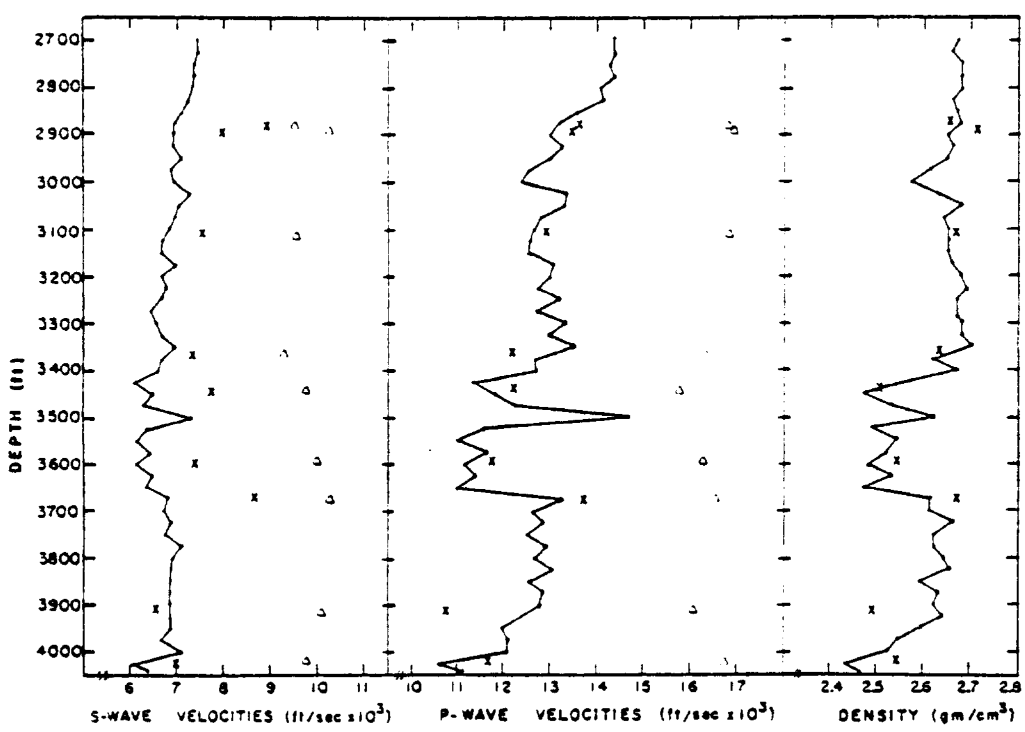


Figure B-5 Comparison of laboratory data (Terra Tek, Inc.) with data from the Birdwell (3-D) log on Columbia Gas System Service Corporation, well #20403. "X" indicates sample orientation parallel to borehole, "Δ" - perpendicular.

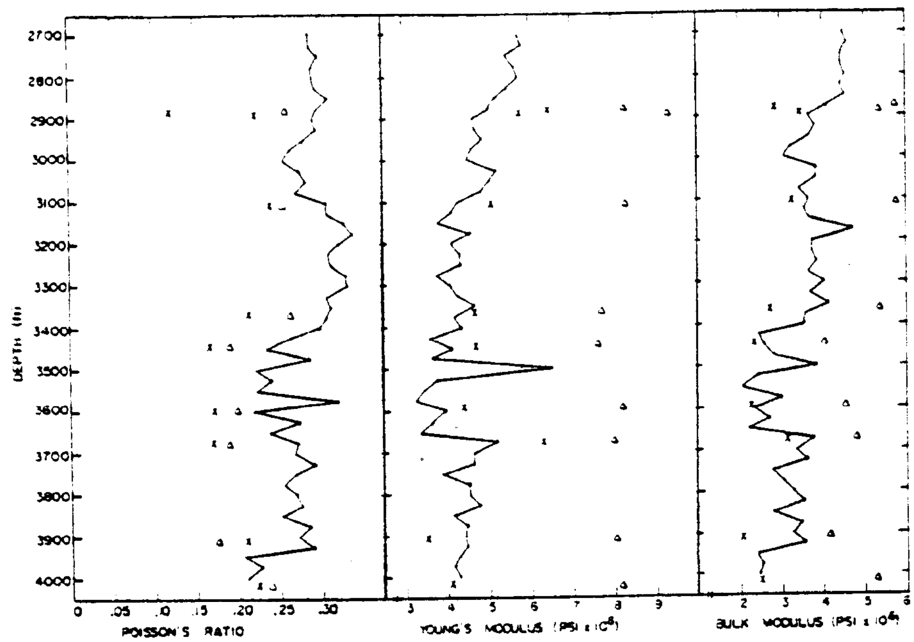

Figure B-6 Comparison of elastic properties derived from laboratory and log (Schlumberger) measurements on Columbia Gas System Service Corporation, well #20403. "X" indicates that the values were calculated from measurements on samples oriented parallel to the borehole, "Δ" - perpendicular.

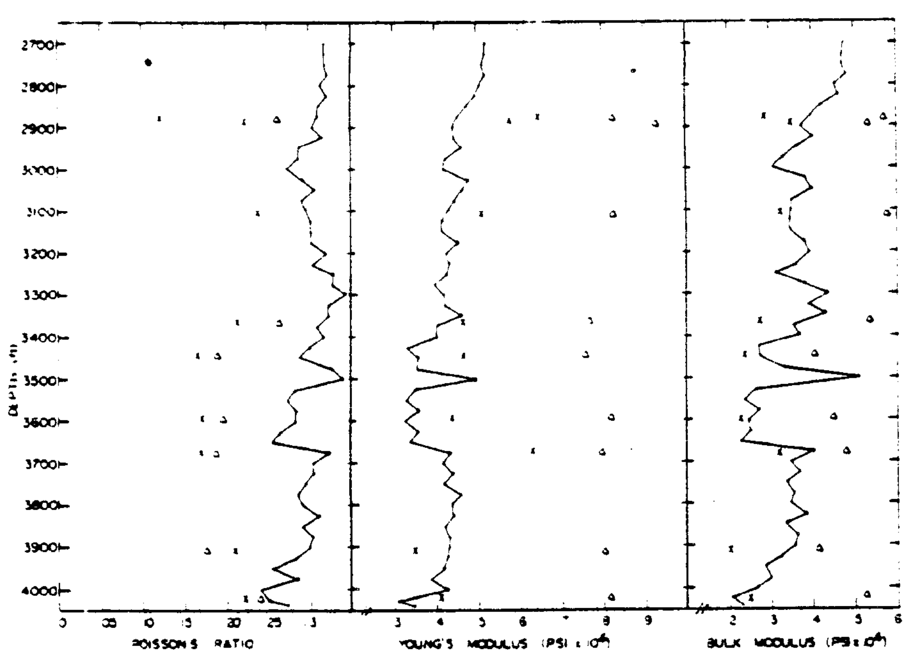

Figure B-7 Comparison of elastic properties calculated from laboratory measurements and data from the Birdwell (3-D) log on Columbia Gas System Service Corporation, well #20403. "X" indicates that the laboratory measurements were made on samples oriented parallel to the borehole, "Δ" - perpendicular.

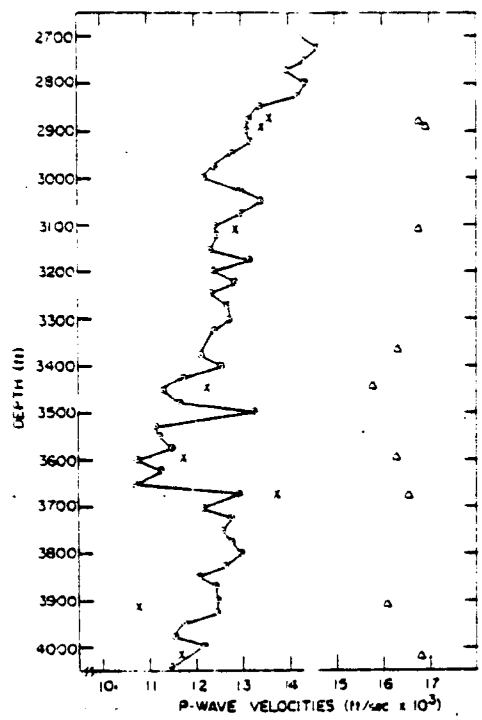


Figure B-8 Comparison of laboratory data with borehole compensated sonic log (Schlumberger) on Columbia Gas System Service Corporation, well #20403. "X" indicates samples oriented parallel to borehole, "Δ" - perpendicular

# APPENDIX C

# METHOD FOR DETERMINING THE PERMEABILITY OF ROCK SAMPLES

Permeability can be measured or estimated by any one of several different methods. Typical laboratory determinations of permeability, however, are usually made using one of the following two techniques:

1. The constant flow or steady-state method which uses a flow meter or positive displacement pump to measure or control the flow rate through the sample. This method requires the flow rate through the material and the pressure drop across the material to be constant at the time of measurement.
2. The transient method imposes a step increase in pressure in a known volume across a sample. The permeability can be calculated from the time-dependent decay of this imposed pressure step.

Each method has advantages and disadvantages over the other depending on the conditions required for the test and the permeability of the sample in question. The first method is generally used for porous media having permeabilities greater than 100 μdarcies, while the second method is more adaptable to low porosity materials such as tight sandstones where the permeabilities are in the tens of microdarcies or lower.

A sketch of a typical test set-up using the transient method for measuring permeability is shown in Figure C1. The sample is placed in a pressure vessel and the pore-pressure inlet and outlet lines are connected to external fittings through the base plug. With this geometry, the sample can be subjected to hydrostatic loading or triaxial compression prior to testing. Pore pressure in the sample can be set at any value less than the confining pressure.

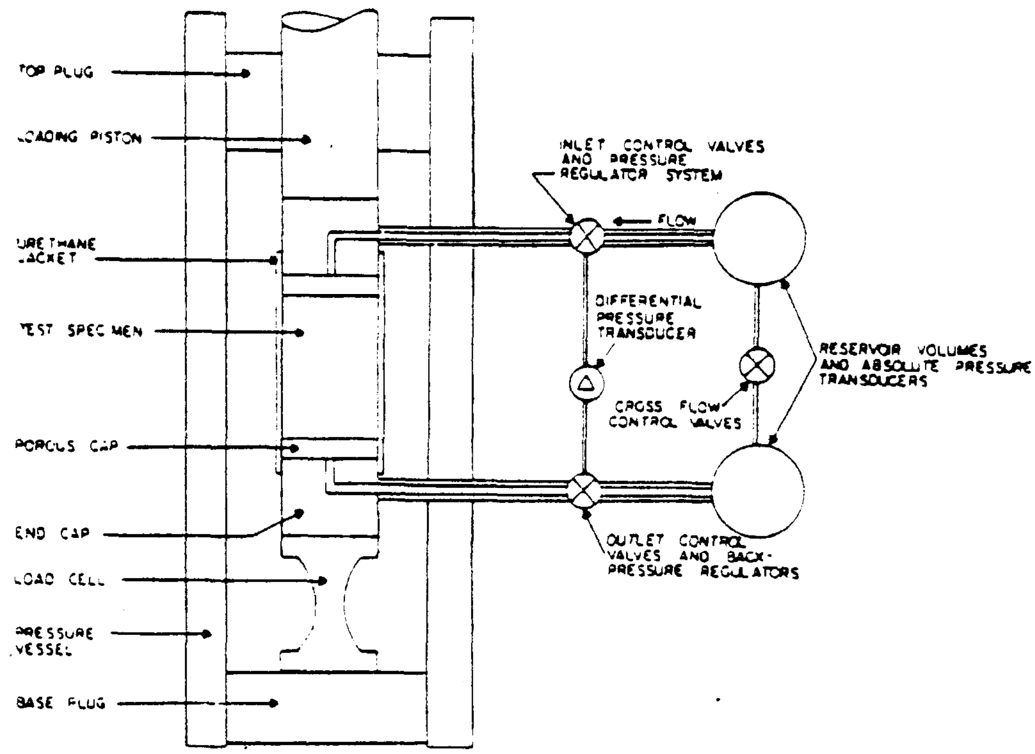


Figure C1. Schematic drawing of the test apparatus used to measure permeability.

Figure C2 illustrates the volumes of fluids on either side of the sample that can be hydraulically connected to allow the pore pressure to equalize. When the sample has reached equilibrium, the volumes are disconnected by closing a valve. The pressure in volume one is then raised slightly. This pressure step should be limited to a small percentage (less than 5 percent) of the absolute pressure in the reservoir volumes. The pressure step decay is monitored accurately through the use of a differential pressure transducer. Variations of sample length and volume of the reservoirs can be changed to allow the test to be completed in a convenient length of time. A brief outline of the theory involved in measuring permeabilities using the transient technique is given below. A detailed treatment of this analysis is presented by Brace, *et al.*, (1968).

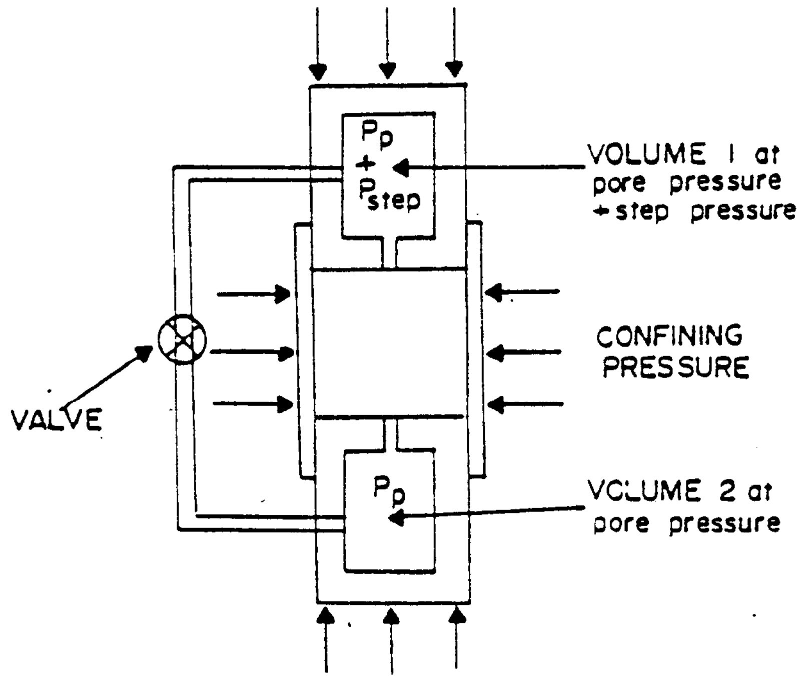


Figure C2. Schematic drawing of a permeability test using the transient technique.

The equation for compressible flow in a compressible media is

$$\nabla^2 p = \frac{\mu \beta}{k} C \frac{\partial P}{\partial t} \quad (1)$$

Where

$\mu$ = fluid viscosity

$\beta$ = fluid compressibility

k = permeabiltiy

C = a term which includes the compressibility of the rock matrix

and

p = pressure

Equation (1) can be solved under the following assumptions concerning fluid flow characteristics:

1. Darcy's law is valid.
2. The fluid flow is laminar.
3. The change in fluid volume in the pores of the rock due to the step pressure change is negligible compared to the amount of fluid flowing through the sample during a test.
4. The pressure step is small compared to the absolute pore pressure so that the physical constants of the fluid (viscosity and compressibility) can be considered constant in all parts of the sample.

Under these conditions the solution to Equation (1) is given by

$$\Delta P = \overline{\Delta P} \frac{V_2}{V_1+V_2} e^{-\alpha t} \tag{2}$$

where

$\overline{\Delta P}$ = Initial pressure step

$\Delta P$ = (Instantaneous pressure) - (Final pressure), i.e., $(P-P_f)$

$V$ = Volume of reservoir at either end of the sample

The permeability k is given by the equation as

$$k = \frac{\alpha \beta \mu \ell}{A(1/V_1 - 1/V_2)} \tag{3}$$

where

$\alpha$ = the slope of the semilog of the natural log of the decaying pressure versus time (as defined in Equation 2)

$\ell$ = the sample length

$A$ = the sample area

Thus, the permeability can be accurately determined for very tight samples with no direct measurement of the flow rate. Another major advantage is the capability for making permeability measurements at high pore pressures.

# APPENDIX D

# FLOW CAPACITY MEASUREMENTS

The flow capacity is reported rather than the permeability because the fracture width is generally not known in the tests.

The flow capacity of the fracture is determined from the equation

$$kw = \frac{2000\ Q_o p_o L\mu}{(p_i^2 - p_o^2)\ h} \quad [\text{md-cm}]$$

where

$k$ = Permeability (millidarcy's)

$Q_o$ = Flow Rate of Outlet Air ($cm^3$/sec)

$p_o$ = Outlet Pressure (Atm absolute)

$p_i$ = Inlet Pressure (Atm absolute)

$\mu$ = Viscosity (centipoises)

$L$ = Length of Sample (cm)

$w$ = Width of Fracture (cm)

$h$ = Height of Fracture (cm).

In the test nitrogen flows in an d out of the pressure vessel through small lines with resulting pressure losses; therefore, a second set of lines were used to sense gas pressures at the ends of the samples. In this way, and for steady state flow, pressures were measured directly and no corrections are needed for line losses. The volume of gas flowed were measured at atmospheric pressure at the end of small flow lines leading from the pressure vessel. The volumetric flow at the outlet end of the sample was determined by making the pressure correction between the flow meter atmospheric pressure and the sample outlet pressure assuming isothermal flow. Figure D1 is a schematic diagram of the experimental set-up.

For the unpropped sample the flow was low enough to be within the measurement range of the equipment used in the transient method, so several tests were made by this technique to cross-check the steady state technique. This data is also given in Table DI and plotted in Figure D2.

After completion of the unpropped flow tests, the sample faces were viewed under a low-power (3x) stereo microscope. The contact points were essentially a discoloration of the surface with little or no visible crushing or deformation. The observations indicate that the points of contact were highly non-uniform. Over a large portion of the faces, perhaps only 5 to 15 percent of the area was marked. In some spots perhaps 60 to 80 percent of the surface was marked. Figure D3 is a photograph of the sample. No attempt was made to quantitatively measure either the surface roughness or the fraction of the surfaces that appeared to make contact when the two halves were fitted back together for the test.

A rough estimate of the efefctive width of the flow channels in the unpropped fracture can be made assuming equivalent permeability for flow between parallel plates (Craft and Hawkins, 1959).

$$k[\text{darcys}] = 54 \times 10^6\ w^2\ [\text{inches}^2]$$

This relationship needs to be modified to account for the rough surface and contact points that hold the crack open. One possible modification might be adapted from Carmen (1970) to give

$$k = \frac{8.38 \times 10^6\ w^2\ \emptyset^3}{T(1 - \emptyset^2)}$$

where

k = permeability in millidarcies

$\emptyset$ = fraction of surface open to flow

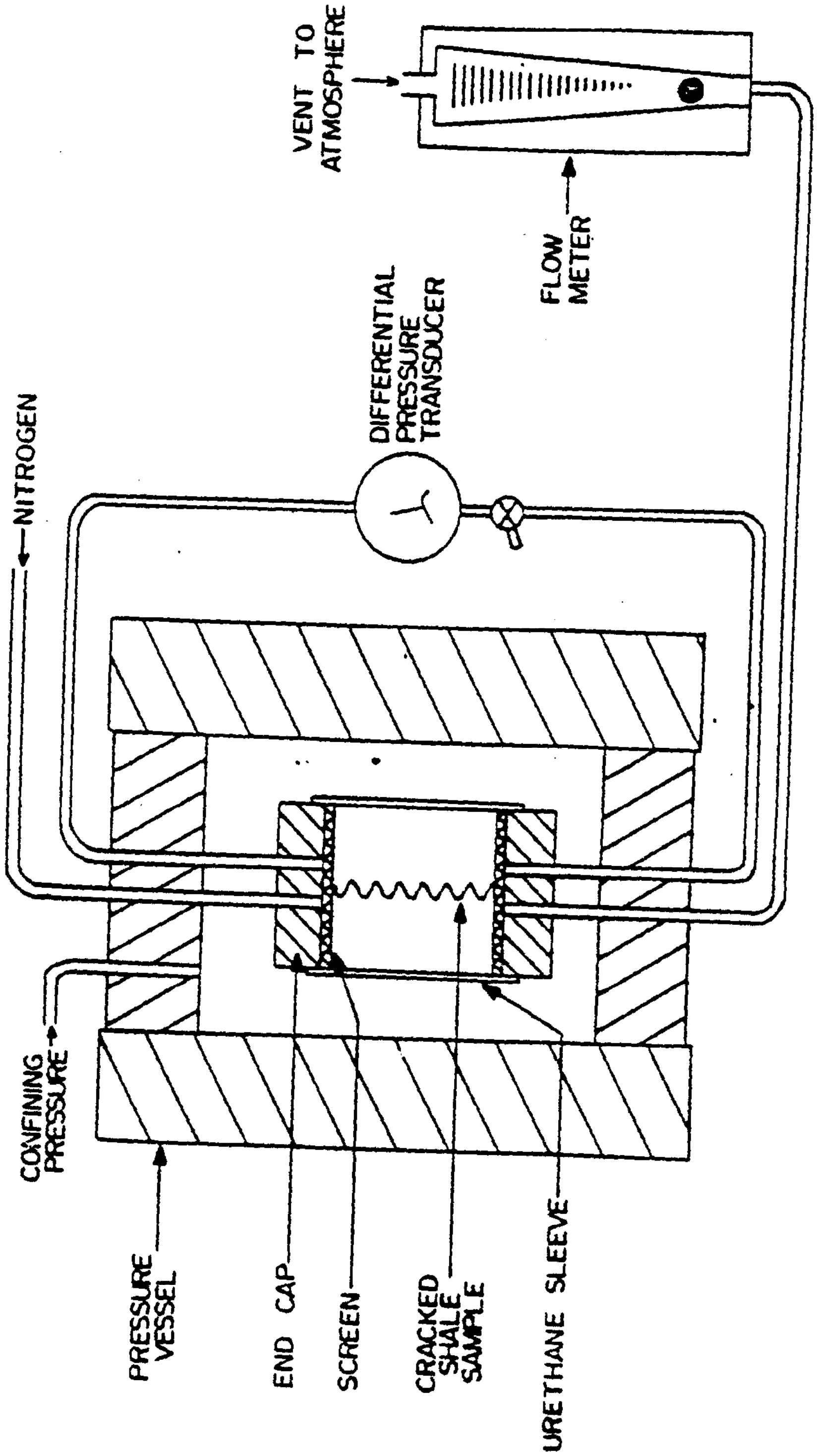


Figure D1. Schematic design of flow test set-up

TABLE DI

Data for Flow Through Unpropped Fracture in Shale*

| Confining psi | Q ml/sec | $P_i$ atm | $P_o$ atm | $1/\bar{P}$ | kw md-cm |
|---|---|---|---|---|---|
| **First Steady State Test** | | | | | |
| 100 | 19.7 | 3.034 | 3.009 | .165 | 9900 |
| 1000 | 17.0 | 9.1 | 8.4 | .057 | 300 |
| 2000 | 41.1 | 10.66 | 1.44 | .083 | 13.5 |
| 2900 | 13.8 | 20.5 | 4.27 | .040 | 3.8 |
| 4000 | 17.3 | 24.9 | 1.36 | .038 | .97 |
| **Transient test** | | | | | |
| 2900 | | | | | 7.1 |
| 4000 | | | | | 3.4 |
| 4000 | | | | | 2.6 |
| **Second Steady State Test** | | | | | |
| 100 | 1.33 | .8574 | .8571 | 1.166 | 56,500 |
| | 4.38 | .8660 | " | 1.161 | 6,240 |
| | 7.08 | .8728 | " | 1.156 | 5,690 |
| | 20.58 | .9027 | " | 1.137 | 5,600 |
| | 15.0 | .8837 | " | 1.149 | 7,020 |
| | 79.2 | 1.0415 | " | 1.053 | 4,940 |
| | 170.0 | 1.3476 | " | 1.907 | 3,430 |
| 1000 | 1.75 | .9150 | .8571 | 1.129 | 370 |
| | 4.55 | .8769 | " | 1.153 | 2,890 |
| | 7.17 | 1.1782 | " | .983 | 240 |
| | 15.33 | 1.4837 | " | .854 | 228 |
| | 11.25 | 1.2701 | " | .940 | 280 |
| | 18.17 | 1.5707 | " | .824 | 229 |
| 2000 | 1.5 | 1.0687 | .8571 | 1.039 | 80.4 |
| | 4.48 | 1.5401 | " | .834 | 59.3 |
| | 3.75 | 1.5095 | " | .845 | 53.0 |
| 4000 | .65 | 1.2293 | .8571 | .959 | 18.3 |
| | 1.92 | 1.5912 | " | .817 | 23.3 |
| | 4.33 | 3.1755 | " | .496 | 10.1 |
| | 4.42 | 3.4721 | " | .462 | 8.5 |
| | 16.67 | 7.8231 | " | .230 | 6.0 |
| | 15.00 | 6.7415 | " | .263 | 7.3 |

* Flow with dry nitrogen

$\mu$ = .018 cp

h = 8.25 cm

L = 5.84 cm

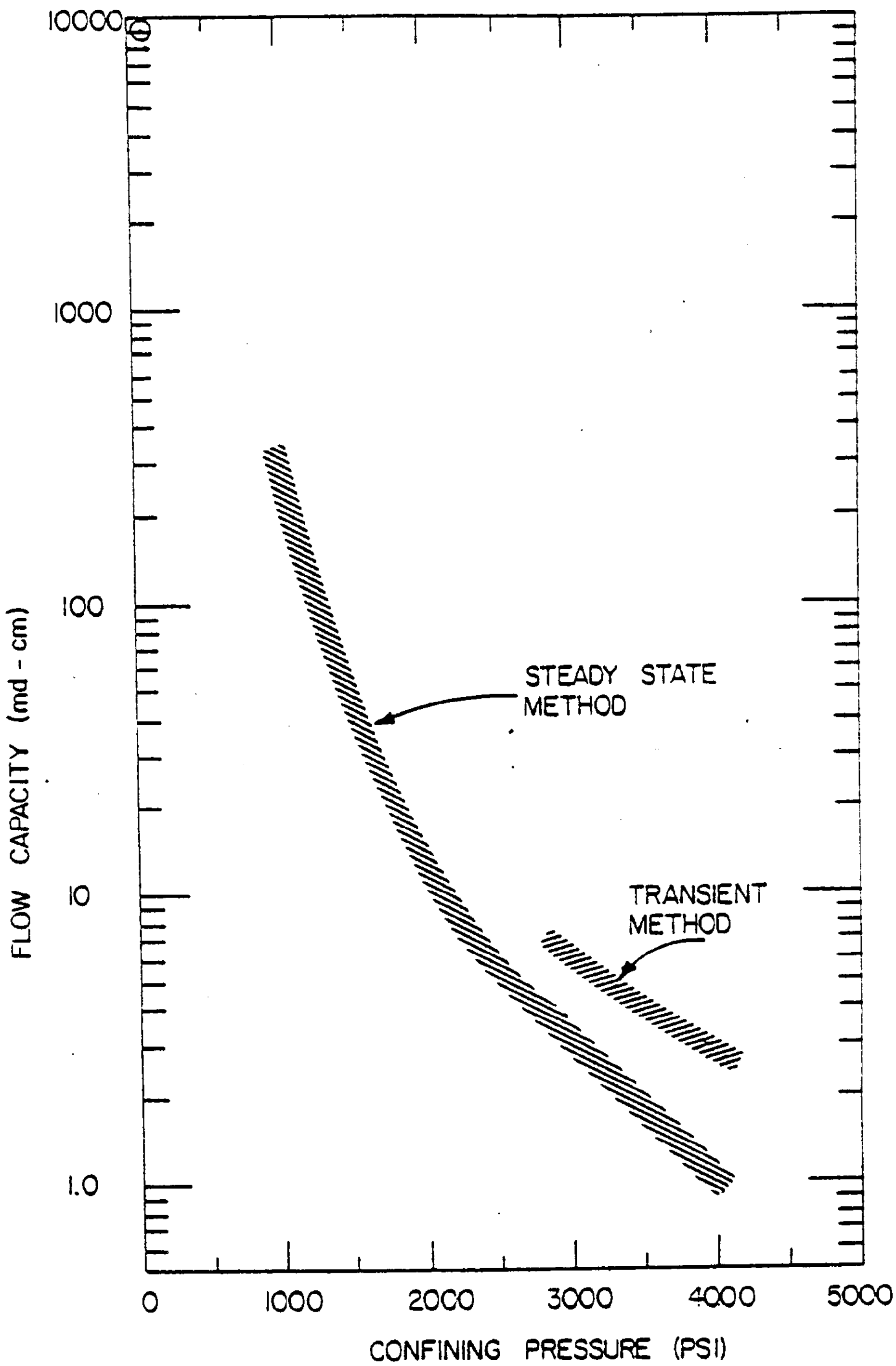


Figure D2. Flow through the unpropped fracture.

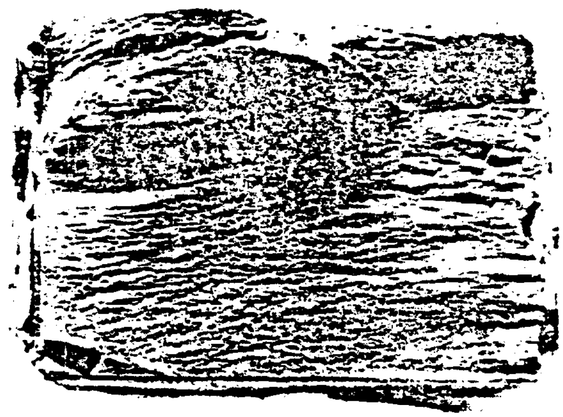

Figure D3. Photograph of test sample

t = tortuosity (actual channel length/straight line)

w = crack width in cm

Multiplying by w and rearranging to solve for w in terms of the flow capacity (kw) gives the equation

$$w \cong \left[\frac{0.12 \times 10^{-6} T \ (1-\emptyset^2) \ kw}{\emptyset^3}\right]^{1/3}$$

It is evident from the data that the flow capacity is significantly dependent on the gas pressure. This is assumed to be the Klinkenberg effect of gas slippage. The pressure-dependent permeability is related to the absolute permeability by the Klinkenberg equation

$$k = k_o \left(1 + b/\overline{P}\right)$$

where

$k_o$ = absolute permeability

$\overline{P}$ = mean pressure in sample

$b$ = Klinkenberg constant

In a plot of kw versus $1/\overline{P}$, the intercept is the absolute flow capacity $k_o w$ and the slope of the line is equal to $k_o wb$ with $\overline{P} = (P_i + P_o)/2$ and the absolute flow capacity is given by

$$k_o w = \frac{2000\ Q_o \mu L}{(P_i + P_o + 2b)\ (P_i - P_o)h}$$

Open File No. 199
Volume 2 - Appendices

# TERRA TEK REPORT

## FRACTURE FLOW CAPACITY OF HYDRAULICALLY FRACTURED DEVONIAN SHALES

# FRACTURE FLOW CAPACITY OF HYDRAULICALLY FRACTURED DEVONIAN SHALES

By

U. Ahmed
L. Buchholdt
A. S. Abou-Sayed

Submitted to

Columbia Gas System Services Corporation
1600 Dublin Road
Columbia, Ohio 53215

Attention: Eric Smith

Submitted by

Terra Tek, Inc.
University Research Park
420 Wakara Way
Salt Lake City, Utah 84108

TR 78-57
Sept 1978

# ABSTRACT

Flow capacities were determined for induced fractures in cores taken from 3445 feet and 3695 feet in the Columbia Gas System Services Corporation Well #20403, located in Lincoln County, West Virginia. The samples from depth 3445 feet were from the 'Middle Brown Shale' and from depth 3695 feet the 'Lower Gray Shale,'. The work was aimed at assessing flow capacity damage potential of a number of water-based fracturing fluids. The fractures were propped with a partial monolayer (0.027 $lb/ft^2$) of 20/40 mesh sand.

At conditions simulating *in situ* closure stress (2700 psi) and temperature (70°F), the 'Middle Brown Shale' fracture flow capacity was reduced to 5 percent of the original flow capacity. For the 'Lower Gray Shale' (the *in situ* closure stress of 2900 psi, temperature 70°F) the reduced flow capacity was close to one percent of the original. In both shales the decrease in flow capacity resulted from sand embedment initiated by fracturing fluid softening of the rock as well as clay flocculation around the imbedded sand.

# TABLE OF CONTENTS

## LIST OF FIGURES

## LIST OF TABLES

# INTRODUCTION

Degradation of matrix and fracture permeability due to the application of hydraulic fracturing fluid has been presented as one reason for the failure of massive hydraulic fractures (Davis, 1974; Clark, 1977). The selection of a fracturing fluid is not only dependent upon the fluids effectiveness in creating the fracture and transporting the proppants; it is also dependent on the degree of formation damage and plugging. In a recent study (Holditch, 1978) the overall productivity decrease in gas production from the combined effects of reservoir damage, relative permeability damage, capillary pressure damage and fracture conductivity damage were investigated. Reduction in fracture conductivity had significant effect on productivity. Thus, the necessity of experimentally determining the damaging effect of fracturing fluid to the flow capacity of the specific formation.

## EXPERIMENTAL PROCEDURE

Core samples taken from Columbia Gas System Services Corporation Well #20403 at depths of 3445 feet and 3695 feet were used in this investigation. The samples for the 3445 feet depth were from the 'Middle Brown Shale' and 3695 feet depth from the 'Lower Gray Shale'. The work was aimed at assessing flow capacity damage of a number of water-based fracturing fluids to fractures propped with a partial monolayer of 20/40 mesh sand.

The core samples were saw cut and propped with a sand concentration of 0.027 $lb/ft^2$. Initially the cores were subjected to confining pressure of 90 psi for the proppants to settle in place. By flowing dry nitrogen gas through the propped channel, flow capacity measurements were taken. The change in flow capacity with effective pressure was determined by varying the confining pressure from 500 psi to 3500 psi; in all cases gas pressure within the fracture was maintained at 300 psi. Cantilevers were placed on the outer core surface to monitor changes in fracture width closure. Fracturing fluid was subsequently flowed through the propped fracture for four hours (to simulate field fracturing time) and the change in flow capacity with effective pressure was determined for the same confining pressure range.

The constituents of the fracturing fluids and the test conditions are presented in Table 1 and 2 respectively. All fracturing fluids were supplied by Dowell. Besides the fracturing fluids saturated nitrogen was flowed through the propped fracture to assess the fracture flow damage from water alone. After each sequence of tests the fractures were examined with an optical microscope to assess the degree of sand embedment, sand crushing, and clay flocculation in the fracture.

TABLE 1

FRACTURING FLUIDS

| SYSTEM | CONSTITUENTS |
|---|---|
| 1. Waterfrac 20-40 | 20-40 #J266/1000 gal + 1 gal F75N/1000 gal w/fresh water |
| 2. Waterfrac 20 W/$CO_2$ | 20 #J160/1000 gal + 10 gal L42/1000 gal + 1 gal F75N/1000 gal w/fresh water |
| 3. Superfoam | 8 gal W22/1000 gal + 10 gal L42/1000 gal w/fresh water |

TABLE 2

TEST CONDITIONS

| | |
|---|---|
| Confining Pressure | 500 - 3500 psi |
| Fluid Pressure within the Fracture | 300 psi |
| Temperature | 70°F |
| Flowing Fluid | Dry Nitrogen |
| Fracturing Fluid Injection Pressure | 850 psi |

## DISCUSSION OF RESULTS

Discussion of results are presented in light of the type of shales.

*Middle Brown Shale:* Figure 1 and Table 3 illustrate the change in the fracture flow capacity with increasing effective pressure for the virgin sample and after exposure to Waterfrac 20 W/$CO_2$ and saturated nitrogen. Figure 2 and Table 4 show the decreasing trend of the calculated effective fracture width with the increase in effective pressure for the same tests. The gentle slope of the curves for the virgin sample in both Figure 1 and 2 suggests that the fracture closed mainly as a result of proppant embedment. Figure 2 also includes a plot of the fracture width (derived from experimentally measuring the closure width) with effective pressure for the virgin sample and upon being interacted by Waterfrac 20 W/$CO_2$. This provides a qualitative and quantitative comparison between calculated and experimentally measured values.

Upon application of the fracturing fluid there is a marked reduction in fracture conductivity. Waterfrac 20 W/$CO_2$ fracturing fluid decreased the original flow capacity by approximately two orders of magnitude. Saturated nitrogen had an even greater effect on the flow capacity. This clearly explains the effect of water on the fracture surface.

Optical microscopic examination of the fracture face after interaction with Waterfrac 20 W/$CO_2$ is shown in Figure 4. Evidence of deep sand embedment is present with signs of clay flocculation around the proppants.

The following reasons can be accepted as causes for the overall decline in flow capacity due to fracturing fluid application:

TABLE 3

COLUMBIA GAS SYSTEM WELL #20403

MIDDLE BROWN SHALE

3445'

COMPARISON OF FRACTURE FLOW CAPACITY

| Effective Pressure psi | Fracture Flow Capacity md-cm | | |
|---|---|---|---|
| | Before Fracturing Fluid Flow | After Fracturing Fluid Flow | |
| | | Waterfrac 20 W/$CO_2$ | Saturated Nitrogen |
| 200 | 92,000 | 2900 | 875 |
| 500 | 78,000 | 2550 | 850 |
| 1000 | 67,000 | 2150 | 810 |
| 2000 | 44,000 | 1880 | 760 |
| 3000 | 30,500 | 1670 | 730 |
| 3200 | 26,750 | 1650 | 720 |

TABLE 4

COLUMBIA GAS SYSTEM WELL #20403

MIDDLE BROWN SHALE

3445'

COMPARISON OF FRACTURE WIDTH

| Effective Pressure psi | Fracture Width cm | | |
|---|---|---|---|
| | Before Fracturing Fluid Flow | After Fracturing Fluid Flow | |
| | | Waterfrac 20 W/$CO_2$ | Saturated Nitrogen |
| 500 | .0220 | .00720 | .00440 |
| 1000 | .0207 | .00717 | .00420 |
| 2000 | .0190 | .00690 | .00392 |
| 3000 | .0170 | .00670 | .00365 |
| 3200 | .0155 | .00668 | .00360 |

1. The water in the water based fracturing fluids helped the fracture face to soften and result in sand proppant embedment.
2. From Figure 3 we have signs of material clusters only around the proppants and no damage to the surface where there were no proppants. This suggests the fracturing fluid has no chemical action; fracture surface damage beneath proppants indicates clay softening. There is no evidence of clay swelling.
3. Fracture flow capacity decrease is due to proppant embedment.

*Lower Gray Shale:* Figure 4 and Table 5 show the change in the fracture flow capacity with increasing effective pressure for the virgin sample and after exposure to Waterfrac 20-40, superfoam and saturated nitrogen. Figure 5 and Table 6 illustrate the decreasing trend of the calculated effective fracture width with the increase in effective pressure for the same tests. Similar to the 'Middle Brown Shale', Figure 4 and 5 suggest that the fracture of the virgin sample closed mainly as a result of sand proppant embedment. Figure 5 also includes a plot of the fracture width (derived from experimentally measuring the closure width) with effective pressure for the virgin sample and upon being interacted by Waterfrac 20-40.

Upon application of the fracturing fluid there is a marked reduction in fracture conductivity similar to that seen for the 'Middle Brown Shale'. Both the Waterfrac 20-40 and Superfoam decreased the virgin flow capacity by roughly three orders of magnitude. Waterfrac 20-40 causing slightly less damage than Superfoam. Saturated nitrogen decreased the virgin flow capacity between one and two orders of magnitude. This is less than the effect seen for 'Middle Brown Shale'. From two seperate studies, Leventhal (1978) and Mcketta (1978) it has been identified that 'Middle Brown Shale' has a higher

TABLE 5

COLUMBIA GAS SYSTEM WELL #20403

LOWER GRAY SHALE

3695'

COMPARISON OF FRACTURE FLOW CAPACITY

| Effective Pressure psi. | Fracture Flow Capacity md-cm | | | |
|---|---|---|---|---|
| | Before Fracturing Fluid Flow | After Fracturing Fluid Flow | | |
| | | Waterfrac 20-40 | Saturated Nitrogen | Superfoam |
| 200 | 88,000 | 380 | 3950 | 140 |
| 500 | 75,000 | 220 | 3600 | 105 |
| 1000 | 63,000 | 130 | 3200 | 77 |
| 2000 | 41,000 | 98 | 2475 | 52 |
| 3000 | 26,500 | 74 | 1910 | 35 |
| 3200 | 24,750 | 69 | 1800 | 33 |

TABLE 6

COLUMBIA GAS SYSTEM WELL #20403

LOWER GRAY SHALE

3695'

COMPARISON OF FRACTURE WIDTH

| Effective Pressure psi | Fracture width cm | | |
|---|---|---|---|
| | Before Fracturing Fluid Flow | After Fracturing Fluid Flow | |
| | | Waterfrac 20-40 | Superfoam |
| 500 | .0210 | .0036 | .00256 |
| 1000 | .0205 | .0026 | .00227 |
| 2000 | .01805 | .00234 | .00193 |
| 3000 | .0160 | .00210 | .00165 |
| 3200 | .0147 | .00201 | .00161 |

percentage of organic materials and calcium oxide (CaO). Organic material absorbs water and calcium oxide absorbs water by chemically reacting with water in the following manner:

$$CaO + 2H_2O \rightarrow 2Ca(OH)_2$$

This explains why the 'Middle Brown Shale' has a lower flow capacity than 'Lower Gray Shale' upon being interacted by saturated nitrogen.

Optical microscopic examination of the fracture face after interaction with Waterfrac 20-40 and Superfoam are shown in Figure 6 and 7 respectively. Evidence of deep sand proppant embedment is present with signs of clay flocculation around the proppants. Fracture face interacted by Superfoam has more flocculated clay.

Reasons for the reduction of flow capacity in the 'Lower Gray Shale' due to the interaction by the fracturing fluids are the same as for the 'Middle Brown Shale'.

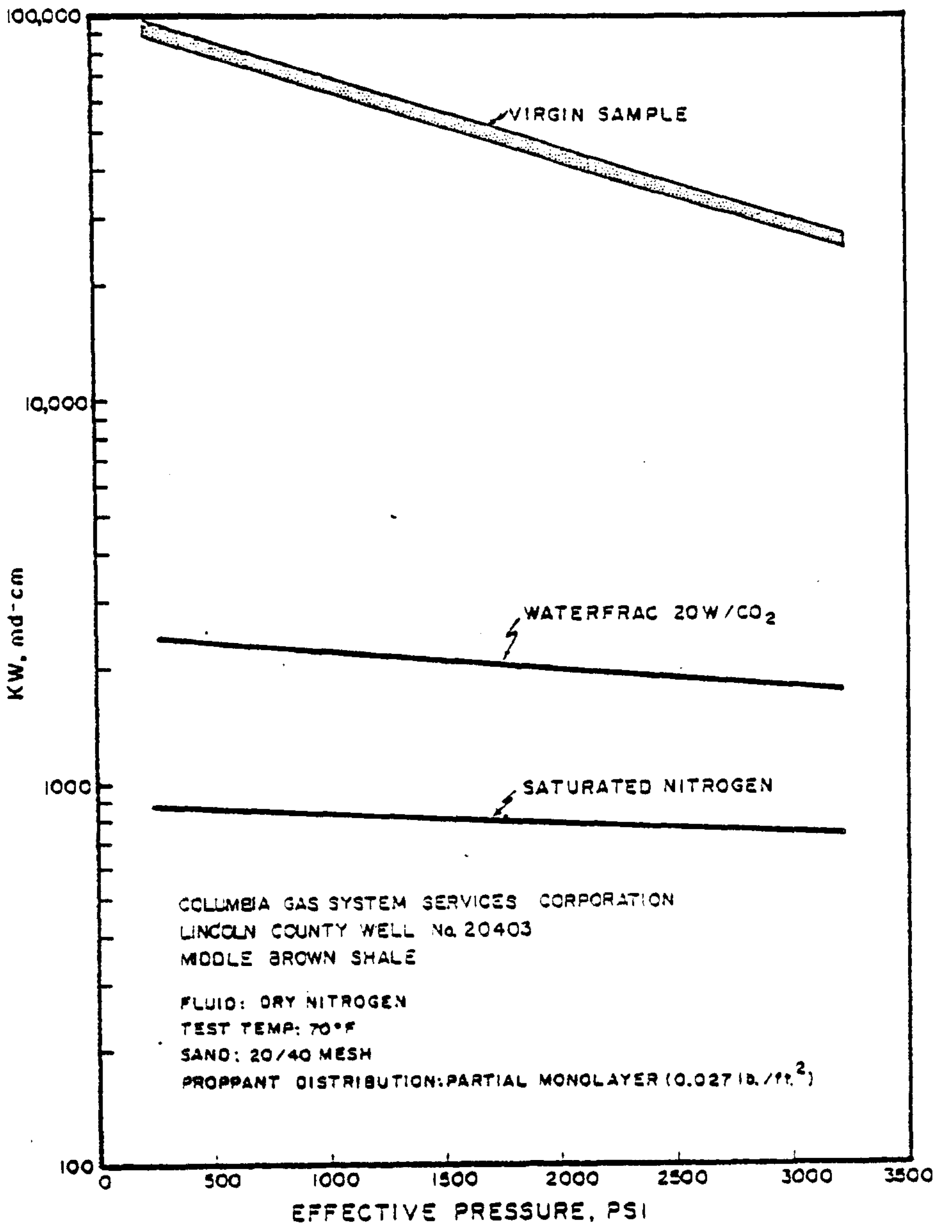


Figure 1. Trend of fracture flow capacity with the increase in effective pressure for 'Middle Brown Shale'.

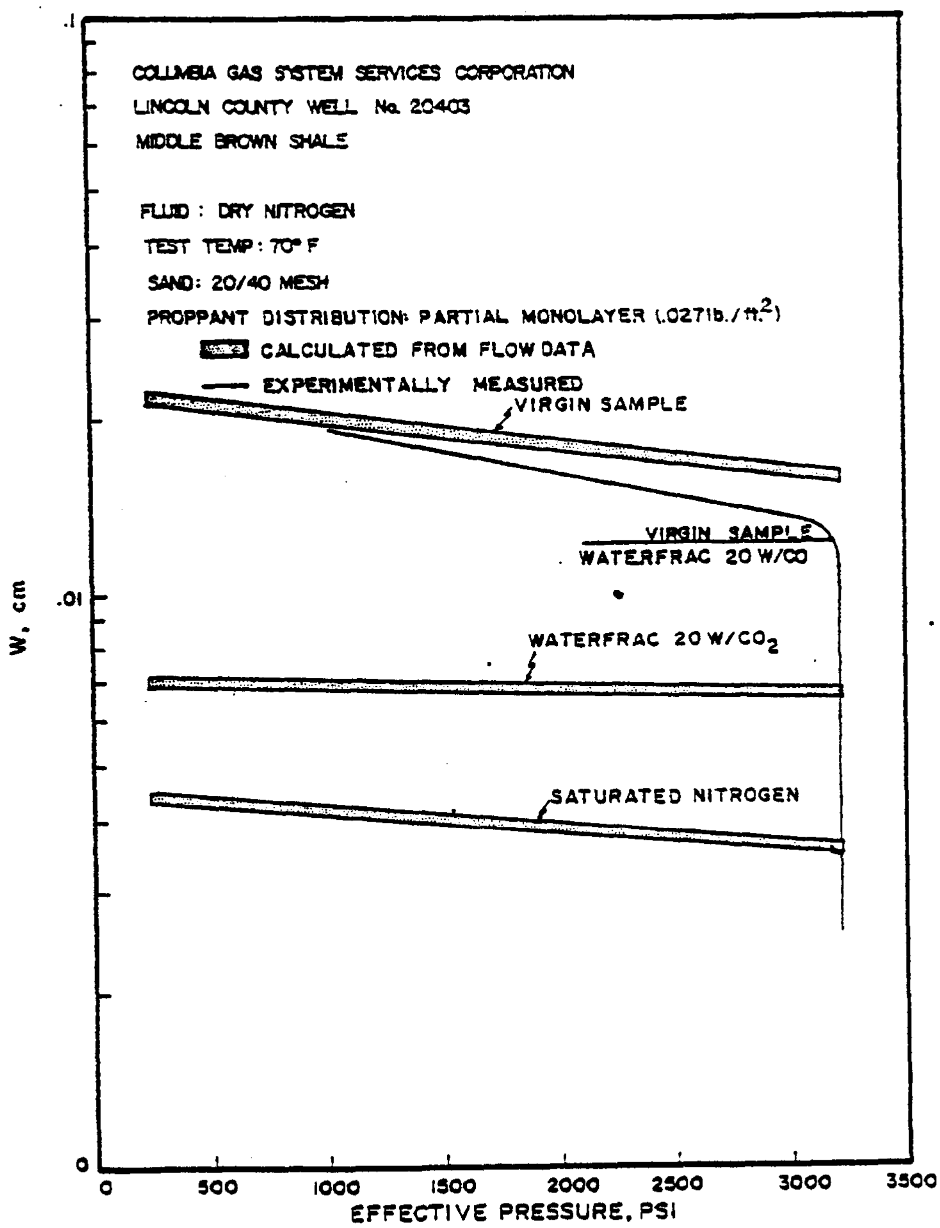


Figure 2. Trend of the effective fracture width with the increase in effective pressure for 'Middle Brown Shale'.

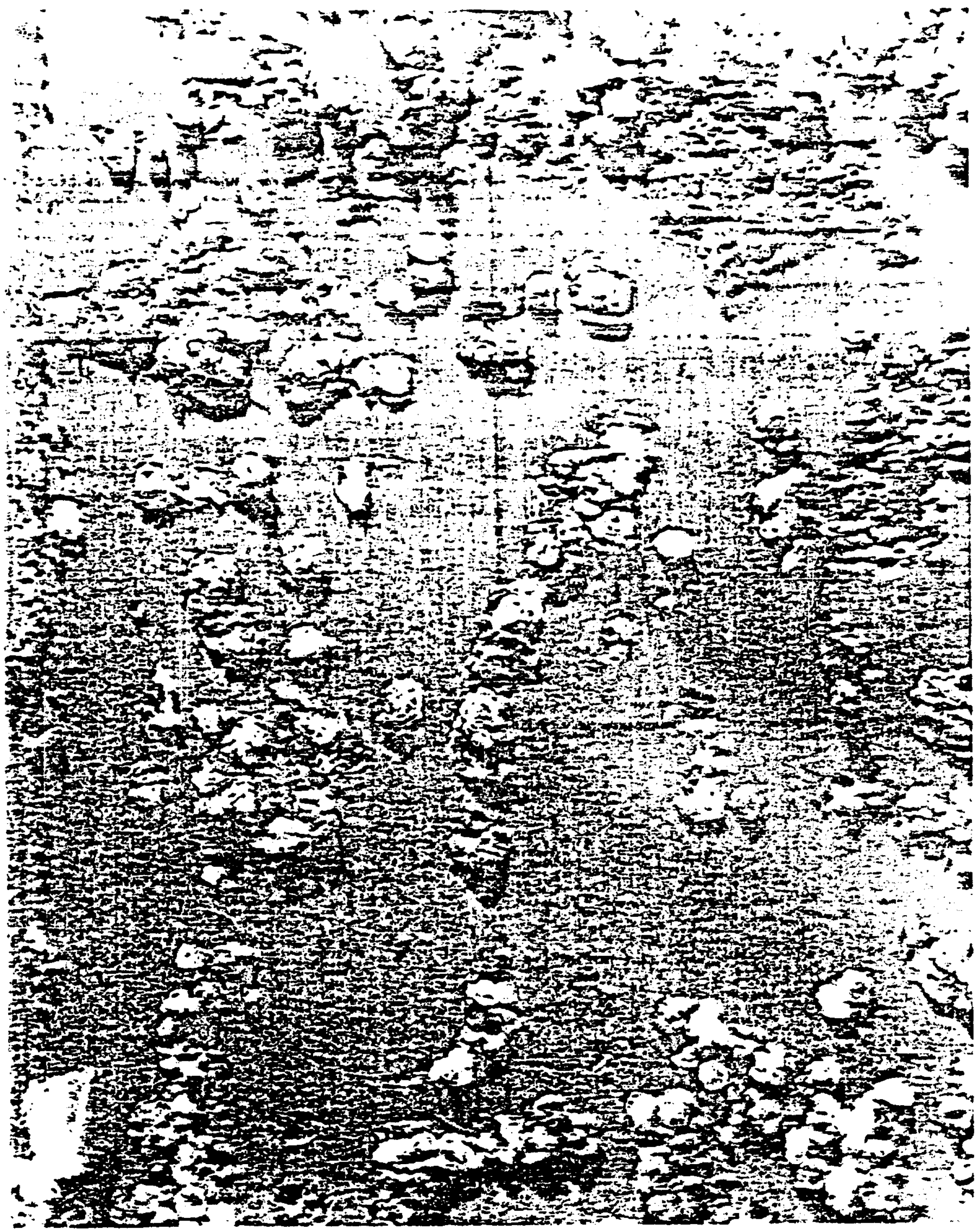

Figure 3. Fracture face of the 'Middle Brown Shale' sample interacted by Waterfrac 20 W/$CO_2$.

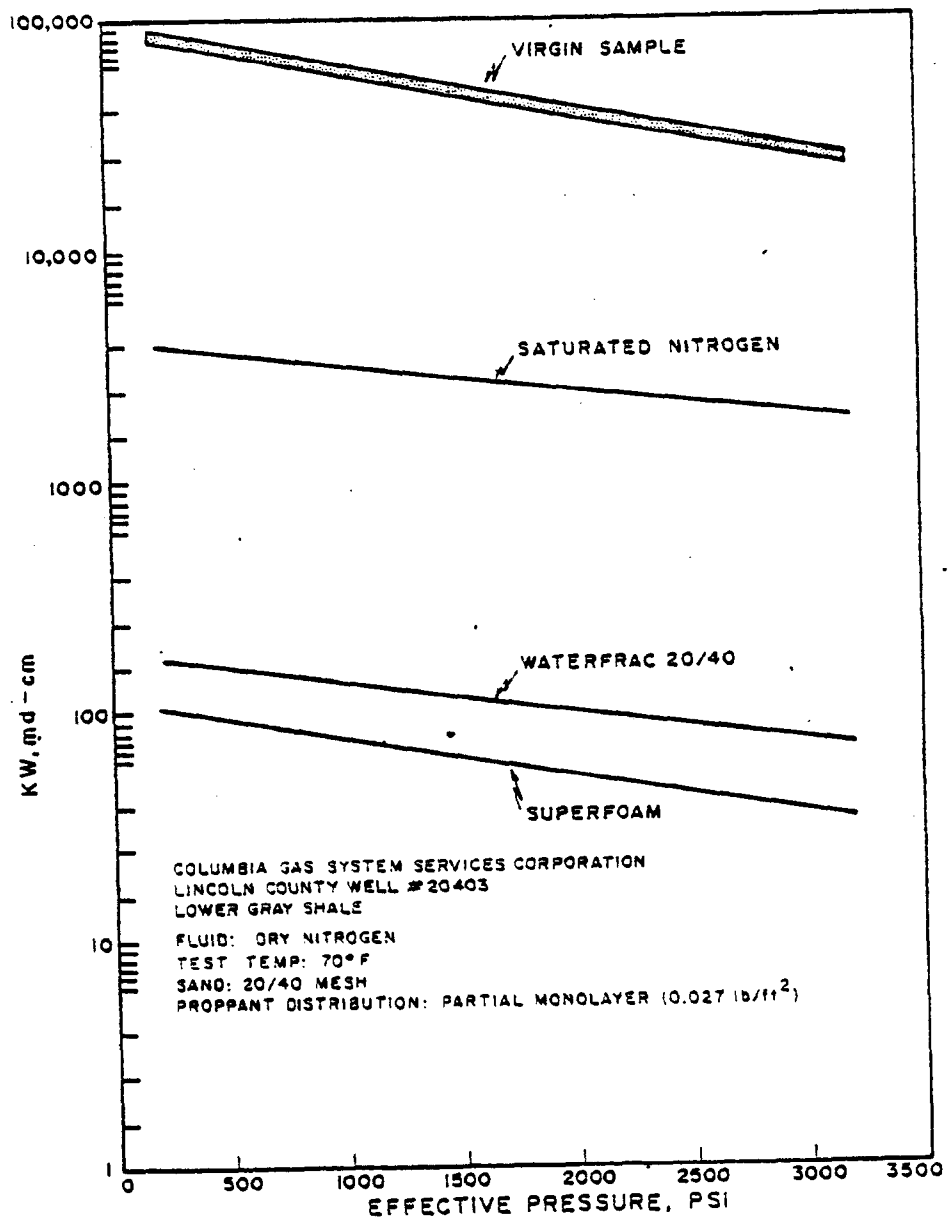


Figure 4. Trend of fracture flow capacity with the increase in effective pressure for 'Lower Gray Shale'.

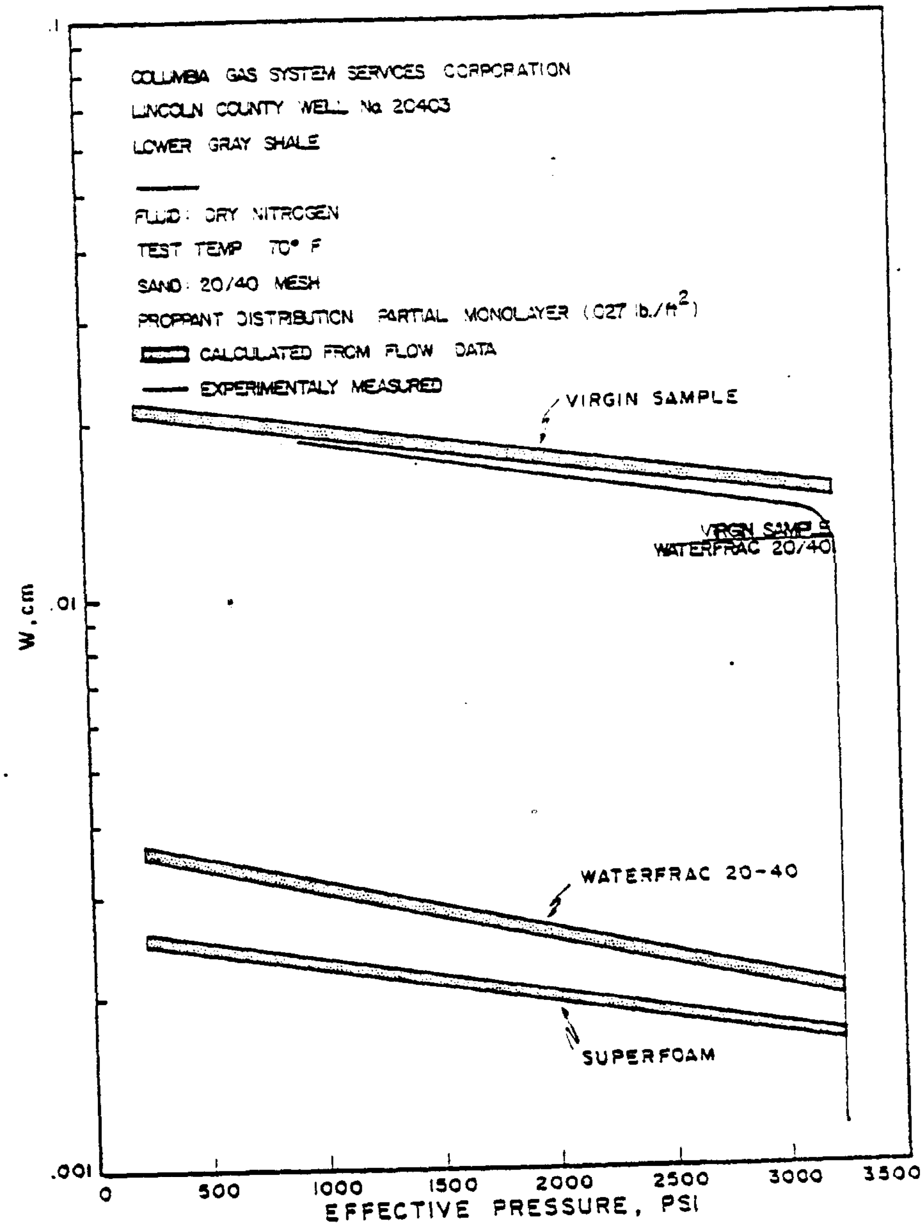


Figure 5. Trend of the effective fracture width with the increase in effective pressure for 'Lower Gray Shale'.

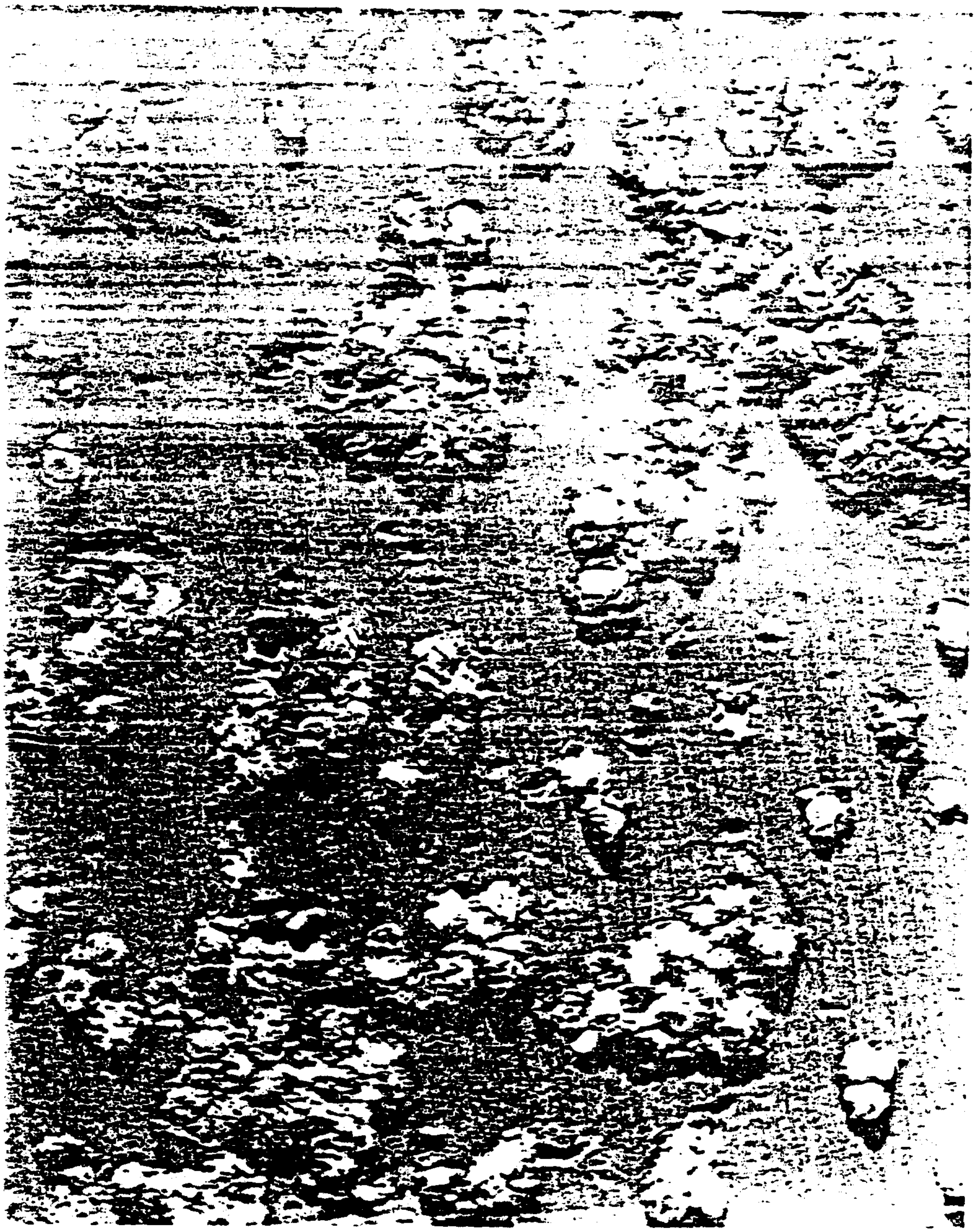

Figure 6. Eracture face of the 'Lower Gray Shale' sample interacted by Waterfrac 20-40.

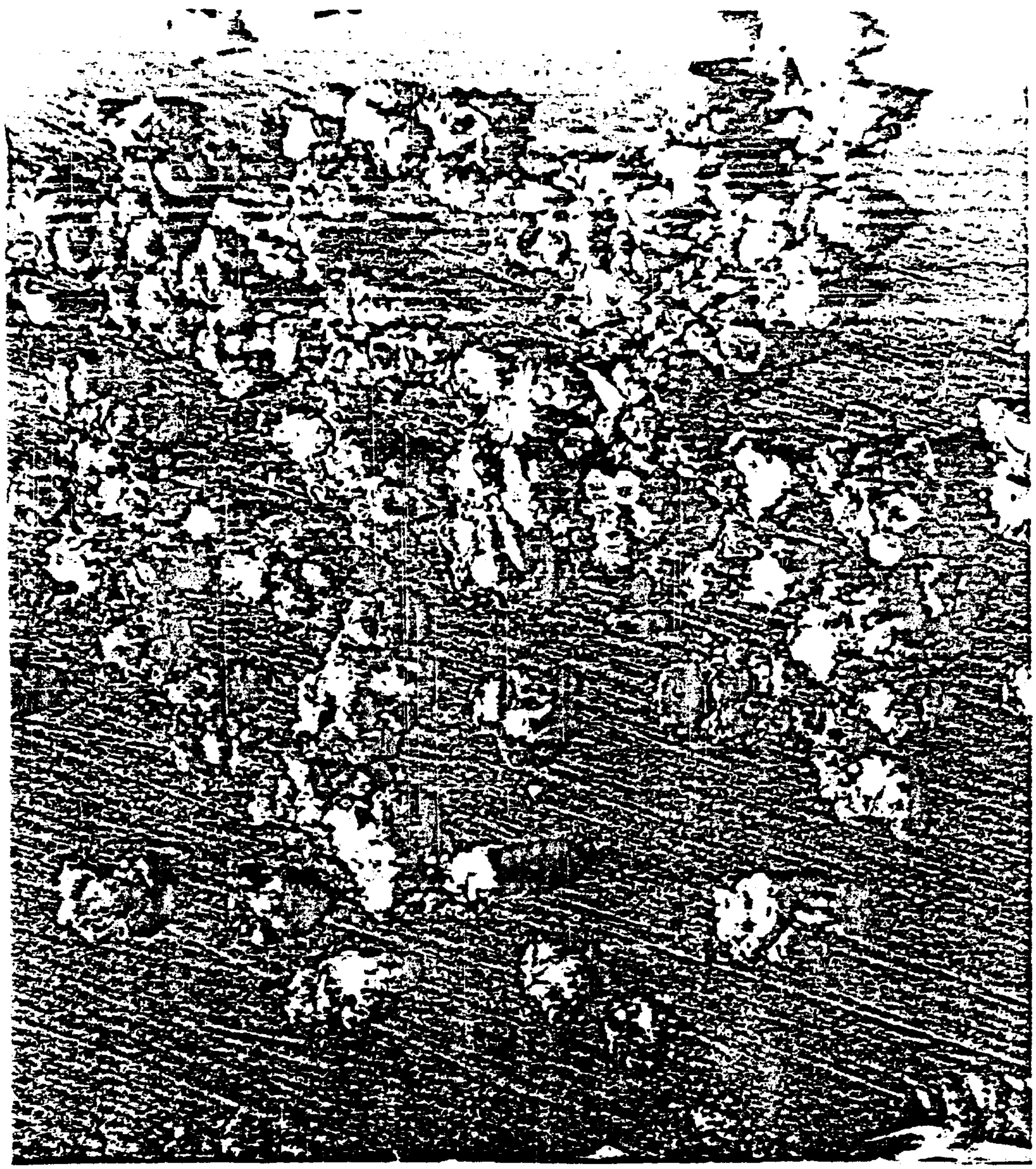

Figure 7. Fracture face of the 'Lower Gray Shale' sample interacted by Superfoam.

# REFERENCES

Amyx, J. S., Bass, D. M., Jr., and Whiting, R. L., "Petroleum Reservoir Engineering - Physical Properties," McGraw Hill, Inc., pp. 70, (1960).

Clark, P. E., Harkin, M. W., Wahl, H. A., and Sievevert, J. A., "Design of a Large Vertical Prop Transport Model," 52nd Annual Fall Technical Conference and Exhibition of the SPE-AIME, Denver, Colorado, (October 9-12, 1977).

Craft, B. C., and Hawkins, M. F., "Applied Petroleum Reservoir Engineering," Prentice-Hall, Inc., Englewood Cliffs, N. J., pp. 882, (1959).

Davis, W. E., Jr., "Consideration for Fracture Stimulation of the Deep Morrow in the Anadarko Basin," SPE paper 5391 presented at Oklahoma City Regional Meeting, Oklahoma City, Oklahoma, (March 24-25, 1975).

Holditch, S. A., "Factors Affecting Water Blocking and Gas Flow from Hydraulically Fractured Gas Wells," SPE paper 7561 presented at the 53rd Annual Fall Technical Conference and Exhibition of the SPE-AIME, Houston, Texas, (October 1-3, 1978).

Leventhal, J. S., "Summary of Chemical Analyses and Some Geochemical Controls Related to Devonian Black Shales from Tennessee, West Virginia, Kentucky, Ohio, and New York," Proceedings from the Second Eastern Gas Shales Symposium, Volume 1, (October 1978).

McKetta, S. F., "Investigation of Hydraulic Fracturing Technology in the Devonian Shale," Proceedings from the Second Eastern Gas Shales Symposium, Volume 1, (October 1978).

# APPENDIX

## FLOW CAPACITY MEASUREMENTS

The flow capacity of a fracture (a product of fracture permeability and width of the fracture) is usually reported instead of the permeability because the fracture width is generally not known.

The calculation of the flow capacity of a fracture follows from a simple derivation of Darcy's law, presented by Amyx, *et al.*, (1960)

$$Q_o = \frac{1 \times 10^{-3} \, KA(P_i - P_o)}{\mu L} \tag{1}$$

where,

$Q_o$ = flow rate of outlet fluid (ml/sec)

K = permeability (millidarcy's)

A = cross-sectional area of flow ($cm^2$)

$P_i$ = inlet pressure (atm absolute)

$P_o$ = outlet pressure (atm absolute)

$\mu$ = viscosity of fluid (centipoises)

L = length of the sample (cm)

For a fracture the cross-sectional area (A) of flow is essentially:

$$A = W \times h \tag{2}$$

where,

W = width of the fracture, cm

h = height of the fracture, cm.

Substitution of Equation (2) into (1) results in the following relationship or the flow capacity, KW, in md-cm.

$$KW = \frac{1 \times 10^{3} \, L\mu Q_o}{h(P_i - P_o)} \tag{3}$$

In the reported tests, nitrogen flowed in and out of the pressure vessel through small lines with resulting pressure losses; therefore, a second set of lines were used to sense gas pressures at the ends of the samples. In this way, and for steady state flow, pressures were measured directly and no corrections were needed for line losses. The gas flow rate was measured at atmospheric pressure at the end of small flow lines leading from the pressure vessel. The volumetric flow through the samples was determined by making the pressure correction between the flowmeter (at atmospheric pressure) and the sample mean pore pressure (assuming isothermal flow at 70°C). Figure 8 is a schematic diagram of the experimental set-up.

An estimate of the width of the flow channels in the unpropped fracture can be made assuming equivalent permeability for flow between parallel plates (Craft and Hawkin, 1959).

$$Q_o = \frac{W^2 A \,(P \;\; - P_o)}{1.74 \times 10^{-6} \mu L} \tag{4}$$

Here again replacing the term A by Equation (2), we have:

$$W = \left\{ \frac{1.74 \times 10^{-6} \mu L \, Q_o}{h(P_i - P_o)} \right\}^{1/3} \tag{5}$$

This same equation can be used to make an estimate of the *effective* width of the flow channels in propped fractures.

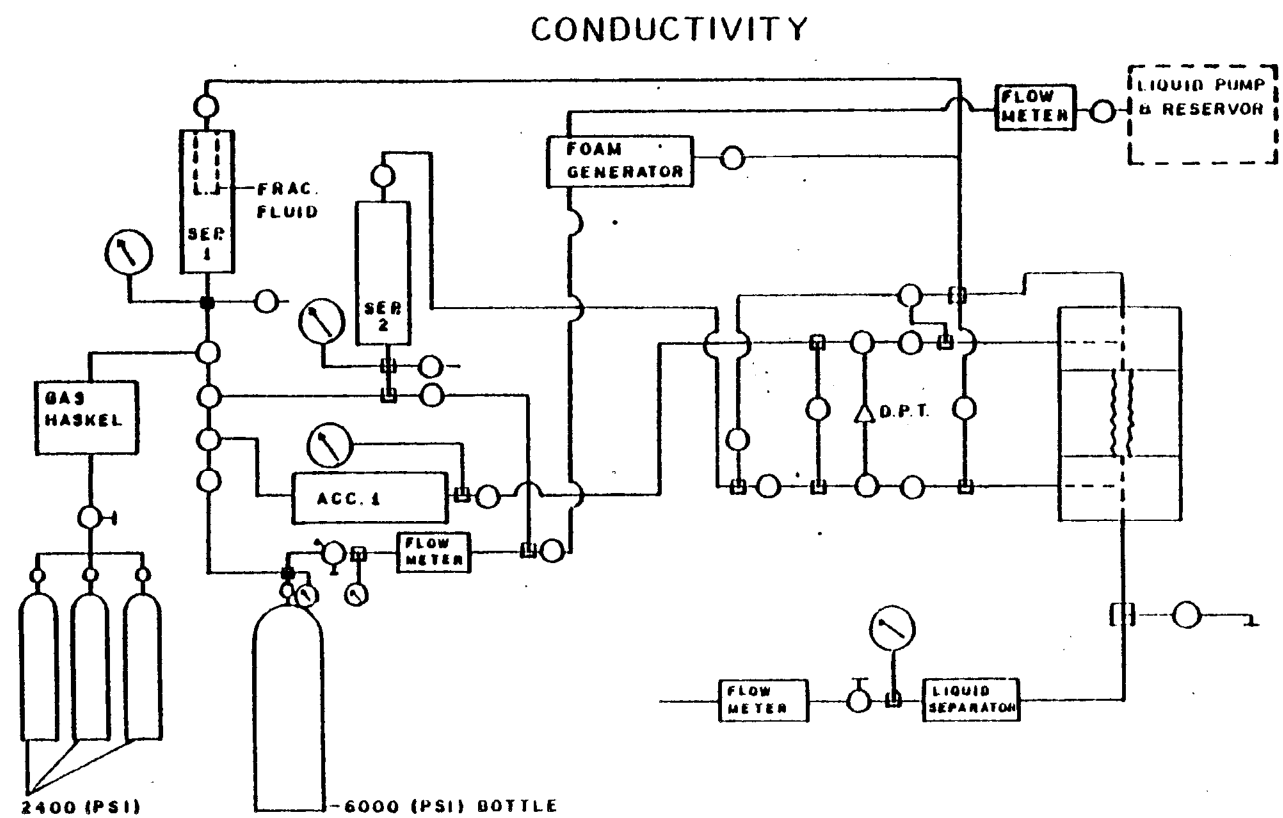


Figure 8. Schematic design of the flow set-up